

LOAD AND RESISTANCE FACTOR DESIGN
OF DRILLED SHAFTS AT THE SERVICE LIMIT STATE

A Dissertation

presented to

the Faculty of the Graduate School

at the University of Missouri-Columbia

In Partial Fulfillment

of the Requirements for the Degree

Doctor of Philosophy

by

THANH THUY VU

Dr. Erik Loehr, Dissertation Supervisor

JULY, 2013

The undersigned, appointed by the dean of the Graduate School, have examined the dissertation entitled

LOAD AND RESISTANCE FACTOR DESIGN

OF DRILLED SHAFTS AT THE SERVICE LIMIT STATE

presented by Thanh Thuy Vu,

a candidate for the degree of

Doctor of Philosophy

and hereby certify that, in their opinion, it is worthy of acceptance.

Dr. Erik Loehr P.E., Supervising Professor

Dr. Douglas Smith P.E., Committee Member

Dr. John Bowders P.E., Committee Member

Dr. Brent Rosenblad, Committee Member

DEDICATION

I am very grateful for my MuGEO family: Wyatt Jenkins, Minh Uong, Taylor Day, Dan Ding, Ahmed Abu El Ela, Sara Grant, Rani Jaafar, Tasneem Khan, David Williams and Daniel Huaco. We could never end our conversations without smiles or laughs. I greatly appreciate our friendship. I have been working hard here, but the time at Mizzou has been very joyful and memorable; thanks to you all.

Most importantly, I would like to thank my husband, Thang Pham, who chose Mizzou for me and who has never stopped encouraging and supporting me; he sacrificed the most for my study. Thanks to my parents Tien Vu and Thanh Ngo for giving me inspiration and determination in life. Also, thanks to my dear daughters, Fonda Pham, Mai Pham and Tracy Pham, for standing by me and for loving me when I live far away from home.

ACKNOWLEDGEMENTS

I would like to gratefully and sincerely thank Dr. Erik Loehr for his guidance, enthusiasm and understanding during my graduate studies at the University of Missouri-Columbia. I have always admired his knowledge, creativity and diligence. I am especially grateful for his encouragement to pursue independent thinking.

I would like express my appreciation to Dr. John Bowders, who always cares for my academic development as well as my life; he is my role model. Many thanks to Dr. Douglas Smith for his valuable help with computer coding. His help made this study go faster. I would also like to thank Dr. Brent Rosenblad for his support of my teaching experiences; I really learned from his teaching skills. Last but not least, many special thanks are to Dr. Richard Hammer, who willingly provided great help for editing.

TABLE OF CONTENTS

ACKNOWLEDGEMENTS.....	ii
TABLE OF FIGURES.....	x
LIST OF TABLES.....	xvii
ABSTRACT.....	xx
Chapter 1. Introduction	1
1.1. Background.....	1
1.2. Problem Statement and Hypothesis	3
1.3. Organization of Dissertation	5
Chapter 2. Literature Review	8
2.1. Introduction.....	8
2.2. Basics of Load and Resistance Factor Design.....	8
2.3. Methods for Predicting Settlement of Drilled Shafts.....	10
2.3.1 Vesic (1977).....	10
2.3.2. Load Transfer Method.....	11
2.3.3. O’Neil and Reese (1999)	12
2.4. Probabilistic Approaches for LRFD Calibration and Reliability-Based Design....	14
2.4.1. First Order Second Moment (FOSM) Method.....	15
2.4.2. First Order Reliability Method (FORM)	15
2.4.3. Monte Carlo Simulation Method.....	16
2.5. Service Limit State’s Target Probability of Failure and Reliability Index.....	17
2.6. Alternative Approaches to Service Limit State Design.....	18

2.7.	Factored Strength versus Factored Resistance	19
2.7.1.	Factored Resistance Approach	19
2.7.1.	Factored Strength Approach	20
2.8.	Service Limit State Reliability-Based Design and LRFD Calibration.....	22
2.8.1.	Misra and Roberts	22
2.8.2.	Zhang and Chu (2009).....	27
2.8.3.	Phoon, Kulhawy and Grigoriu (1995)	30
2.8.4.	Wang, Au and Kulhawy (2011)	31
2.8.5.	Important Findings and Limitations of Previous Work.....	32
2.9	Summary	34
Chapter 3. Deterministic Prediction of Drilled Shaft Settlement		35
3.1.	Introduction.....	35
3.2.	The t - z Method.....	35
3.2.1.	Finite Element Formulation	38
3.2.2.	Newton Raphson Approach	41
3.3.	Modeling an Actual Case for Code Checking	46
3.4.	Summary	50
Chapter 4. Probabilistic Prediction of Drilled Shaft Settlement		51
4.1.	Input Parameters for Probabilistic Analysis of SLS.....	51
4.2.	Monte Carlo Simulation	52
4.2.1.	Number of Simulations	54
4.2.2.	Random Number Generation of Variables	56

4.3. Summary	59
Chapter 5. Interpretation of Load Transfer from Field Load Tests	60
5.1. Drilled Shaft Load Test Program.....	60
5.1.1. Site Conditions and Soil/Rock Properties	60
5.1.2. Test Shaft Characteristics	73
5.1.3. Test Shaft Instrumentation and Measurements	75
5.1.4. Load testing procedure.....	81
5.2. Analysis and Interpretation.....	84
5.2.1. Procedure for Establishing Load Distribution along Shafts	84
5.2.2. Analysis of Load Transfer in Side Resistance	88
5.2.3. Analysis of Load Transfer in Tip Resistance.....	91
5.2.4. Summary of load test results.....	93
5.3. Development of Normalized Load Transfer Curves	95
5.3.1. Normalized Load Transfer Using Maximum Measured Values	96
5.3.2. Normalized Load Transfer Using Predicted Ultimate Resistance.....	107
5.4. Important findings of the chapter.....	114
5.5. Summary	116
Chapter 6. Development of Load Transfer Models	117
6.1. Introduction.....	117
6.2. Approach to Model Development	117
6.3. Options for regression analyses	118
6.3.1 Ordinary Least Squares versus Weighted Least Squares Regression	119

6.3.2	Collective versus Individual Regression Analyses	121
6.4.	Regression Analyses for Side Resistance – Normalized to Maximum Measured Resistance.....	124
6.4.1.	Regression Analyses for Side Resistance - Collective Measurements.....	125
6.4.2.	Regression Analyses for Side Resistance –Individual Measurements.....	143
6.5.	Regression Analyses for Side Resistance - Normalized to Predicted Ultimate Resistance.....	153
6.6.	Regression Analyses for Tip Resistance –Normalized to Maximum Measured Resistance.....	155
6.6.1.	Regression Analyses for Tip Resistance - Collective Measurements	155
6.6.2.	Regression Analyses for Tip Resistance – Individual Measurements.....	169
6.7.	Regression Analyses for Tip Resistance - Normalized to Predicted Ultimate Resistance.....	176
6.8.	Probabilistic Simulation of Load Transfer Curves	178
6.9.	Comparison of Simulated Data for Collective and Individual Measurements.	180
6.9.1.	Generation of Load Transfer Data - Side Resistance.....	181
6.9.2.	Generation of Load Transfer Data - Tip Resistance.....	187
6.10.	Important Findings of this Chapter	195
6.11.	Selection of Load Transfer Models.....	198
6.12.	Summary.....	199
Chapter 7.	Evaluation of Probabilistic and Deterministic Variables	201
7.1.	Introduction.....	201

7.2.	Framework for Load and Resistance Factor Design at Service Limit State	201
7.3.	Calibration of Resistance Factors for Service Limit State	203
7.3.1.	Probabilistic Analysis	203
7.3.2.	Resistance Factor Calibration:	206
7.4.	Parameter Normalization	208
7.5.	Impossible Cases	211
7.6.	Sensitivity Analyses	214
7.6.1.	Inputs for Sensitivity Analyses	214
7.6.2.	Effect of Variability of Probabilistic Variables	216
7.6.3.	Effect of Normalized Load on SLS Resistance Factor	218
7.6.4.	Effect of Dead Load over Live Load Ratio	221
7.6.5.	Effect of Target Probability of Failure	222
7.6.6.	Effect of Normalized Shaft Dimension	223
7.6.7.	Effect Reinforced Concrete Young's Modulus	226
7.6.8.	Effect of Adding Probabilistic Variables	227
7.7.	Important Findings of this Chapter	232
7.8.	Summary	233
 Chapter 8. Procedure for Evaluation of Service Limit State for Drilled Shafts Using LRFD235		
8.1.	Introduction	235
8.2.	Input Parameters	235
8.2.1.	Inputs for SLS probabilistic Analyses	235
8.2.2.	Variable Combination and Reduction	238

8.3. Resistance Factors for Drilled Shaft at Service Limit State	242
8.4. Equation to Calculate SLS Resistance Factor.....	246
8.5. Resistance Factor Equation Verification	249
8.5.1. Example 1	250
8.5.2. Example 2	250
8.5.3. Comparisons with Resistance Factor Curves.....	251
8.6. Possible and Impossible Case.....	253
8.6.1. Example 1	256
8.6.2. Example 2	258
8.7. Resistance Factor Calibrated Using Load Transfer Normalized to Predicted Ultimate Values.....	260
8.8. Side Resistance Factor and Tip Resistance Factor	265
8.9. Summary	270
Chapter 9. Application Procedure for Service Limit State Design Using LRFD	271
9.1. Introduction.....	271
9.2. Procedure for Drilled Shaft Design at the Service Limit State	272
9.3. Illustrative Example	276
9.4. Summary	282
Chapter 10. Summary, Findings, Practical Implications and Conclusions	283
10.1. Summary of the Study.....	283
10.2. Findings and Practical Implications	286
10.2.1. Load Transfer Characteristics	286

10.2.2. Regression Approaches	288
10.2.3. Sensitivity of SLS Resistance Factors on Variables	290
10.2.4. Proposed Procedure and Resistance Factors for SLS Design	293
10.3. Conclusions.....	295
10.4. Recommendations for Future Research	295
APPENDIX	298
Appendix A. MATLAB® Code for Shaft Top Displacement Calculation	298
Appendix B. As-built Shaft Information	302
Appendix C. Measured Side and Tip Resistances.....	340
Appendix D. Measured and Predicted Ultimate Resistance	346
Appendix E. Weighted Least Square Regression Code	356
Appendix F. Simulation of Load transfer Data/Curves.....	359
Appendix G. Computer Codes for Resistance Factor Calibration	365
Appendix H. Drilled Shaft SLS Resistance Factors	371
References	378
Vita.....	382

TABLE OF FIGURES

Figure 2.1. Probability of failure and reliability index (From Allen, 2005).	9
Figure 2.2. Normalized load transfer, or $t-z$ and $q-w$ curves.	12
Figure 2.3. Load transfer model and load transfer curves.	13
Figure 2.4. O’Neil and Reese (1999) $t-z$ and $q-w$ curves.	14
Figure 2.5. Shaft-soil interface load-displacement relationship (a) the ideal elasto-plastic and (b) hyperbolic nonlinear spring-slider system, (Misra and Roberts 2009)	24
Figure 2.6. Service limit state resistance factors versus COV of.....	26
Figure 3.1 The $t-z$ method model and load transfer curves.	37
Figure 3.2 Nodes and elements.	39
Figure 3.3 Forces and displacements of nodes.....	40
Figure 3.4 Shaft F7 (Frankford, MO) with O-Cell and strain gages.	47
Figure 3.5 Mobilized unit side resistance versus displacement of shear zone.	48
Figure 3.6 Mobilized unit tip resistance versus displacement of shaft tip.	48
Figure 3.7 Load-displacement curves for Shaft F7 (Frankford, MO).	50
Figure 4.1. Schematic of Monte Carlo Simulation.	53
Figure 4.2. Resistance factor versus number of Monte Carlo Simulations.	56
Figure 4.3. Normal (left) and lognormal distributions (right).....	57
Figure 5.1. Drilled shaft test sites in Missouri.....	61
Figure 5.2. Cross-section of the Frankford Load Test Site showing measured uniaxial compressive strengths.	63
Figure 5.3. Layout of test shafts at the Frankford site.....	64

Figure 5.4. Cross-section of the Frankford Load Test Site showing the drilled shafts.	65
Figure 5.5. Measured uniaxial compressive strengths at the Frankford site.	66
Figure 5.6. Cross-section of the Warrensburg Load Test Site showing measured uniaxial compressive strengths.	68
Figure 5.7. Layout of test shafts at Warrensburg site.	69
Figure 5.8. Cross-section of the Warrensburg Load Test Site showing the drilled shafts.	70
Figure 5.9. Measured uniaxial compressive strengths from the Warrensburg site.	72
Figure 5.10. Shaft F7 with O-Cell and strain gauge elevations.	74
Figure 5.11. O-Cell® welded to top and bottom plates at the end of a rebar cage.	78
Figure 5.12. Vibrating wire strain gauge attached to rebar cage.	79
Figure 5.13. Load displacement curves for shaft F7.	82
Figure 5.14. Force in test shaft F7 at each loading during testing.	85
Figure 5.15. Mobilized unit side resistance versus displacement for test shaft F-7.	91
Figure 5.16. Mobilized unit tip resistance versus displacement for test shaft F-7.	93
Figure 5.17. Normalized load transfer response in side resistance for uncased segments of test shafts at the Frankford site.	97
Figure 5.18. Normalized load transfer response in side resistance for uncased segments of test shafts at the Warrensburg site.	97
Figure 5.19. Normalized load transfer response in side resistance for cased segments of test shafts at the Frankford site.	98
Figure 5.20. Normalized load transfer response in side resistance for cased segments of test shafts at the Warrensburg site.	99

Figure 5.21. Normalized unit side resistance curves from tests at the Frankford site with O’Neil and Reese (1999) curves (bold black lines) superimposed for comparison. 101

Figure 5.22. Normalized unit side resistance curves from tests at the Warrensburg site with O’Neil and Reese (1999) curves (bold black lines) superimposed for comparison. 101

Figure 5.23. Normalized load transfer response in tip resistance for test shafts at the Frankford site. 103

Figure 5.24. Normalized load transfer response in tip resistance for test shafts at the Warrensburg site. 103

Figure 5.25. Normalized unit tip resistance curves from tests at Frankford site with O’Neil and Reese (1999) curves (bold black lines) superimposed for comparison. 106

Figure 5.26. Normalized unit tip resistance curves from tests at Warrensburg site with O’Neil and Reese (1999) curves (bold black lines) superimposed for comparison. 106

Figure 5.27. Normalized load transfer response in side resistance with respect to predicted ultimate values for uncased segments of test shafts at the Frankford site... 109

Figure 5.28. Normalized load transfer response in side resistance with respect to predicted ultimate values for uncased segments of test shafts at the Warrensburg site. 110

Figure 5.29. Normalized load transfer response in tip resistance with respect to predicted ultimate values of test shafts at the Frankford site. 113

Figure 5.30. Normalized load transfer response in tip resistance with respect to predicted ultimate values of test shafts at the Warrensburg site. 113

Figure 6.1. Illustration of regression under assumptions of: (a) constant standard deviation and (b) non-constant standard deviation (after Ang and Tang, 1974).....	120
Figure 6.2. Flowchart of regression analyses for both side and tip resistances.....	124
Figure 6.3. Power function from ordinary least squares regression.	126
Figure 6.4. Power function from weighted least squares regression.....	126
Figure 6.5. Power function from ordinary	128
Figure 6.6. Power function from weighted.....	128
Figure 6.7. Exponential function from ordinary least squares regression.	130
Figure 6.8. Exponential function from weighted least squares regression.....	130
Figure 6.9. Logarithm function from ordinary least squares regression.	132
Figure 6.10. Logarithm function from weighted least squares regression.....	132
Figure 6.11. Rational function from ordinary least squares regression.	135
Figure 6.12. Rational function from weighted least squares regression.....	135
Figure 6.13. Rational fitting for side resistance from	136
Figure 6.14. Rational function from weighted.....	137
Figure 6.15. Hyperbolic function of fit from ordinary least squares regression.	138
Figure 6.16. Hyperbolic function of fit from weighted least squares regression.	138
Figure 6.17. Five fitting models for unit side resistance.....	142
Figure 6.18. Fitting models for shaft segment F7-12.....	144
Figure 6.19. Hyperbolic fitting model for shaft segment F7-12.	145
Figure 6.20. Histogram of hyperbolic fitting parameters a and b	152
Figure 6.21. Hyperbolic function from ordinary least squares regression	154

Figure 6.22. Hyperbolic function from weighted least squares regression.....	154
Figure 6.23. Power function for tip resistance	156
Figure 6.24. Power function for tip resistance	157
Figure 6.25. Exponential function for tip resistance.....	159
Figure 6.26. Exponential function for tip resistance.....	159
Figure 6.27. Logarithm function for tip resistance	161
Figure 6.28. Logarithm function for tip resistance	162
Figure 6.29. Rational function for tip resistance	163
Figure 6.30. Rational function for tip resistance	164
Figure 6.31. Hyperbolic function for tip resistance	165
Figure 6.32. Hyperbolic function for tip resistance from weighted least squares regression	166
Figure 6.33. Five functions for tip resistance from ordinary least squares regression. .	167
Figure 6.34. Unreasonable tip resistance fit (Shaft W3).....	171
Figure 6.35. Reasonable tip resistance fit (Shaft W12)	171
Figure 6.36. Histograms of hyperbolic fitting parameters for tip resistance.	175
Figure 6.37. Hyperbolic function for tip resistance	177
Figure 6.38. Hyperbolic function for tip resistance	177
Figure 6.39 Comparison of simulated (\diamond) and measured (+) side resistances	182
Figure 6.40. Comparison of simulated (\diamond) and measured (+) side	182
Figure 6.41. Comparison of simulated (\diamond) and measured (+) side resistances	183
Figure 6.42. Comparison of simulated (\diamond) and measured (+) side resistances	184

Figure 6.43. Simulated normalized unit side resistance curves from the collective approach.	186
Figure 6.44. Simulated normalized unit side resistance curves	187
Figure 6.45. Comparison of simulated (\diamond) and measured (+) tip resistances	189
Figure 6.46. Comparison of simulated (\diamond) and measured (+)tip resistances	189
Figure 6.47. Comparison of simulated (\diamond) and measured (+) tip resistances	190
Figure 6.48. Comparison of simulated (\diamond) and measured (+) tip resistances	191
Figure 6.49. Simulated normalized unit tip resistance curves from the collective approach.	193
Figure 6.50. Simulated normalized unit tip resistance curves.....	193
Figure 7.1. Histogram and probability density curve for vertical top shaft displacement	205
Figure 7.2. Resistance factors for different loads,	211
Figure 7.3. Impossible case: the probability of failure cases.....	212
Figure 7.4. Displacement histogram from 300 simulations.....	213
Figure 7.5. Frequency distribution of random values load and resistance	214
Figure 7.6. Resistance factors versus COV of each probabilistic variable.	217
Figure 7.7. Resistance factors for different normalized loads Θ from 0.2 to 0.6.	219
Figure 7.8. Non-linearity of load transfer curve.	220
Figure 7.9. Resistance factor for different dead load/live load ratios.....	221
Figure 7.10. Resistance factor for P_f of 1/25-1/100.....	223
Figure 7.11. Resistance factors for different L/D.....	225

Figure 7.12. Resistance factors for concrete Young's moduli	226
Figure 7.13. Comparing effects of adding probabilistic variables.	228
Figure 8.1. Resistance factor for drilled shafts at SLS for (L/D = 10).	243
Figure 8.2. Resistance factor for drilled shafts at SLS L/D = 30.	244
Figure 8.3. Coefficient $C_{L/D}$	248
Figure 8.4. Comparisons of resistance factors obtained from Equation 8.7	253
Figure 8.5. Boundaries of possible and impossible cases with L/D of 10.	255
Figure 8.6. Possible/impossible case boundary for Equation 8.7 with L/D of 30 and Pf=1/100.....	258
Figure 8.7. The t - z curves for a) normalized to maximum measured unit resistance ...	261
Figure 8. 8. Resistance factors for two approach of normalization.	264
Figure 8.9. Side resistance factors.	268
Figure 8.10. Tip resistance factors.....	269
Figure 9.1. Sketch of design problem for a single drilled shaft.	276
Figure 9.2. Resistance factors for unit side resistance for strength limit sates.....	278
Figure 9.3. Resistance factors for unit tip resistance for strength limit sates.....	278

LIST OF TABLES

Table 2.1 SLS partial factors for drilled shafts (Zhang and Chu, 2009).....	29
Table 2.2. Deformation factors for Drilled Shafts under undrained conditions.....	30
Table 3.1. Input parameters for Shaft F7.....	47
Table 4.1. Input Parameters for Sample Cases.	55
Table 5.1. Uniaxial compressive strength statistics for the Frankford site.	67
Table 5.2. Uniaxial compressive strength statistics for the Warrensburg site.	71
Table 5.3. Summary of test shaft characteristics at the Frankford site.....	74
Table 5.4. Summary of test shaft characteristics at the Warrensburg site.	75
Table 5.5. Summary of instrumentation used for the Frankford test shafts.....	76
Table 5.6. Summary of instrumentation used for the Warrensburg test shafts.	76
Table 5.7 Shaft F7 as built parameters.	80
Table 5.8. Maximum O-Cell pressures and loads for tests at Frankford site.....	83
Table 5.9. Maximum O-Cell pressures and loads for tests at Warrensburg site.....	83
Table 5.10. Load Test Results for Test Shaft F7 –Side resistance.	93
Table 5.11. Load Test Results for Test Shafts at Frankford – Tip Resistance.....	94
Table 5.12. Load Test Results for Test Shafts at Warrensburg – Tip Resistance.	95
Table 6.1. Summary of fitting models for side resistance normalized to maximum measured values using a collective approach.	141
Table 6.2. Fitting parameters for side resistance data	146
Table 6.2 continued. Fitting parameters for side resistance data.....	147

Table 6.3. Fitting parameters for side resistance data	148
Table 6.3 continued. Fitting parameters for side resistance data	149
Table 6.4. Fitting parameters and their statistics for side resistance data	150
Table 6.5. Fitting parameters and their statistics for side resistance data for collective and individual approaches.....	151
Table 6.6. Summary of fitting models for tip resistance normalized to maximum measured values using collective approach.	168
Table 6.7. Fitting parameters for tip resistance data	169
Table 6. 8. Fitting parameters for tip resistance data	170
Table 6.9. Fitting parameters and their statistics from individual approach for tip resistance.....	173
Table 6.10. Fitting parameters and their statistics for tip resistance.....	174
Table 6. 11. Fitting parameters and the variability of simulated data and field test data for side resistance.....	185
Table 6.12. Fitting parameters and the variability of simulated data and field test data for tip resistance.	192
Table 6.13. Summary of load transfer models and their quantified variability	199
Table 7.1. Inputs for SLS probability analyses and resistance factor calibration.	204
Table 7.2. Input for SLS probabilistic analyses.....	215
Table 7.3. Notation for resistance factor lines.	228
Table 8.1. Input parameters for the calibration of SLS probabilistic analyses.	236
Table 8.2. Probability of failure for different.....	237

Table 8. 3. Coefficient c_{pf}	247
Table 8.4.Coefficient $c_{L/D}$	247
Table 8.5. Combinations for impossible case with L/D of 10.	254
Table. 8.6. Side and tip resistance factors.	266
Table 9.1. Calculation of factored settlements.....	281

LOAD AND RESISTANCE FACTOR DESIGN
OF DRILLED SHAFTS AT THE SERVICE LIMIT STATE

Thanh Thuy Vu

Dr. Erik Loehr, Dissertation Supervisor

ABSTRACT

A practical and efficient procedure for evaluation of drilled shafts at the service limit state is proposed. The procedure uses Load and Resistance Factor Design (LRFD) concepts to achieve target probabilities of failure without requiring case-specific probabilistic analyses. Proposed resistance factors are primarily dependent on four parameters: the normalized load, the coefficient of variation of the geomaterial strength, the target probability of failure, and the shaft length-to-diameter ratio. The proposed procedure can be implemented using several charts or analytical equations provided.

Chapter 1. Introduction

This chapter provides background about load and resistance factor design of drilled shaft at the service limit state. The problem statement, hypotheses and objectives of this dissertation are addressed. The organization of the dissertation is also described.

1.1. Background

Geotechnical engineers recently have been working to transition from allowable stress design (or working stress design), which has been used for many years, to load and resistance factor design (LRFD). In allowable stress design, every input parameter is treated as deterministic, and the uncertainty in each design step is combined into one global factor called the “factor of safety.” Allowable stress design is the traditional design method, and its safety margin has gained widespread acceptance within the engineering community. The factor of safety for each type of structure is chosen based on past experience. However, design engineers seldom explicitly know the reliability of their designs or the probability of failure. On the other hand, LRFD often is linked explicitly to reliability analysis. An LRFD design often is targeted at a known level of reliability. The LRFD approach, therefore, provides the potential to achieve more consistent and uniform reliability. The American Association of State Highway

Administration Officials (AASHTO) has made utilization of LRFD mandatory on all federally-funded new bridge projects since 2007, (AASHTO, 2007).

In LRFD, a design starts with identifying all possible failure modes or limit states. The design reaches a limit state when a component of the structure does not fulfill its prescribed function. The LRFD limit states often are separated into strength limit states (ULS) and service limit states (SLS) categories. The strength limit state relates to geotechnical strength failures; for example, when the applied load is just equal to the resistance. The service limit state is when a component of the structure deforms beyond a prescribed amount; for example, when the vertical displacement of a drilled shaft is larger than the prescribed limiting settlement.

In current geotechnical practice, resistance factors for strength limit states are relatively well established. However, resistance factors for service limit states are not (AASHTO, 2007; O'Neil & Reese, 1999). In current AASHTO design specifications (AASHTO, 2007), the resistance factor for service limit states (except for extreme events) for *all* cases and for *all* geomaterials, takes the value of 1.0, implying that more research is needed. The resistance factor of 1.0 implies that the design is treated as deterministic, while LRFD is based on reliability and probability analysis. This research focuses on the SLS design for drilled shafts, develops models and a design procedure for the SLS, and contributes to the development of load and resistance factor design at the SLS.

1.2. Problem Statement and Hypothesis

Methods for LRFD or probability-based design of drilled shafts at the service limit state are not well established in current design practice. Recent research has focused on the issue (Fenton & Griffiths, 2007; Haldar & Babu, 2008; Misra & Roberts, 2009; Wang et al., 2011); however, the state-of-the-art is still immature. All of the resistance factors that have been proposed for service limit states were calculated for cases of specific diameters and/or shaft lengths, were based on specific reliability indices, or the designs were based on extensive probability analyses for each individual design. In other words, current SLS designs are drawn up on a case-by-case basis.

In current design practice, some load transfer models exist for drilled shaft (Reese and O'Neil, 2010); however, a specific load transfer model for drilled shafts in shale has not been identified. Furthermore, the variability and uncertainty of load transfer models in any kind of material are not quantified. The dependence of reliability of drilled shaft settlement predictions on deterministic and probabilistic parameters is not fully understood. To date, there is no closed-form equation to calculate resistance factors for SLS design for drilled shafts incorporating sources of input uncertainty, probability of failure or other important parameters. Even the design procedure used for design of drilled shafts at SLS is not well established.

It is hypothesized that: 1) resistance factors for design of drilled shafts at the SLS are strongly dependent on the load transfer model uncertainty as well as the variability and uncertainty in the strength of the soil and/or rock, and are less sensitive to non-soil

parameters such as the diameter or the length of drilled shafts; and 2) an equation can be developed to calculate resistance factors for SLS design that do not require probabilistic calculations on a case-by-case basis. In order to evaluate this hypothesis, the following objectives were established for this dissertation: 1) identifying appropriate load transfer models for drilled shafts in shale; 2) quantifying the variability and uncertainty in load transfer models based on full-scale field load tests; 3) understanding the primary parameters affecting the reliability of settlement predictions; 4) identifying the associated resistance factors and developing a closed-form equation to calculate the resistance factors, and; 5) establishing a design procedure to assess the service limit state for drilled shafts.

In order to achieve the objectives, work has been done on interpreting experimental data to identify rational and appropriate load transfer models for drilled shafts in shale. A sensitivity study was also conducted to help understand the dependence of resistance factors on the calibration process's input parameters. This work led to a process of combining, normalizing and eliminating input parameters so that LRFD can be practically implemented. Finally, work was performed to develop a design procedure for the service limit state that is not based on case-specific probabilistic analyses.

1.3. Organization of Dissertation

The work performed to evaluate the hypotheses and to develop an approach to evaluate load and resistance factor design for drilled shafts at the service limit states is documented in this thesis. The document is organized into ten chapters.

A review of literature is presented in Chapter 2. The chapter covers several methods used to develop deterministic predictions of drilled shafts settlement and the choices involved in those methods. The chapter also describes some available probabilistic tools and the current state-of-the-art for SLS design. The literature review examines several studies on resistance factors for drilled shafts at the service limit state.

Chapter 3 describes a method for predicting shaft displacement from a given load based on load-displacement relationships, or t - z curves. The t - z method is a rigorous method, which can determine displacement of a drilled shaft based on load transfer curves developed from load test data. A finite element method implementation of the t - z method used for the present work is also presented.

Chapter 4 describes the Monte-Carlo simulation method used for predicting the probabilistic displacement of a shaft under a given load. A computer code written for probabilistic analysis to find the resistance factor for a drilled shaft at the service limit state, and its verification are described.

Chapter 5 describes the development of load transfer curves based on field test data. Load transfer curves were developed using two different approaches for

normalizing unit side and tip resistance. Load transfer curves established from one of the methods are compared with the widely-used O'Neil and Reese (1999) method.

Field test data regression analyses are presented in Chapter 6. This chapter covers the development of mathematical models for load transfer curves for side resistance and tip resistance. Statistical analyses conducted to determine load transfer curve characteristics are described and the variability of the load transfer curves is quantified in this chapter. Also, two different approaches for modeling and generating load transfer data are presented. Simulated load transfer data using the two approaches is compared with field test data to identify the better approach.

One of the more important parts of this study is presented in Chapter 7, which is evaluating dependency of service limit state resistance factors on a variety of input parameters. Sensitivity analyses performed to investigate the effects of different deterministic and probabilistic variables on the overall resistance factor for a drilled shaft at the service limit state are presented. The dependency of the resistance factors on the number of probabilistic variables is also covered.

Chapter 8 describes the proposed approach for implementation of service limit state evaluations for drilled shafts in shale using LRFD. Resistance factors for drilled shaft at the service limit state are presented in the form of charts. A closed-form equation to calculate SLS resistance factors is also provided.

Chapter 9 provides a step-by-step design procedure for service limit state design of drilled shafts, making use of the proposed resistance factors, along with an example

to illustrate application of the proposed method. Finally, Chapter 10 provides a summary of this dissertation, along with notable findings, conclusions, and practical implications of the work described this dissertation. Recommendations for future research are also presented in this chapter.

Chapter 2. Literature Review

2.1. Introduction

This chapter describes important background information that serves as the basis for the research described in this dissertation. The chapter covers several deterministic methods for predicting shaft displacement as well as probabilistic tools for calibration of service limit state (SLS) resistance factors. This chapter also introduces several concepts, including SLS performance functions and distribution types of probabilistic variables. Discussions of the current state-of-the-art for load and resistance factor design are included along with reliability-based design of drilled shafts at the service limit state.

2.2. Basics of Load and Resistance Factor Design

Load and resistance factor design (LRFD), by definition (AASHTO, 2007), is “a reliability-based design methodology in which force effects caused by factored loads are not permitted to exceed the factored resistance of the components.” The load and resistance factors “have been developed from the theory of reliability based on current statistical knowledge of load and structural performance.”

Design following LRFD is usually separated into evaluation of strength limit states and service limit states. A limit state design must be based on a performance function.

In a general form, the performance function, denoted as g , is the difference between the nominal resistance and the nominal load as

$$g = R - Q . \quad (2.1)$$

When the performance function g is equal to or less than zero, it defines an unsatisfactory performance region; and g larger than zero indicates a satisfactory performance region.

For probabilistic analyses, the resistance R and load Q are probabilistic parameters, each having its own distribution as shown in Figure 2.1.a. The performance function g , therefore, takes on a probability distribution as presented in Figure 2.1.b. The overlap area under the two curves in Figure 2.1a is associated with the area of failure region (where performance function is equal to or less than zero in Figure 2.1b), which is the probability of failure of the design.

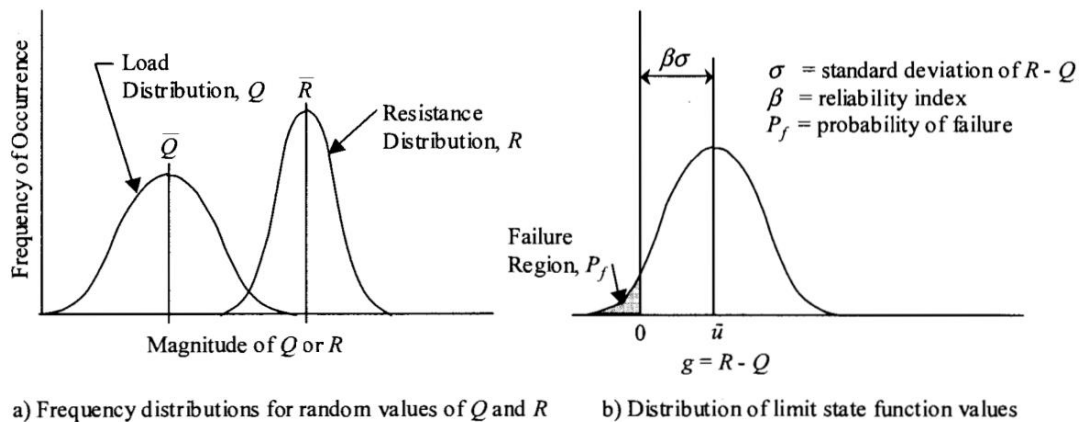


Figure 2.1. Probability of failure and reliability index (From Allen, 2005).

The general governing equation that can be applied to a number of different limit states for LRFD is

$$\gamma Q \leq \phi R_n \quad (2.2)$$

where

Q = nominal load component,

γ = load factor,

R_n = nominal resistance, and

ϕ = resistance factor.

2.3. Methods for Predicting Settlement of Drilled Shafts

To deal with the service limit state, a method to predict the load-displacement response of drilled shafts is essential. Several methods have been described in the literature, which include Vesic's (1977) method, the load-transfer, or t - z method, and the O'Neil and Reese (1999) method. Descriptions of each of these methods follow.

2.3.1 Vesic (1977)

Vesic (1977) proposed an approximate method for prediction settlement of deep foundations. In the method, the settlement of the shaft top is taken to be the sum of three components. The equation to calculate settlement of the shaft top w_T is:

$$w_T = w_c + w_{bb} + w_{bs} \quad (2.3)$$

where

w_c = elastic compression of the shaft,

w_{bb} = settlement of the shaft tip due to load transferred to the tip, and

w_{bs} = settlement of the shaft tip, due to the load transferred along shaft side.

Elastic compression of the shaft is a function of shaft length, cross sectional area of the shaft, composite elastic modulus for the reinforced concrete, load applied to the shaft, and mobilized side resistance. The settlement of the shaft tip is due to load transferred to the tip, and the settlement of the tip due to the load transferred along the side of the shaft, are based on empirical relationships. More details on the method can be found in “Drilled shafts: Construction Procedures and LRFD Design Methods,” (Brown et al., 2010). This method is recommended for preliminary analysis, and is not used in this research.

2.3.2. Load Transfer Method

Another method to predict shaft settlement is the so-called “load transfer” or “ $t-z$ ” method. The mainstays of the method are use of normalized unit side resistance versus local shear zone displacement relationships, or $t-z$ curves, and normalized unit tip resistance versus tip displacement relationships, or $q-w$ curves (Figure 2.2). The method also requires some prediction models to establish ultimate side and tip resistances from geomaterial properties. The normalized unit side and tip resistances are multiplied by these ultimate resistances to obtain the overall shaft resistance.

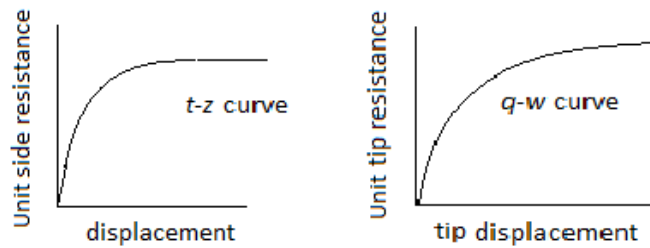


Figure 2.2. Normalized load transfer, or t - z and q - w curves.

Solving for shaft settlement usually requires iterations; thus, a computer program often is needed. Figure 2.3 shows the shaft sectioned or divided into a number of elements. Inputs for the method are shaft dimensions, shaft stiffness, the load transfer models, and the ultimate side and tip resistance prediction models. The general analytical process is that a load at the top of the shaft is specified, given all of the input parameters, from which the program computes the following: the settlement associated with that load; the displacement of any element along the shaft; and the distribution of stress/load along the length of the shaft (including the load at the shaft tip). More details are provided in Chapter 3.

2.3.3. O'Neil and Reese (1999)

Another drilled shaft settlement prediction method is proposed by O'Neil and Reese (1999). This method is widely used, and is recommended for use by ASSHTO (2007) and Brown et al. (2010). The method of O'Neil and Reese (1999), which is similar to the load transfer method, is the normalized relation of load and settlement, which are based on data from full-scale load tests. The dimensionless forms of normalized ultimate side load transfer and normalized ultimate end bearing in cohesive soils are

shown in Figure 2.4. Under an applied load, mobilized side and tip resistances of the shaft depend on the settlement of the shaft and shaft diameter. The procedure for design is iterative, and may be performed in a similar manner as that presented in Section 2.3.2 for the t - z method.

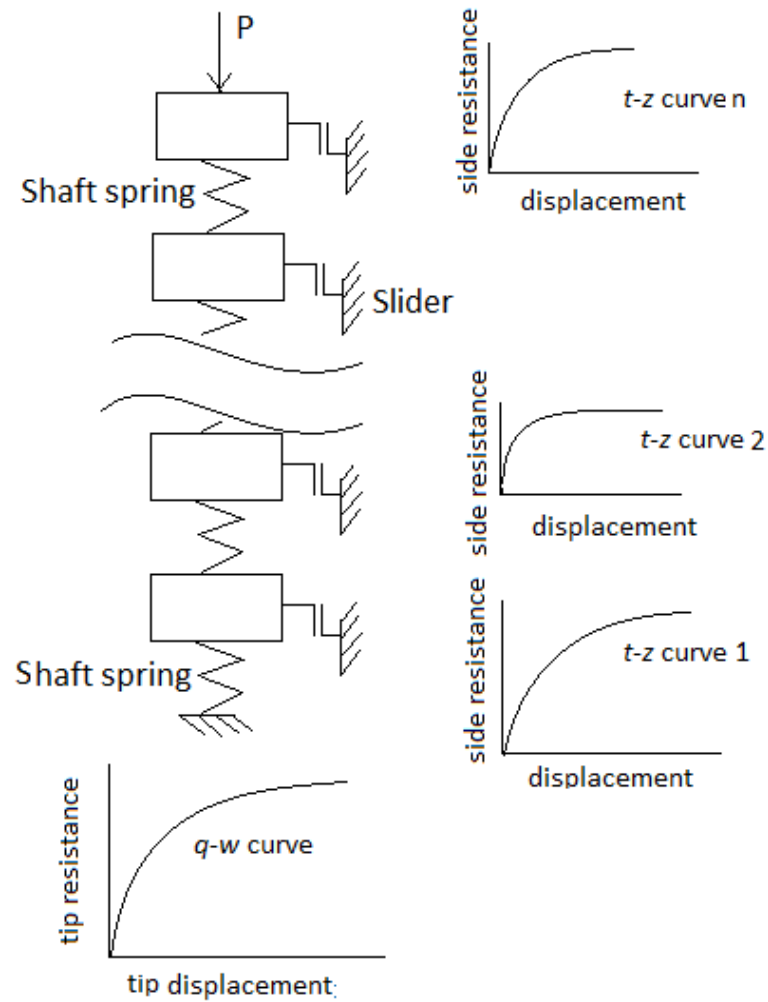


Figure 2.3. Load transfer model and load transfer curves.

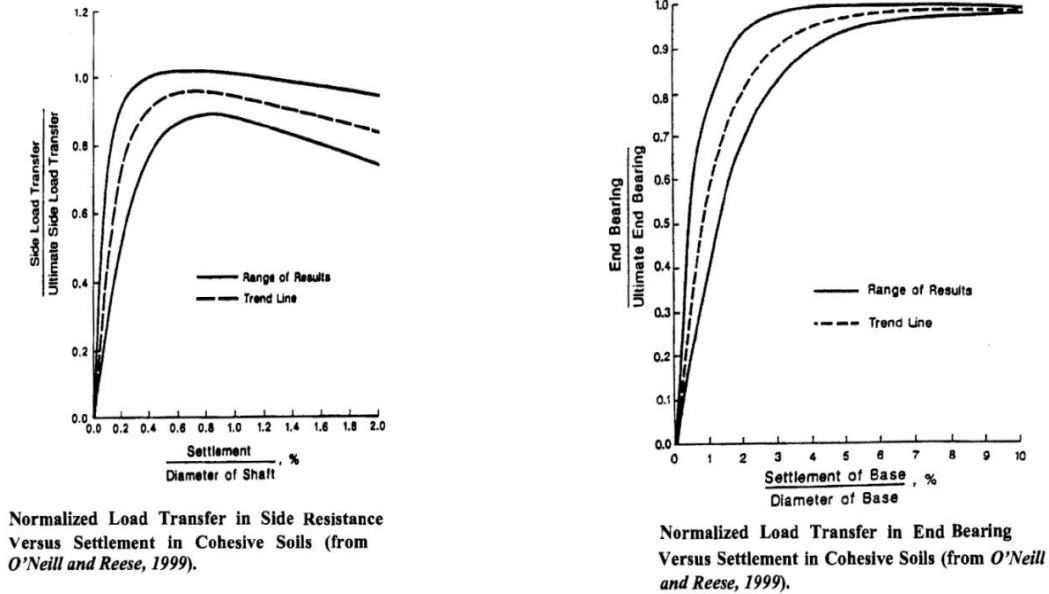


Figure 2.4. O'Neil and Reese (1999) t - z and q - w curves.

The t - z method is considered to be the more rigorous of these methods, and it is usually based on any load transfer models developed from load test data. In this research, the t - z method was used for all analyses.

2.4. Probabilistic Approaches for LRFD Calibration and Reliability-Based Design

Several probabilistic approaches often are used in reliability-based design and in the LRFD resistance factor calibration process. The most frequently used methods are the First Order Second Moment (FOSM) method, the First Order Reliability Method (FORM), and the Monte Carlo simulation method. Details about the methods have been described in the literature (Ang & Tang, 2004; Baecher & Christian, 2003; Griffiths & Fenton, 2007; Harr, 1987). Brief descriptions of the methods follow.

2.4.1. First Order Second Moment (FOSM) Method

The FOSM is an approximation method (Baecher and Christian, 2003) based on a Taylor series expansion of a performance function, g . Several steps are involved in the method. The first step is to find mean values, variances, correlation coefficients and auto correlation lengths of all probabilistic input variables. After computing the expected value $E[g]$ of the performance function, the partial derivatives of the function with respect to the variables are found. This step usually employs some form of numerical differencing. The contributions of each variable to the systematic and spatial variance, σ_g , for the performance function are calculated next. The last step is to compute the variance in the performance function, and based on the variance, to compute the reliability index, β , using the following equation:

$$\beta = \frac{E[g]-1}{\sigma_g} \quad (2.4)$$

where

$E[g]$ = expected value of the performance function, and

σ_g = spatial variance for the performance function.

2.4.2. First Order Reliability Method (FORM)

The first order reliability method (FORM) is a linear approximation of a limit state (Phoon et al., 2003; Phoon, 2008). The method utilizes a performance function g that is defined to be zero at the limit state. The approach is based on assumptions that all input parameters are normally distributed, and that the limit state also is a normally

distributed variable. The approach requires transforming the original random variables into independent, standard normal variables. Then an approximate linear limit state function is used instead of the actual limit state function. The nearest point from the origin to the approximate linear limit state function is the most likely failure point, and is called “the design point.” In the new standard space, a reliability index is determined by the distance from the origin to the design point.

2.4.3. Monte Carlo Simulation Method

The Monte Carlo simulation method utilizes random number simulation to extrapolate probability density function values (Baecher and Christian, 2003; Harr, 1995). The inputs for a simulation process for a variable are its mean value, standard deviation or coefficient of variation (COV), and type of distribution. In the Monte Carlo simulation method, any input can be set as a probabilistic variable as long as its mean value, standard of deviation or COV, and distribution function type are provided. According to Baecher and Christian (2003), the Monte Carlo technique has the advantage that it is relatively easy to implement on a computer and can deal with a wide range of functions. The major disadvantage is that the results may converge very slowly. As stated by Allen et al. (2005), when “a closed-form solution is either not available or is considered to be too approximate, Monte Carlo simulation can be performed.” The method is flexible and is gaining popularity for use in geotechnical reliability-based design. More detailed description of the Monte Carlo approach is provided in Chapter 4.

The first order second moment and the first order reliability method cannot be used with different types of variable distributions. Also, the two approaches usually provide some 'first order' approximations. The Monte Carlo simulation method is more flexible and rigorous, and if enough simulations are generated, the results approach exact solutions; however, the drawback is that it requires a large number of simulations for the results to converge. Despite the intensity of the calculations, the Monte-Carlo simulation method was still chosen in this research for probabilistic analyses.

2.5. Service Limit State's Target Probability of Failure and Reliability Index

There are two common probabilistic measures of the safety of a design. They are the probability of failure and the reliability index (Figure 2.1b). The relationship between probability of failure and reliability index depends on the distribution type of the variable (Allen, 2005). Probability of failure, P_f , as its name indicates, directly represents the probability that a service limit state (SLS) *failure* will happen. A SLS failure happens when the foundation deformation is larger than the predefined allowable or limiting deformation (usually settlement for a drilled shaft). The target probability of failure for service limit states is usually greater than that for ultimate limit states and often lies in the range of 1/15 to 1/150. The reliability index β , on the other hand, is an indirect way of expressing probability of failure, which reflects the number of standard deviations between the mean settlement and the limit condition (Fig. 2.1b). The greater the reliability index, the lower the probability of failure and the safer the design.

For the service limit state, the target probability index is often assigned values ranging from 1.5 (P_f of 0.067) in Eurocode (Orr & Farrell, 1999) to 2.6 (P_f of 0.0047) (Phoon et al., 1995). Huaco et al. (2012) recommended four different values of P_f , ranging from 0.01 to 0.04 for drilled shafts at the service limit state for different bridge categories.

2.6. Alternative Approaches to Service Limit State Design

The service limit state represents when a component of a structure deforms beyond a prescribed amount; for instance, when the settlement of a drilled shaft is larger than an allowable or limiting settlement. The design criterion for the service limit state can be represented by a performance function, g , that reflects the degree to which the criterion is satisfied. The design reaches the service limit state when g is equal to or less than zero. For the service limit state, there are two alternative forms of performance function. The first form of performance function compares displacement with allowable displacement, which is specified as:

$$g = y_a - y = y_a - y(Q) \quad (2.5)$$

where

g = performance function,

y = settlement calculated from design load Q ,

y_a = allowable settlement, and

Q = design load.

The second form compares the design load with a load determined from the allowable displacement:

$$g = Q_{ya} - Q \quad (2.6)$$

where

Q_{ya} = load calculated from given allowable settlement, y_a , and

Q = nominal load.

Which form to use is a choice. Both forms share equal coverage and credibility in the literature (Misra & Roberts, 2006a; Phoon & Kulhawy, 2008). The first form is used in this research.

2.7. Factored Strength versus Factored Resistance

In LRFD, there are two approaches to applying resistance factors to achieve a certain level of probability: 1) the factored *resistance* approach, in which the overall resistance is factored, and; 2) the factored *strength* approach, in which the geomaterial's strength is factored (Becker, 1996). Details of each approach follow.

2.7.1. Factored Resistance Approach

In the factored resistance approach, the resistance factor is applied directly to the overall resistance. This overall resistance factor accounts for all of the uncertainty and variability in the resistance and its use is similar to that of the factor of safety. In using the displacement-based performance function (Equation 2.5) for the service limit

state, the allowable displacement is analogous to resistance for strength limit states. Therefore, the resistance factor can be applied to allowable displacement as follows.

$$y_a * \varphi_y - y \geq 0 \quad (2.7)$$

where

y = settlement calculated from predicted or design load,

y_a = allowable settlement, and

φ_y = resistance factor (which is applied to allowable settlement for use in Equation 2.7).

Within this factored resistance approach, several researchers have used different equations (Honjo et al., 2005; Paikowsky & Lu, 2006) as per the following:

$$y_a - \varphi_d \cdot y \geq 0 \quad (2.8)$$

where φ_d = resistance factor applied to predicted settlement. Note that the resistance factor φ_d in Equation 2.8 is the reciprocal of φ_y in Equation 2.7 ($\varphi_d > 1$ and $\varphi_y < 1$). The principles are very similar. The only difference is the term where the resistance factor is applied.

2.7.1. Factored Strength Approach

The factored strength approach applies the resistance factor to geomaterial strength parameters, which contribute to the overall shaft resistance. The strength parameters can be cohesion, friction angle, uniaxial compressive strength (UCS) or

others. Most of the drilled shaft designs in shales/rocks are based on UCS. In this case, the SLS resistance factor is applied to the UCS to obtain a factored UCS^* for use in SLS design.

$$UCS^* = \varphi * UCS \quad (2.9)$$

where

UCS^* = factored uniaxial compressive strength

φ = resistance factor, and

UCS = uniaxial compressive strength.

Then, a factored displacement is computed at some nominal load Q using the factored uniaxial compressive strength UCS^* and the condition:

$$y_a - y^*_{(UCS^*)} \geq 0 \quad (2.10)$$

is checked, where

$y^*_{(UCS^*)}$ = factored predicted settlement computed using factored strength, and

y_a = allowable or limiting settlement.

Becker (1996) stated that the factored strength approach "Follows the original work of Brinch Hansen and the Danish Code where specified partial factors are applied to the individual soil strength properties of cohesion and internal friction." The approach has been used widely in Europe. However, in North America, the factored resistance approach is often utilized. The factored strength approach has the potential

of being more sophisticated because the resistance factor is related to the types of strength parameters (Becker 1996). The factored strength approach was chosen for use in this research.

2.8. Service Limit State Reliability-Based Design and LRFD Calibration

As discussed in Chapter 1, AASHTO (2007) and Brown et al. (2010) currently recommend a SLS resistance factor of 1.0, which implies that SLS design is treated as deterministic. Recently, probabilistic applications for serviceability limit state design of deep foundations have been studied by some researchers. This research has led to procedures and suggestions for improved design procedures and proposed resistance factors, but only in some specific cases and conditions. Summaries of the more notable efforts are presented below.

2.8.1. Misra and Roberts

Misra and Roberts (Misra & Roberts, 2006a, 2006b; Misra & Roberts, 2009; Roberts et al., 2008; Roberts & Misra, 2010) have described several studies of probability analyses for drilled shafts at serviceability limit states. Misra and Roberts (2006, 2009) adopted factored load criteria (Equation 2.6) in their analyses, and have proposed resistance factors that are multiplied by the shaft resistance at the associated allowable shaft displacement. If the factored resistance is greater than or equal to the nominal load then the SLS design is considered adequate.

$$\varphi * Q_{ya} > Q \quad (2.11)$$

where

Q_{ya} = load calculated from given allowable settlement, y_a , and

Q = nominal load.

The following equation proposed by Baecher and Christian (2003) is used to compute the resistance factor ϕ for a given target reliability index.

$$\phi = \frac{\lambda_R \left(\frac{\gamma_D E(Q_D)}{E(Q_L)} + \gamma_L \right) \sqrt{\frac{1 + \Omega_{QD}^2 + \Omega_{QL}^2}{1 + \Omega_R^2}}}{\left(\lambda_{QD} \frac{E(Q_D)}{E(Q_L)} + \lambda_{QL} \right) e^{\beta_T} \sqrt{\ln[(1 + \Omega_R^2)(1 + \Omega_{QD}^2 + \Omega_{QL}^2)]}} \quad (2.12)$$

λ_R = the bias of the resistance,

$\lambda_{QD}, \lambda_{QL}$ = bias of the dead load and live load,

γ_D, γ = load factor for dead load and live load,

$\Omega_{QD}, \Omega_{QL}, \Omega_R$ = COV of dead load, live load and resistance (capacity),

$E(Q_D), E(Q_L)$ = expected values of dead load and live load, and

β_T = target reliability index.

In the above equation, a bias factor (also known as the model factor) is the ratio of measured or actual quantity over the predicted quantity. A dead load over live load ratio of 2.0 was used, and the reliability index, β , was 2.6. Misra and Roberts (2006, 2009) used the Monte-Carlo simulation method to develop the cumulative distribution histogram for shaft capacity based on allowable settlement. Then the cumulative

distribution histogram of load capacity was used to find the variability, Ω_R , to calibrate the resistance factor.

Misra and Roberts used the t - z method to predict load-displacement behavior with two models of shaft-soil interface interaction for homogenous soil: an elasto-plastic model and a hyperbolic model (Figure 2.5). Figure 2.5 shows the shaft-soil interface load-displacement relationship where K is the shear modulus of shaft-soil interface subgrade reaction; K_i is the initial tangent shear modulus of the shaft-soil interface subgrade reaction; q_o is the yield strength or ultimate (asymptotic) strength of the shaft-soil interface; and u_o is the interface displacement at yield. The two models illustrated in Figure 2.5 were both used in Misra and Roberts' studies.

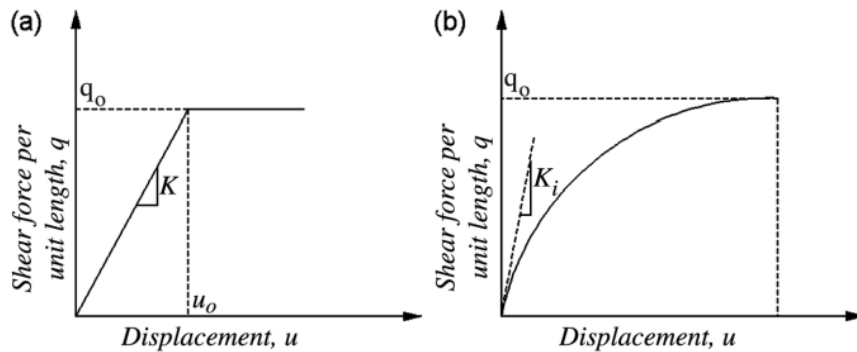


Figure 2.5. Shaft-soil interface load-displacement relationship (a) the ideal elasto-plastic and (b) hyperbolic nonlinear spring-slider system, (Misra and Roberts 2009) .

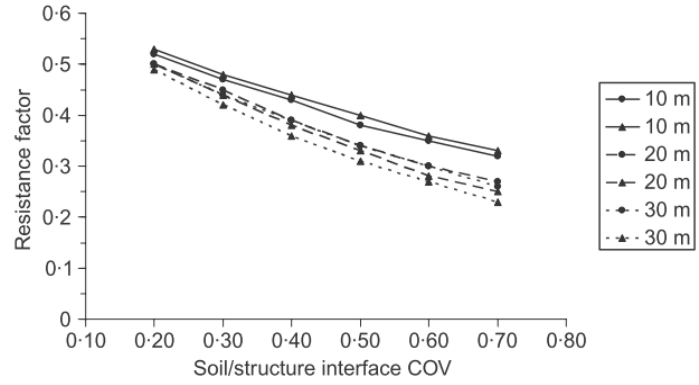
Shaft-soil interface parameters were considered to be probabilistic variables characterized by a lognormal probability distribution function. Misra and Roberts (2009) back-analyzed field test data given by Phoon et al. (1995) to establish mean values for the shaft-soil interface model parameters K , K_i , and q_o . Misra and Roberts (2009)

showed how the COVs of the parameters were “. . . determined to be approximately 0.30 for each parameter. However the COV for each random variable was varied from 0.20 to 0.70 in the simulations.”

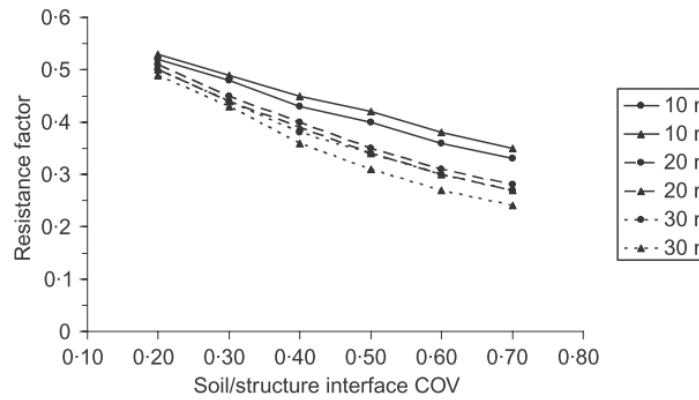
Resistance factors determined by Misra and Roberts are presented in Figure 2.6. Their research considered shaft diameters of 910 mm, 1210 mm and 1520 mm and shaft lengths of 10 m, 20 m and 30 m. There are six curves; the continuous curves are for a shaft length of 10 m, dashed curves are for a shaft length of 20 m, and dotted curves are for a shaft length of 30 m. The symbol “●” is for allowable head displacement of 10 mm, and Δ is for allowable head displacement of 20 mm.

Misra and Roberts found that SLS resistance factors:

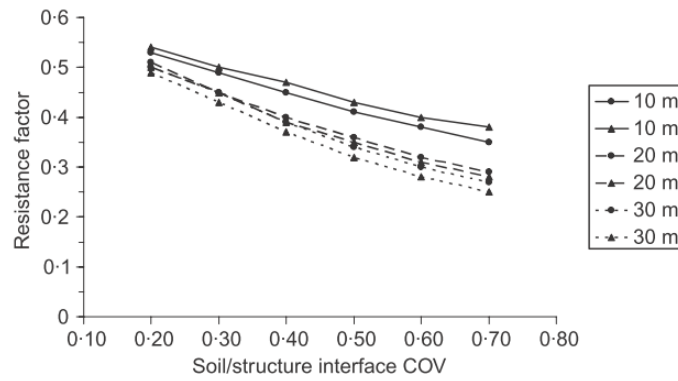
- increase with the diameter of the drilled shaft, albeit not significantly, by about 0.01-0.02 when the diameter increased from 910 mm to 1520 mm;
- decrease with increasing shaft length, by 0.03 when COV of shaft/soil interface is 0.2 and by 0.1 when COV of shaft/soil interface is 0.7;
- decrease substantially when the shaft/soil interface COV increase in a range from 0.20 - 0.25;



(a)



(b)



(c)

Figure 2.6. Service limit state resistance factors versus COV of shaft/soil interface parameters. (From Misra and Roberts, 2009)

(a) Diameter = 910 mm; (b) 1210 mm; (c) 1520 mm; shaft lengths of 10, 20 and 30 m.

- decrease as the nominal values of the shaft/soil interface parameters increase. The amount of change was small and Misra and Roberts (2009) suggested identical values of resistance factors should be used in design (i.e., same resistance factors should be used regardless of the change of nominal values of the shaft/soil interface parameters), and
- depend on allowable drilled shaft head displacement; however, their effects on the allowable displacements (of 10 mm and 20 mm) are negligible.

2.8.2. Zhang and Chu (2009)

Zhang and Chu (2009 a, 2009b) probabilistically analyzed the service limit state for large diameter bored-piles (or drilled shafts) using load-transfer methods based on drilled shaft load test data from Hong Kong. They used the first order reliability method (FORM), considering both estimated settlement and limiting tolerable settlement as lognormally distributed random variables . Their *partial factors* have a function similar to that of a resistance factor, but partial factors are applied for both estimated settlement and limiting tolerable settlement.

The estimated settlement is considered to be a random variable resulting from uncertainty of the load transfer method. The ratio between the measured settlement and the predicted settlement is the bias factor (or model factor) λ_s . The mean value of λ_s and its COV were used to develop partial factors for evaluation of the service limit state.

For the limiting settlement, Zhang and Chu based their conclusions on research conducted by Zhang and Ng (2005), who found that the SLS resistance factor depends on the mean value as well as the COV of limiting settlement. Zhang and Ng compiled data based on the performance of built structures and found the mean and standard deviation of limiting tolerable settlement for deep foundations are 96mm and 56 mm, respectively. These two values of mean and COV of limiting settlement were used by Zhang and Chu (2009 a, 2009 b). The performance function for the service limit state in their study was:

$$g = S_t - \lambda_s S_e R_s T_s = 0 \quad (2.13)$$

where:

S_t = limiting tolerable displacement,

S_e = estimated settlement,

λ_s = model factor,

R_s = group settlement ratio, and

T_s = system settlement ratio,

Zhang and Chu assumed a value of the group settlement ratio $R_s = 1.75$ for drilled shafts, and assumed a system settlement ratio T_s of 1.0. Zhang and Chu used partial resistance factors applied to both the estimated settlement and the limiting tolerable settlement. Accordingly, the proposed design equation for the service limit state is expressed as:

$$\phi_{st} S_t = \phi_{se} \lambda_s S_e R_s T_s \quad (2.14)$$

where

ϕ_{st} = partial factor for limiting tolerable displacement, and

ϕ_{se} = partial factor for estimated settlement.

Zhang and Chu derived the partial factors using a first order reliability method, which used variable transformation to obtain independent standard normal random variables. Zhang and Chu calculated and introduced a table for the partial factors (Table 2.1). The partial factors were proposed for four different reliability indices.

Table 2.1. SLS partial factors for drilled shafts (Zhang and Chu, 2009).

Soil/Rock	Partial factors for limiting settlement				Partial factors for estimated settlement			
	$\beta=2.5$	$\beta=2.0$	$\beta=1.5$	$\beta=1.0$	$\beta=2.5$	$\beta=2.0$	$\beta=1.5$	$\beta=1.0$
Soil	0.28	0.35	0.44	0.55	1.56	1.41	1.27	1.15
Rock	0.26	0.33	0.42	0.54	1.35	1.26	1.18	1.1

All of the above partial factors (or resistance factors) were calibrated at a load of 50% of the shaft capacity. Also note that the resistance factors in the above table were calculated for the case where the mean and standard deviation of the limiting tolerable settlements for deep foundation were 96 mm and 56 mm, respectively. The resistance factors are very specific, i.e., case specific.

2.8.3. Phoon, Kulhawy and Grigoriu (1995)

Phoon et al. (1995) used the load transfer method and a hyperbolic model with its curve fitting parameters obtained from data in their study. Phoon et al. utilized a performance function similar to Equation 2.6, which is based on the comparison of load and allowable load. They used the FORM approach to calculate deformation factors (i.e., SLS resistance factors) for drilled shafts in medium, stiff and very stiff clay with different COV for the undrained shear strength, S_u , as shown in Table 2.2. They found that the deformation factors for drilled shafts in a drained condition depend on the COV of soil strength. Due to the broad range of geotechnical COVs, the resistance factors could not be given a single value to meet the need for the design to achieve a prescribed reliability index. Therefore, the deformation factors were presented in the table depending on the COV of soil strength to achieve a uniform target reliability level, which they chose β^{SLS} to be 2.6.

Table 2.2 Deformation factors for Drilled Shafts under undrained conditions
(Summarized from Phoon, 1995).

Clay	COV of S_u (%)	Deformation factors (SLS resistance factors)
Medium	10-30	0.65
	30-50	0.61
	50-70	0.56
Stiff	10-30	0.64
	30-50	0.59
	50-70	0.52
Very stiff	10-30	0.63
	30-50	0.56
	50-70	0.48

2.8.4. Wang, Au and Kulhawy (2011)

Wang, Au and Kulhawy (2011) offered an expanded approach to assess the reliability of drilled shaft design at the service limit state, called the 'expanded reliability-based design approach' – or RBD^E. This is an approach to perform probabilistic analyses, and Wang et al. (2011) suggest that it be used instead of LRFD. In their approach, they argue that shaft diameter B typically is controlled by auger size, and values of shaft length D are frequently rounded by 0.1 to 0.2 m for construction convenience; hence, B and D were treated as discrete variables. They determined the probability of failure corresponding to the designs of various shaft length and shaft diameter combinations and selected the design based on economic evaluations. Their procedural steps are as follows:

1. Establish the deterministic model for calculating the design loads and capacities of drilled shafts;
2. Model the geotechnical-related uncertainties of loads, geology site interpretations, geotechnical properties, and calculation models. The uncertainties are characterized by probabilistic functions. Numbers of uncertain quantities are *chosen* by the designers;
3. Perform Monte Carlo simulations, count the number of failure cases, and calculate the probability of failure by counting the number of cases failed;
4. Identify a pool of feasible designs, and;
5. Select the final design among the pool based on economic evaluations.

Basically, the RBD^E approach recommends performing probability analysis using a Monte Carlo simulation for each specific design. Wang et al. (2011) stated that this method allows design engineers to adjust the reliability index easily and offers design engineers insights into how the expected design performance level changes as B and D change.

2.8.5. Important Findings and Limitations of Previous Work

There are load transfer models for drilled shafts in clay and sand; however, there are no load transfer models specifically developed for drilled shafts in shales. To utilize the t - z method for drilled shafts in shale, a model must be developed. Furthermore, to account for the variability of the model in reliability analyses, the variability/uncertainty of the model must be quantified.

Three different methods to assess the probability of failure and/or resistance factors for deep foundations at the service limit state have been presented. The resistance factors for drilled shafts at the service limit state were found to depend on a variety of parameters including: nominal load; nominal value of the shaft/soil interface parameter; coefficients of variation of geomaterial strengths; shaft length; shaft diameter; and even allowable settlement. The resistance factors proposed were calibrated for some fixed values of the reliability index, β (Misra and Roberts (2009), Zhang and Chu (2009), Phoon et al. (1995)). This makes it difficult for design engineers to adjust the level of safety during the design process.

The proposed SLS resistance factors from Misra and Roberts (2009) were calibrated for several predetermined shaft lengths and diameters and allowable settlements. For other conditions, the resistance factors should “. . . ideally be computed for each design scenario using site specific data and variability,” (Misra and Roberts, 2009). Similarly, for Zhang and Chu (2009), the resistance factors were calibrated for a fixed value of working load (50 percent of shaft capacity), and a fixed value for allowable settlement (96 mm). All of these restrictions limit the applicability of the proposed methods for routine design.

The more general Expanded Reliability-based design approach proposed by Wang et al. (2011) is flexible enough to accommodate specific needs of a particular project. However, the approach recommends reliability analyses for each specific case.

In summary, no clear design procedure exists for design of drilled shafts at the service limit state. All the methods are restricted to some specific given condition or require design engineers to perform Monte Carlo simulations and probability analyses on a case-by-case basis. Resistance factors for design of drilled shafts at the service limit state, therefore, need to change for different projects with different parameters, e.g., shaft diameter, shaft length, applied load, limiting settlement or reliability index, or even load. This is determined on a case-by-case basis and requires geotechnical engineers to perform intensive probabilistic analyses, which takes extra effort and time that is not often available for many projects.

2.9 Summary

This chapter provides a basic background of load and resistance factor design. Deterministic and probabilistic tools for research on load and resistance factor designs were reviewed. The t - z method and the Monte Carlo simulation approach were selected for this research and are presented in more detail in Chapter 3 and Chapter 4. The current state of the art for load and resistance factor design and reliability-based design at the service limit state was also discussed. The resistance factors that have been proposed were calibrated based on specific design conditions. In other conditions, service limit state design of drilled shaft is recommended to be based on case-by-case analyses for the specific conditions present. This provides the context for subsequent analyses and the findings of this research.

Chapter 3. Deterministic Prediction of Drilled Shaft Settlement

3.1. Introduction

The deterministic prediction of drilled shaft settlement using the load transfer or t - z method is described in this chapter. The finite element method was used in a computer code written using MATLAB®. Details of the finite element implementation of the load transfer method to calculate shaft displacement are described. An actual load test case was modeled as an example of deterministic displacement calculation using the computer code and is presented in this chapter.

3.2. The t - z Method

As briefly discussed in Chapter 2, the load transfer, or t - z method, is a rigorous method used to determine vertical (axial) displacement of drilled shafts. The method is based on nonlinear load transfer curves that usually are obtained from actual load test results. Normalized unit side resistance versus displacement at the shaft-soil interface is modeled using so-called “ t - z curves”, and normalized unit tip resistance versus tip displacement is modeled using “ q - w curves” as illustrated in Figure 3.1.

Inputs for the method include shaft dimensions, shaft stiffness, load transfer models for side resistance along the length of the shaft, a load transfer model for tip resistance at the tip of the shaft, predicted values for ultimate unit side and tip

resistance, and geomaterial strengths. The general process is that a load at the top of the shaft is specified, the program computes the following based on all input parameters: the shaft settlement associated with that load; the displacement of any element along the shaft; and the distribution of stress/load along the length of the shaft (including the load at the shaft tip).

The shaft is divided into a number of elements. Shaft stiffness for each element is represented by the product of shaft cross sectional area, A , and the concrete modulus E , EA . Figure 3.1 is a sketch of the $t-z$ and $q-w$ models. If the shaft is in layered soils/shales, each element may have its own $t-z$ curve to reflect differences in load transfer and the ultimate load in each layer.

For an element, from its vertical displacement, the corresponding mobilized unit side resistance can be obtained using the $t-z$ curve. Similarly for tip resistance, the corresponding mobilized unit tip resistance can be obtained using the $q-w$ curve and the displacement of the tip,. The normalized unit side resistance, or tip resistance (for tip element), is multiplied by the ultimate side or tip resistance and the associated area to obtain the mobilized resistance of the element. The ultimate side resistance and ultimate tip resistance depend on the geomaterial strength (UCS for drilled shafts in shales/rocks, usually) and can also be obtained from load test data. The integral (summation) of the mobilized resistance of all elements is the mobilized shaft resistance.

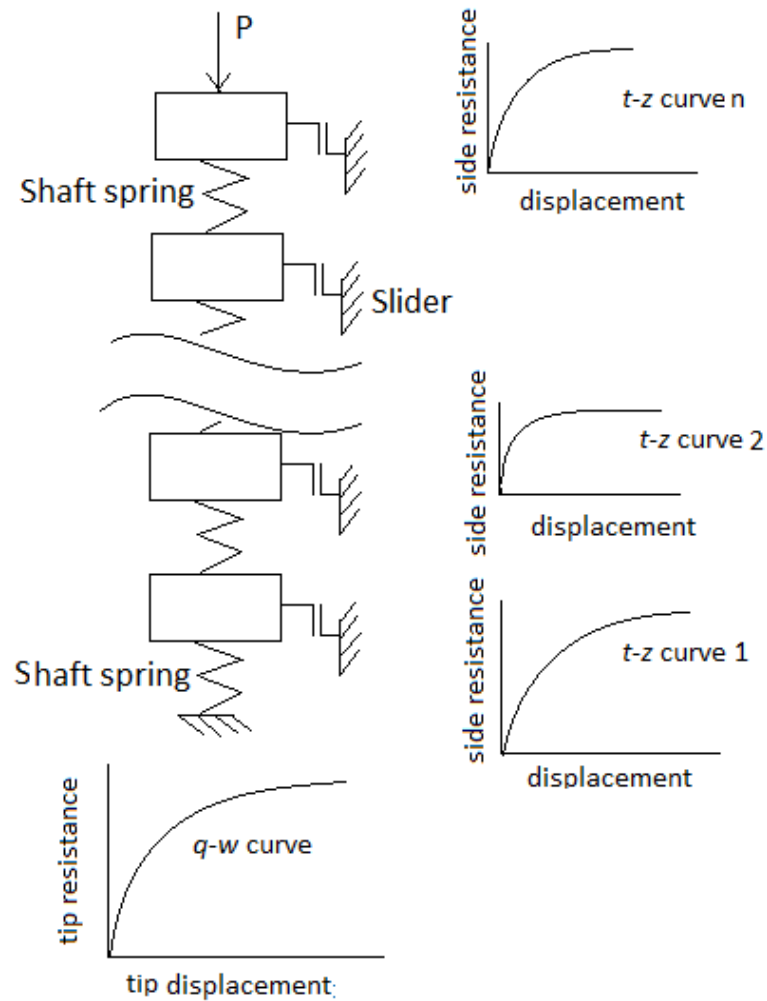


Figure 3.1. The $t-z$ method model and load transfer curves.

The load transfer curves are highly nonlinear, so iterations are needed to solve for shaft head displacement under an applied load. The finite element method and the Newton-Raphson optimization method are utilized to solve the problem. A detailed description of how the finite element method was used is presented in the next section. A computer program using the finite element method was written in MATLAB and is

attached in Appendix A. Details of the basic finite element formulation and the application of the Newton-Raphson approach are as follows.

3.2.1. Finite Element Formulation

A shaft with only an axial load is considered to be a truss problem with a linear shape function. The governing equation for a linear, one-dimensional truss system is (Fish and Belytschko, 2007):

$$\{F\} = [K] * \{U\} \quad (3.1)$$

where

$\{U\}$ = vector of displacements at each node,

$[K]$ = global stiffness matrix, and

$\{F\}$ = vector of forces at each node.

3.2.1.a. Stiffness Matrix

The shaft is sectioned into n elements, and each element is represented by a spring with spring constant k_i and two nodes, i and $i+1$, one at each end of the element. The first element is the one that contains the tip of the shaft. A typical mesh is illustrated in Figure 3.2. The notation adopted is: displacement of the i^{th} node is u_i , and the mobilized side or tip resistance force obtained at that node is $Q_i(u_i)$, as shown in Figure 3.3. For the first node, the mobilized tip resistance force $Q_1(u_1)$ is obtained from the tip resistance $q-w$ curve; for all other nodes, the mobilized side resistance force, $Q_i(u_i)$, is obtained from the respective side resistance $t-z$ curves. The external force

acting at the i^{th} node is called P_i , so the given load on the shaft top is on node $n+1$ and is P_{n+1} .

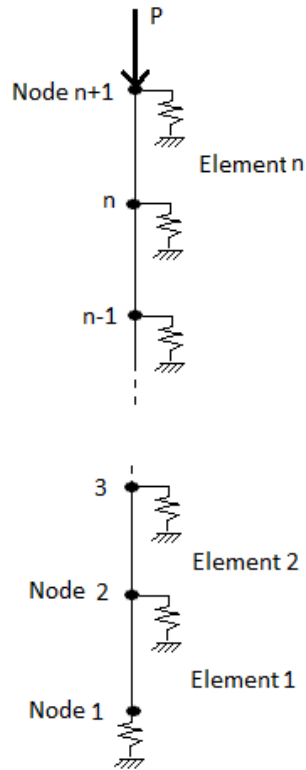


Figure 3.2. Nodes and elements.

The spring constant k_i for element i is given by:

$$k_i = \frac{A_i * E_i}{L_i} \quad (3.2)$$

where

A_i = the cross sectional of the shaft element,

E_i = Young's modulus of the shaft element, and

L_i = the length of the element.

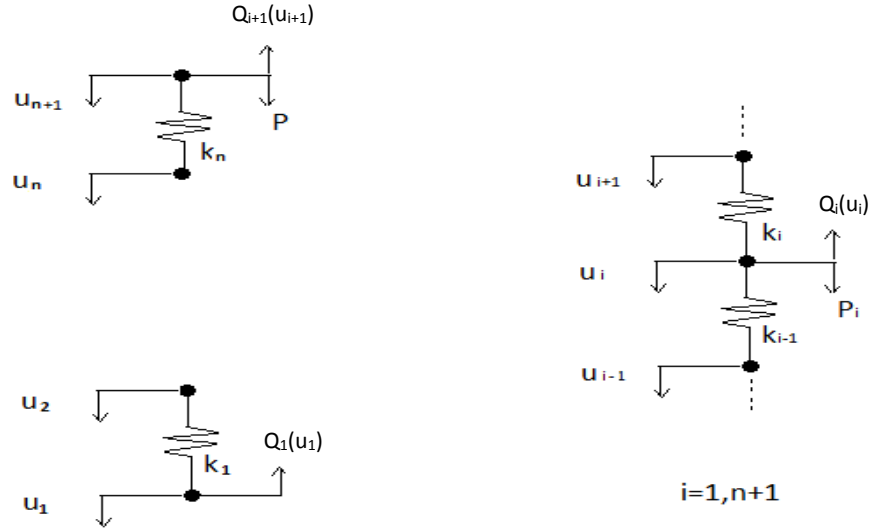


Figure 3.3. Forces and displacements of nodes.

For a truss problem, the element stiffness matrix is:

$$K_i^e = k_i \begin{bmatrix} 1 & -1 \\ -1 & 1 \end{bmatrix} \quad (3.3)$$

For this 1-D problem, the global stiffness matrix is:

$$[K] = \begin{bmatrix} k_1 & -k_1 & 0 & 0 & 0 & 0 & 0 & 0 \\ -k_1 & k_1 + k_2 & -k_2 & 0 & 0 & 0 & 0 & 0 \\ 0 & -k_2 & k_2 + k_3 & -k_3 & 0 & 0 & 0 & 0 \\ 0 & 0 & -k_3 & \cdot & \cdot & 0 & 0 & 0 \\ 0 & 0 & 0 & \cdot & \cdot & -k_{n-2} & 0 & 0 \\ 0 & 0 & 0 & 0 & -k_{n-2} & k_{n-2} + k_{n-1} & -k_{n-1} & 0 \\ 0 & 0 & 0 & 0 & 0 & -k_{n-1} & k_{n-1} + k_n & -k_n \\ 0 & 0 & 0 & 0 & 0 & 0 & -k_n & k_n \end{bmatrix} \quad (3.4)$$

3.2.1.b Force Vector

Consider node i in Figure 3.3, force equilibrium at a node is:

$$F_i = (k_i + k_{i-1})u_i - (k_i)u_{i+1} - (k_{i-1})u_{i-1} - P_i + Q_i(u_i) \quad (3.5)$$

where

F_i = sum of force at node i ,

P_i = external force acting at node i ,

u_i = displacement at node i , and

$Q_i(u_i)$ = mobilized side or tip resistance force.

The force vector of the entire system is:

$$\{F\} = \begin{bmatrix} k_1 u_1 - k_1 u_2 + Q_1(u_1) \\ (k_2 + k_1)u_2 - k_2 u_3 - k_1 u_1 + Q_2(u_2) \\ (k_3 + k_2)u_3 - k_3 u_4 - k_2 u_2 + Q_3(u_3) \\ \vdots \\ (k_i + k_{i-1})u_i - k_i u_{i+1} - k_{i-1} u_{i-1} + Q_i(u_i) \\ \vdots \\ k_n u_{n+1} - k_n u_n + Q_{n+1}(u_{n+1}) - P \end{bmatrix} \quad (3.6)$$

3.2.2. Newton Raphson Approach

The general formulation for dealing with the non-linearity of the load transfer curves when using the t - z method is described in this section. Iteration is required to find the displacement vector, and the Newton Raphson method (Chapra, 2005) is utilized to compute the root of nonlinear equations. Using this method, the displacement vector at the $(l+1)^{th}$ iteration is calculated based on the displacement

vector of iteration number I^{th} . At iteration $(I+1)^{th}$, displacement vector $\{U_{I+1}\}$ is calculated as:

$$\{U_{I+1}\} = \{U_I\} - \frac{\{F(U_I)\}}{J[F(U_I)]} \quad (3.7)$$

where

U_I = displacement vector for I^{th} iteration,

$F(U_I)$ = force vector at I^{th} iteration, and

J = Jacobian of force vector at I^{th} iteration.

Defining the vector $\{X\}$ as the difference between the displacement vectors for two successive iterations, then from Equation 3.7,

$$\{X\} = \{U_I\} - \{U_{I+1}\} = J[F(U_I)]^{-1}\{F(U_I)\}. \quad (3.8)$$

As similar to Equation 3.1,

$$\{F(U_I)\} = [K] * \{U_I\} \quad (3.9)$$

then

$$J[F(U_I)] * \{X\} = [K] * \{U_I\}. \quad (3.10)$$

The force vector's Jacobian is needed to substitute into Equation (3.10) to solve for root $\{X\}$ and displacement vector $\{U\}$. To determine the Jacobian matrix of the force vector, the partial derivative of the force F (Equation 3.6) is taken with respect to each displacement variable:

$$\frac{\partial F_i}{\partial u_i} = k_i + k_{i-1} + \frac{\partial Q_i(u_i)}{\partial u_i} \quad (3.11)$$

$$\frac{\partial F_i}{\partial u_{i-1}} = -k_{i-1} \quad (3.12)$$

$$\frac{\partial F_i}{\partial u_{i+1}} = -k_i. \quad (3.13)$$

Substitute Equations 3.11 through 3.13 into 3.6, the Jacobian matrix of force vector becomes

$$\{U\} = \begin{bmatrix} k_1 + Q'_1(u_1) & -k_1 & 0 & 0 & 0 & 0 \\ -k_1 & k_1 + k_2 + Q'_2(u_2) & -k_2 & 0 & 0 & 0 \\ 0 & -k_2 & \cdot & \cdot & 0 & 0 \\ 0 & 0 & \cdot & \cdot & -k_{n-1} & 0 \\ 0 & 0 & 0 & -k_{n-1} & k_{n-1} + k_n + Q'_n(u_n) & -k_n \\ 0 & 0 & 0 & 0 & -k_n & k_n + Q'_{n+1}(u_{n+1}) \end{bmatrix} \quad (3.14)$$

The next step is finding partial derivatives of the mobilized side resistance force on the Jacobian matrix of the force vector. The mobilized side resistance force at node i is the sum of one half of the side resistance for element i and one half of the side resistance for element $i+1$. The mobilized side resistance along a shaft element is the product of the normalized unit side resistance, the ultimate unit side resistance, and the shear area of the element. The normalized unit side resistance obtained from the load transfer t - z curve is associated with the displacement of the node. The value of the ultimate unit side resistance is obtained from a predictive model as a function of the geomaterial strength. The mobilized side resistance force for node i can be calculated as:

$$Q_i(u_i) = A_{S_i} * t_i(u_i) * t_{ult} \quad (3.15)$$

Where

$Q_i(u_i)$ = normalized side resistance associated with displacement u_i ,

A_s = the shear area of an element, which is equal to the circumference of the shaft times the length of the element,

$t_i(u_i)$ = normalized unit side resistance associated with displacement u_i , and

t_{ult} = the ultimate unit side resistance.

Taking the partial derivative with respect to u_i gives

$$\frac{\partial Q_i(u_i)}{\partial u_i} = A_{S_i} * t_{ult} * \frac{\partial t_i(u_i)}{\partial u_i} \quad (3.16)$$

The normalized unit side resistance t_i at displacement u_i is determined from an appropriate t - z model. If the t - z model is taken to have hyperbolic form (Chapter 5), the normalized unit side resistance is:

$$t_i(u_i) = \frac{u_i}{a_t * u_i + b_t} \quad (3.17)$$

where with a_t and b_t are fitting coefficients for the t - z curve. Taking the derivative with respect to u_i yields

$$\frac{\partial t_i(u_i)}{\partial u_i} = \frac{b_t}{(a_t * u_i + b_t)^2} \quad (3.18)$$

so

$$Q'_i(u_i) = \frac{\partial Q'_i(u_i)}{\partial u_i} = A_{S_i} * t_{ult} * \frac{b_t}{(a_t * u_i + b_t)^2} \quad (3.19)$$

For the first node with $i = 1$, the external mobilized force acting at the node is the tip resistance force, which is the product of the normalized unit tip resistance, the ultimate unit tip resistance, and tip area of the shaft. The normalized unit tip resistance obtained from the load transfer $q-w$ curve, is associated with the displacement of the shaft tip. The value of the ultimate unit tip resistance is obtained from a predictive model as a function of the geomaterial strength. The mobilized tip resistance force for node 1 can then be calculated as:

$$Q_1(u_1) = A_B * q(u_1) * q_{ult} \quad (3.20)$$

where

A_B = cross section area of the shaft tip,

$q_1(u_1)$ = normalized unit tip resistance obtained from $q-w$ curve, and

q_{ult} = the maximum or ultimate unit tip resistance.

Taking the partial derivative with respect to u_1 yields

$$\frac{\partial Q_1(u_1)}{\partial u_1} = A_B * q_{ult} * \frac{\partial q(u_1)}{\partial u_1} . \quad (3.21)$$

The normalized unit tip resistance $q_1(u_1)$ at displacement u_1 is determined from $q-w$ curve, which also has a hyperbolic form:

$$q_1(u_1) = \frac{u_1}{a_q * u_1 + b_q} \quad (3.22)$$

where a_q and b_q are fitting coefficients for $q-w$ curve. Taking the derivative with respect to u_1 yields

$$\frac{\partial Q_1(u_1)}{\partial u_1} = \frac{b_q}{(a_q * u_1 + b_q)^2} \quad (3.23)$$

so that

$$Q'_1(u_1) = \frac{\partial Q_1(u_1)}{\partial u_1} = A_B * q_{ult} * \frac{b_q}{(a_q * u_1 + b_q)^2} \cdot \quad (3.24)$$

Substituting $Q'_i(u_i)$ found in Equations 3.19 and 3.24 into Equation 3.14, the Jacobian matrix of F is obtained. The stiffness matrix, force vector and Jacobian are then substituted back into Equation 3.6 to solve for the root $\{X\}$, where $\{X\}$ is the difference of displacement vector $\{U\}$ at iteration $l+1$ and the previous iteration l . The process is carried out until the differences in values of the two consecutive iterations are less than a predetermined precision value, which was chosen to be 10^{-4} inches. The last displacement vector represents the displacements of nodes along the shaft under the applied load.

3.3. Modeling an Actual Case for Code Checking

Test shaft F7 at the Frankford site (Chapter 5) was chosen as an example application for the deterministic calculation of shaft performance. The shaft has a diameter of 3.2 ft., and length of 34.7 ft.; other shaft parameters are presented in Table 3.1. A sketch of the shaft with the shale layers and the position of the O-Cell and strain gauges is shown in Figure 3.4. The measured mobilized unit side and tip resistance curves are presented in Figures 3.5 and 3.6.

Table 3.1. Input parameters for Shaft F7.

Shaft diameter (as constructed)	38.4 (inches)
Length(as constructed)	34.7 (ft.)
Concrete strength at testing	4271 (psi)
Area of Steel	20.3 (in ²)
Concrete Young's modulus	3725 (ksi)

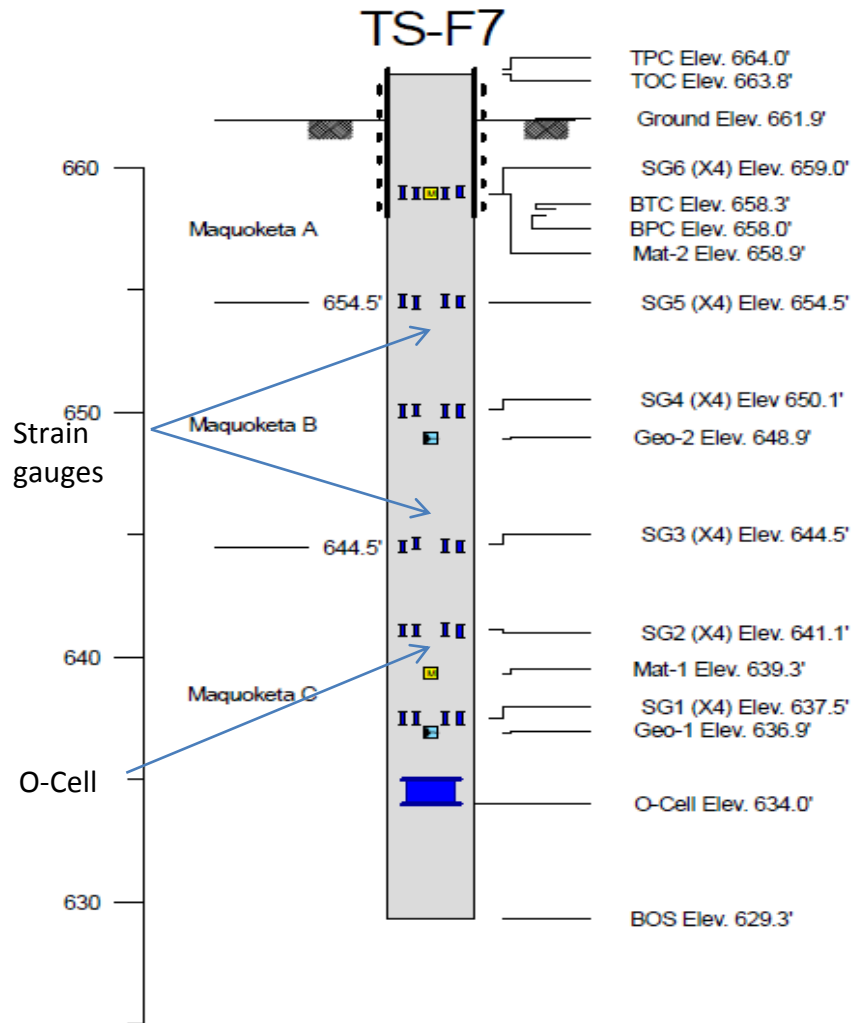


Figure 3.4. Shaft F7 (Frankford, MO) with O-Cell and strain gages.

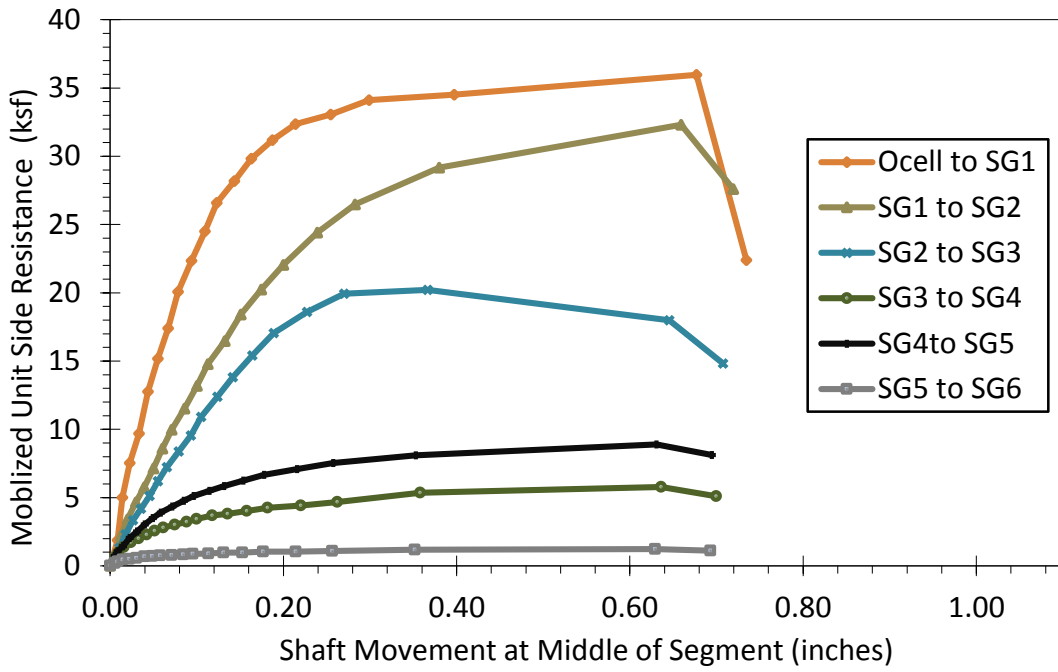


Figure 3.5. Mobilized unit side resistance versus displacement of shear zone.

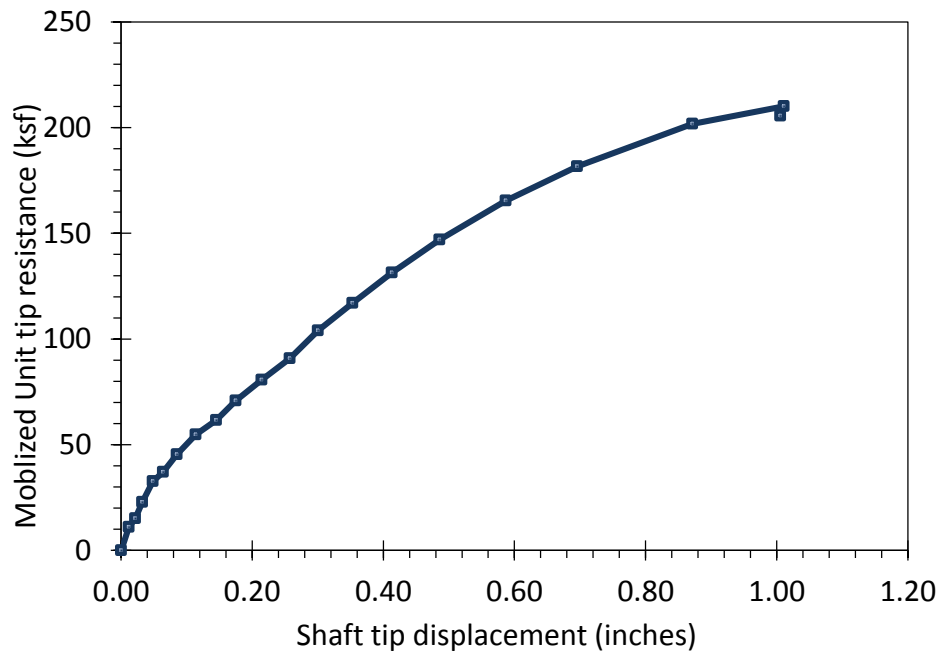


Figure 3.6. Mobilized unit tip resistance versus displacement of shaft tip.

Input to the program also requires determining the unit side resistance versus displacement relationship, the t - z curve, and the unit tip resistance versus displacement relationship, the q - w curve - all derived from the load test. For this example, the subsoil is considered as one layer, with t - z and q - w curves obtained from regression analysis on data shown on Figures 3.4 and 3.5. The following function is obtained from regression analysis for t - z curve of Shaft F7:

$$t = \frac{z}{0.86*z+0.096} \quad (3.25)$$

Similarly, for tip resistance, the q - w function is:

$$q = \frac{w}{0.588*w+0.408} \quad (3.26)$$

These models were used in the computer code to develop a predicted load-settlement curve. The load-displacement curves from load test data are presented in Figure 3.7. Two curves are shown: a “measured” curve and a measured curve “adjusted for shaft elastic compression”. For comparison, the digitized measured curves from LoadTest® are imposed with the calculated load-displacement curve, as shown in Figure 3.7.

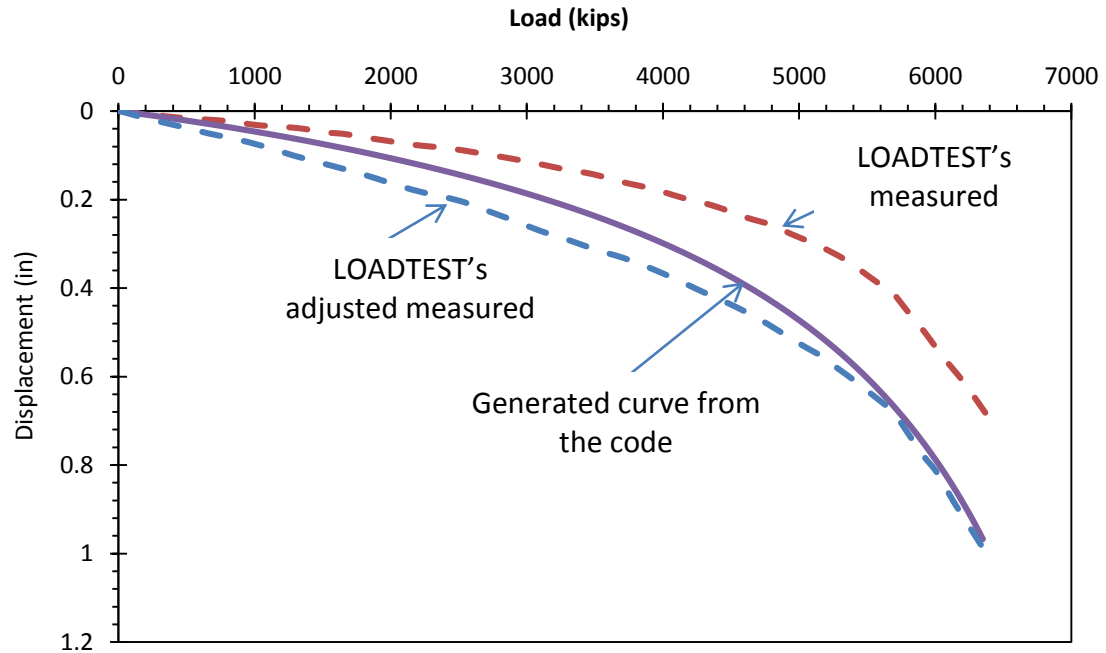


Figure 3.7. Load-displacement curves for Shaft F7 (Frankford, MO).

The calculated curve lies between the measured curve and the adjusted measured curve. At larger loads (>5500 kips), the predicted curve is almost coincident with the adjusted measured curve.

3.4. Summary

The basics of the t - z method to calculate deterministic shaft displacement are described in this chapter. The chapter also presents utilization of the t - z method with the finite element method and describes how the Newton-Raphson approach is used to calculate the distribution of load and displacement within the shaft. An example was presented to illustrate how the deterministic calculation can be solved using the computer code. The computer code is used in both probabilistic analyses and in the calibration process discussed subsequently in Chapters 7 and 8.

Chapter 4. Probabilistic Prediction of Drilled Shaft Settlement

This chapter describes a method used for probabilistic prediction of settlement for drilled shafts. A detailed description of the Monte Carlo simulation method, which is an important probabilistic tool used in this research, is also provided.

4.1. Input Parameters for Probabilistic Analysis of SLS

For service limit state (SLS) design based on the t - z method, there are total of 24 deterministic and probabilistic variables as inputs, not including type of probabilistic distribution. The shaft length and the probability of failure are the only variables that are considered deterministic. All 24 variables (22 probabilistic and two deterministic) are listed below:

- a) Geomaterial strength and its variability /uncertainty, represented by its coefficient of variation (two variables);
- b) Dead load and its variability /uncertainty (two variables);
- c) Live load and its variability /uncertainty (two variables);
- d) Shaft length, considered deterministic (one variable);
- e) Shaft diameter and its variability /uncertainty (two variables);

- f) Concrete Young's modulus and its variability /uncertainty (two variables);
- g) Probability of failure, considered deterministic (one variable);
- h) t - z and q - w fitting parameters (four variables for two pairs of fitting parameters) and their standard deviations (two variables), and;
- i) Ultimate unit side resistance (two variables for two parameters), ultimate unit tip resistance (two variables for two parameters) and their coefficients of variation (two more variables).

4.2. Monte Carlo Simulation

As briefly described in Chapter 2, inputs for a Monte Carlo simulation of a problem include the variable's mean value, coefficient of variation (COV) or standard deviation, and its distribution type. From the inputs, Monte Carlo simulation uses random number simulations to establish the probability density function of parameter values. The process is carried out to obtain a probability density function for every probabilistic variable, which are then input into the deterministic model to obtain a probability density function for the problem of interest.

Figure 4.1 illustrates how the Monte Carlo simulation approach is used to create an output probability density function. To the figure's left are deterministic and probabilistic input variables in the form of a probability density function. All 24 listed parameters introduced at the beginning of this chapter are utilized when using Monte

Carlo simulation to generate the probability density function of the output (in service limit state (SLS) design, it is a shaft head vertical displacement under a load). For one simulation, one value is taken from the probability density function of each probabilistic parameter, and then, along with the other deterministic variable values, all values are put into a load-transfer model to calculate one value of shaft head vertical displacement. The process is repeated n times, or n simulations are performed to obtain the shaft head displacement probability density function.

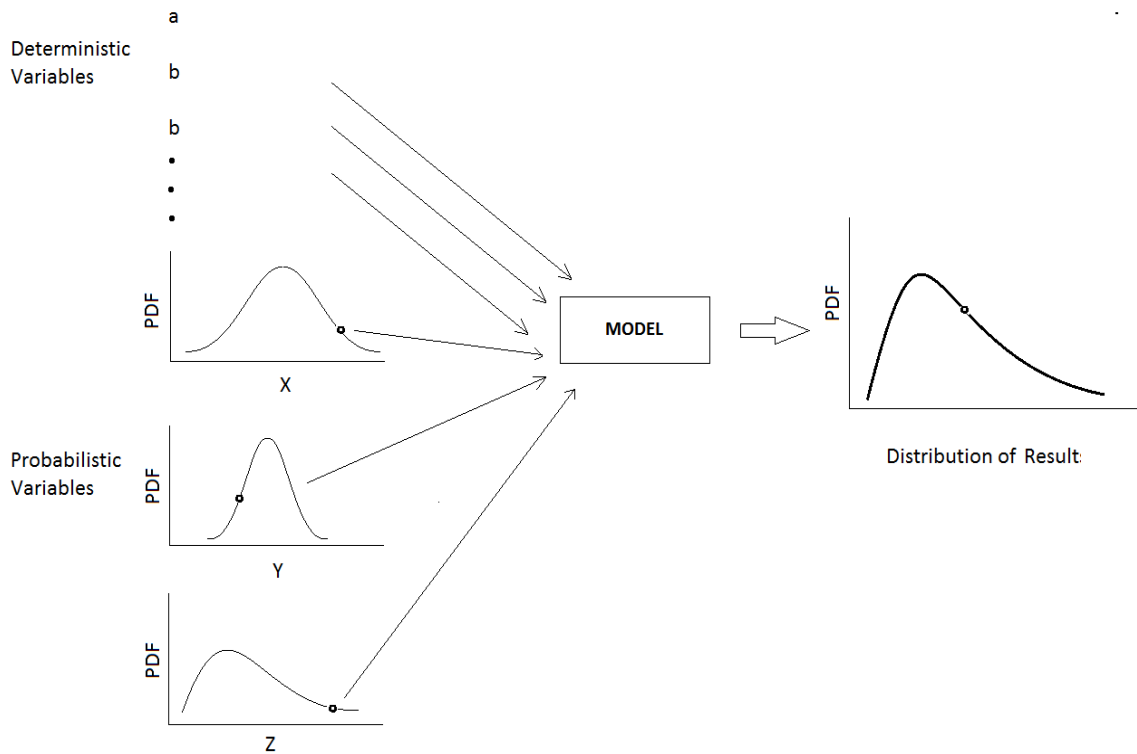


Figure 4.1. Schematic of Monte Carlo Simulation.

4.2.1. Number of Simulations

The Monte Carlo simulation method is an approximate method. The accuracy of Monte Carlo analyses is largely dictated by the number of simulations that are performed. Thus, one important aspect of a Monte Carlo analysis is establishing the number of simulations needed to accurately determine the probabilistic distribution of an output parameter.

The accuracy approaches a true solution as the number of simulations increases. Allen et al. (2005) stated that 5,000 to 10,000 simulations or more are needed to adequately define the distribution of the limit state function (Section 2.2) for a probability index of $\beta_T=2.3$ to 3.0, which is greater than is usually required for SLS. Harr (1987) used the binominal distribution function (number of success trials in total trials) and reliability theory to show that if it is desired that “the Monte Carlo simulation not to differ by more than 1% from the estimated value with 99% confidence”, 16,641 trials would be required

To establish an adequate number of simulations for the specifics of this research, two different sample cases were analyzed with different numbers of simulations. The examples were set up to determine an SLS resistance factor, which is an indirect measure related to the reliability or probability of failure (Chapter 2). The input parameters for the sample cases are given in Table 4.1.

The resulting resistance factors are plotted in Figure 4.2. The resistance factors are almost identical when the number of simulations exceeds 5000. In this research, in

order to be confident with reasonable accuracy, and to account for possible different input variability sources, the number of simulations chosen was 30,000.

Table 4.1. Input Parameters for Sample Cases.

Parameters	Sample Case 1		Sample Case 2	
	Mean	COV	Mean	COV
UCS	20 ksf	0	35 ksf	0.25
Dead load	1000 kips	0.1	2500 kips	0.1
Live load	500	0.12	1250 kips	0.12
Shaft length	30 ft.	Deterministic	45 ft.	Deterministic
Shaft diameter	3 ft.	0.15	5 ft.	0.15
Concrete Young's modulus	30,000 ksi		30,000 ksi	
Probability of failure	1/25	Deterministic	1/100	Deterministic
<i>t-z</i> fitting parameters	1.071 and 0.13	0	1.071 and 0.13	0.172
<i>q-w</i> fitting parameters	1.098 and 0.721	0	1.098 and 0.721	0.14
Unit side prediction parameters	0.76 and 0.79	0	0.76 and 0.79	0.26
Unit tip prediction parameters	14.0 and 0.71	0	14.0 and 0.71	0.254

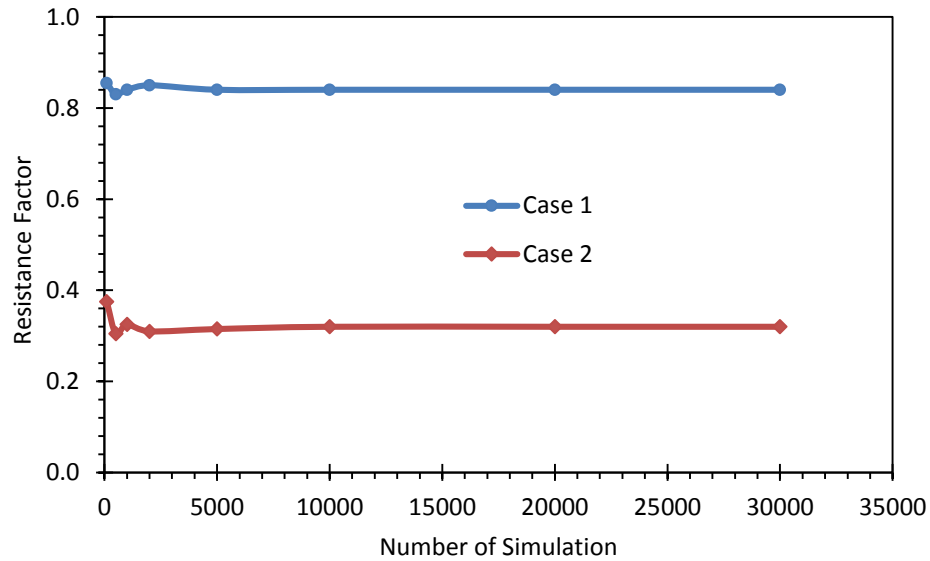


Figure 4.2. Resistance factor versus number of Monte Carlo Simulations.

4.2.2. Random Number Generation of Variables

An important consideration in probability analyses is the type of distribution used to represent variability and uncertainty in the input parameters. In geotechnical engineering, the most frequently used distribution types for probabilistic variables are the normal and log-normal distributions (Phoon and Kulhawy, 1999; Duncan, 2000; Baecher and Christian, 2003; Allen et al., 2005).

The appeal of the normal distribution are that it is mathematically convenient, it accurately reflects many measurements, and it is commonly used in practice. The normal distribution is bell-shaped (Figure 4.3). However, the normal distribution often includes some negative values which are impractical and unacceptable for many SLS design problems, e.g., it is not appropriate for strength or stiffness parameters to be negative. In some cases, when the number of negative values is relatively small (e.g.,

when the distribution is narrow, or the mean is quite large), the normal distribution can be used effectively, and it often is a reasonable representation of variability and uncertainty. However, when the number of negative values is larger, it poses challenges and may not appropriately reflect the variability and uncertainty of many parameters. This is true despite its popularity for random number generation.

The log-normal distribution type reflects data where the natural logarithms of the data are normally distributed. The shape of the distribution is an eccentric bell with a much longer tail (Figure 4.3). This type of distribution is strictly non-negative, and thus is frequently used in practice to represent values that should be non-negative.

In general, the choice of whether to use a normal or a lognormal distribution depends upon which is a better reflection of the variability and uncertainty for the respective parameters. In later probabilistic analyses, the types of distributions for the input variables are chosen based on field test data, or taken from well-established literature.

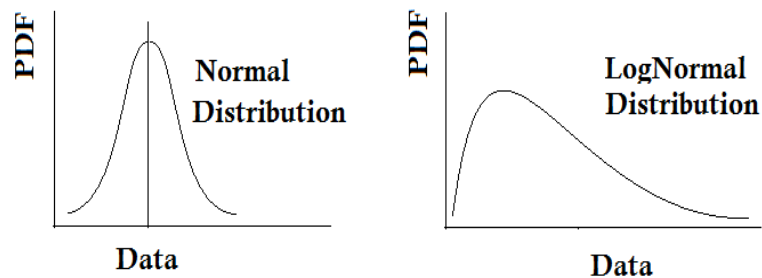


Figure 4.3. Normal (left) and lognormal distributions (right).

4.2.2.a. Generation of Normally Distributed Parameter Values

If the mean, standard deviation, and distribution type of a parameter are known, the Monte Carlo approach is able to simulate n numbers of random parameter values that have the same mean, standard deviation and distribution type. In MATLAB®, for a variable that is normally distributed with mean μ and standard deviation σ , a random parameter value set from n simulations can be produced using the following equation:

$$X = \mu + \sigma * randn(1, n) \quad (4.1)$$

where *randn* is a command to generate an array of n random numbers that have standard normal distribution with mean of zero and standard deviation of unity.

If the data are highly variable and the standard deviation σ is large, it is possible for the process to produce negative values that are non-real. The negative values must be removed from the population. In this research, generated negative values are replaced with positive, near-zero values (10^{-6} for all cases), and the calculation process is continued. This approach is more beneficial than to assume a lognormal distribution, even though the data show normal distribution characteristics as is sometimes used in literature.

4.2.2.b Generation of Lognormally Distributed Parameter Values

In order to generate a set of variables L (i.e., Lognormal) which is lognormally distributed with mean μ and standard deviation σ , a transformation step must be

performed. The logarithm of the variable L is $N = \ln(L)$. N is a normally distributed variable with mean λ and standard deviation ξ .

The relationships between mean λ and standard deviation ξ of variables L and mean μ and standard deviation σ of the normally distributed variable N are:

$$\xi = \sqrt{\ln\left(1 + \frac{\sigma^2}{\mu^2}\right)} \quad (4.2)$$

$$\lambda = \ln\mu - \frac{\xi^2}{2} \quad (4.3)$$

The variable N can be generated using following function:

$$N = \lambda + \xi * randn(1, n) \quad (4.4)$$

The final step to obtain the data set L is by taking the exponential of the values in N :

$$L = e^N \quad (4.5)$$

In this research, these procedures are executed in MATLAB®. The generated parameter values were used in the Monte-Carlo and probabilistic analyses.

4.3. Summary

This chapter describes the input parameters for a probabilistic analysis of the service limit state. The chapter also describes Monte Carlo simulation and the procedure of generating random parameter values for such simulations. The critical inputs for probabilistic analyses at the service limit state are the load transfer models and their variabilities, which are addressed in Chapters 5 and 6.

Chapter 5. Interpretation of Load Transfer from Field Load Tests

Twenty-five load tests were conducted on full-scale drilled shafts in the state of Missouri. Data from the load tests were analyzed and used to develop load transfer relationships. This chapter covers the details of the drilled shaft load test program, the process of interpreting data and the development of normalized load transfer curves.

5.1. Drilled Shaft Load Test Program

Twenty-five drilled shafts were constructed and load tested at two sites in Frankford and Warrensburg, Missouri. The site conditions, test shaft instrumentation and testing procedures are described in this section.

5.1.1. Site Conditions and Soil/Rock Properties

Locations for the two sites are shown in Figure 5.1. One site is referred to as the “Frankford Load Test Site” and the other as the “Warrensburg Load Test Site.” Ten shafts were constructed and tested at the Frankford site, and fifteen at the Warrensburg site. Ground conditions and the geomaterials strength, i.e., the uniaxial compressive strength (UCS), are described as follows.

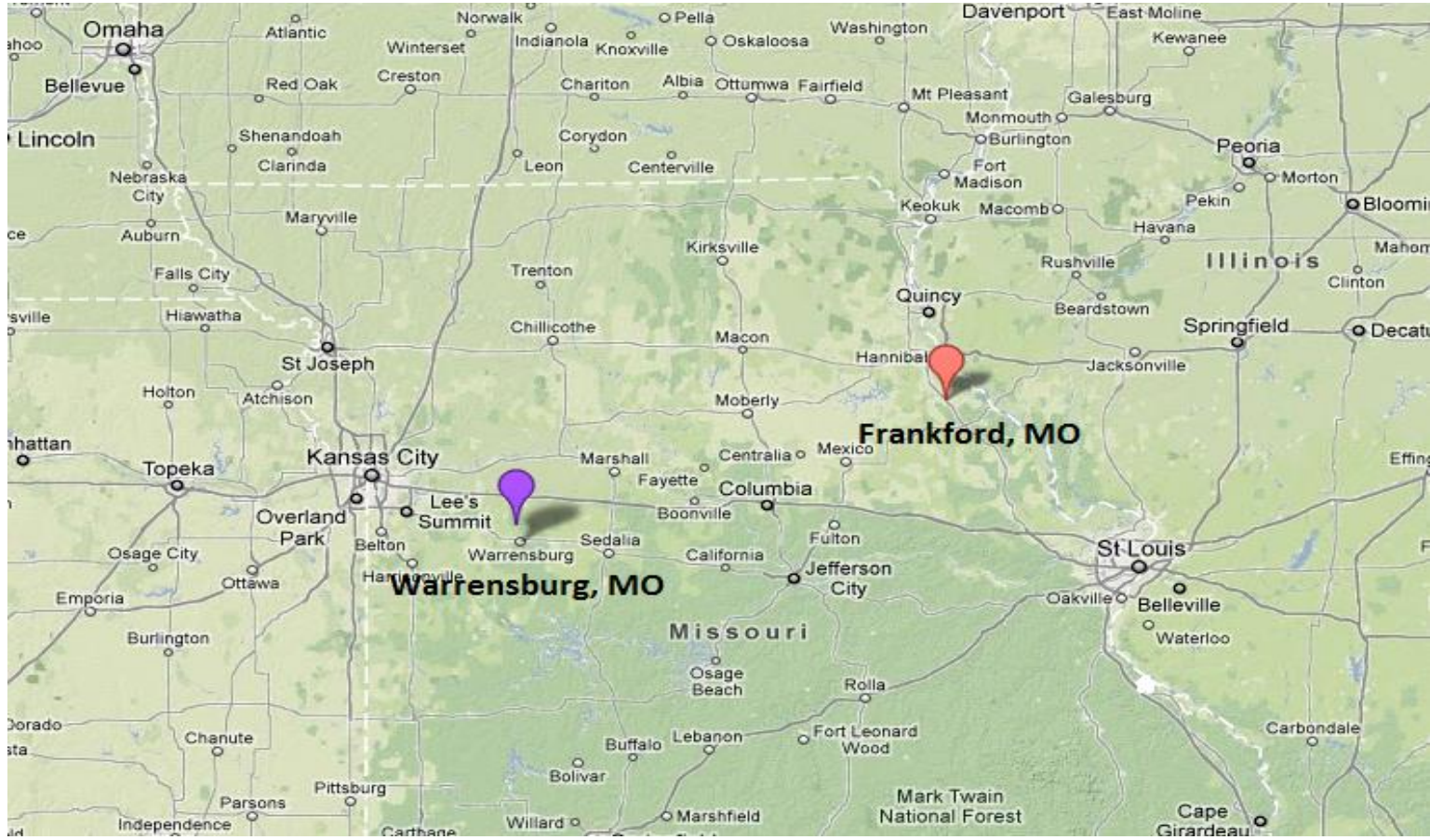


Figure 5.1. Drilled shaft test sites in Missouri.

5.1.1.a. Frankford site condition

Ground conditions at the Frankford site are generally uniform, including three strata from a single formation with different strengths and varying degrees of weathering as illustrated in Figure 5.2. Ten shafts in the Frankford site were arranged in a line, as shown in Figures 5.3 and 5.4.

The thicknesses of the weathered stratum increase to the south of the site as shown in Figure 5.3. The Frankford site is a relatively uniform site, with three layers of shale strata: Maquoketa Formations A, B and C.

Measured uniaxial compressive strengths (UCS) from the Frankford site are shown in Figures 5.2 and 5.5. The weathered shales, designated as Maquoketa Formations A and B, have uniaxial compressive strengths ranging from 3 to 10 ksf, and the unweathered shale, Maquoketa Formation C, has UCS ranging from 50 to 100 ksf. The standard deviation of UCS values in each stratum range from 1.31 to 240.7 ksf. Table 5.1 summarizes the mean value, standard deviation, and distribution type for UCS within each stratigraphic layer at the Frankford site.

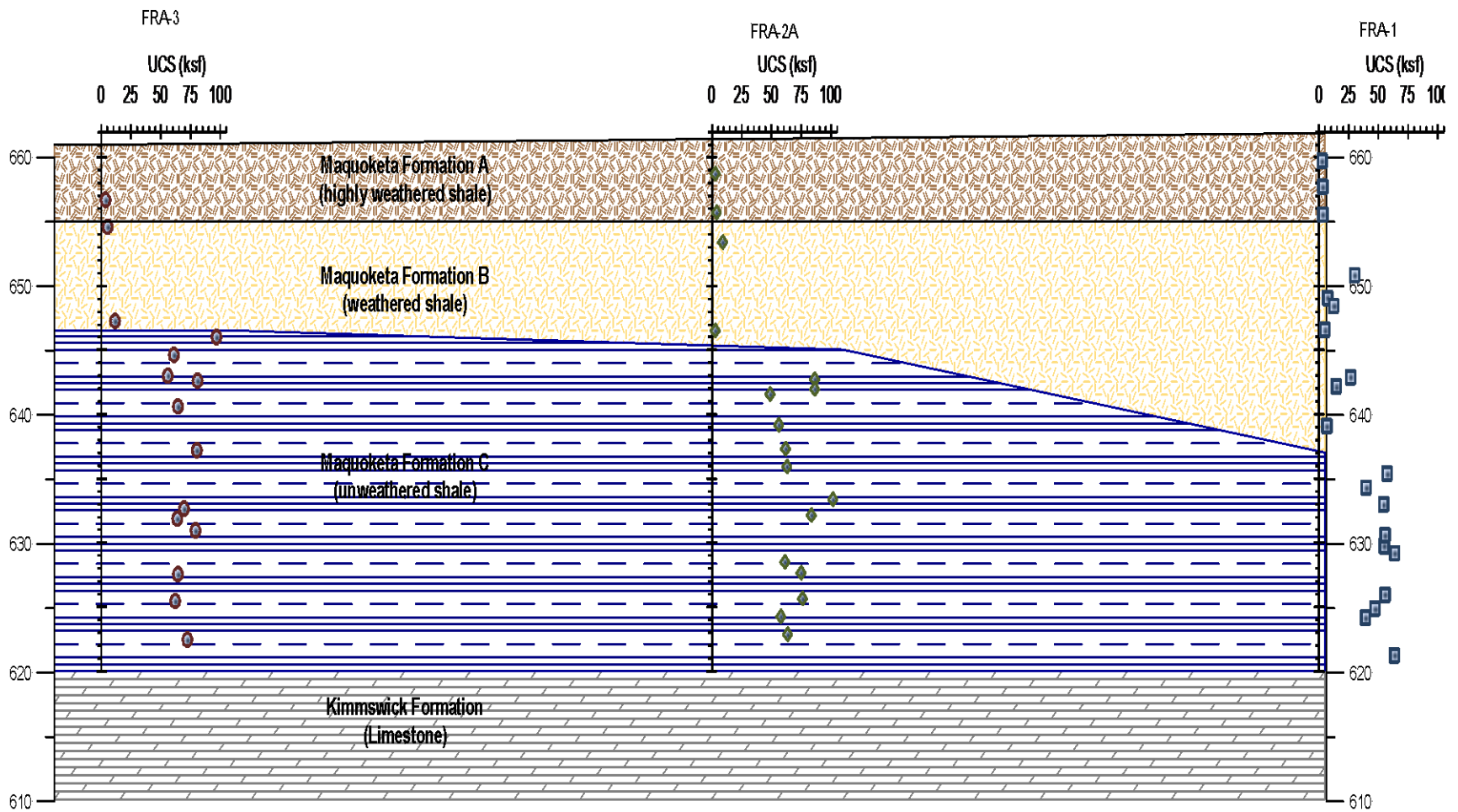


Figure 5.2. Cross-section of the Frankford Load Test Site showing measured uniaxial compressive strengths.

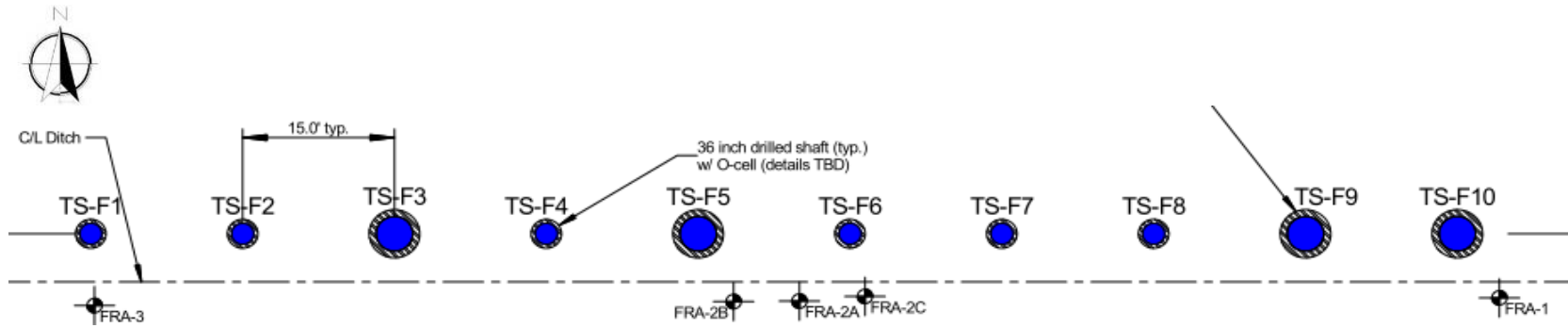


Figure 5.3. Layout of test shafts at the Frankford site.

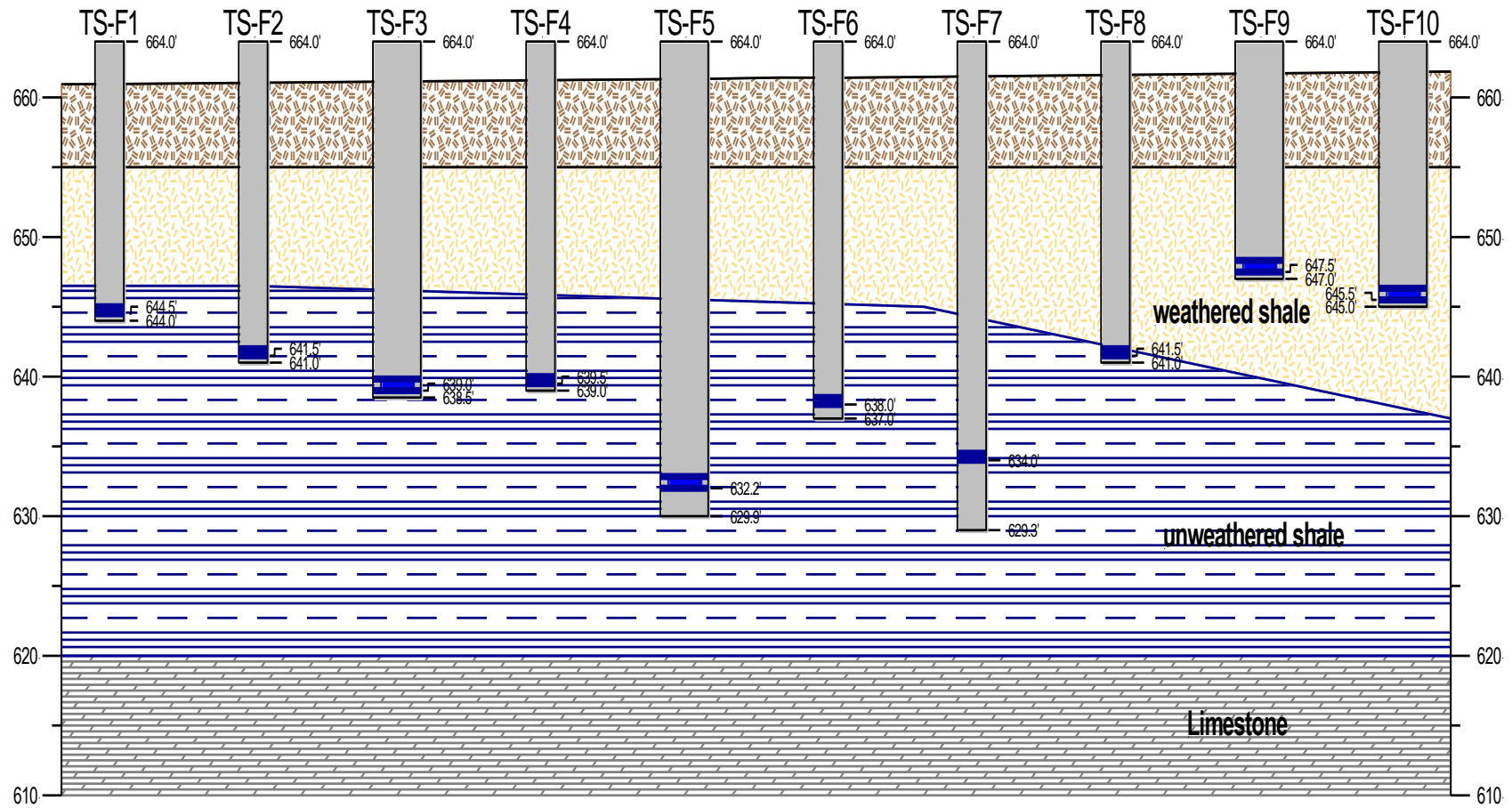


Figure 5.4. Cross-section of the Frankford Load Test Site showing the drilled shafts.

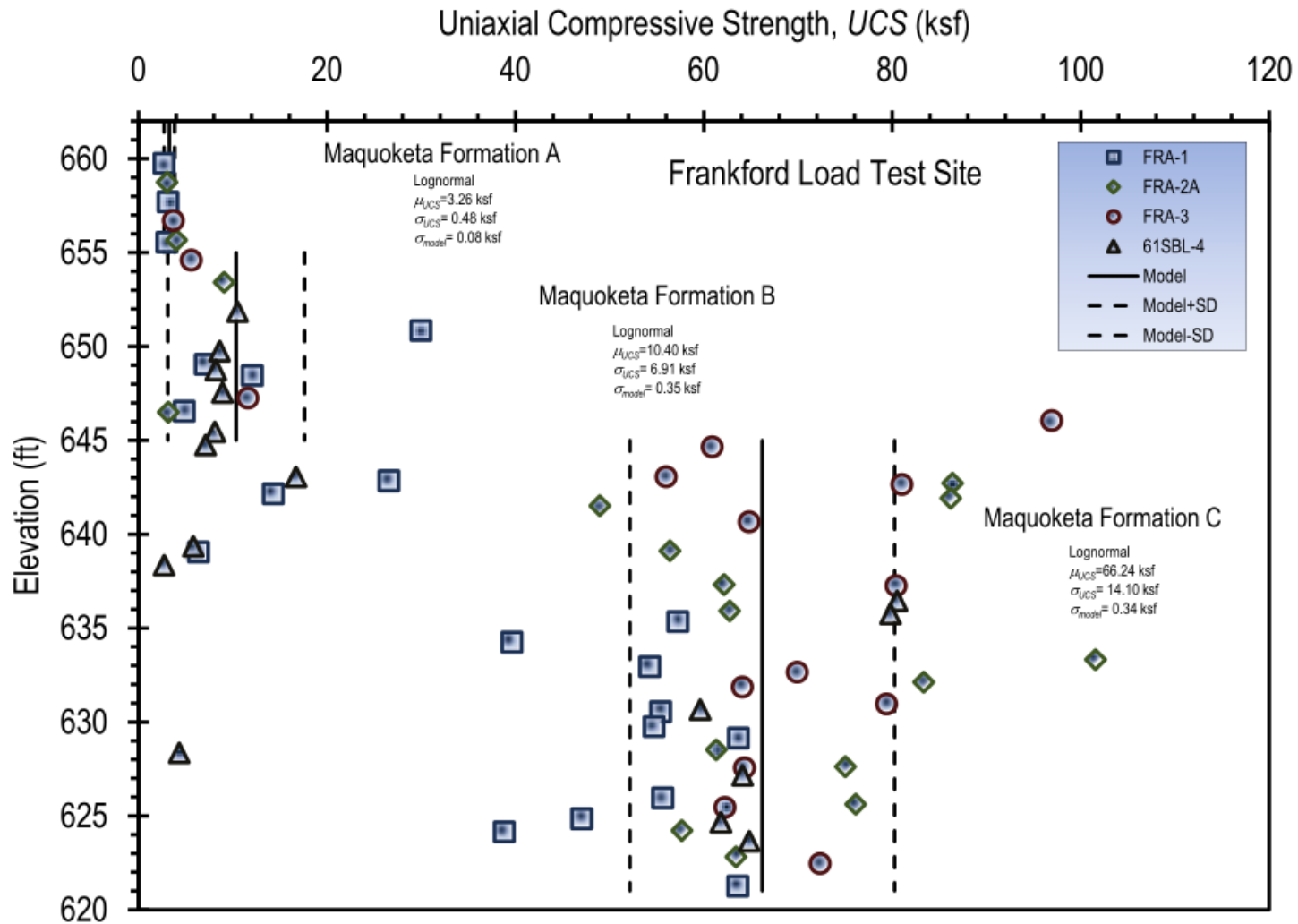


Figure 5.5. Measured uniaxial compressive strengths at the Frankford site.

Table 5.1. Uniaxial compressive strength statistics for the Frankford site.

Frankford Site	UCS Statistics		
	Mean (ksf)	Standard deviation (ksf)	Distribution type
Maquoketa Formation A	3.26	0.48	Lognormal
Maquoketa Formation B	10.4	6.91	Lognormal
Maquoketa Formation C	66.25	14.1	Lognormal

5.1.1.b. Warrensburg site condition

The Warrensburg site is composed of five to seven layers of different soils and shales, including a silty clay soil overburden overlying variable soft and hard shales as well as interbedded shales with some sandstone (Figure 5.6). The fifteen shafts at the Warrensburg site were constructed in a triangular arrangement, as shown in Figures 5.7 and 5.8.

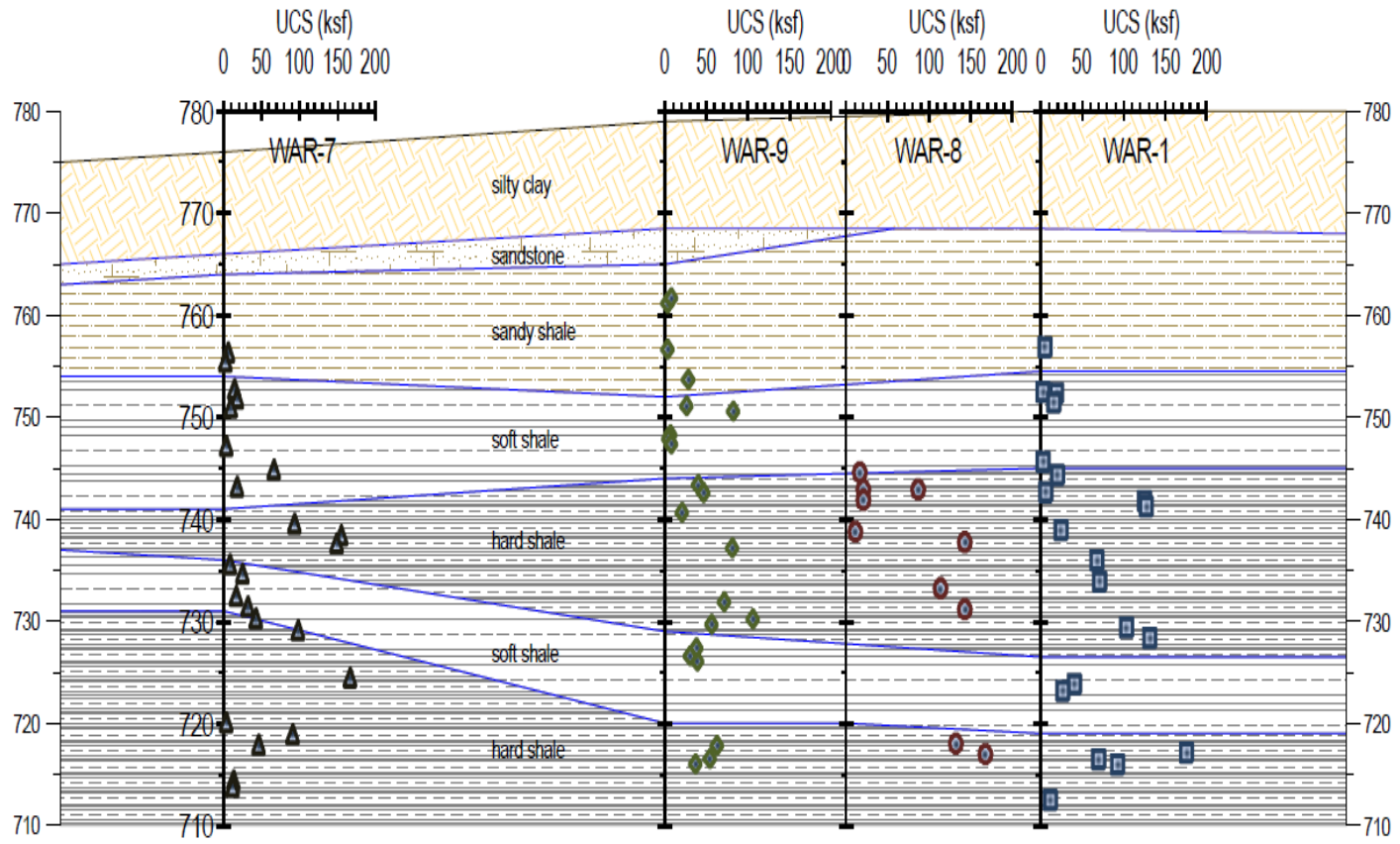


Figure 5.6. Cross-section of the Warrensburg Load Test Site showing measured uniaxial compressive strengths.

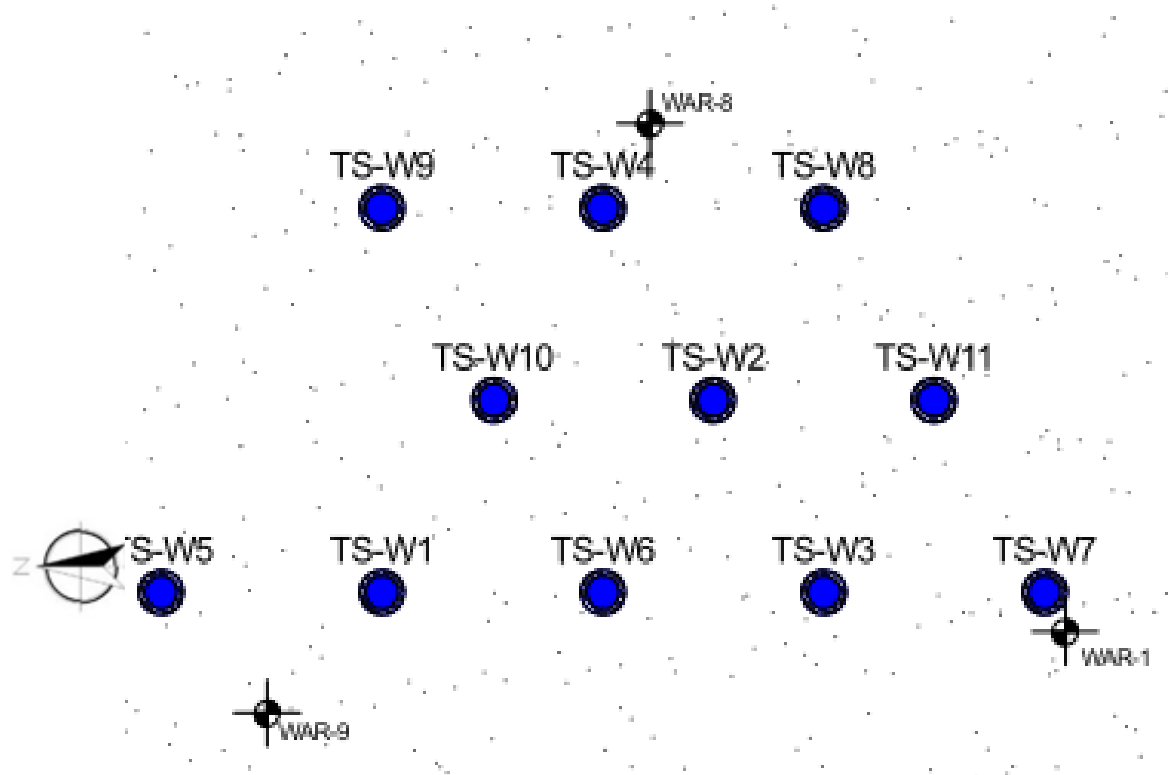


Figure 5.7. Layout of test shafts at Warrensburg site.

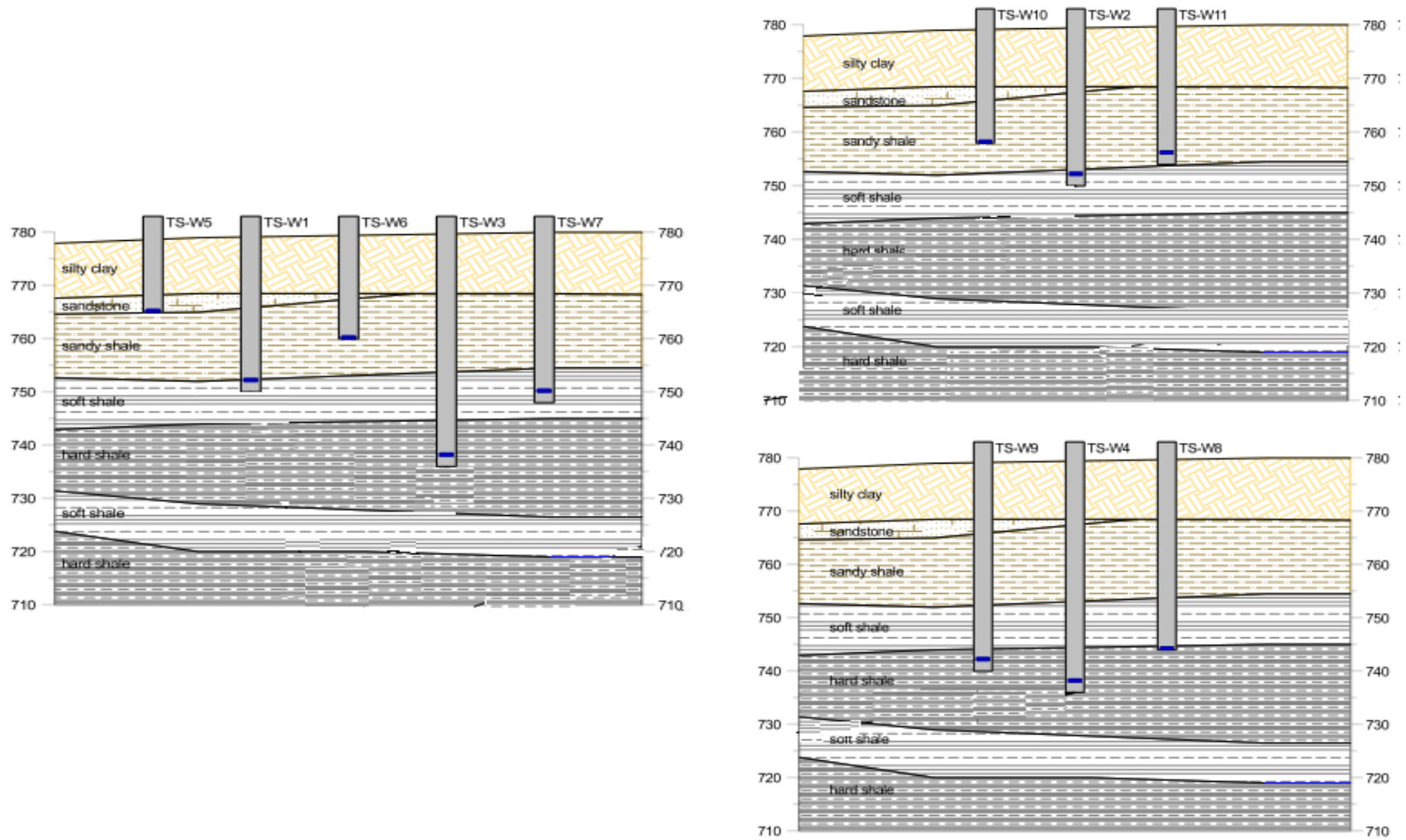


Figure 5.8. Cross-section of the Warrensburg Load Test Site showing the drilled shafts.

The Warrensburg site includes: stiff clay overburden; the Croweburg and Fleming Formations; Mineral Formation A; Mineral Formation B; and the Scammon Formation. The high variability of UCS at the Warrensburg site is shown in Figures 5.6 and 5.9. The UCS values of the soil layers vary from 3 to 150 ksf, with the standard deviation varying from 1.31 to 240 ksf. The mean value of UCS, standard deviation and distribution type for UCS within each soil layer are summarized in Table 5.2.

Table 5.2. Uniaxial compressive strength statistics for the Warrensburg site.

Warrensburg site	UCS Statistics		
	Mean (ksf)	Standard deviation (ksf)	Distribution type
Stiff clay overburden	3.35	1.31	Lognormal
Croweburg Formation	13.73	11.29	Lognormal
Fleming Formation	81.78	96.52	Lognormal
Mineral Formation A	30.14	11.11	Normal
Mineral Formation B and Scammon Formation	133.23	240.7	Lognormal

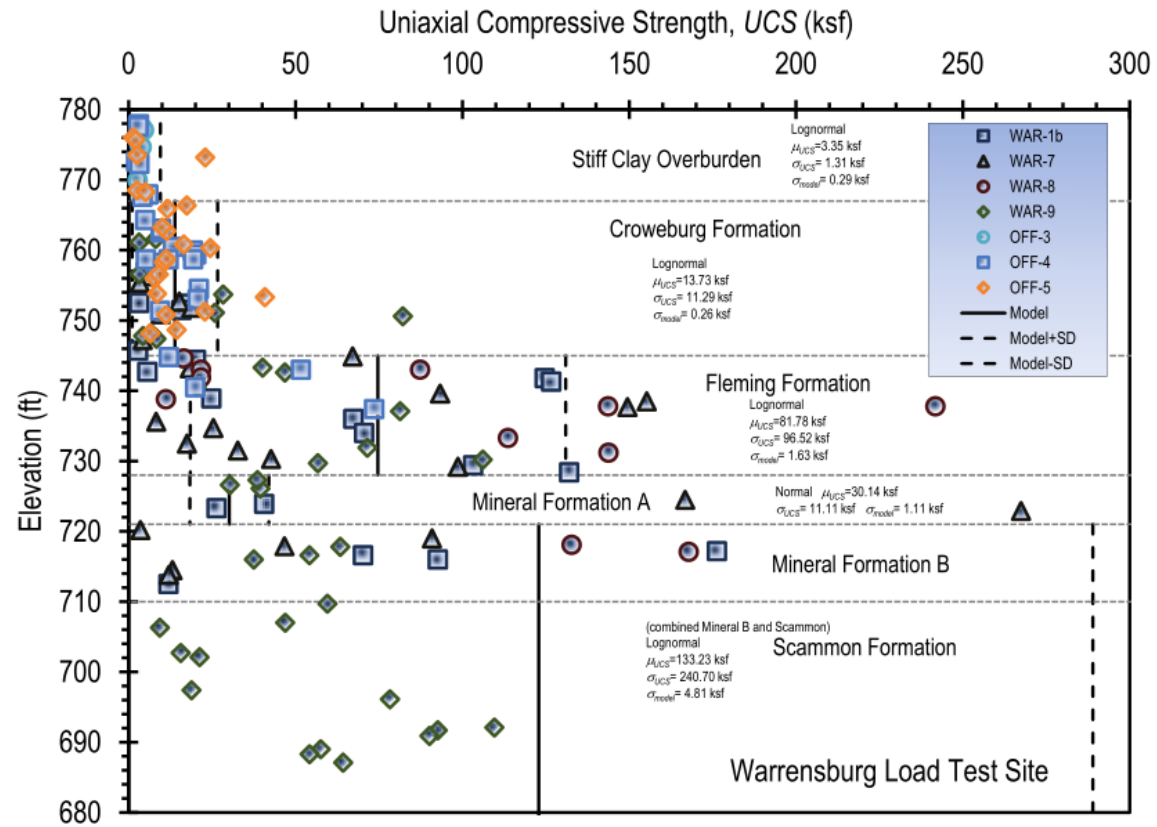


Figure 5.9. Measured uniaxial compressive strengths from the Warrensburg site.

5.1.2. Test Shaft Characteristics

Test shafts at both sites have nominal lengths varying from 15 to 50 feet, and nominal diameters of 3 feet and 5 feet. A summary of information about shaft tip elevations, shaft lengths, and nominal diameters is provided in Table 5.3 (Frankford site) and Table 5.4 (Warrensburg site). These tables also contain information for as-constructed (or as-built) parameters such as tip diameters, elevations of O-Cell bottom plates, and diameters of O-Cell bottom plates that are used in later calculations and analyses.

Figure 5.10. shows a typical as-built drawing for test shaft F-7. The figure also shows the O-Cell position, strain gauge elevations and casing length. Similar as-built drawings for each test shaft are provided in Appendix B.

Table 5.3. Summary of test shaft characteristics at the Frankford site.

Shaft	Tip Elevation (ft.)	Shaft length (ft.)	Nominal Diameter (ft.)	As Constructed Tip Diameter (ft.)	Elevation of O-Cell Bottom Plate (ft.)	Diameter O-Cell Bottom Plate (in.)
F1	643.2	20.6	3	3.18	644.4	18
F2*	640.9	22.8	3	3.22	641.8	24
F3	638.5	25.2	5	5.18	639	47
F4	637.6	26.2	3	3.28	638	23
F5	629.9	33.6	5	5.09	632.2	47
F6	636.6	27.3	3	3.23	637.1	23
F7	629.3	34.4	3	3.2	634	23
F8*	640.9	23.3	3	3.38	641.3	24
F9	647	16.7	5	5.25	647.7	48
F10	645.2	18.6	5	4.88	645.8	42

*Rim-Cell used.

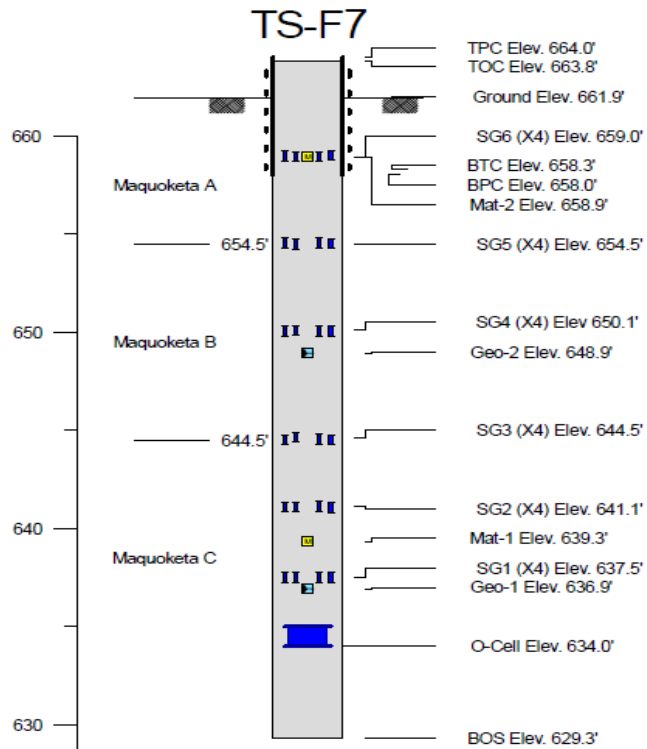


Figure 5.10. Shaft F7 with O-Cell and strain gauge elevations.

Table 5.4. Summary of test shaft characteristics at the Warrensburg site.

Shaft	Tip Elevation (ft.)	Shaft length (ft.)	Nominal Diameter (ft.)	As Constructed Tip Diameter (ft.)	Elevation of O-Cell Bottom Plate (ft.)	Diameter O-Cell Bottom Plate (in.)
W1	750.4	32.5	3	3.08	752.4	24
W2	749.5	33.4	3	3.11	751.6	24
W3	735.8	47.1	3	3.02	738.3	24
W4	733.4	49.4	3	3.13	738.8	24
W5	756.5	27.1	3	3.03	757.1	16
W6	749.9	33.1	3	3.16	751.7	24
w7	749.1	34	3	3	749.2	20
W8	735.1	48.1	3	3.26	736.5	21
W9	735.2	47.8	3	3.06	735.6	21
W10*	746.2	38.8	3	3.3	747	24
W11*	745.9	38.7	3	3.2	747.3	24
W12	749.3	33.6	3	3.14	750.6	24
W13	749.9	32.9	3	3.08	752	24
w14	749.6	32.8	3	2.97	752.5	24
W15	749.6	33.3	3	3.13	751.8	24

*Rim-Cell used.

5.1.3. Test Shaft Instrumentation and Measurements

Each test shaft was instrumented to acquire data about shaft top and shaft tip movements, strain at certain levels and concrete quality could be obtained. A summary of instrumentation installed in each test shaft is provided in Tables 5.5 and 5.6. Additional descriptions of specific types of instrumentation are provided below.

Table 5.5. Summary of instrumentation used for the Frankford test shafts.

Instrument	Test shafts at Frankford site									
	F1	F2	F3	F4	F5	F6	F7	F8	F9	F10
O-Cell	X		X	X	X	X	X		X	X
Rim Cell		X						X		
Strain Gauges	X	X	X	X	X	X	X	X	X	X
Inclinometer Casing	X	X	X	X	X	X	X	X	X	X
Concrete Maturity Meters										
Geophones	X	X	X	X	X	X	X	X	X	X
CSL Tubes					X		X			
Tell-tales	X	X	X	X	X	X	X	X	X	X

Table 5.6. Summary of instrumentation used for the Warrensburg test shafts.

Instrument	Test shafts at Warrensburg Site														
	W1	W2	W3	W4	W5	W6	W7	W8	W9	W10	W11	W12	W13	W14	W15
O-Cell	X	X	X	X	X	X	X	X	X			X	X	X	X
Rim Cell										X	X				
Strain Gauges	X	X	X	X	X	X*	X	X	X	X	X	X*	X*	X*	X*
Inclinometer Casing	X	X	X	X	X	X	X	X	X	X	X	X	X	X	X
Concrete Maturity Meters	X	X	X												
Geophones	X	X		X	X	X	X	X	X	X	X	X	X	X	X
CSL Tubes	X	X													
Tell-tales	X	X	X	X	X	X	X	X	X	X	X	X	X	X	X

* Two strain gauges were used at each level

All test shafts were load tested using the Osterberg Cell® (or “O-Cell”) testing method, or a variation of the O-Cell method referred to as a “Rim-Cell.” An O-Cell is a hydraulically driven device that was welded onto steel plates (top plate and bottom

plate) and attached to the reinforcing cage. Figure 5.11 shows an O-Cell® attached at the end of a rebar cage. During a test, pressure in the O-Cell is increased to create a pair of forces, upward and downward, that are equal to the mobilized resistance of shaft segments above and below the O-Cell. A Rim-Cell functions conceptually in the same manner; however, it is a slightly different device in that instead of having an enclosed steel cylinder as found in an O-Cell, has an open steel and concrete cylinder. Only four shafts – F2, F8, W10 and W11 as indicated in Tables 5.5 and 5.6 - were equipped with a Rim-Cell. Herein, both the O-Cell and Rim-Cell are referred as the O-Cell.

The O-Cells were sometimes placed on the bottoms of the shafts and sometimes elevated above the shaft tip in order to try to balance the upward and downward resistance. An O-Cell “load” is derived by O-Cell pressure divided by the O-Cell cylinder’s cross sectional area, to be used for later analyses.

Telltale, LVDTs, and a LEICA Laser Level System were used to measure the displacement of the O-Cell top and bottom plates at each load step. Tell-tale pipes were installed in each shaft and were directly connected to the O-Cell top and bottom plates. For most test shafts, two telltale pipes extended from above the shaft down to the top plate, and three pipes extended from above the shaft down to the bottom plate. The pipes were welded to the respective O-Cell plates. Before the load test for each shaft, tell-tale rods were placed inside the pipes and threaded into a plug installed at the bottom of the pipe. Tell-tales and LVDTs provided measurements of the relative movement of the shaft top and the top and bottom plates. Absolute movements of the

shaft top were measured using the LEICA Laser Level System. From the relative and absolute movements, the absolute movements of upper and lower plates were obtained. The absolute plate movements were used to determine shaft segment displacements for different load steps during testing.



Figure 5.11. O-Cell® welded to top and bottom plates at the end of a rebar cage.

Strain at specific levels in each shaft was measured using Geokon Model 4200 Vibrating Wire Concrete Embedment strain gauges. The strain gauges were mounted to the rebar cages at six elevations (six levels) within each shaft (Figure 5.12). Four strain gauges were placed at each level for most test shafts. Two strain gauges were placed at each level in shafts W-6, W-12, W-13, W-14, and W-15 at the Warrensburg site. The strain measurements were typically recorded following application of each load increment and at 1, 2, 4, and 8 minutes after application of each load increment. The

strain gauge measurements were used for data interpretation to determine the load in the shaft at each strain gauge level.

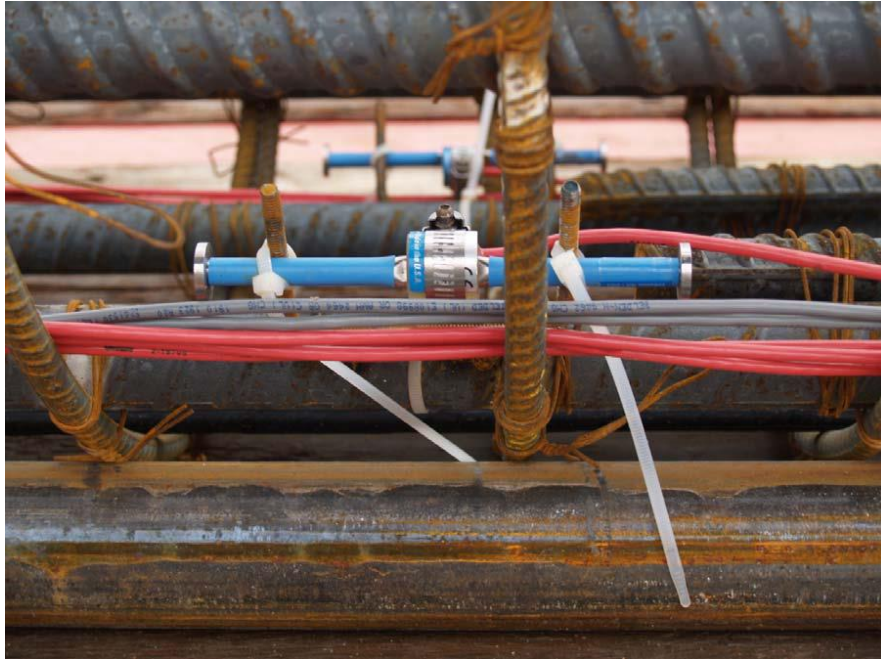


Figure 5.12. Vibrating wire strain gauge attached to rebar cage.

The quality of concrete in drilled shaft construction plays an important role in interpreting load test results. A number of additional measurements were taken to facilitate interpretation of the test shaft performance. Additional instrumentation, including geophones and cross hole sonic logging tubes, was installed in select test shafts to support interpretations of shaft quality and concrete modulus. These measurements included the following:

- Measurements of concrete strength from test cylinders taken for each test shaft;

- Measurements of concrete stiffness for each test shaft using cross-hole sonic logging (CSL) or direct arrival measurements with geophones embedded in select shafts. The geophones installed were Geospace 20DM-40-270 sensors. Olson Instruments CSL equipment was used to evaluate shaft quality and concrete modulus in two test shafts at each site;
- “Sonic” caliper measurements of the cross-section and diameter at 1-ft intervals in each test shaft.

Table 5.7 provides a summary of as-built parameters for test shaft F-7 that includes elevations of the O-Cells, strain gauges, shaft tip, shaft top, area of steel as well as the measured diameter of the test shaft at relevant elevations for the shaft. Similar tables are provided in Appendix B for other test shafts.

Table 5.7 Shaft F7 as built parameters.

Parameters	Elevation (ft.)	Shaft Diameter (ft.)	Area of Steel (in ²)
Shaft Tip	629.3	3.2	
O-Cell Bottom plate	634	3.2	20.3
O-Cell Top plate	635.1	3.2	20.3
SG1	637.5	3.2	20.3
SG2	641.1	3.1	20.3
SG3	644.5	3.2	20.3
SG4	650.1	3.2	20.3
SG5	654.5	3.2	20.3
SG6	659.0	3.0	25.0
Shaft Top	664.0	3.0	25.0

5.1.4. Load testing procedure

LoadTest, Inc. performed the O-Cell® load testing generally following the Quick Loading Procedure in ASTM D1143 - *Standard Test Methods for Deep Foundations under Static Axial Compressive Load* (2009). In the Quick Test Method, each load increment is usually held for four minutes. The testing process followed was to incrementally increase the O-Cell pressure until the shaft failed in either side resistance or tip resistance or until the maximum capacity of the O-Cell® was reached. All shafts were tested until failure occurred either in side resistance or tip resistance or both. Load increments were selected based on predicted shaft resistance seeking to have approximately ten load increments in each test. In fact, some tests required more than twenty load increments before failure (Test shafts F3 and W8), and some failed with as few as three load increments (Test shaft W10).

Typical measured O-Cell load-displacement curves for test shaft F7 are shown in Figure 5.13. Two separate curves are shown. The upper curve reflects the response of the upper portion of the shaft above the O-Cell top plate while the lower curve reflects the response of the shaft below the O-Cell bottom plate. Test shaft F7 failed in side resistance when the O-Cell load reached 3389 kips, as evidenced by the dramatic upward movement of the top plate at that load. The O-Cell pressures and O-Cell loads at which failure occurred are summarized in Table 5.8 for test shafts at the Frankford site, and in Table 5.9 for shafts at the Warrensburg site.



Osterberg Cell Load-Displacement
F7 Test Pile - Missouri Research Project - Frankford, MO

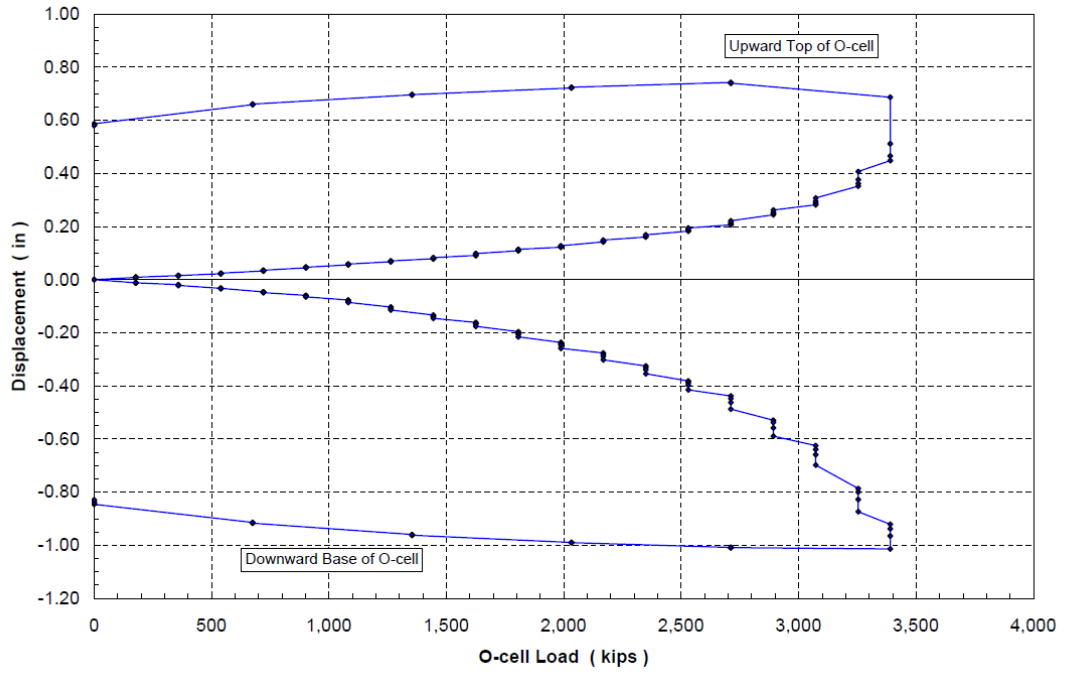


Figure 5.13. Load displacement curves for shaft F7.

Table 5.8. Maximum O-Cell pressures and loads for tests at Frankford site.

Shaft	Maximum O-Cell Pressure (psi)	Maximum O-Cell Load (kips)
F1	6,065	863
F2	2,530	1,051
F3	14,400	3,251
F4	10,385	2,343
F5	15,000	5,361
F6	10,950	2,472
F7	15,000	3,389
F8	1,944	808
F9	4,950	701
F10	6,010	854

Table 5.9. Maximum O-Cell pressures and loads for tests at Warrensburg site.

Shaft	Maximum O-Cell Pressure (psi)	Maximum O-Cell Load (kips)
W1	2,650	375
W2	3,750	529
W3	6,000	1,353
W4	5,395	1,217
W5	1,600	150
W6	3,920	556
W7	2,840	404
W8	8,840	1,996
W9	5,250	1,182
W10	605	252
W11	1,209	502
W12	4,160	591
W13	3,010	426
W14	3,010	423
W15	4,000	569

5.2. Analysis and Interpretation

Load transfer from the drilled shafts to the surrounding ground in side and tip resistance is a fundamental behavior necessary to predict settlement of drilled shafts. Such behavior can be established from load test measurements like those described in this chapter, which subsequently can be used to establish appropriate load transfer models for prediction of drilled shaft settlement. Measurements from each of the load tests performed were, therefore, analyzed to establish the “measured” load-displacement response for both side and tip resistance as described in more detail in the following sections.

5.2.1. Procedure for Establishing Load Distribution along Shafts

The load distribution along each shaft for a given loading increment was established from strain gauge measurements at different levels in the shaft and from measurements of the O-Cell load. Figure 5.14 shows an example distribution of load along the shaft at different loading increments for test shaft F7 from the Frankford site. As shown in the figure, the load in the shaft is greatest at the location of the O-Cell and diminishes with distance from the O-Cell due to load transfer in side resistance.

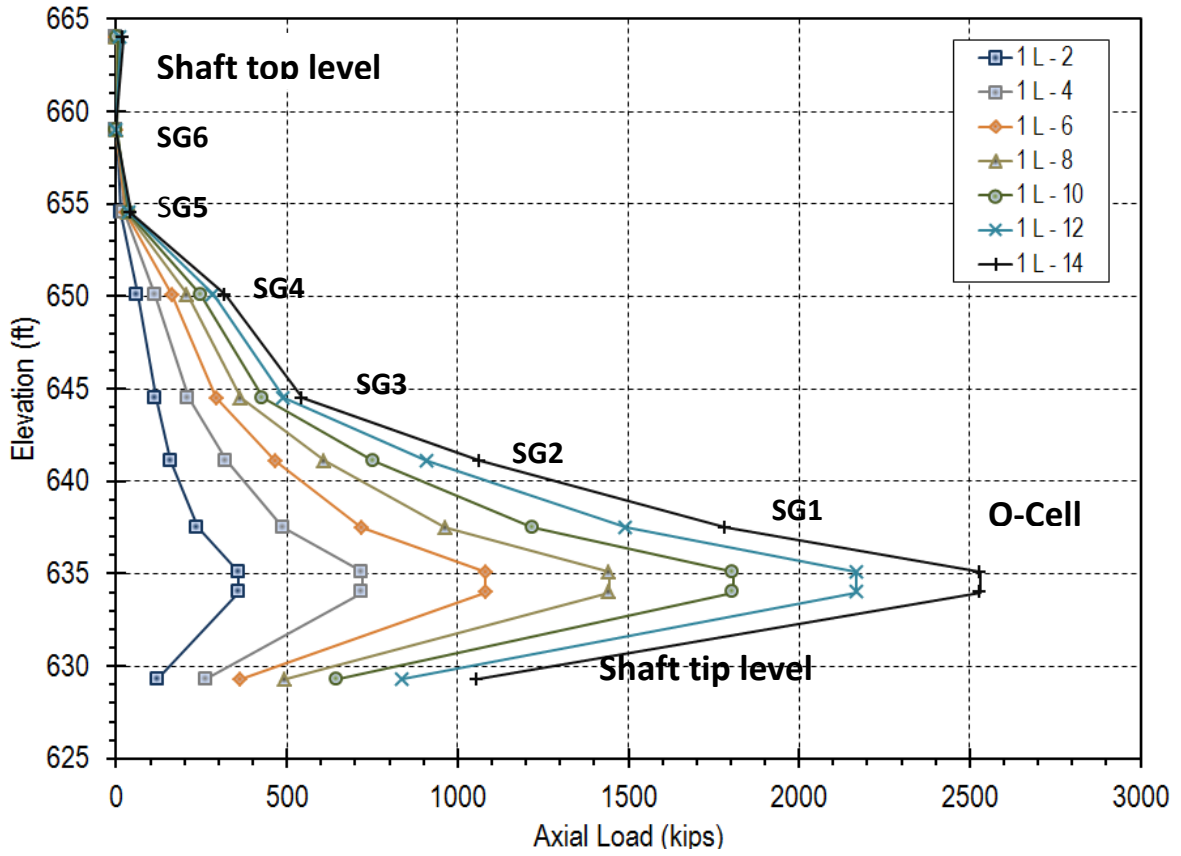


Figure 5.14. Force in test shaft F7 at each loading during testing.

The distribution of load in the shaft for a given value of applied load was established as follows:

1. The magnitude of the load at the top and bottom of the O-Cell was taken to be equal to the calibrated O-Cell load (derived from the measured fluid pressure in the O-Cell divided by the cross-sectional diameter of the O-Cell cylinder);
2. The magnitude of the load at the location of each strain gauge level was computed from the average strain reading at that level as:

$$P_i = \varepsilon_{avg} * AE = \varepsilon_{avg} * (A_c * E_c + A_s * E_s) \quad (5.1)$$

where

ε_{avg} = the average strain at each level of strain gauges,

EA = the composite shaft stiffness,

A_c = the cross-sectional area of the shaft concrete at the strain gauge level (the measured area of shaft cross section minus the area of steel),

E_c = Young's modulus of the concrete calculated from compressive strength tests performed on the day of load testing,

A_s = the cross sectional area of reinforcing steel, and

E_s = Young's modulus of the reinforcing steel (29,000 ksi).

In Equation 5.1, the concrete Young's modulus E_c was estimated from results of compressive strength tests performed on the day of the load tests as

$$E_c = 57000 * \sqrt{f'_c} \quad (5.2)$$

where

E_c = concrete Young's modulus in *psi*, and

f'_c = the concrete compressive strength in *psi*.

3. The magnitude of the load at the ground surface was taken to be zero since no load or reaction was applied at the top of the shaft;
4. The magnitude of the load at the tip of the shaft was calculated as equal to the O-Cell load minus the load transferred in side resistance below the O-Cell.

$$P_{Tip} = P_{Cell} - P_{BO} \quad (5.3)$$

where

P_{Tip} = load at the tip of the shaft

P_{Cell} = load applied by the O-Cell, and

P_{BO} = load transferred in side resistance below the O-Cell.

The load transferred in side resistance between the O-Cell and the shaft tip was determined assuming that the unit side resistance for the shaft segment below the O-Cell was equal to the unit side resistance of the segment right above O-Cell. The side resistance force between the O-Cell and shaft tip is, thus, equal to

$$P_{BO} = f_1 * A_{BO} \quad (5.4)$$

where

f_1 = unit side resistance of the first shaft segment right above O-Cell, and

A_{BO} = side area of the shaft below O-Cell.

The side area the shaft segment below the O-Cell is

$$A_{BO} = \frac{1}{4} \pi * D_{BO}^2 * L_{BO} \quad (5.5)$$

where

L = distance from O-Cell to shaft tip, and

D_{BO} = average as-built diameter of the shaft segment below O-Cell.

Figure 5.14 illustrates results of such calculations for test shaft F-7 from the Frankford load test site and represents seven load increments during the test.

5.2.2. Analysis of Load Transfer in Side Resistance

Once the load distribution was established for each load increment, the mobilized side resistance in each shaft segment (between adjacent strain gauge levels, and between the O-Cell and the first strain gauge level) was determined using the following procedure:

1. The total load transfer in side resistance for each segment was calculated as the difference in mobilized load across the segment:

$$\Delta P_i = P_i - P_{i-1} \quad (5.6)$$

where

ΔP_i = total load transferred in side resistance for shaft segment i

P_i = mobilized load in the shaft at strain gage level i , and

P_{i-1} = mobilized load in the shaft at strain gage level $i-1$;

2. The mobilized unit side resistance for each shaft segment was calculated as:

$$f_i = \Delta P_i / A_i \quad (5.7)$$

where

f_i = mobilized unit side resistance for segment i , and

A_i = shaft-soil interface area for shaft segment i .

The shaft-soil interface area for the shaft segment is

$$A_i = \frac{1}{4} \pi * D_i^2 * L_i \quad (5.8)$$

where

L_i = length of shaft segment i , and

D_i = average as-built diameter of shaft segment i .

3. Elastic compression δ_i^e of a shaft segment between two consecutive strain gage levels or between the O-Cell and the strain gage immediately above the O-Cell is calculated from the load in the shaft segment, length of the shaft segment, and shaft stiffness,

$$\delta_i^e = \frac{(P_i + P_{i-1})}{2} * \frac{L}{EA} \quad (5.9)$$

where

P_i = mobilized load in the shaft at strain gage level i

P_{i-1} = mobilized load in the shaft at strain gage level $i-1$, or in the O-Cell load if the first shaft segment is considered,

L = length of the shaft segment, and

EA = shaft stiffness.

The length of the shaft segment is obtained from elevations of two consecutive strain gage levels at the two ends of the shaft segment, or from the distance between the O-Cell and the first strain gage level immediately above the O-Cell;

4. The “local” average displacement for each shaft segment was calculated progressively from the lower shaft segments, and the average displacement of the first shaft segment was calculated from the measured O-Cell upper plate movement and the calculated elastic compression of the shaft segment.

Average displacement for shaft segment i is

$$d_i = d_{i-1} - (\delta_i^e + \delta_{i-1}^e)/2 \quad (5.10)$$

where

d_i, d_{i-1} = average displacement for shaft segment i and $i-1$, and

$\delta_i^e, \delta_{i-1}^e$ = elastic compression of the shaft segment i and $i-1$.

The average displacement for the shaft segment between the first strain gage level and the O-Cell is:

$$d_1 = d_0 - (\delta_1^e)/2 \quad (5.11)$$

where

d_1 = average displacement for shaft segment 1

d_0 = measured O-Cell upper plate movement, and

δ_1^e = elastic compression of the first shaft segment above the O-Cell.

Given the mobilized unit side resistance and local displacement for each shaft segment and load increment, load transfer curves were constructed as illustrated in

Figure 5-15 for test shaft F-7. The same procedure was carried out for every shaft, and the results were used subsequently to establish normalized load transfer curves.

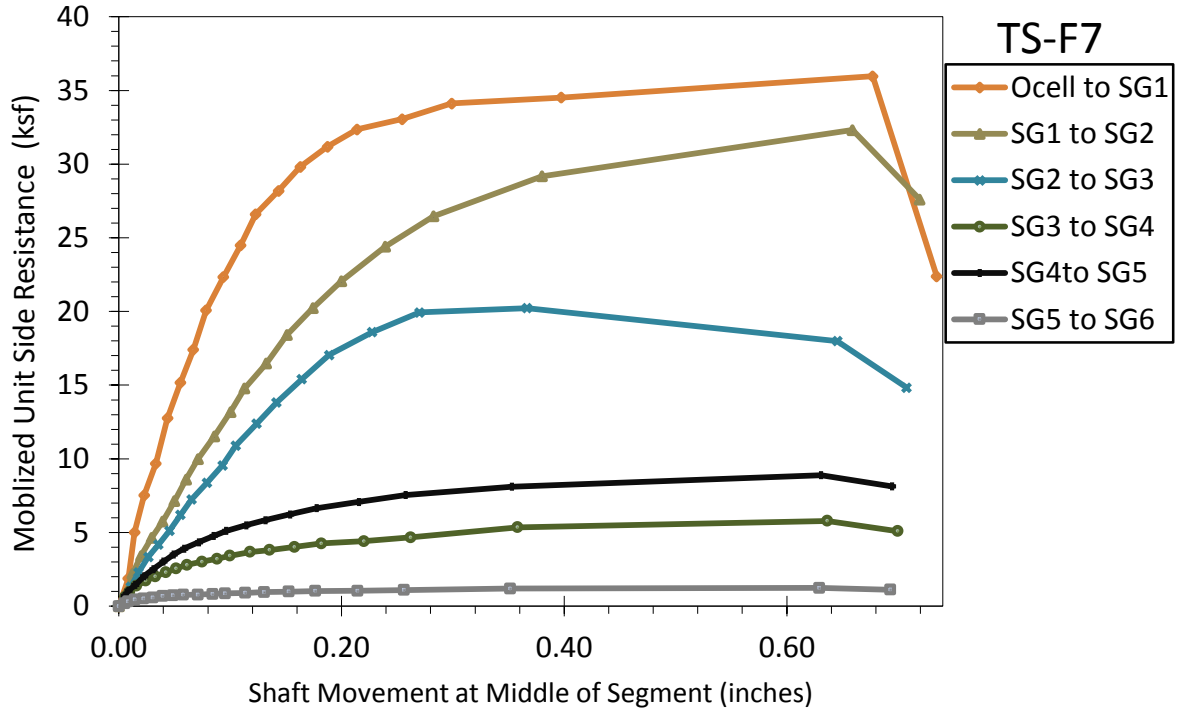


Figure 5.15. Mobilized unit side resistance versus displacement for test shaft F-7.

5.2.3. Analysis of Load Transfer in Tip Resistance

The procedure to establish load transfer in tip resistance is as follows:

1. Obtain the mobilized unit tip resistance by dividing the force at the tip of the shaft P_{Tip} in Equation 5.3 and divide it by the as-built shaft tip area. Shaft tip area is calculated from as-built tip diameter in Table 5.7;
2. Elastic compression of the shaft segment below the O-Cell is:

$$\delta_{BO}^e = (P_{Tip} + P_{Cell})/EA \quad (5.12)$$

where

δ_{BO}^e = elastic compression of the shaft segment below the O-Cell,

P_{Cell} = O-Cell load, and

EA = average shaft stiffness for the shaft segment;

3. Obtain the shaft tip displacement by subtracting the elastic compression of the shaft segment below the O-Cell from the bottom plate movement.

$$d_{Tip} = d_{BO} - \delta_{BO}^e \quad (5.13)$$

where

d_{Tip} = displacement of shaft tip, and

d_{BO} = measured O-Cell lower plate movement;

4. Construct the mobilized unit tip resistance versus displacement of shaft tip from results of steps 1 and 3 as in Figure 5-16.

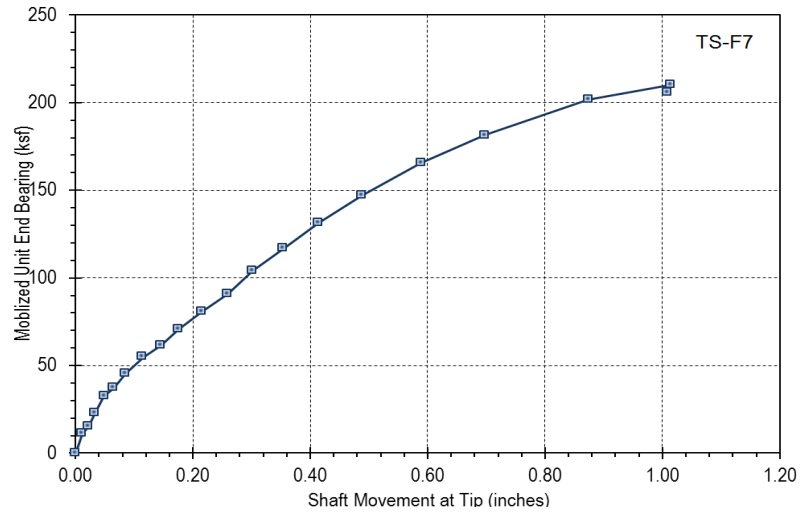


Figure 5.16. Mobilized unit tip resistance versus displacement for test shaft F-7.

5.2.4. Summary of load test results

Table 5.10 shows the average UCS for each segment of test shaft F7. Table 5.10 also presents the maximum mobilized resistance, predicted ultimate resistance (based on predictive models described in Section 5.3.2) and mobilized displacement at the ultimate resistance for test shaft F-7. Because the data are extensive, similar information for all test shafts is presented in Appendix C.

Table 5.10. Load Test Results for Test Shaft F7 –Side resistance.

Shaft F-7	Mean UCS (ksf)	Measured Maximum Mobilized Resistance (ksf)	Predicted Ultimate Resistance (ksf)	Displacement at Maximum Resistance (% of shaft diameter)
O-SG1	66.2	36.0	20.9	1.9
SG1-SG2	66.2	32.3	20.9	1.8
SG2-SG3	66.2	18.0	20.9	1.8
SG3-SG4	10.4	5.8	4.8	1.8
SG4-SG5	10.4	8.9	4.8	1.8
SG5-SG6	3.3	1.2	2.0	1.7

Tables 5.11 and 5.12 summarize information for each of the tests performed at the Frankford and Warrensburg sites, respectively, including the mean UCS at the shaft tip, the maximum mobilized tip resistance, and the mobilized tip displacement at the ultimate resistance. The tables also present the estimated value of measured ultimate resistance (in %), the estimated ultimate measured tip resistance, and the predicted ultimate tip resistance for all shafts that are used for establishing normalized tip load transfer response as presented later in Section 5.3.2.

Table 5.11. Load Test Results for Test Shafts at Frankford – Tip Resistance.

Test Shaft	Mean UCS (ksf)	Measured Maximum Resistance (ksf)	Estimated % of Measured Ultimate (ksf)	Estimated Ultimate Measured Resistance (ksf)	Predicted Ultimate Resistance (ksf)	Displacement at Maximum Resistance (%D)
F1	66.2	78.1	31	252	275	0.65
F2	66.2	114.6	48	239	275	0.3
F3	66.2	134.2	54	249	275	0.54
F4	66.2	259.9	100	260	275	9.02
F5	66.2	190	76	250	275	1.34
F6	66.2	286.4	31	924	275	13
F7	66.2	210.1	85	247	275	2.63
F8	66.2	80.4	34	237	275	0.26
F9	10.4	27.2	35	78	74	0.37
F10	10.4	44.5	52	86	74	0.73

Table 5.12. Load Test Results for Test Shafts at Warrensburg – Tip Resistance.

Test Shaft	Mean UCS (ksf)	Measured Maximum Resistance (ksf)	Estimated % of Measured Ultimate (ksf)	Estimated Ultimate Measured Resistance (ksf)	Predicted Ultimate Resistance (ksf)	Displacement at Maximum Resistance (%D)
W1	5.4	41.5	42	99	46	0.81
W2	5.4	60.4	63	96	46	1.44
W3	74.7	171.4	50	343	299	1.07
W4	74.7	131.3	36	365	299	0.89
W5	15	100.3	100	100	96	6.65
W6	5.4	58.7	59	99	46	1.85
W7	5.4	175.3	100	175	46	22.98
W8	74.7	251.6	72	349	299	1.88
W9	74.7	158.9	45	353	299	1.95
W10	5.4	32.1	31	103	46	5.99
W11	5.4	57.9	40	145	46	2.92
W12	5.4	53.7	95	57	46	3.29
W13	5.4	39.9	85	47	46	0.61
W14	5.4	45.1	50	90	46	0.55
W15	5.4	66.4	60	111	46	0.54

5.3. Development of Normalized Load Transfer Curves

It is common to normalize load transfer curves to account for differences in shaft size or ultimate capacity (e.g., O’Neil and Reese, 1999) so that load transfer models can be utilized for other shaft sizes and for other site conditions. The mobilized side or tip resistance is commonly normalized using the “ultimate” side or tip resistance, while displacements are generally mobilized relative to the shaft diameter.

Two different approaches can be used to normalize the mobilized unit side or tip resistance like the data considered in this chapter: normalizing the mobilized unit

resistance using the maximum *measured* values for the unit resistance, and normalizing the mobilized unit resistance using the maximum *predicted* values for unit resistance. The first approach presumes that the maximum measured resistance represents the ultimate condition, which may or may not be appropriate for specific data. The latter approach, in contrast, assumes that a reasonable prediction method exists for the materials present. Both of these approaches were utilized for the load test measurements from the Frankford and Warrensburg test sites as described in the following sections.

5.3.1. Normalized Load Transfer Using Maximum Measured Values

Mobilized side and tip resistance values for each shaft segment from the load tests performed at the Frankford and Warrensburg test sites were normalized using the maximum measured values for side or tip resistances. Displacements for each shaft segment were normalized by the measured shaft diameters of the respective segments.

5.3.1.a Mobilized Side Resistance – Normalized to Maximum Measured Values

Normalized load transfer curves for side resistance using maximum measured values are plotted in Figures 5.17 through 5.20. The curves shown in Figures 5.17 and 5.18 represent results obtained from tests at the Frankford and Warrensburg sites, respectively, for shaft segments without permanent casing.

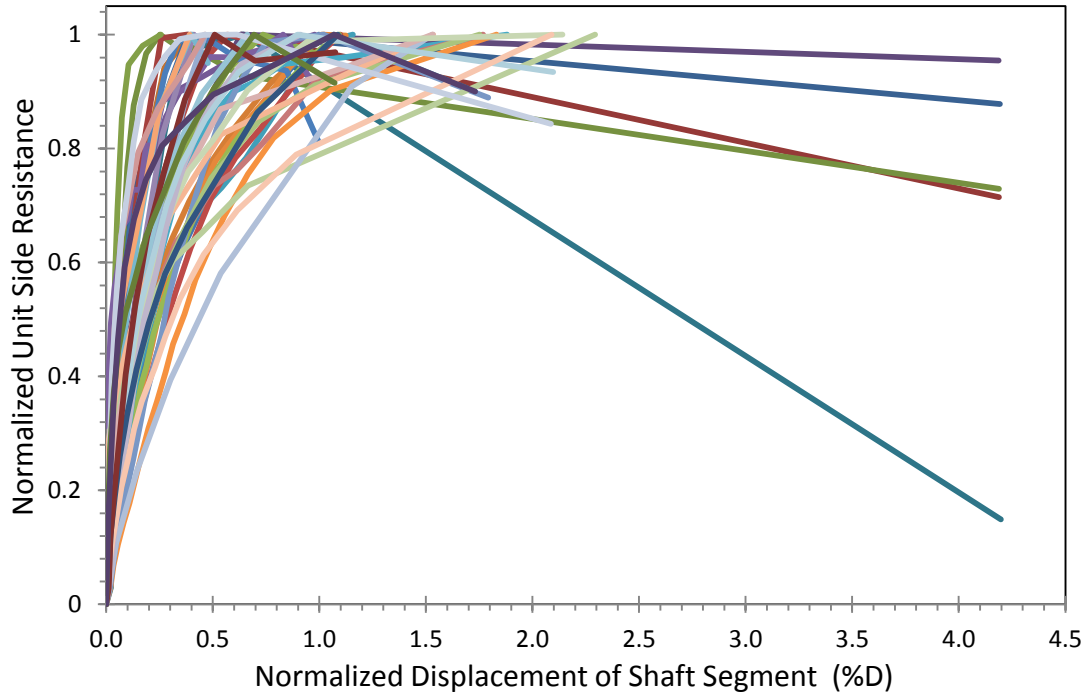


Figure 5.17. Normalized load transfer response in side resistance for uncased segments of test shafts at the Frankford site.

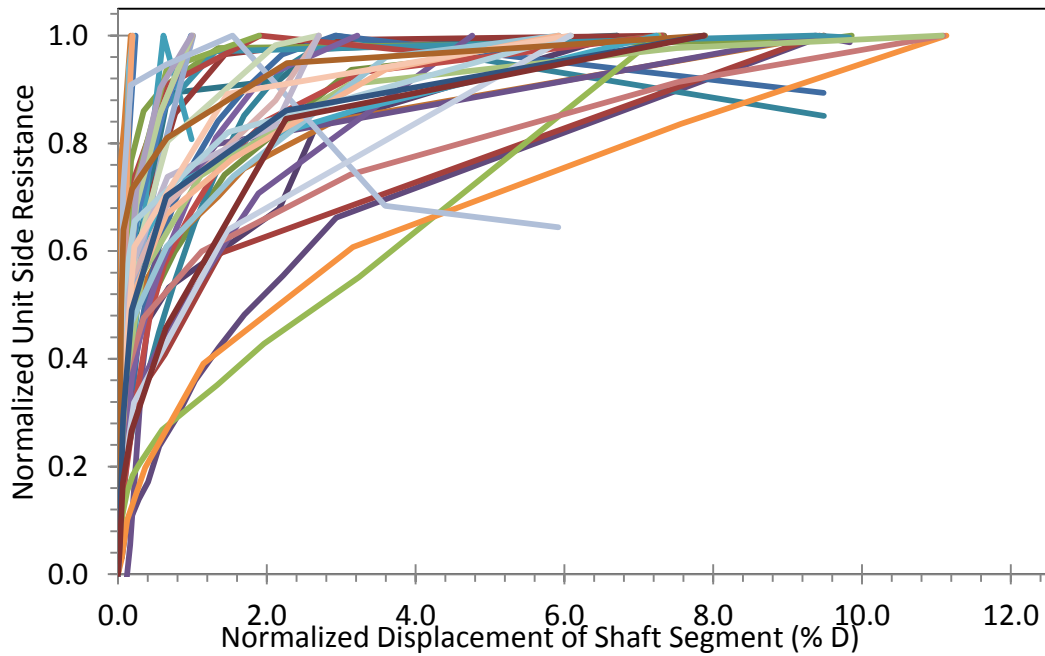


Figure 5.18. Normalized load transfer response in side resistance for uncased segments of test shafts at the Warrensburg site.

Results of load transfer responses of cased segments were plotted separately because they were different from those of uncased segments. The curves shown in Figures 5.19 and 5.20 represent results for shaft segments with permanent casing, which clearly exhibited different load transfer responses from uncased segments as well as greater scatter and some non-typical response. The cased segment data were not included in later analyses.

As shown in Figure 5.17, mobilization of side resistance at the Frankford site was relatively consistent for all shaft segments. The maximum measured side resistance was mobilized at displacements of approximately 0.3 to 2% of the respective shaft diameter. Measured side resistance at greater displacements generally decreased, suggesting that the ultimate side resistance was generally mobilized for all shaft segments.

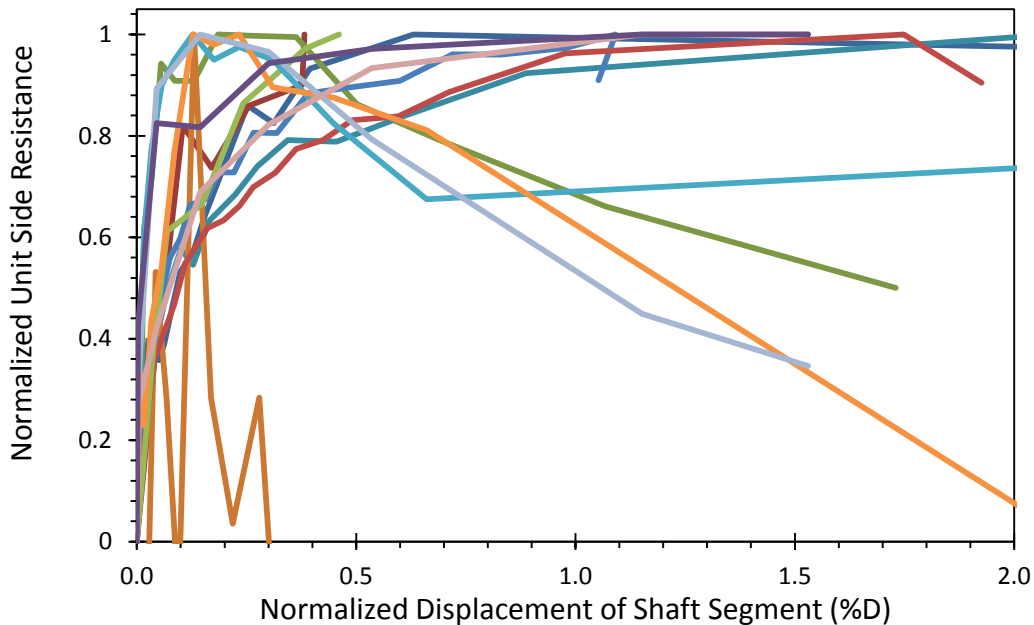


Figure 5.19. Normalized load transfer response in side resistance for cased segments of test shafts at the Frankford site.

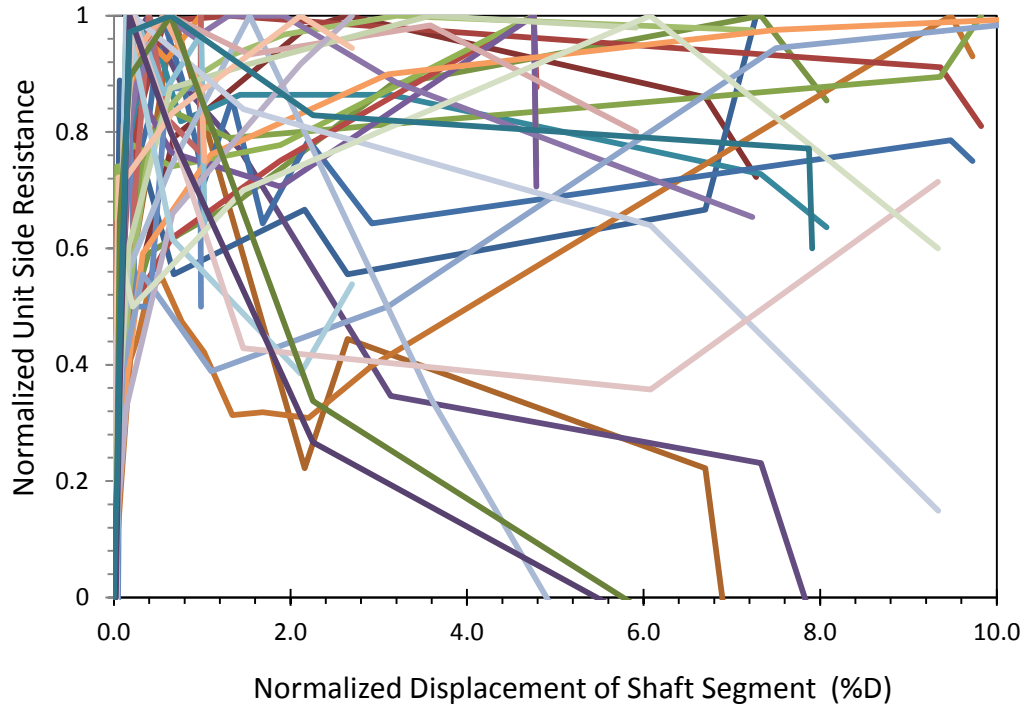


Figure 5.20. Normalized load transfer response in side resistance for cased segments of test shafts at the Warrensburg site.

Results plotted in Figure 5.18 for the Warrensburg site show much greater variability. The maximum measured side resistance for these tests was mobilized at displacements of as little as 0.2 percent of the shaft diameter for some shaft segments. However, for other shaft segments, displacements as great as 11 percent of the shaft diameter were required to mobilized the maximum measured resistance. As was the case for results from the Frankford site tests, the measured side resistance generally decreased at greater displacements, which indicates that the maximum measured resistance reflects the ultimate condition. The greater variability in the load transfer response observed at the Warrensburg site is attributed to the highly variable ground conditions at that site (Fig. 5.4).

O'Neil and Reese (1999) presented the Load Transfer method, with the relationship between normalized unit side and tip resistance versus normalized shaft displacement (Chapter 2). The method also provides ranges of variability for the load transfer curves in cohesive soil. Since the geomaterials for both the Frankford and Warrensburg sites are mostly shales, which falls between hard cohesive soil to soft rock, the developed load transfer curves are compared with the O'Neil and Reese curves. The O'Neil and Reese curves were digitized and superimposed on the curves obtained from load test data for comparison.

Figures 5.21 and 5.22 show the normalized mobilization of side resistance from Figures 5.17 and 5.18 with normalized load transfer curves from O'Neil and Reese (1999) superimposed for comparison. Results shown in Figure 5.21 for tests at the Frankford site are largely consistent with both the trend and range shown for the O'Neil and Reese curves, although the range of the O'Neil and Reese curves is slightly lower than that observed from tests at the Frankford site. Results shown in Figure 5.22 for tests at the Warrensburg site are not as consistent with the O'Neil and Reese curves. The normalized responses for some shaft segments at the Warrensburg site are generally consistent with the O'Neil and Reese relation. However, the normalized response for a large number of shaft segments at the Warrensburg site is substantially less stiff than suggested by the O'Neil and Reese relation and the range of the normalized response is substantially greater than that suggested by O'Neil and Reese.

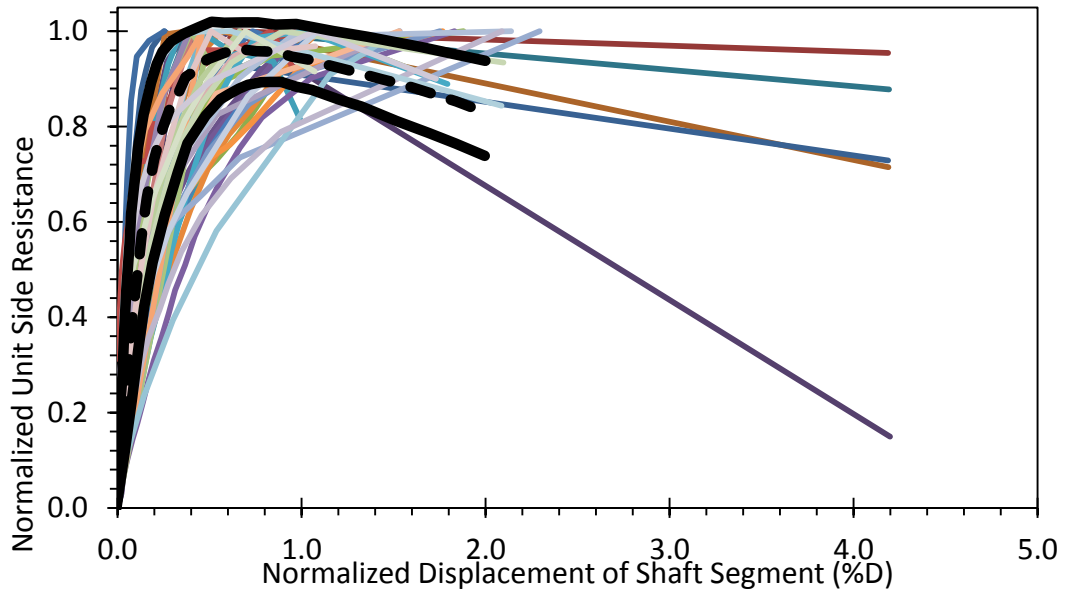


Figure 5.21. Normalized unit side resistance curves from tests at the Frankford site with O'Neil and Reese (1999) curves (bold black lines) superimposed for comparison.

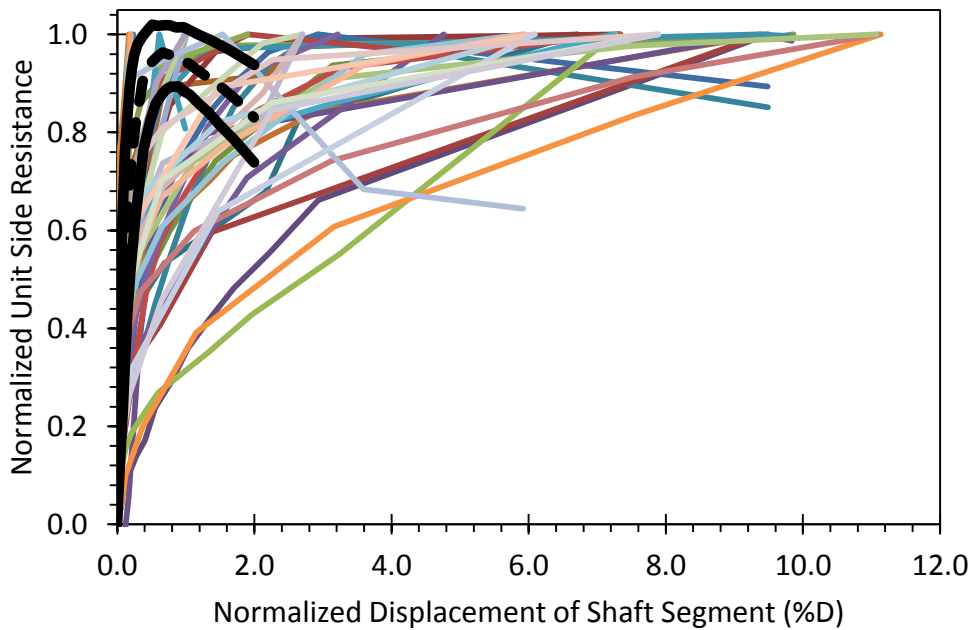


Figure 5.22. Normalized unit side resistance curves from tests at the Warrensburg site with O'Neil and Reese (1999) curves (bold black lines) superimposed for comparison.

The finding that relatively large displacements (up to 11% D) may be required for side resistance to fully mobilize possibly affects the service limit state design. In practice, shafts are considered to gain their ultimate resistance when the settlement is about 5% of the shaft diameter (ASSHTO 2007), meaning that both side and tip resistance are considered fully mobilized at displacements of 5% D. The data show that the required shaft displacement may be much larger to obtain the ultimate side resistance. Furthermore, the range of results in O'Neil and Reese data is significantly smaller than that from the load test data used in this dissertation, which means that if this research relied on the O'Neil and Reese (1999) range for analyses, the variability of the results and the actual probability of failure of designs would be larger than the target.

5.3.1.b. Mobilized Tip Resistance – Normalized to Maximum Measured Values

Normalized load transfer curves for tip resistance using maximum measured values are plotted in Figures 5.23 and 5.24 for tests conducted at the Frankford and Warrensburg sites, respectively. The development of normalized load transfer curves for tip resistance from the test measurements is not as straightforward as for side resistance because many of the tests did not achieve the ultimate condition at the tip (either because the shaft above the O-Cell failed or because the capacity of the O-Cell was reached prior to mobilization of ultimate tip resistance). The maximum measured values of tip resistance are, therefore, not the ultimate values for all tests.

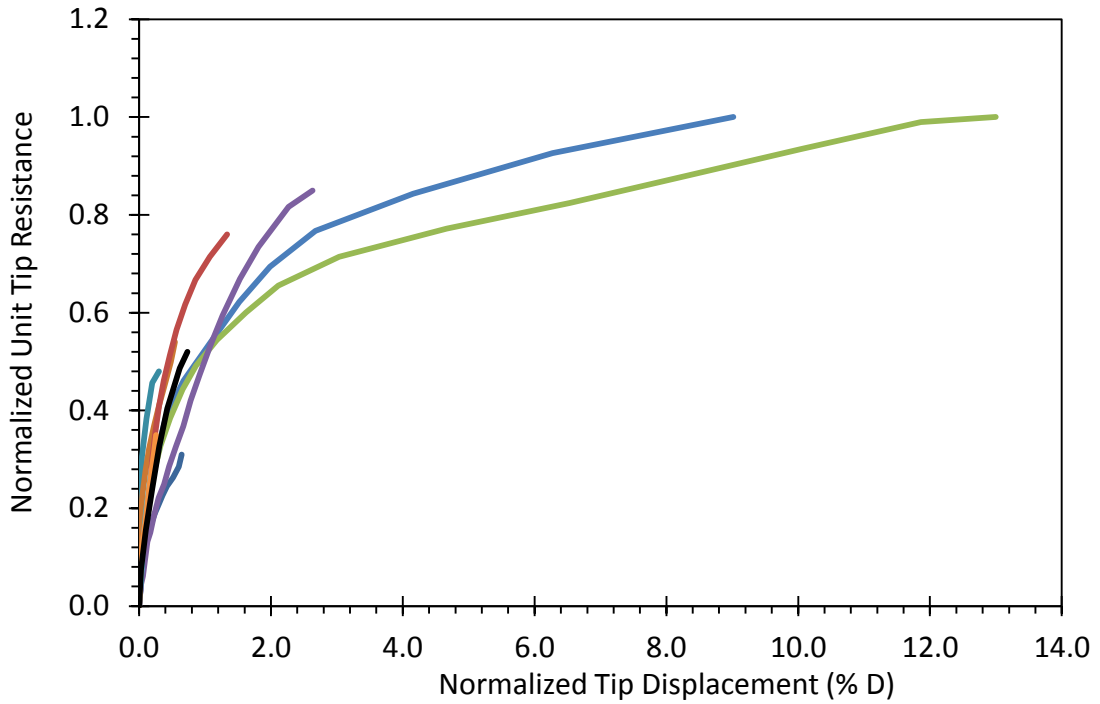


Figure 5.23. Normalized load transfer response in tip resistance for test shafts at the Frankford site.

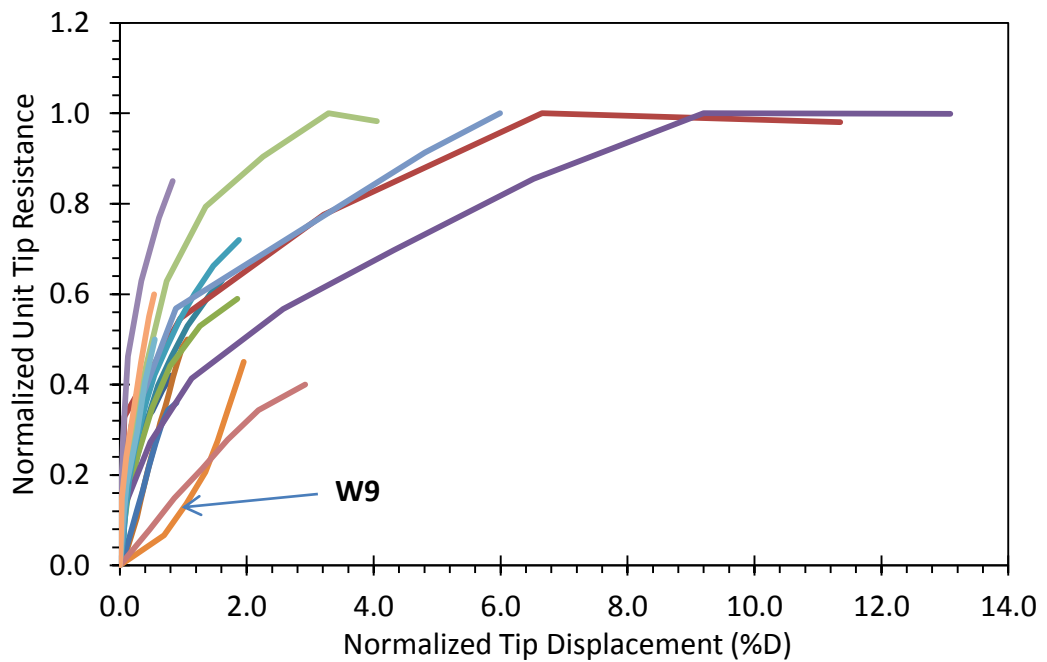


Figure 5.24. Normalized load transfer response in tip resistance for test shafts at the Warrensburg site.

In order to allow normalization of test results for those shafts where the ultimate tip resistance was not reached, extrapolation was used to estimate an ultimate capacity based on the shapes of the curves, the magnitudes of displacement achieved, and the magnitudes of resistance reached relative to predicted tip resistance derived from tests where the ultimate tip resistance was achieved. These extrapolated estimates are summarized in Tables 5.11 and 5.12, and were used to normalize the measured resistances.

Results plotted in Figure 5.23 for shafts from the Frankford test site indicate relatively consistent responses from all shafts. The response can be characterized by an initial, nearly linear mobilization of resistance that occurred to normalized displacements of approximately 2 percent of the shaft diameter and normalized unit tip resistance of 0.7 to 0.8 of the ultimate resistance. This initial mobilization was followed by additional mobilization of resistance with additional displacement at a dramatically reduced rate for tests where loading exceeded the initial near linear portion of the load transfer curve. The tip displacement required to fully mobilize tip resistance ranged from 8 to 12 percent of the diameter where the ultimate condition was reached.

Results shown in Figure 5.24 for shafts from the Warrensburg test site are less consistent than results from the Frankford site, as can be expected based on the relative variability of rock strength at the two test sites. The tip load transfer curves again have a nearly linear portion at small displacements, followed by a “softened” response with

additional displacement prior to achieving the ultimate resistance at much greater displacements. The near linear portion of the load transfer curve generally extends to normalized displacements of approximately 1 percent and to normalized loads between 0.4 and 0.8 of the ultimate resistance. The ultimate condition is reached at normalized displacements between 3 and 9 percent of the shaft diameter.

One of the normalized tip load transfer curves in Figure 5.24, for Test Shaft W9 from the Warrensburg site, shows a response that differs from all other tests. This curve indicates an initial “soft” response, followed by stiffer response at greater displacements. Such a response is indicative of a “soft bottom” condition.

Figures 5.25 and 5.26 show the normalized tip resistance mobilization curves from tests at the Frankford and Warrensburg sites, respectively, with the O’Neil and Reese load transfer curves (1999) superimposed as black, bold curves. For results from the Frankford site, the normalized load transfer data reasonably follow the curves from O’Neil and Reese in terms of both the trend and the range of load transfer response at displacements less than about 2 percent of the shaft diameter. However, the measured responses for test shafts F4 and F6, which are the two shafts with the most complete measurements, differ from the O’Neil and Reese curves at greater displacements. Measurements for these shafts suggest that the O’Neil and Reese curves may overestimate mobilized tip resistance, particularly as loads approach the ultimate

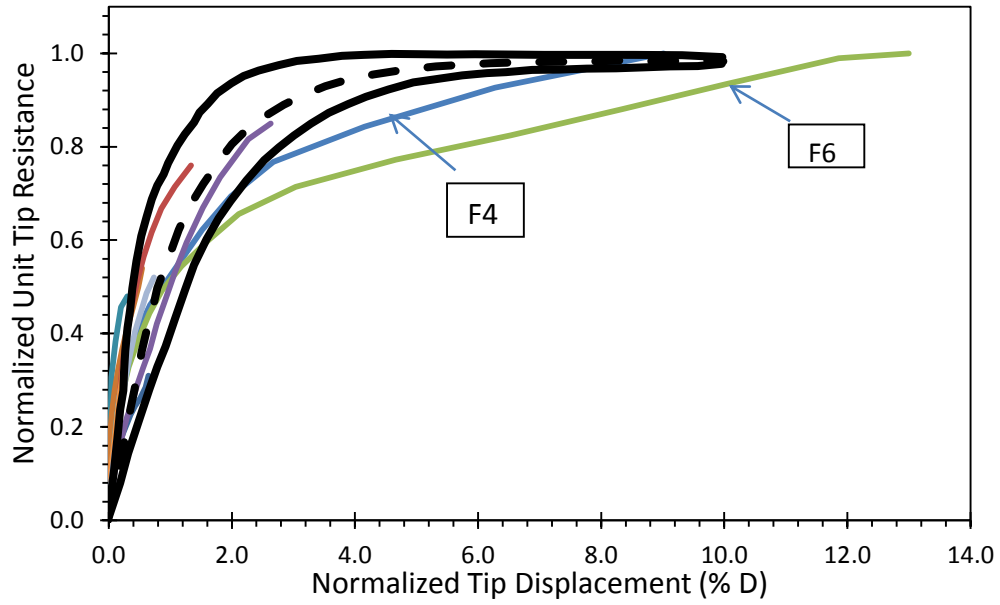


Figure 5.25. Normalized unit tip resistance curves from tests at Frankford site with O'Neil and Reese (1999) curves (bold black lines) superimposed for comparison.

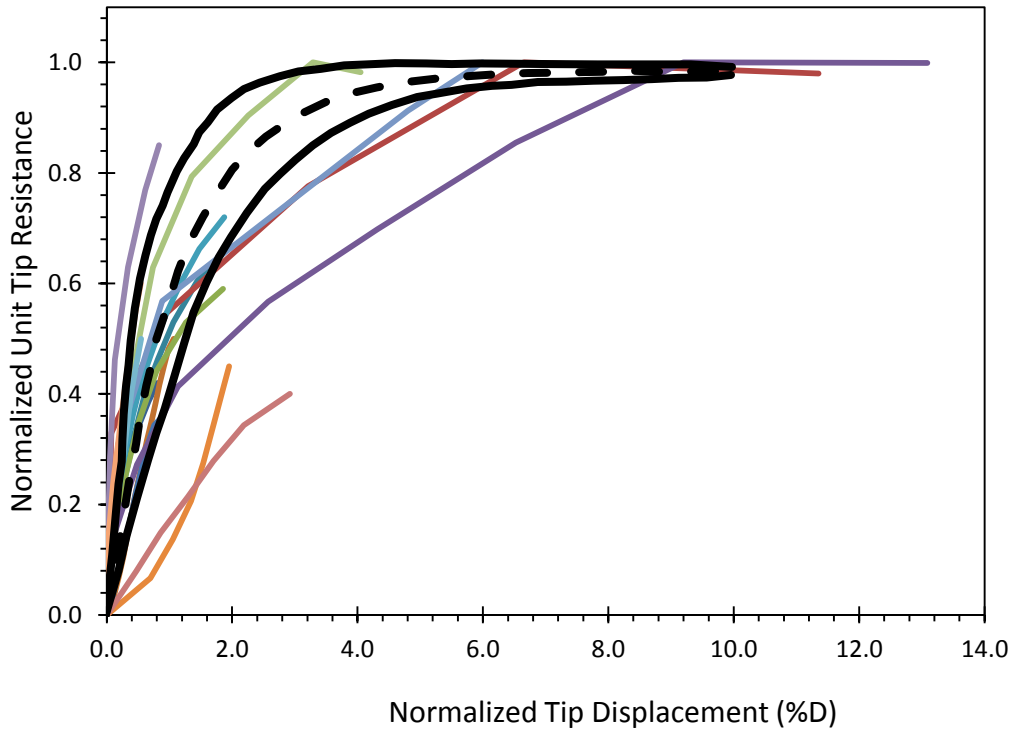


Figure 5.26. Normalized unit tip resistance curves from tests at Warrensburg site with O'Neil and Reese (1999) curves (bold black lines) superimposed for comparison.

resistance, and may underestimate displacements for loads greater than approximately 70 percent of the ultimate resistance. Measurements for these two shafts also suggest that displacements of 8 to 10 percent of the shaft diameter may be required to mobilize the ultimate resistance, as compared to the 2 to 5 percent of the diameter suggested by the O'Neil and Reese curves.

The normalized load transfer shown in Figure 5.26 for tests at the Warrensburg site compares favorably with the O'Neil and Reese curve favorably when the tip displacement is less than approximately 2 percent of the shaft diameter or when the mobilized unit tip resistance is less than 75% of the ultimate resistance. Outside of that range, the measured curves seem to be more scattered. Results also reveal that the ranges shown in the O'Neil and Reese load transfer curves are smaller than the range observed for the load tests at both the Frankford and Warrensburg test sites.

5.3.2. Normalized Load Transfer Using Predicted Ultimate Resistance

Mobilized side and tip resistance values for each shaft segment from the load tests performed at the Frankford and Warrensburg test sites were normalized using predicted values for ultimate unit side or tip resistance. Predicted values used for normalization for each shaft segment were established using a predictive model derived from the results of all load tests at the Frankford and Warrensburg sites, as well as from additional load tests performed for drilled shafts in shale from Missouri and surrounding states (Loehr et al., 2013). As was done previously, displacements for each shaft

segment were also normalized by the measured shaft diameter of the respective segments.

5.3.2.a. Predicted Ultimate Unit Side and Tip Resistance

Predicted values for ultimate unit side and tip resistances were obtained from the relationship provided in the Missouri Department of Transportation's Engineering Policy Guidelines for Design of Drilled Shafts (Loehr et al., 2011). These design relationships were developed based on analyses of the load test results described in this chapter as well as results from additional load tests conducted in the Central U.S. for drilled shafts in shale. The predictive models for ultimate side and tip resistance were developed for use in shales with uniaxial compressive strength (UCS) between 5 and 100 ksf.

The ultimate unit side resistance, q_s , for a shaft segment is computed as

$$q_s = 0.76 \times UCS^{0.79} \leq 30 \text{ ksf} \quad (5.14)$$

where UCS is the mean uniaxial compressive strength of the shale stratum along the shaft segment in units of ksf. The value of q_s is in units of ksf and is limited to a maximum value of 30 ksf. The ultimate unit tip resistance, q_p , at the shaft is computed similarly as

$$q_p = 14 \times UCS^{0.71} \leq 400 \text{ ksf} \quad (5.15)$$

where q_p is in units of ksf and is limited to a maximum value of 400 ksf.

5.3.2.b. Mobilized Side Resistance – Normalized to Predicted Ultimate Values

Figures 5.27 and 5.28 show the normalized load transfer responses in side resistance for the load test measurements at the Frankford and Warrensburg sites, respectively, using predicted ultimate values for normalization. The results showed the uncased segments to be consistent with what had been presented previously for normalization using the maximum measured resistance. The load transfer data for cased segments have different patterns and were not used in subsequent analyses.

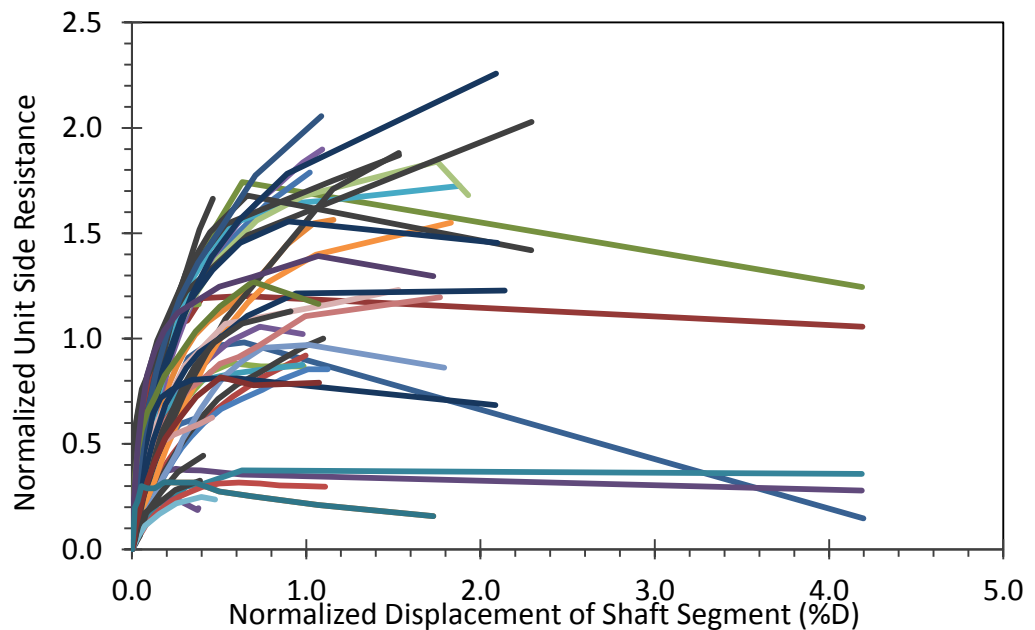


Figure 5.27. Normalized load transfer response in side resistance with respect to predicted ultimate values for uncased segments of test shafts at the Frankford site.

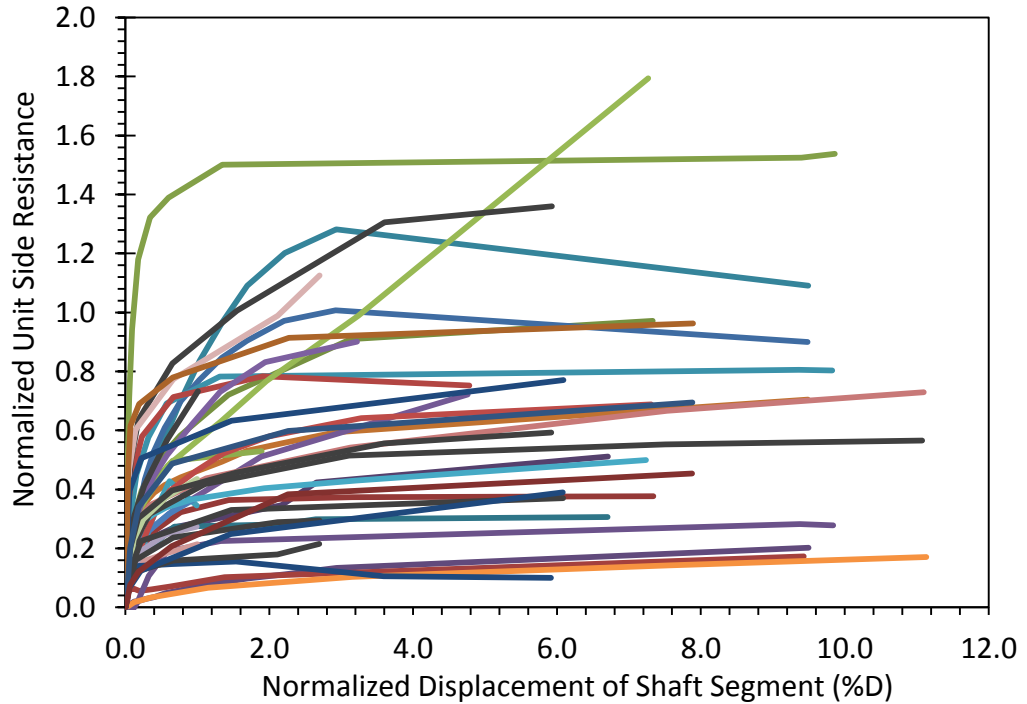


Figure 5.28. Normalized load transfer response in side resistance with respect to predicted ultimate values for uncased segments of test shafts at the Warrensburg site.

As shown in Figures 5.27 and 5.28, the variability of these normalized load transfer curves is greater than observed when the load transfer curves are normalized using the maximum measured resistance presented previously in Figures 5.17 and 5.18. The additional variability is a result of including variability and uncertainty in the predicted ultimate resistance, in addition to variability and uncertainty in the mobilization of resistance. Furthermore, additional scatter is introduced because Figures 5.27 and 5.28 include results from different strata and the predicted ultimate resistance from some strata may be greater than or less than the actual measured ultimate resistance in individual strata. The magnitude of normalized unit side resistance ranges from 0.0 to 2.3, not 0.0 to 1.0 as enforced when normalizing to the

maximum measured resistance. It is interesting to note that the maximum mobilized resistance for load transfer curves from the Frankford site (Fig. 5.27) is generally distributed around unity, while the maximum mobilized resistance for the Warrensburg site (5.28) largely fall below unity. This suggests that the prediction model (Eq. 5.3) used better reflects the ultimate resistance for the Frankford site than for the Warrensburg site.

The magnitudes of displacements required to mobilize the ultimate resistance is not affected by the normalization method, so the discussions about the displacements required to mobilize the ultimate resistance for the normalized to maximum measured values in Section 5.3.1 apply here. For the Frankford site, the displacement required to mobilize the ultimate side resistance is approximately 0.3 to 2% of the shaft diameter, while for Warrensburg site, displacements in the range of from 0.2 to 11% of the shaft diameter are required.

5.3.2.c. Mobilized Tip Resistance – Normalized to Predicted Ultimate Values

Figures 5.29 and 5.30 show the normalized load transfer response in tip resistance for load test measurements at the Frankford and Warrensburg sites, respectively, using predicted ultimate values for normalization. The predicted ultimate values were calculated from Equation 5.15. Unlike when normalizing using the maximum measured resistance, *no* extrapolation for the ultimate tip resistance was needed when normalizing with predicted ultimate values.

For the Frankford site, the curves are very concentrated with much less scatter compared to the same type of curves obtained when normalizing to the maximum measured resistance in Figure 5.23. The two shafts with the most complete measurements, F4 and F6, are almost on top of each other. One of the attributes for the concentration of the curves is that most of shaft tips rest on the same layer of shale (Figure 5.4), thus the tip resistances of most shafts were normalized with the same predicted ultimate values. Furthermore, no extrapolation was used in obtaining these normalized unit tip resistance curves.

Curves from tests at the Warrensburg site are more scattered when normalizing to the maximum measured resistance in Figure 5.24. This is considered to be a result of both the mobilization and the scatter in the geomaterial strength of the Warrensburg load test site.

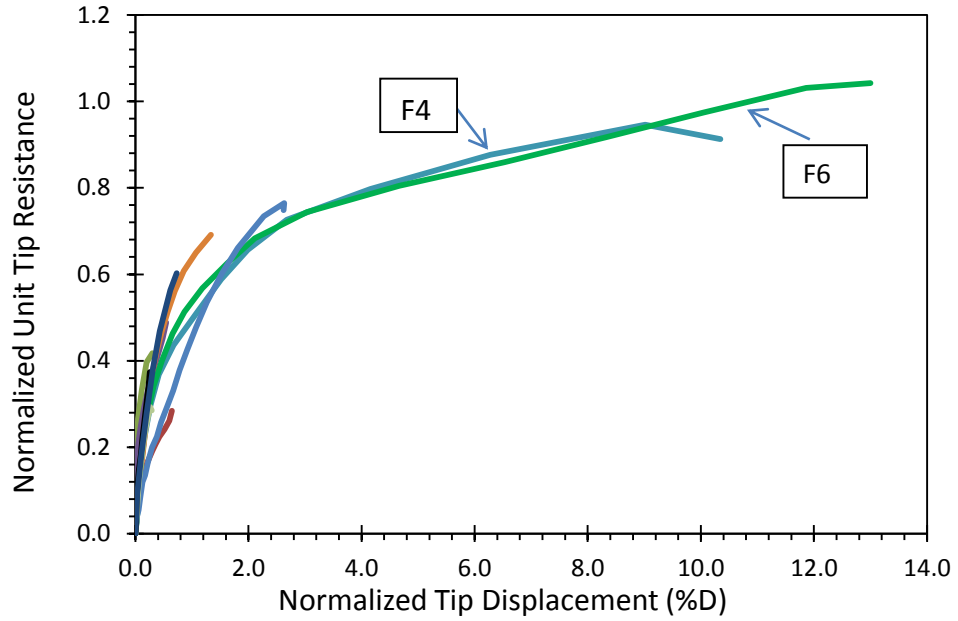


Figure 5.29. Normalized load transfer response in tip resistance with respect to predicted ultimate values of test shafts at the Frankford site.

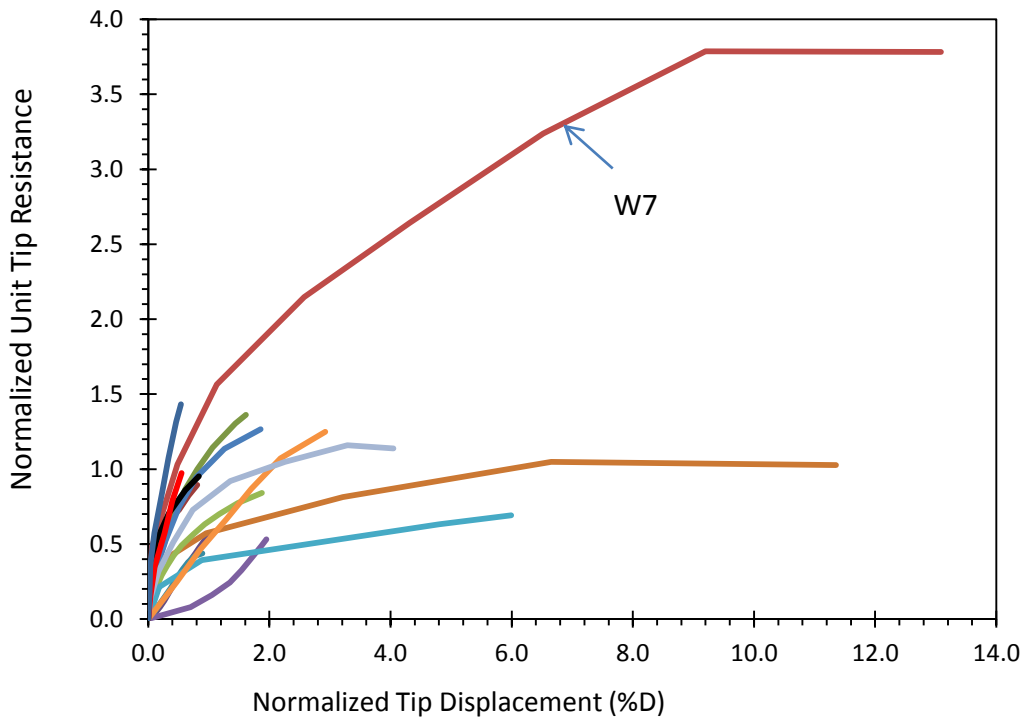


Figure 5.30. Normalized load transfer response in tip resistance with respect to predicted ultimate values of test shafts at the Warrensburg site.

For the unit tip resistance, the response normalized to the maximum predicted resistance for both the Frankford and Warrensburg sites are concentrated below unity. This, however, does not indicate that the predictive model is good or poor, because the ultimate tip resistance was not reached for many test shafts. For the Warrensburg site, a curve that has a magnitude of normalized unit tip resistance as large as 3.8 exists, and it seems to be an outlier. The shaft was W7. The curve follows a common pattern, and its slope is similar to those for other test shafts; therefore, it was judged as normal and the curve was not eliminated from later analyses.

5.4. Important findings of the chapter

Compared to the O'Neil and Reese curves (O'Neil and Reese, 1999), the measured load-transfer curves from load tests at the Frankford and Warrensburg sites are somewhat different. The displacement required to fully mobilize side resistance is greater than the 2% of shaft diameter suggested by the O'Neil and Reese curves and can be as much as 10% of the shaft diameter. Similarly for tip resistance, displacement required to mobilize the ultimate resistance exceeds 5% and may reach as much as 12% of the shaft diameter. This may affect the conventional drilled shaft service limit state design, which considers that shaft resistance is fully mobilized after the shaft displacement reaches 5% of the diameter.

The range of variability of the normalized unit side and tip resistances in shale is significantly larger than the range provided by O'Neil and Reese (1999). This indicates that if O'Neil and Reese's range of variability were to be used for later probabilistic

analyses for the service limit state, the results would be unconservative, and the target probability of failure may not reflect the actual probability of failure.

Differences in the amount of scatter for load transfer curves normalized using the maximum measured resistance (or estimated values of the maximum measured resistance when considering tip resistance) and using the predicted ultimate resistance are attributed to the fact that the scatter reflects different sources of variability and uncertainty. Load transfer curves normalized to the maximum measured resistance include no scatter due to variability and uncertainty in the ultimate resistance, and therefore, reflect only the variability and uncertainty in mobilization of the resistance. In contrast, load transfer curves normalized to the predicted ultimate resistance include variability and uncertainty that can be attributed to both mobilization of the resistance as well as the magnitude of the ultimate resistance.

Normalizing using predicted values for ultimate unit side and tip resistance avoids the problem described in Section 5.3.1.b, where extrapolation is needed to estimate the ultimate resistance when the test loads do not mobilize the ultimate resistance. However, normalization using predicted values also introduces additional scatter into comparison of normalized load transfer curves because the measured or actual ultimate resistance for a particular shaft segment may not be consistent with the ultimate resistance predicted using a given model. As such, the resulting normalized unit resistance will not necessarily approach a value of unity, but may approach values

greater than or less than unity depending on the relative magnitude of the predicted and measured ultimate resistance.

5.5. Summary

Results of a series of full-scale load tests were presented. Data from the load tests were processed and used to develop load-transfer curves. The load-transfer curves were developed using two different approaches to normalization: normalizing to the maximum measured resistance and normalizing to the predicted ultimate resistance. The developed load transfer curves were used for regression analyses to establish load transfer models and their variability and uncertainty as presented and described in Chapter 6. The developed load transfer curves are the critical component for the calibration of service limit state resistance factors and will be discussed further in later chapters.

Chapter 6. Development of Load Transfer Models

6.1. Introduction

This chapter describes work performed to develop load transfer models to reflect the field load test data presented in Chapter 5. Analyses of the data were performed using several regression approaches. The variability and uncertainty were quantified for the best model(s) fitted to the measurements.

6.2. Approach to Model Development

Models to reflect mobilization of side and tip resistance for drilled shafts in shale were empirically developed by performing regression analyses for the measurements described in Chapter 5. The observational data were fitted using five different functional forms; each form is a nonlinear combination of model parameters and axial displacement. These include a *power* function:

$$f(x) = m * x^n \quad (6.1)$$

an *exponential* function:

$$f(x) = 1 - \exp(c * x) \quad (6.2)$$

a *logarithm* function:

$$f(x) = d * \ln(x) + e \quad (6.3)$$

a *rational* function:

$$f(x) = \frac{p_1x+p_2}{x+q_1} \quad (6.4.)$$

and a *hyperbolic* function:

$$f(x) = \frac{x}{ax+b} . \quad (6.5)$$

In Equations 6.1 through 6.5, m , n , c , d , e , p_1 , p_2 , q_1 , a and b are fitting parameters. Each of these functions is “reasonably” simple and practical, and each is capable of representing the general load transfer response observed in the load test measurements.

Each function was fitted to the normalized load transfer measurements and analyzed to find the model that best reflects the data and their variability/uncertainty. Important criteria used for choosing the best model is based on the coefficient of determination (R^2) and/or the root-mean-square error ($RMSE$). R^2 is most often used to predict future outcomes and is used to describe how well a regression line fits a particular set of data. Values of R^2 range from 0 to 1.0. The greater the R^2 value, the better the regression line represents (fits) the data. The $RMSE$ is a frequently used measure of the differences between values predicted by the regression model and the observed data, with lower values of $RMSE$ indicating better model fits. The relationship between R^2 and $RMSE$ is inversely proportional, and both were used in this research to evaluate the quality of the model fits.

6.3. Options for regression analyses

Unit side and tip resistance can be normalized using maximum measured values or predicted ultimate values when developing load transfer curves (Chapter 5).

Regression analyses were performed for the data normalized using each normalization approach. Additionally, both ordinary least squares and weighted least squares were performed. Finally regression analyses were performed for the collective set of data from all load tests as well as for individual load transfer curves from each test. These options are described in more detail in the following subsections.

6.3.1 Ordinary Least Squares versus Weighted Least Squares Regression

Two different types of regression analyses were performed: *ordinary least squares* regression and *weighted least squares* regression. Figure 6.1 illustrates the differences between these two regression analysis procedures. Ordinary least squares regression is based upon an assumption that the data exhibit constant variance (or constant conditional standard deviation) about the trend line (Ang and Tang, 2004). The constant standard deviation, $\sigma_{y/x}$, over the range of the data, is shown in Figure 6.1a by the parallel bounds. The assumption of constant variance is commonly exhibited in many data sets. In ordinary least squares regression, parameter estimates for the selected regression functions are found by minimizing the sum of the squared residuals between the data points and the predicting model.

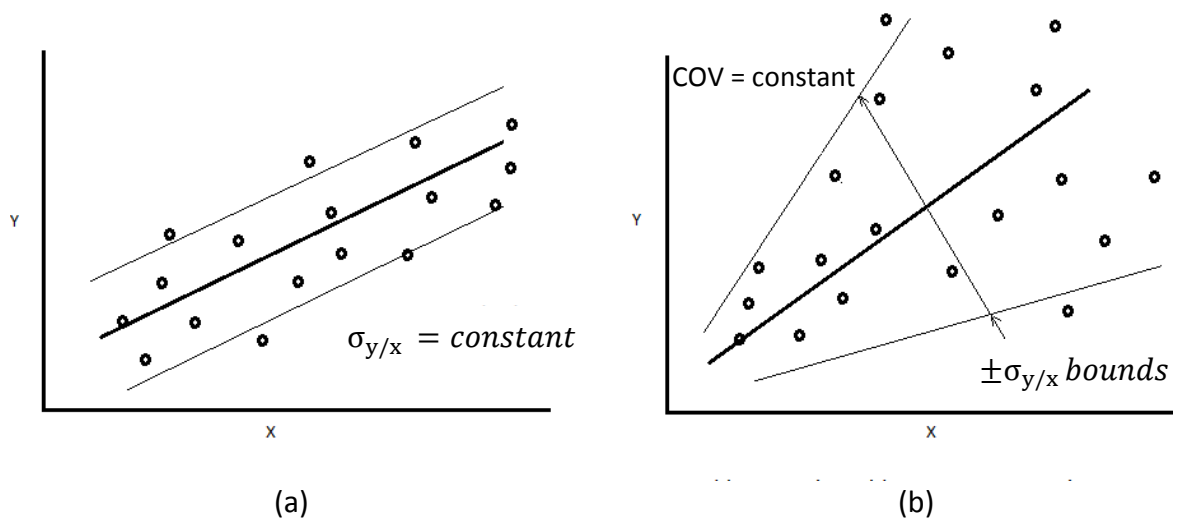


Figure 6.1. Illustration of regression under assumptions of: (a) constant standard deviation and (b) non-constant standard deviation (after Ang and Tang, 1974).

In contrast, some data sets may not exhibit constant standard deviation about the trend, but rather may exhibit standard deviation that depends on the value of the predictor variable, as illustrated in Figure 6.1b. In such cases, weighted least squares regression is preferable to ensure that each data point has an appropriate influence on the final parameter estimates. In weighted least squares regression, the *weighted* sum of the squared residuals between the data points and the predicting model is minimized to determine the parameter estimates.

A variety of different weights can be used in weighted least squares regression, with the weights dictating the values of the parameter estimates as well as how the conditional standard deviation varies with the magnitude of the predictor variable. This study used regression weights that were chosen to be inversely proportional to the magnitudes of the predictions, i.e., to be equal to $1/y$, where y is the value of the prediction for a given x (Ang and Tang, 1974). Using such weights produces the convenient result of having a constant coefficient of variation (standard deviation

divided by the mean), while also often representing the scatter about the regression line well for many data sets.

Ordinary least squares regression analyses were conducted using standard and customized MATLAB[®] functions. Weighted least squares analyses were performed using MATLAB[®] computer program provided in Appendix F (Loehr, 2010). Both ordinary and weighted least squares regression analyses were performed for each of the functional forms described above, and comparisons were made to establish which form(s) best fit with the measured load test results as described later in this chapter.

6.3.2 Collective versus Individual Regression Analyses

Regression analyses were performed considering the “collective” set of load test measurements, as well as considering each load transfer measurement “individually” (i.e., load transfer measurements for a single shaft segment). Regression using the collective set of available measurements produces a single load transfer model for side resistance and a single load transfer model for tip resistance based on the collection of load transfer measurements from shaft segments of all tests. Regression analyses for individual segments of each shaft produce a “best fit” load transfer model for each shaft segment. The best fit parameters for each shaft segment can then be collectively analyzed to determine mean values for the function parameters and the variability of the parameters. These mean values can be used to establish one model for unit side resistance and one model for tip resistance. In this document, the former approach is referred to as the “collective” approach while the latter is referred to as the “individual”

approach. The individual approach was used by Phoon and Kulhawy (2009). Regression analyses for both collective and individual approaches were performed for this research.

The methods for representing variability and uncertainty of a model depend on the approach of analyses. For “collective” models established from regression on the collective set of load transfer curves, the variability and uncertainty of the respective models are established from the variability of specific measurements about the model trend, and are represented by the conditional standard deviation about the best fit trend. If Y_{model} is a vector of N predictions, and Y is the vector of the true values, then the unbiased conditional standard deviation is calculated using the following equation:

$$\sigma = \sqrt{\frac{1}{N-k} \sum_{i=1}^N (y_i - y_{model})^2} \quad (6.6)$$

where k is the number of variables. For the load transfer model, k is equal to 2 (normalized unit resistance variable, and normalized displacement variable). The *RMSE* of a fitting model, which is one of the outcomes of regression analyses, is calculated as:

$$RMSE = \sqrt{\frac{1}{N} \sum_{i=1}^N (y_i - y_{model})^2} \quad (6.7)$$

Equations 6.6 and 6.7 are similar and usually give the same result if a large quantity of data is considered. *RMSE* is often considered to be the prediction of the conditional standard deviation for regression analyses, where the bias of the regression model is considered to be zero. The sample size of the field test data for this study is large, because N is 1405 for side resistance and 242 for tip resistance. The large quantity of data results in an *RMSE* similar to the conditional standard deviation. The variability

and uncertainty of the respective models from collective approach are represented by the conditional standard deviation, which is taken to be equal to the *RMSE* in this project.

For regression analyses performed for individual shaft segments, an *RMSE* is obtained for each each shaft segment. *RMSE* for a single shaft segment is usually small because little scatter exists within the data of one shaft segment. If the variability of load transfer for all data were represented by the average value of *RMSE* from all shaft segments, it would be small, and variability and uncertainty of the load transfer model would not be correctly reflected. For individual approach, the variability and uncertainty of the model is represented by the variability and uncertainty in the model parameters determined from the individual regression analyses.

Figure 6.2 shows a flowchart depicting the regression analyses presented in this chapter. “OLS” and “WLS” in the figure represent ordinary least squares regression and weighted least squares regression, respectively. Products of the regression analyses presented in this chapter are two “final models” for load transfer in side and tip resistance for both measurements normalized to the maximum measured resistance and normalized to the predicted ultimate resistance.

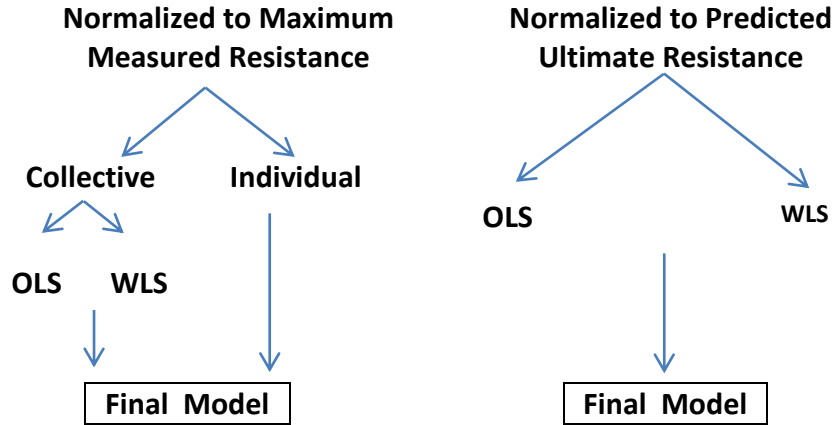


Figure 6.2. Flowchart of regression analyses for both side and tip resistances.

The final models for side resistance and tip resistance from each approach of normalization were found from regression analyses. The data from the two approaches were different, so the best models from the approaches could not be compared directly, but subsequently were used for SLS probabilistic analyses. Comparisons of the models from the two approaches then can be made to choose the better approach of the two, as presented in Chapter 8.

6.4. Regression Analyses for Side Resistance – Normalized to Maximum Measured Resistance

This section reports the regression analyses for unit side resistance normalized to maximum measured values. As discussed in previous sections, two pairs of options exist for performing regression analyses. The first option is to use ordinary least squares regression, with the assumption of constant standard deviation, or weighted least squares regression, which leads to a constant coefficient of variation. The second option is to perform regression on the collective data set versus performing regression on

individual test results. Both methods are used in the regression analyses to choose the load transfer model as presented in the following sections. The subsections which follow demonstrate the regression analyses using two choices - the collective approach (6.4.1) and the individual approach (6.4.2).

6.4.1. Regression Analyses for Side Resistance - Collective Measurements

Results of regression analyses for the collective side resistance data normalized to the maximum measured resistance is presented in this section. Five functional models were used for the analyses. The analysis was performed using both ordinary least square regression and weighted least square regression as follows.

The *Power function* was used for the ordinary least squares regression and the equation obtained is:

$$t = m * x^n = 0.75 * z^{0.22} \quad (6.8)$$

where

t = normalized unit side resistance,

z = normalized displacement of local shear zone, and

m and n = fitting parameters.

The regression analysis gave an R^2 of 0.56 and an $RMSE$ of 0.20. Weighted least squares regression using a similar function produced the equation:

$$t = m * x^n = 0.84 * z^{0.34} \quad (6.9)$$

with the *RMSE* of 0.50. Ordinary least squares and weighted least squares gave two equations, with slightly different fitting parameters. The regression lines, the data and the confidence bounds for new observations at 68.2% ($\pm\sigma_{y/x}$) are presented in Figure 6.3 for ordinary least squares regression and in Figure 6.4 for weighted least squares regression.

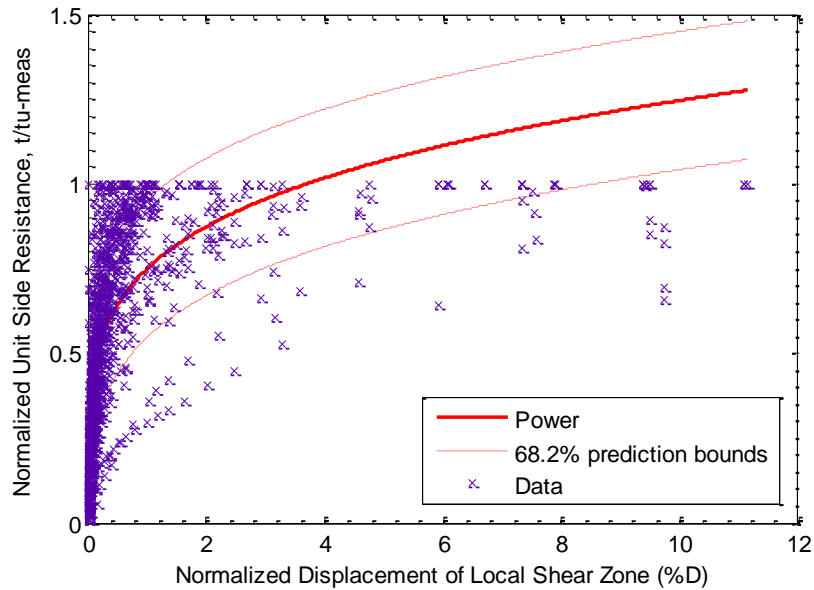


Figure 6.3. Power function from ordinary least squares regression.

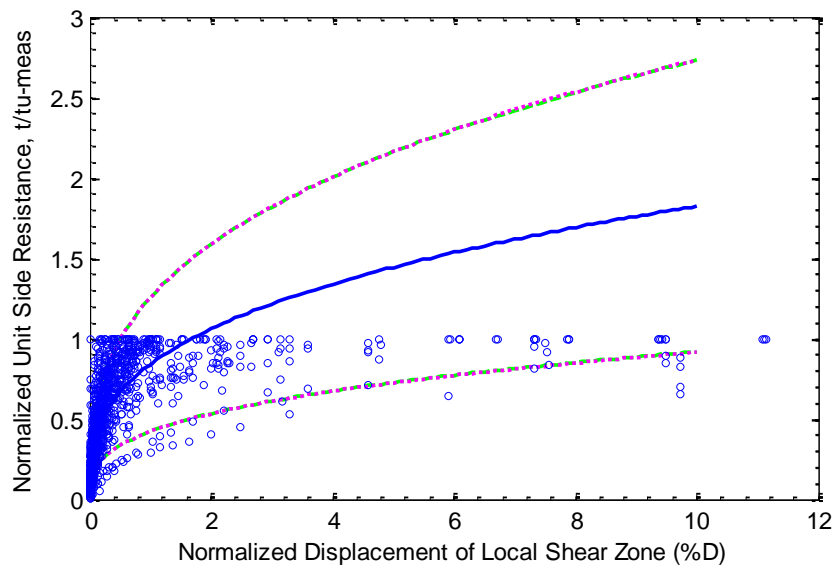


Figure 6.4. Power function from weighted least squares regression.

The regression lines fit the data well at normalized displacements less than about 4% (ordinary least squares) and 2% (weighted least squares). Then the models overestimate the mobilized unit side resistance at greater normalized displacements. This overestimation increases without bound, and it is unfavorable.

The 68.2% prediction bounds for ordinary least squares regression are “parallel” to the regression line (Figure 6.3 and expanded scale in Figure 6.5). The vertical distance from a bound to the regression line is a constant and is equal to the model’s *RMSE* (or one conditional standard deviation $\pm\sigma$). In contrast, the 68.2% prediction bounds for weighted least squares regression are further from the regression line, resulting in a constant coefficient of variation (COV). The prediction bounds from both ordinary and weighted least squares regressions seem to underestimate the variability at displacements less than 0.05% D (Figure 6.4 and expanded scale in Figure 6.6). The prediction bounds of the model from weighted least squares are wider (higher *RMSE* 0.50) compared to those from ordinary least squares (lower *RMSE* of 0.20). Because the fitting parameters n of 0.22 and 0.34 (Equations 6.8 and 6.9), which are less than 1.0, the power functions have a disadvantage in that the initial slopes of the functions are infinite. This poses numerical problems in modeling load transfer, which is a practical problem. In general, the power function may not be the best choice to model the data and their variability.

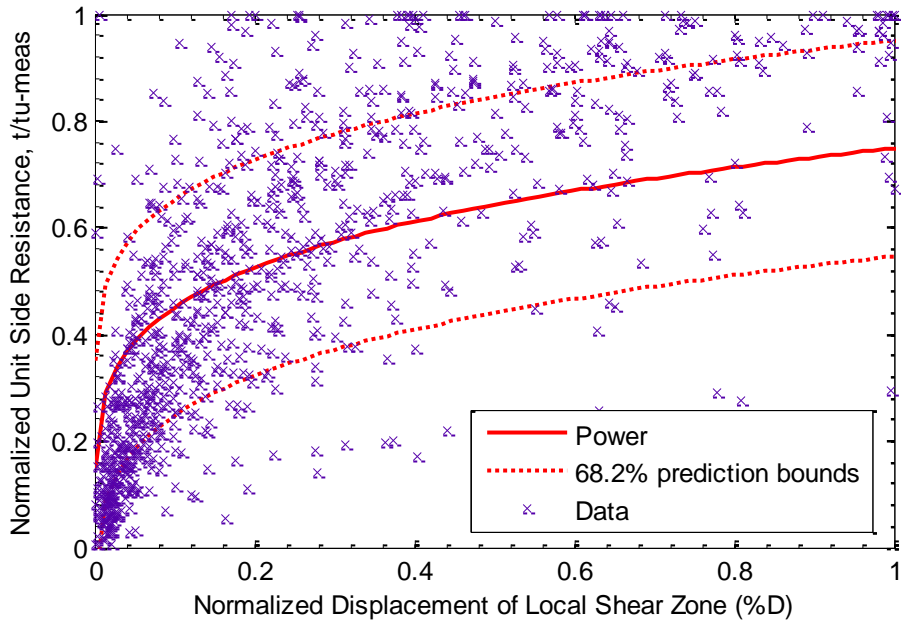


Figure 6.5. Power function from ordinary least squares regression—expanded scale.

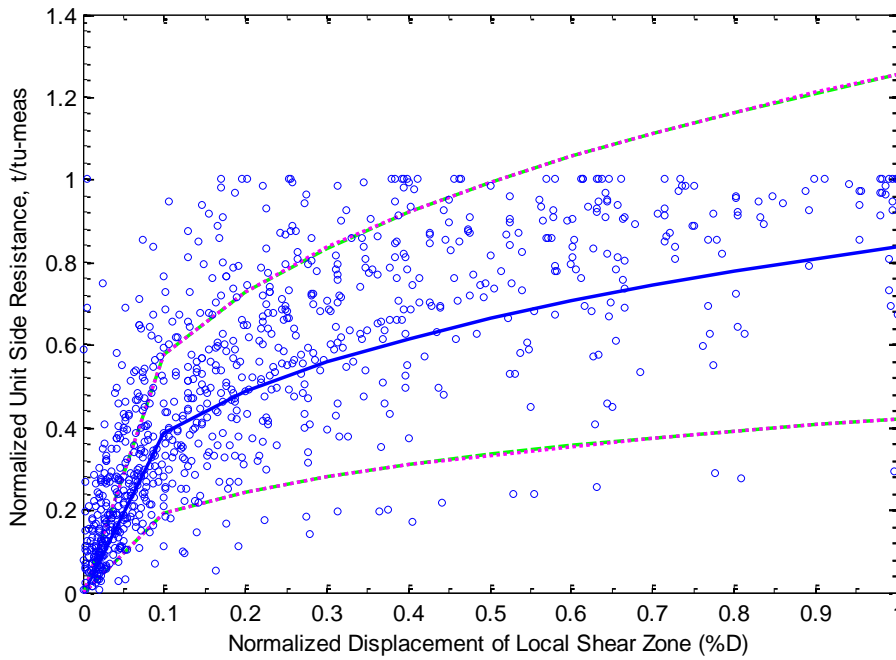


Figure 6.6. Power function from weighted least squares regression—expanded scale.

The *exponential function* obtained from ordinary least square regression is in the form:

$$t = 1 - \exp(c * z) = 1 - \exp(-4.06 * z) \quad (6.10)$$

where

t = normalized unit side resistance,

z = normalized displacement of local shear zone, and

c = fitting parameter.

The fit has R^2 of 0.60 and $RMSE$ of 0.19. Using the weighted least square regression, the exponential equation is:

$$t = 1 - \exp(c * z) = 1 - \exp(-9.67 * z) \quad (6.11)$$

with a large value of $RMSE$ of 1.41. Ordinary least squares and weighted least squares regressions gave different equations with significantly different fitting parameters. The models, the data and the confidence bounds for new observations at 68.2% are presented in Figure 6.7 for ordinary least squares regression and in Figure 6.8 for weighted least squares regression.

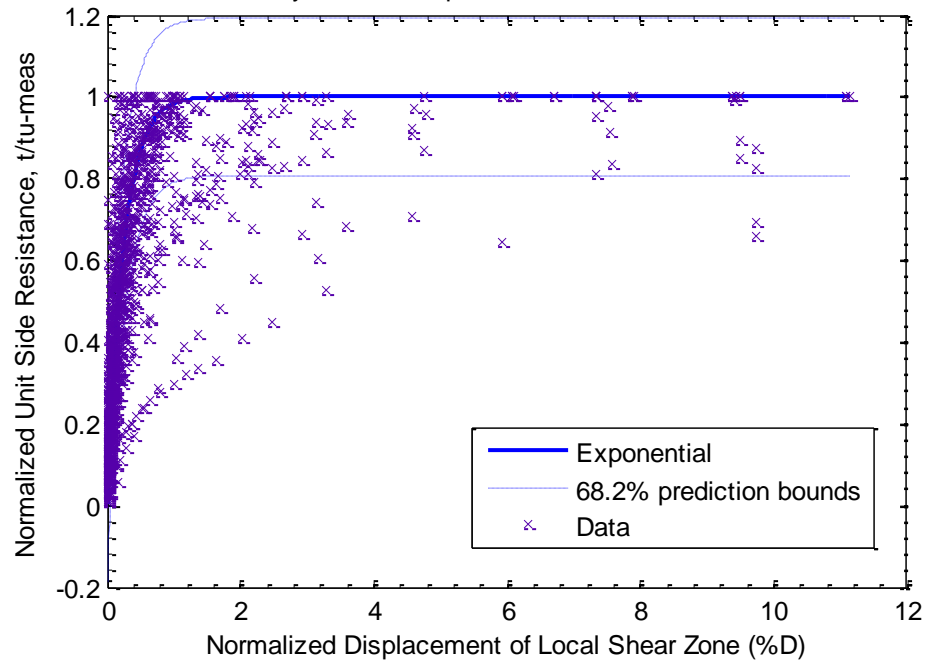


Figure 6.7. Exponential function from ordinary least squares regression.

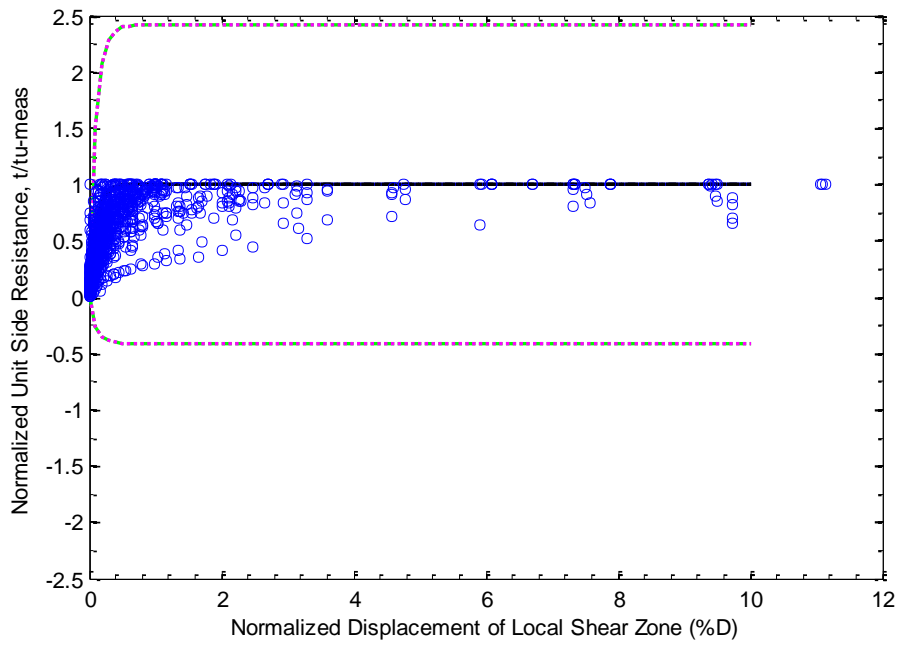


Figure 6.8. Exponential function from weighted least squares regression.

The exponential models track the load transfer data well for the area where most of the data points are clustered. The regression lines also match the upper bound well. They do not match some of the curves that are “outliers.” If only displacement less than 2% D is considered, the exponential function would be the best of the five functions. The prediction bounds obtained from ordinary least squares appear to fit with the data; however, the bounds obtained from weighted least squares regression appear unreasonable with the lower bound passing to a value of -0.5 . The two bounds seem to cover 100% of the data points, not about 68%, as should be the case.

The *logarithm function* obtained using ordinary least squares regression is in the form:

$$f(x) = d * \ln(x) + e = 0.15 * \ln(z) + 0.79 \quad (6.12)$$

where d and e are fitting parameters. The ordinary least squares regression gave an R^2 of 0.63 and an *RMSE* of 0.19. The logarithm function from weighted least squares is

$$f(x) = d * \ln(x) + e = 0.09 * \ln(z) + 0.67 \quad (6.13)$$

The weighted least squares regression gave an *RMSE* of 0.48. The fitting models with the plus and minus one standard deviation prediction bounds are shown in Figures 6.9 (ordinary least squares) and 6.10 (weighted least squares).

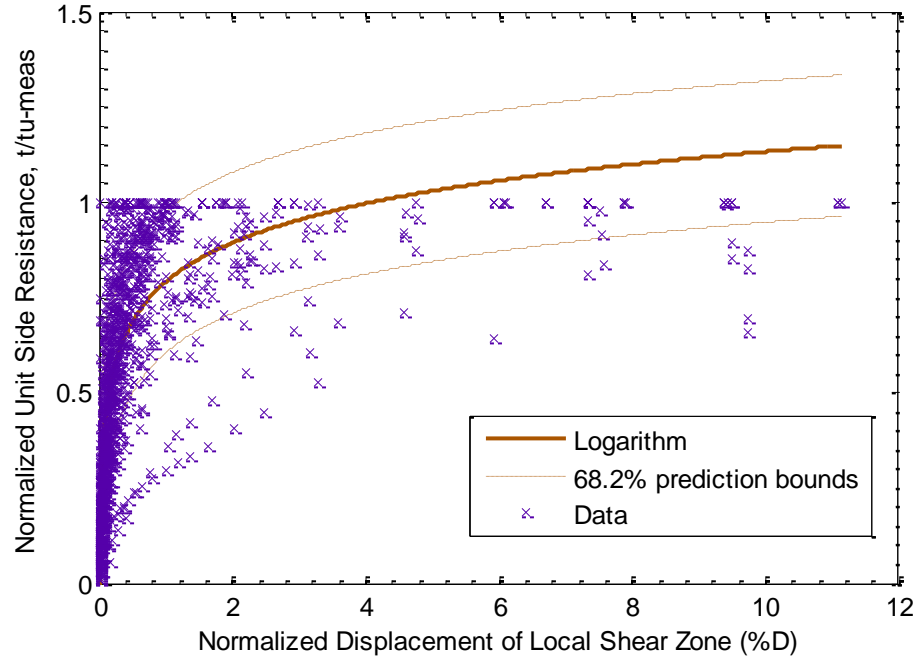


Figure 6.9. Logarithm function from ordinary least squares regression.

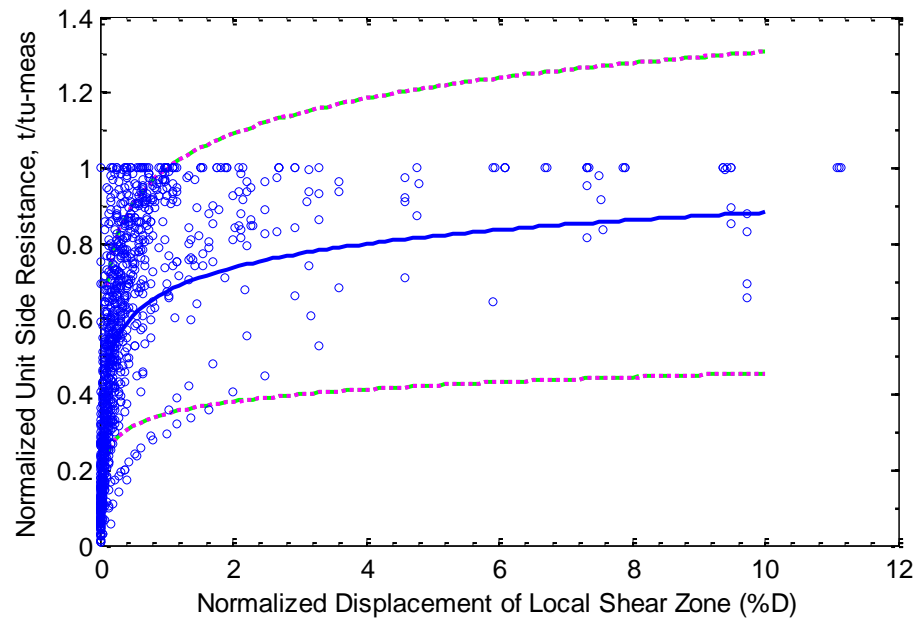


Figure 6.10. Logarithm function from weighted least squares regression.

The regression line of ordinary least squares regression reflects the data well when the normalized displacement is small, and the model overpredicts future outcomes at greater displacements, i.e., when the displacement exceeds 4% of the shaft diameter. The plus and minus one standard deviation bounds are parallel to the model, with the vertical distance from the model of 0.19, which are similar to results for the power and exponential functions.

The regression line from the weighted least squares regression analysis reflects the observed load transfer data well, where the model lies in the center of the of the data cluster for the whole range of the displacements. The logarithm regression line obtained from weighted least squares better reflects data than the model obtained from the ordinary least squares. The model from weighted least squares regression gave much higher variability/uncertainty of prediction bounds for future outcomes (*RMSE* of 0.48) than the prediction bounds from ordinary least squares analysis (*RMSE* of 0.19), which is unfavorable.

The *rational function* that was obtained from ordinary least squares regression is represented by the equation:

$$t = \frac{p_1x+p_2}{x+q_1} = \frac{0.95*z+0.007}{z+0.14} \quad (6.14)$$

where p_1 , p_2 , and q_1 are fitting parameters. The fit gave an R^2 value of 0.68 and an *RMSE* of 0.17. The R^2 is high, and the *RMSE* is the lowest value of the four functional models considered so far, which means that the rational model predicts future data with the lowest variability and uncertainty. The model obtained from weighted least square regression yields an *RMSE* of 0.49 and the equation:

$$t = \frac{p1*z+p2}{z+q1} = \frac{1.01*z+0.02}{z+0.21} \quad (6.15)$$

The fitting models with the plus and minus one standard deviation prediction bounds are shown in Figures 6.11 (ordinary least squares) and 6.12 (weighted least squares). Both rational regression lines follow the data pattern well.

Figures 6.13 and 6.14 present the rational fitting models in an expanded scale for a magnified view of the origin zone. When the displacement is less than 0.05% D, the prediction bounds for the ordinary least squares regression seems to overpredict the variability of the data, and the bounds from the weighted least squares regression better reflect the variability of the data. However, with larger displacements, prediction bounds from ordinary least square regression seem to cover 68.2% of the data as they should . The bounds from weighted least squares regression overestimate the variability of the future outcomes when the bounds cover up to 90% of the data, which is unfavorable.

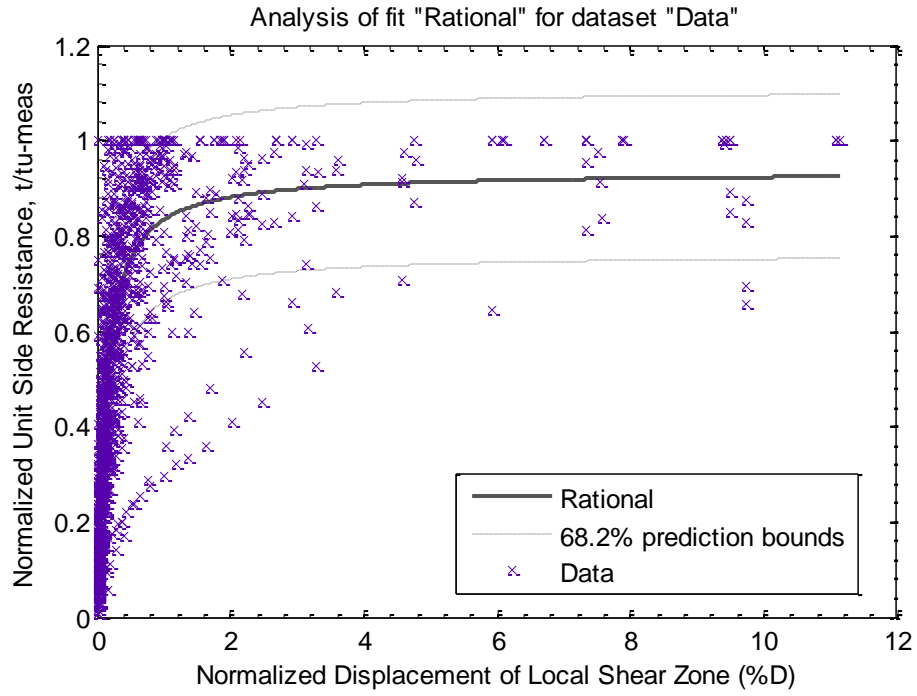


Figure 6.11. Rational function from ordinary least squares regression.

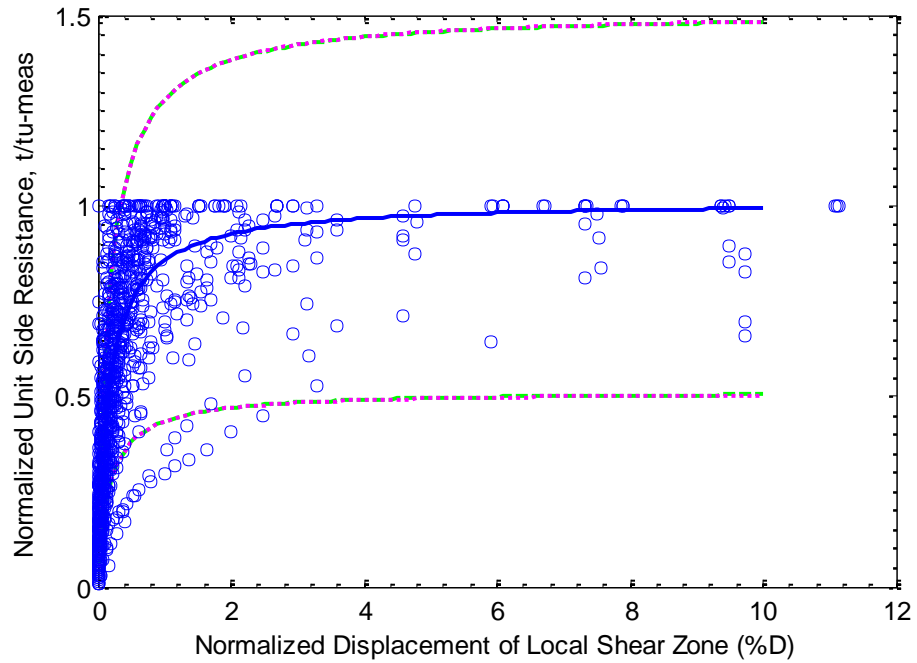


Figure 6.12. Rational function from weighted least squares regression.

The rational model regression line obtained from ordinary least squares regression passes through the origin, while the regression line from weighted least squares regression does not. The rational model obtained from weighted least squares regression is not considered a good fit in terms of either the regression line or the prediction bounds.

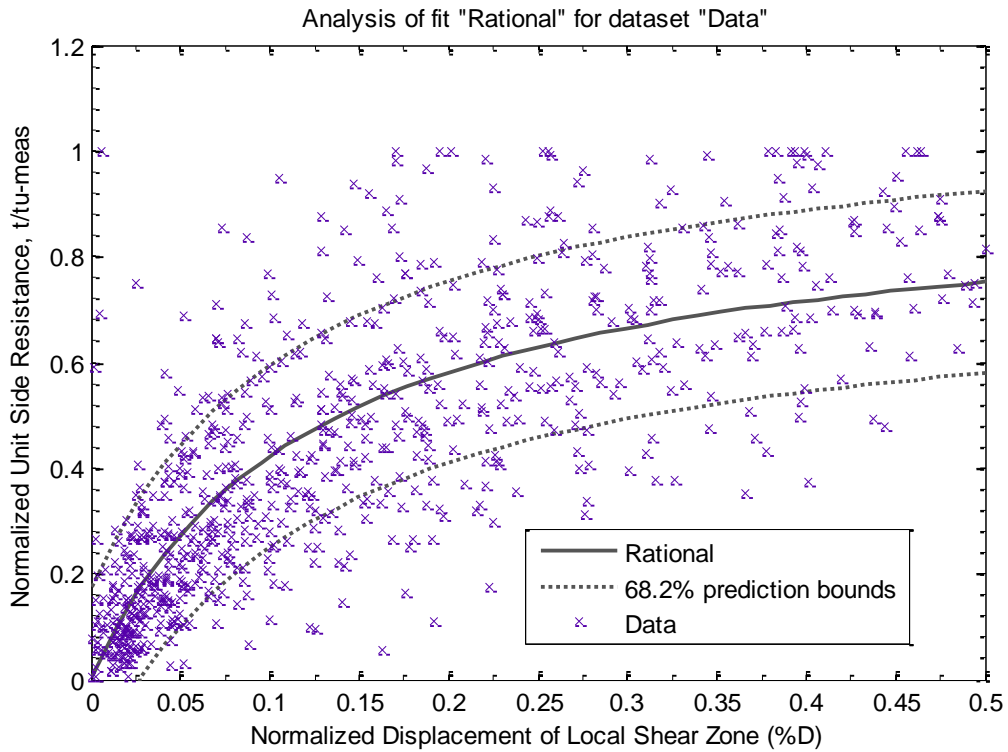


Figure 6.13. Rational fitting for side resistance from ordinary least squares regression—expanded scale.

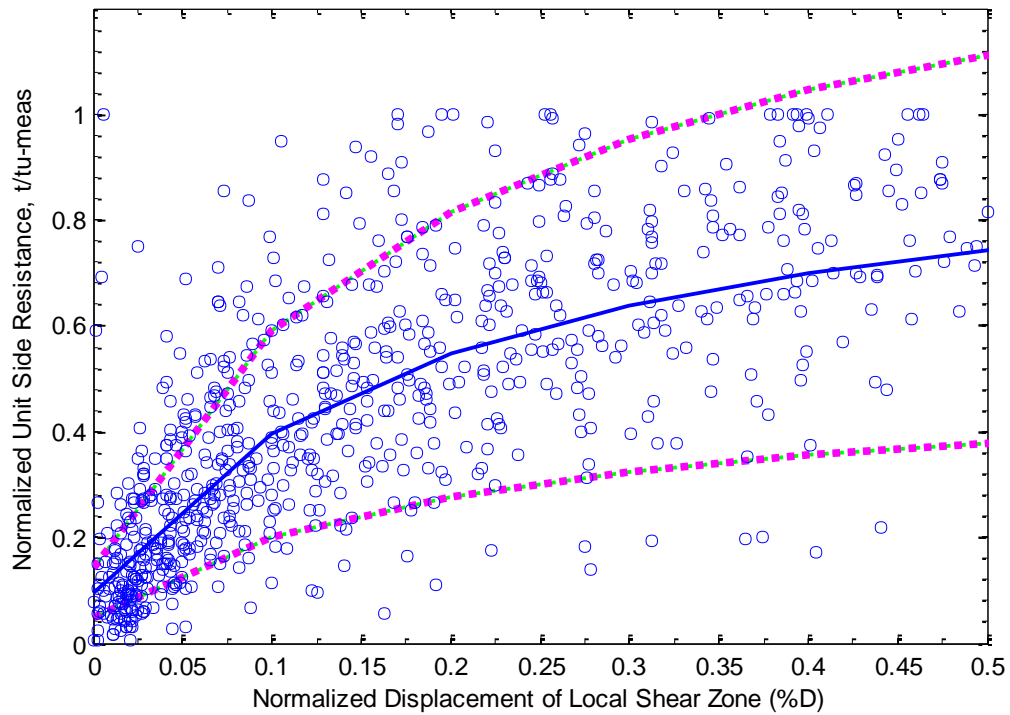


Figure 6.14. Rational function from weighted least squares regression—expanded scale.

The *hyperbolic function* obtained when using ordinary least squares analysis gives:

$$t = \frac{z}{az+b} = \frac{z}{1.07*z+0.13} \quad (6.16)$$

where a and b are fitting parameters. The regression analysis had an R^2 of 0.68, and gave the lowest $RMSE$ of 0.17. The hyperbolic model from the weighted least square regression is:

$$t = \frac{z}{az+b} = \frac{z}{1.07*z+0.13} \quad (6.17)$$

where the $RMSE$ is 0.62. The models, data and prediction bounds are shown in Figures 6.15 and 6.16.

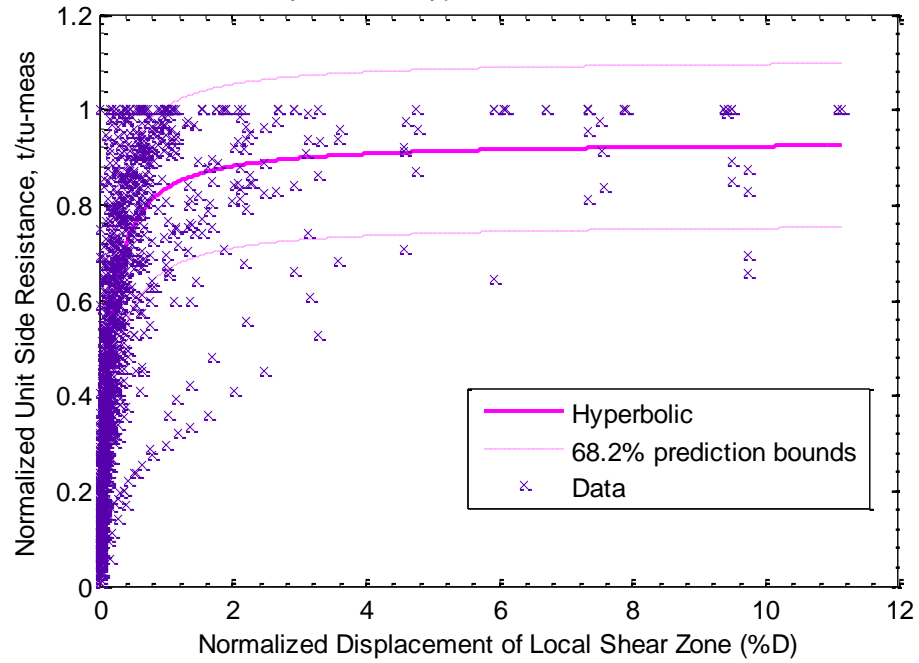


Figure 6.15. Hyperbolic function of fit from ordinary least squares regression.

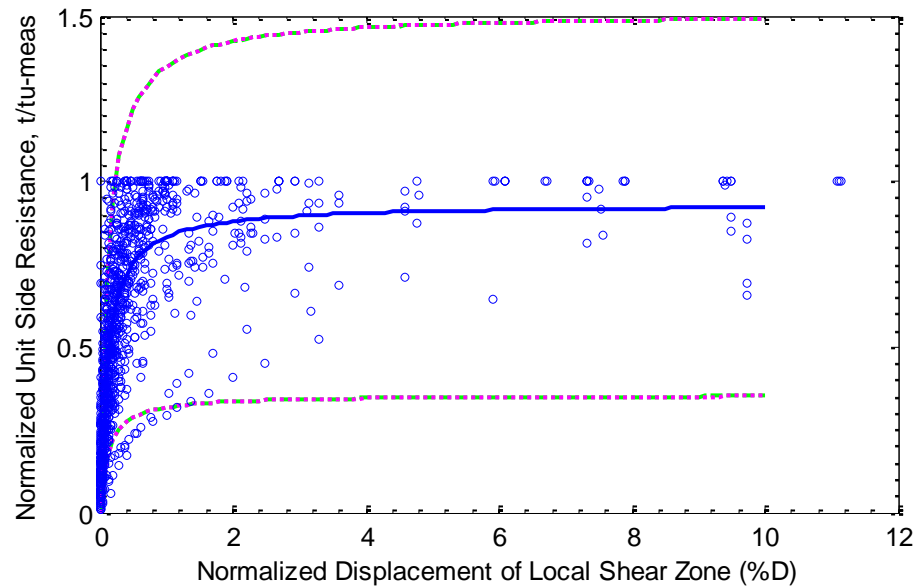


Figure 6.16. Hyperbolic function of fit from weighted least squares regression.

The hyperbolic model is a special form of the rational model, where the fitting parameter p_2 of the rational model is taken to equal zero. This guarantees the regression line always passes through the origin. The favorable feature of the hyperbolic model is

that the regression parameters have physical meaning where parameter a is the reciprocal of the horizontal asymptote, and parameter b is the reciprocal of the initial slope of the regression line or the model.

The ordinary least squares and weighted least squares regression analyses gave the same hyperbolic equation (when two significant numbers are considered for the fitting parameters). This is the only function out of the five functions for which the equations obtained from ordinary least squares and weighted least squares coincide. The model reflects the data well.

The prediction bounds from the two models are different, however. The weighted least squares regression produces a relatively high *RMSE* of 0.48 compared to the ordinary least squares *RMSE* of 0.17. The discussions of the prediction bounds from hyperbolic model are similar to those of the rational models. For ordinary least squares (Figure 6.14), it seems that about 68.2% of the data points are really bounded by prediction bounds and the bounds reflect the variability of the data well.

Within most of the models considered for normalized unit side resistance, the prediction bounds from weighted least squares regression better predict the variability of the data when the displacement is relatively small, usually just less than 0.05% D . When the displacement is larger, the prediction bounds from weighted least square regression always over predict the data variability. The weighted least squares regression gave *RMSE* values that were significantly higher than the *RMSE* values from ordinary least squares regression. Thus, the weighted least squares regression does not properly fit the collective unit side resistance data normalized to the maximum

measured values. Resulting models from ordinary least squares regression are therefore chosen for further analysis.

Table 6.1 summarizes the functions, the R^2 and the $RMSE$ values obtained from the regression analyses. The $RMSE$ s obtained from weighted least squares regression vary significantly. The $RMSE$ range from 0.48 for logarithmic analyses to 1.41 for the exponential function. However, the range of $RMSE$ from ordinary least squares regression is small, from 0.17 (hyperbolic and rational) to 0.2 (power). This indicates that the ordinary least squares regression gives models with little differences in the conditional standard deviation.

Table 6.1. Summary of fitting models for side resistance normalized to maximum measured values using a collective approach.

Type of Function	Regression Type	Equation	R ²	RMS E	Comments
Power	Ordinary least squares	$t = 0.7482 * z^{0.2215}$	0.56	0.2	– Does not fit well when displacement is large; infinity slope at origin; low R ² and high RMSE.
	Weighted least squares	$t = 0.84 * z^{0.34}$	-	0.50	
Exponential	Ordinary least squares	$t = 1 - \exp(-4.057 * z)$	0.6	0.19	+ Fits well when displacement is large; traces the upper bound well. – Low R ² , and high RMSE.
	Weighted least squares	$t = 1 - \exp(-9.67 * z)$	-	1.41	
Logarithm	Ordinary least squares	$t = 0.15 * \ln(z) + 0.79$	0.63	0.19	+ Fits the data relatively well. – Lower R ² , and relatively high RMSE.
	Weighted least squares	$t = 0.09 * \ln(z) + 0.67$	-	0.48	
Rational	Ordinary least squares	$t = \frac{0.95 * z + 0.007}{z + 0.14}$	0.68	0.17	– Does not pass through origin.
	Weighted least squares	$t = \frac{1.01 * z + 0.02}{z + 0.21}$	-	0.49	
Hyperbolic	Ordinary least squares	$t = \frac{z}{1.07 * z + 0.13}$	0.68	0.17	+ Best reflects data, highest R ² and low RMSE.
	Weighted least squares	$t = \frac{z}{1.07 * z + 0.13}$	-	0.62	

Figure 6.17 shows the data with the five regression lines obtained from ordinary least squares regression. The power and logarithm functions underestimate future data when the displacement is smaller than about 4% D, and overestimate future data when the displacement is larger than 4% D. The exponential regression line best reflects the observed data when the displacement is less than about 1% D, and then follows the upper bound of the data when the displacement is larger. However, as discussed

before, the exponential model prediction bounds are too large and overestimate the variability of future outcomes. The other two models, which are rational and hyperbolic, have regression lines that are very close together, both of which reflect the data well. A subtle difference between the two models is that, when the displacement is zero, from the rational equation, unit side resistance is 0.007, which is not strictly zero. The hyperbolic model obtained from ordinary least squares regression best reflects the data measured unit side resistance normalized by maximum measured values.

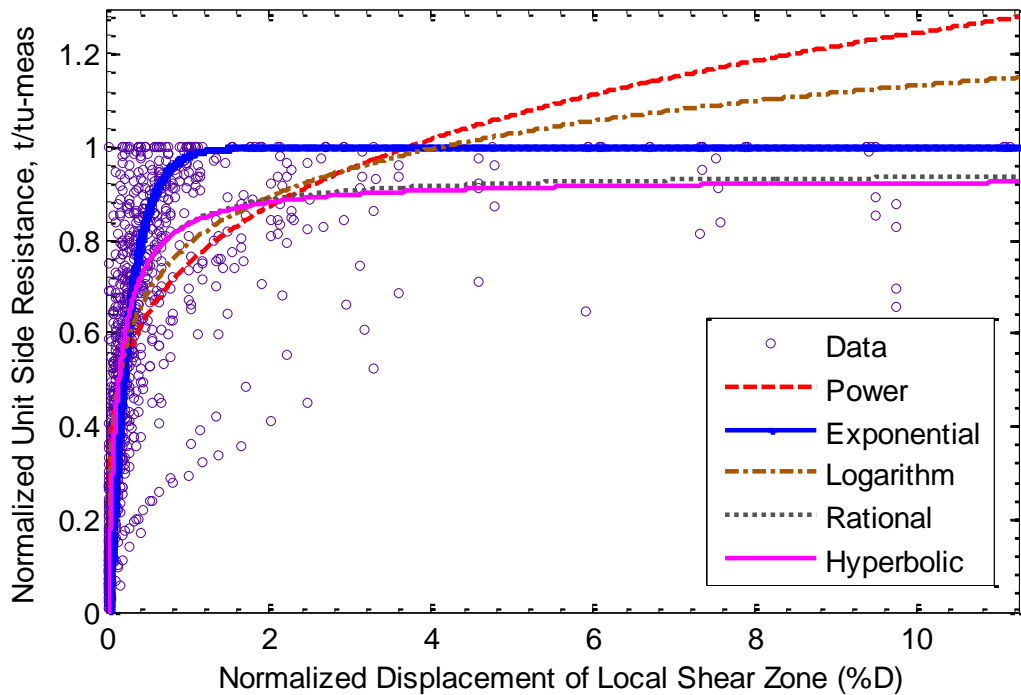


Figure 6.17. Five fitting models for unit side resistance from ordinary least squares regression.

In conclusion, the hyperbolic function is the best function for modeling unit side resistance data normalized to maximum measured values. The hyperbolic regression line best reflects the data, does not contain practical issues such as an infinite slope at

the origin as does the power function, and does not have non-zero response at zero displacement as does the rational function. The model also gives the lowest *RMSE* (0.17) and narrowest conditional standard deviation prediction bounds. The regression parameters have physical meanings - where a parameter is the reciprocal of the horizontal asymptote, and b parameter is the reciprocal of the initial slope of the t - z curve. The hyperbolic function obtained from the above analysis happens to be in the same form as the hyperbolic model favored by Duncan and Chang (1970), and Phoon and Kulhawy (2009). The mathematic expression of the hyperbolic model for side resistance factor is in Equation 6.17.

The variability and uncertainty in the model (Equation 6.17) is reflected by the conditional standard deviation of the data about the model. As discussed in Section 6.5, this conditional standard deviation is considered the same as *RMSE* from the regression analyses and is equal to 0.17. The model and its variability are used subsequently for comparison and further analyses.

6.4.2. Regression Analyses for Side Resistance –Individual Measurements

Previous sections cover regression analyses that were performed collectively for the entire set of load transfer data. This section presents ordinary least squares regression analyses performed for each individual segment. The analyses are for the measure unit side resistance normalized to maximum measured values.

An example of fitting models for data from the shaft segment between strain gauge (SG) 1 and 2 (denoted as F7-12) for test shaft F7 is shown in Figure 6.20. The

rational model is not included because it has a line that coincides with the hyperbolic model. The four regression lines are close to one another. Identifying the best model for each and every shaft segment is difficult. Adopting the results from previous sections, the hyperbolic model was used for analysis in this section. The hyperbolic model for the shaft segment is shown in Figure 6.21.

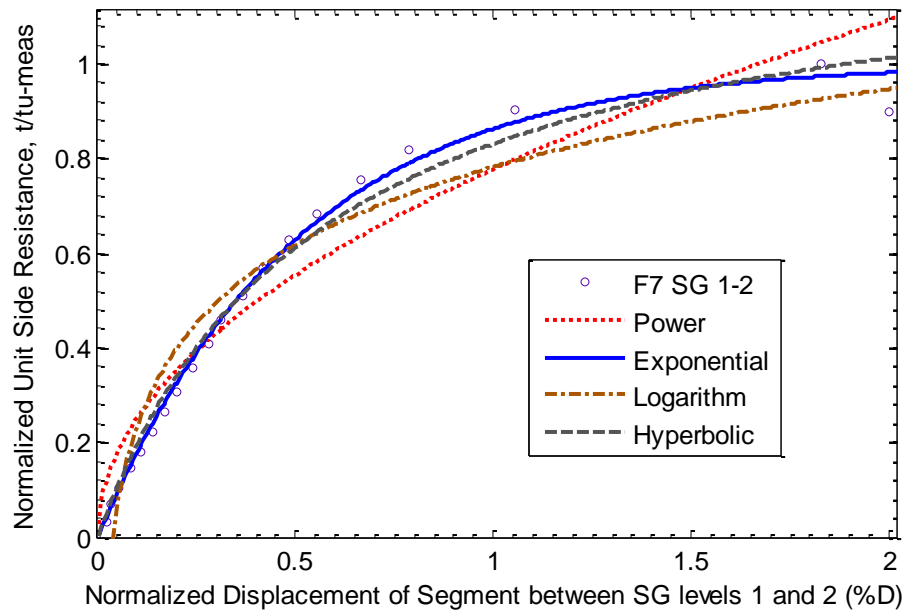


Figure 6.18. Fitting models for shaft segment F7-12.

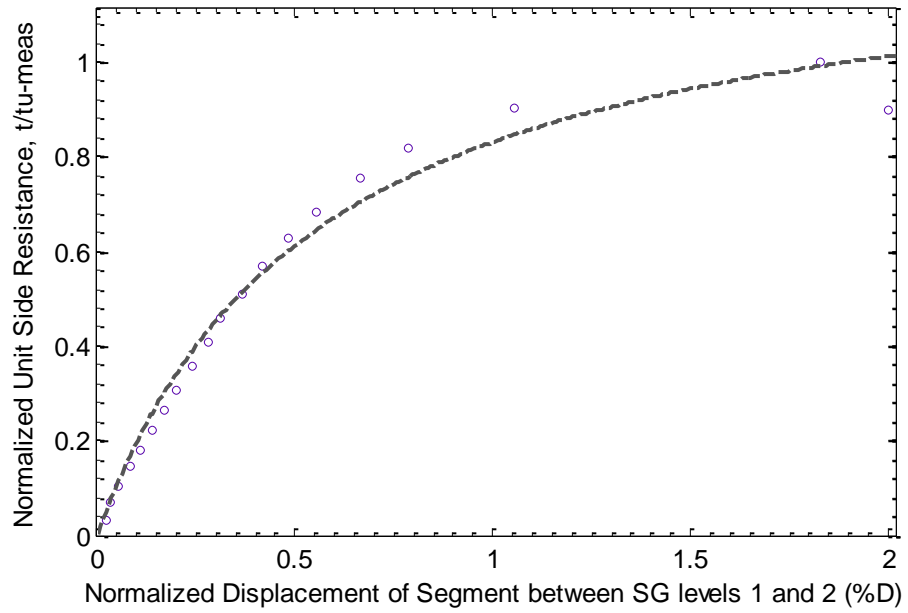


Figure 6.19. Hyperbolic fitting model for shaft segment F7-12.

Regression analyses were performed for each shaft segment. The obtained hyperbolic fitting parameters a and b are summarized in Table 6.2 (Frankford site) and Table 6.3 (Warrensburg site).

Table 6.2. Fitting parameters for side resistance data at Frankford site. Table continued on next page.

(Notation: *F1-12* is for Shaft F1, SG levels 1 to 2).

Shaft Segment	Hyperbolic Parameter <i>a</i>	Hyperbolic Parameter <i>b</i>
<i>F1 01</i>	0.62	0.18
<i>F1 12</i>	0.87	0.07
<i>F1 23</i>	0.67	0.21
<i>F1 34</i>	0.85	0.05
<i>F1 45</i>	0.83	0.14
<i>F2 12</i>	0.58	0.14
<i>F2 23</i>	0.74	0.10
<i>F2 34</i>	0.63	0.12
<i>F2 45</i>	0.98	0.02
<i>F3 12</i>	0.84	0.24
<i>F3 23</i>	0.83	0.17
<i>F3 34</i>	0.99	0.09
<i>F3 45</i>	0.96	0.08
<i>F3 56</i>	1.14	0.02
<i>F4 01</i>	0.82	0.19
<i>F4 12</i>	0.70	0.24
<i>F4 23</i>	0.80	0.18
<i>F4 34</i>	0.95	0.31
<i>F4 45</i>	0.92	0.04
<i>F4 56</i>	1.08	0.07
<i>F5 01</i>	0.85	0.20
<i>F5 12</i>	0.75	0.29
<i>F5 23</i>	0.81	0.14
<i>F5 34</i>	0.98	0.08
<i>F5 45</i>	0.92	0.08
<i>F6 01</i>	0.81	0.26
<i>F6 12</i>	0.69	0.32
<i>F6 23</i>	0.84	0.14
<i>F6 34</i>	0.70	0.35
<i>F6 45</i>	0.74	0.29
<i>F6 56</i>	0.98	0.06

Table 6.3 continued. Fitting parameters for side resistance data at Frankford site.

<i>Shaft Segment</i>	Hyperbolic Parameter <i>a</i>	Hyperbolic Parameter <i>b</i>
<i>F7 01</i>	0.81	0.21
<i>F7 12</i>	0.69	0.46
<i>F7 23</i>	0.74	0.31
<i>F7 34</i>	0.95	0.19
<i>F7 45</i>	0.87	0.23
<i>F7 56</i>	1.01	0.10
<i>F8 01</i>	0.53	0.19
<i>F8 12</i>	0.69	0.12
<i>F8 23</i>	0.81	0.08
<i>F8 34</i>	0.51	0.23
<i>F8 45</i>	0.96	0.04
<i>F9 23</i>	0.95	0.13
<i>F9 34</i>	1.09	0.01
<i>F10 01</i>	1.04	0.10
<i>F10 12</i>	0.62	0.57
<i>F10 23</i>	0.94	0.14
<i>F10 34</i>	1.20	0.00

Table 6.4. Fitting parameters for side resistance data at Warrensburg site. Table continued on next page.

Shaft Segment	Hyperbolic Parameter <i>a</i>	Hyperbolic Parameter <i>b</i>
W1 12	1.20	0.16
W1 23	1.01	0.08
W2 12	0.97	0.16
W2 23	1.00	0.36
W3 01	0.79	2.08
W3 12	0.94	0.56
W3 23	1.13	0.26
W3 34	0.95	0.36
W4 01	1.19	0.34
W4 12	0.99	0.06
W4 23	0.88	0.62
W4 34	0.97	0.12
W5 01	1.12	0.00
W5 12	0.87	0.05
W5 23	0.57	0.09
W6 01	1.03	0.05
W6 12	1.00	0.09
W6 23	0.94	0.63
W6 34	1.09	0.20
W7 01	0.81	0.25
W7 23	0.94	0.12
W7 34	0.90	0.07
W8 01	0.92	0.53
W8 12	0.88	2.43
W8 23	0.98	0.40
W8 34	1.10	0.20
W8 45	0.93	0.20
W9 01	0.87	2.08
W9 23	1.11	0.29
W9 34	1.02	0.22
W9 45	1.01	0.23
W10 23	0.95	0.02
W10 34	0.86	0.04

Table 6.5 continued. Fitting parameters for side resistance data at the Warrensburg site.

Shaft Segment	Hyperbolic Parameter a	Hyperbolic Parameter b
<i>W11 01</i>	0.88	0.19
<i>W11 12</i>	0.99	0.07
<i>W11 23</i>	0.89	0.13
<i>W11 34</i>	0.84	0.15
<i>W12 01</i>	1.19	0.13
<i>W12 12</i>	1.14	0.14
<i>W12 23</i>	1.07	0.04
<i>W13 01</i>	1.20	0.08
<i>W13 12</i>	0.96	0.15
<i>W13 23</i>	1.19	0.08
<i>W14 01</i>	1.09	0.06
<i>W14 12</i>	1.00	0.13
<i>W14 23</i>	0.96	0.58
<i>W15 01</i>	1.06	0.05
<i>W15 12</i>	1.03	0.20
<i>W15 23</i>	0.93	0.62

Table 6.4 shows the mean values, standard deviations, COVs and the correlation coefficient for the fitting parameters for the Frankford site and the Warrensburg site. As shown in the table, the variability of the hyperbolic fitting parameter b is very high; for the Warrensburg site, the COV of b parameter was as high as 154.5%. This shows the variability of the initial slope of the load transfer curve.

The correlation coefficient ρ_{ab} is negative, indicating that a and b have an inverse relationship, meaning that the initial slope and the horizontal asymptote of the load transfer curves are inversely proportional. Correlation coefficient ρ_{ab} is -0.607 for the Frankford site, and -0.32 for the Warrensburg site.

Table 6.6. Fitting parameters and their statistics for side resistance data using individual approach.

Site	Frankford		Warrensburg	
Fitting parameters	Hyperbolic parameter <i>a</i>	Hyperbolic parameter <i>b</i>	Hyperbolic parameter <i>a</i>	Hyperbolic parameter <i>b</i>
Mean	0.84	0.17	0.99	0.33
Standard Deviation	0.16	0.12	0.12	0.51
COV (%)	19.0	70.6	12.1	154.5
Correlation Coefficient	-0.61		-0.32	

Table 6.5 shows the average values of fitting parameters a_{avg} and b_{avg} from all the shaft segments for both sites from the individual approach as well as the fitting parameters from the collective approach. The variability of the fitting models obtained is also in the table. The model for side load transfer for the individual approach was established from the fitting parameters $a_{avg} = 0.91$ and $b_{avg} = 0.25$. The recommended t - z model, which is based on individual analysis of the side load transfer measurements, is represented by the equation

$$t = \frac{z}{a_{avg} * z + b_{avg}} = \frac{z}{0.91 * z + 0.25} \quad (6.18)$$

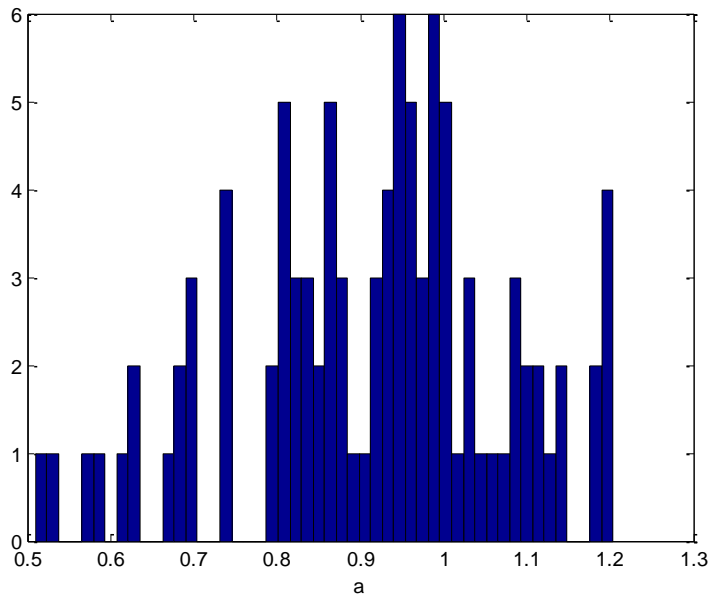
The variability and uncertainty of the recommended hyperbolic model for the individual approach (Equation 6.18) is reflected by the standard deviation and/or the COV of the two fitting parameters. This is different from the collective analysis of the data, where the variability and uncertainty in the established model are addressed by the conditional standard deviation of the fitting model.

Table 6.7. Fitting parameters and their statistics for side resistance data for collective and individual approaches.

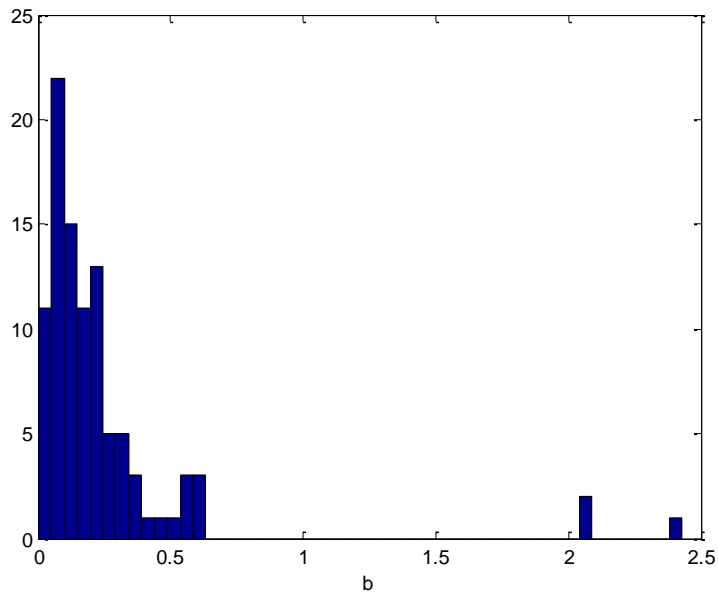
Parameters	Individual approach		Collective approach	
	Hyperbolic Parameter a	Hyperbolic Parameter b	Hyperbolic Parameter a	Hyperbolic Parameter b
Mean	0.91	0.25	1.071	0.13
Standard Deviation	0.16	0.38	0.17	
COV (%)	17.6 %	152.0 %		
Correlation Coefficient	-0.15			

The collective approach gives a more *intuitive* picture of the variable range of data, with one estimate of standard deviation of 0.17. The variability and uncertainty of the data for the individual approach are reflected by the standard deviations of the fitting parameters, which makes it more difficult to get a picture of how variable the range of data is. However, the individual approach gives a picture of how the reciprocal of the initial slope (parameter b , standard deviation of 0.38) and the horizontal asymptote (parameter a , standard deviation of 0.16) of the load transfer curves vary. The comparisons of the simulated load transfer data/curves of the collective and individual approaches are presented in Section 6.9.

The distributions of the parameters also are known. Figure 6.20 shows the histogram of parameter a has a bell-shaped distribution and has normal distribution, and the histogram of parameter b has a longer tail and is considered to follow a lognormal distribution. The correlation coefficient and the distribution of the fitting parameters are used to generate and simulate load transfer curves.



a) Histogram of a parameter.



b) Histogram of b parameter.

Figure 6.20. Histogram of hyperbolic fitting parameters a and b

6.5. Regression Analyses for Side Resistance - Normalized to Predicted Ultimate Resistance

When developing load transfer curves, the unit side resistance can be normalized by maximum measured values or maximum predicted values. The regression analyses covered in Section 6.4 were performed on the resistance normalized to maximum measured values. Presented below are the regression analyses for the resistance normalized to predicted ultimate values. Ordinary least squares and weighted least squares regression analyses were performed using a hyperbolic function.

The ordinary least squares regression gave the function:

$$t = \frac{z}{az+b} = \frac{z}{1.10*z+0.12} \quad (6.19)$$

with an R^2 of 0.34 and an $RMSE$ of 0.35. The weighted least squares regression analysis gave the function:

$$t = \frac{z}{az+b} = \frac{z}{1.24*z+0.08} \quad (6.20)$$

and an $RMSE$ of the fitting model of 1.00. The regression lines, the data and the plus and minus conditional standard deviation bounds are shown in Figures 6.21 and 6.22.

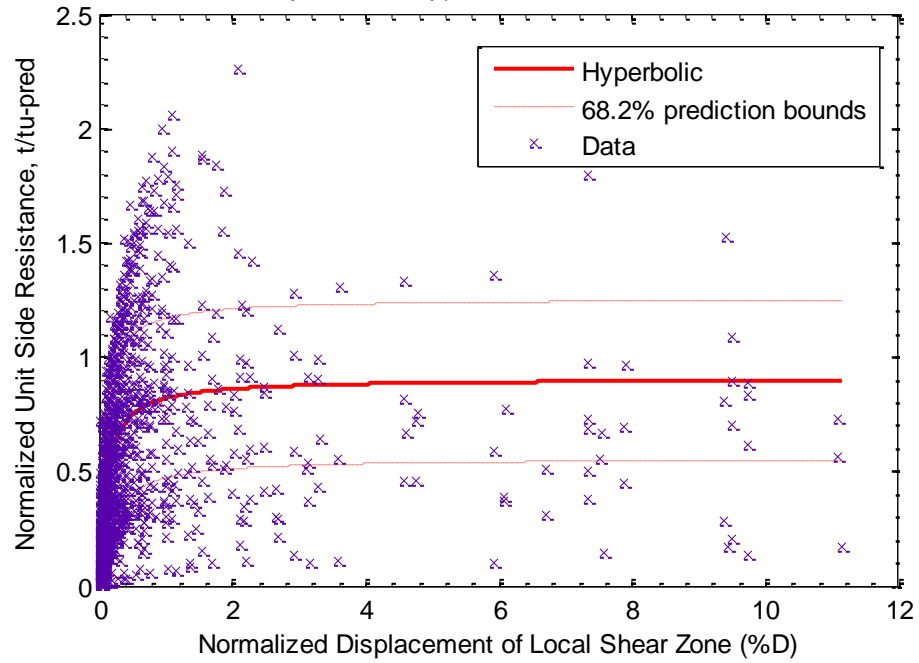


Figure 6.21. Hyperbolic function from ordinary least squares regression for side resistance normalized by predicted ultimate values.

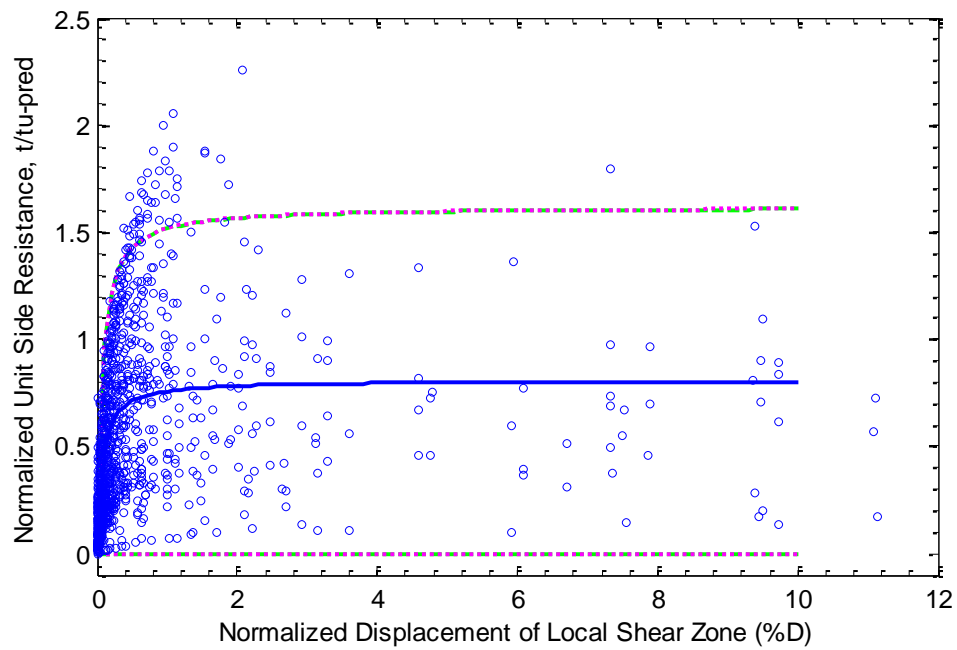


Figure 6.22. Hyperbolic function from weighted least squares regression for side resistance normalized by predicted ultimate values.

Both regression lines from ordinary and weighted regression analyses fit the data well. However, the prediction bounds from the weighted least squares regression are much wider, which again over predict the variability of future data. The weighted least squares regression analysis gave the value of *RMSE* of 1.0, which is significantly greater than the *RMSE* of 0.35 from the ordinary least squares regression analysis. This again indicates that a better model is obtained from the ordinary least squares analysis. Therefore, the model obtained from ordinary least squares regression, Equation 6.19, is used for subsequent analyses.

6.6. Regression Analyses for Tip Resistance –Normalized to Maximum Measured Resistance

Similar to what has been done for unit side resistance, regression analyses were performed using the collective and individual regression analyses, and the options of ordinary least squares and weighted least squares regression. The following subsections present the analyses for the collective interpretation and the individual interpretation.

6.6.1. Regression Analyses for Tip Resistance - Collective Measurements

The unit tip resistance data normalized to maximum measured values was fitted using five functions to find the tip load transfer *q-w* model. The functions are power, exponential, logarithm, and rational hyperbolic. Details follow.

The *power function* obtained from the ordinary least squares regression follows:

$$q = m * x^n = 0.48 * w^{0.34} \quad (6.21)$$

where

q = normalized unit tip resistance,

w = normalized displacement of shaft top, and

m and n = fitting parameters.

The analysis gave an R^2 of 0.73 and an $RMSE$ of 0.13. Using weighted least squares regression, the function is:

$$q = m * x^n = 0.48 * w^{0.39} \quad (6.22)$$

The $RMSE$ for this model is 0.40. The regression lines, the data and the one conditional standard deviation bounds are presented in Figures 6.23 and 6.24.

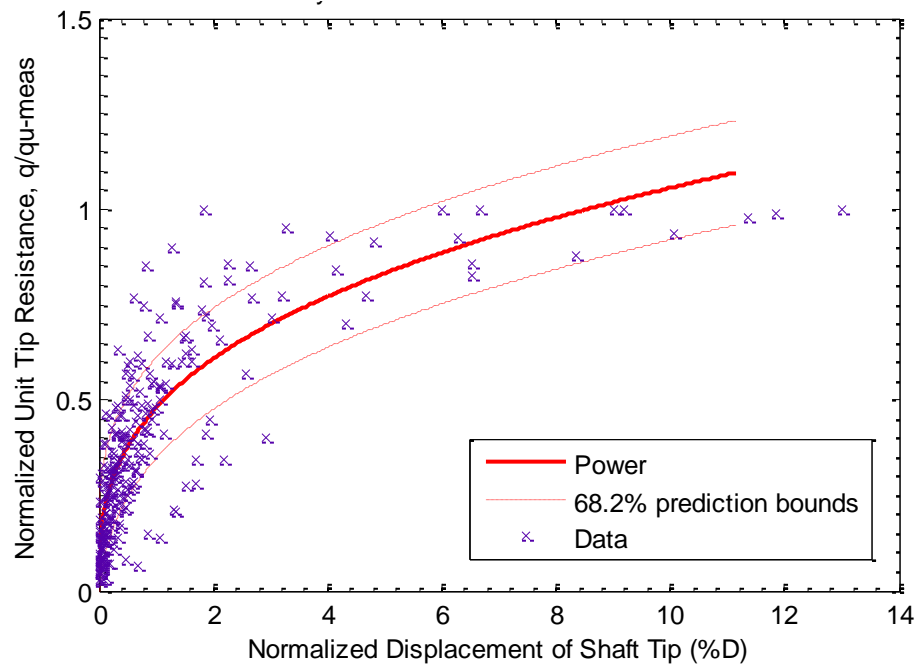


Figure 6.23. Power function for tip resistance from ordinary least squares regression.

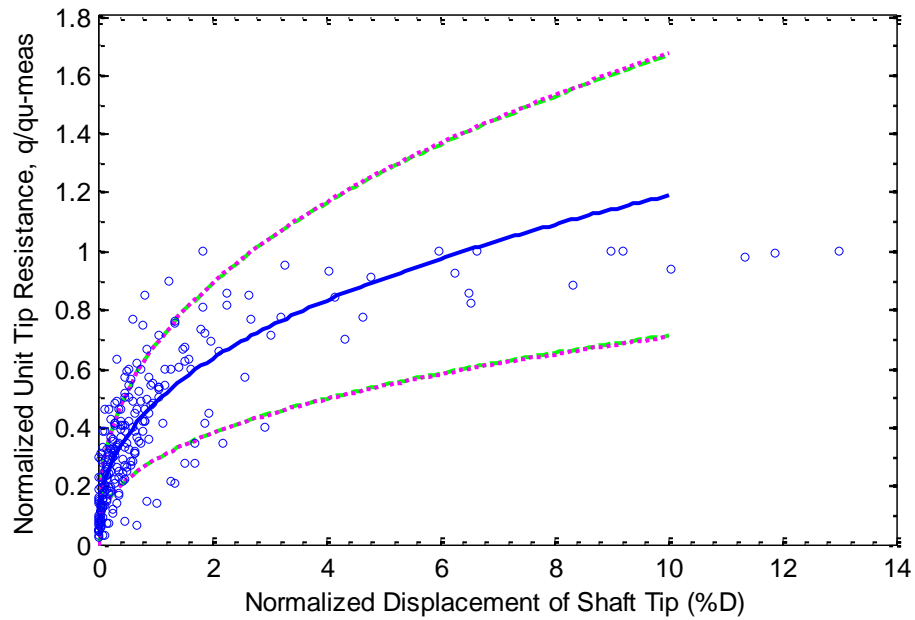


Figure 6.24. Power function for tip resistance from weighted least squares regression.

As in Figure 6.23, the fit obtained from ordinary least squares appears to track the data well. When the displacement is larger than about 10% of the shaft diameter, the model tends to overestimate the unit tip resistance. However, in practice, the SLS design usually limits the displacement of less than 10% D; thus, this is not an issue. The bounds are parallel to the regression line and cover a large amount (about 70%) of observed data, further indicating that the model obtained is reasonable.

On the contrary, the fit obtained from weighted least squares does not appear to model the data as well as that from ordinary least squares. When the displacement is larger than about 6% shaft diameter, the model rises above the observed data. This is not preferable because most of the normalized resistance curves have a tendency to flatten, or even decrease after the displacement is large. In addition, the bounds start

from the origin together with the model, and only reasonably predict the data variability when the tip displacement is less than about 3% of shaft diameter. Thus, the power function from weighted least squares is not a good choice to model tip load transfer data.

The *exponential function* obtained using ordinary least squares regression analysis on the load transfer data for tip resistance is:

$$q = 1 - \exp(c * z) = 1 - \exp(-0.78 * w) \quad (6.23)$$

where

q = normalized unit tip resistance,

w = normalized displacement of shaft top, and

c = fitting parameter.

The R^2 of 0.6 and an $RMSE$ of 0.16 were obtained from the ordinary least squares regression. Weighted least squares regression gave the function:

$$q = 1 - \exp(c * z) = 1 - \exp(-2.55 * w) \quad (6.24)$$

with the $RMSE$ of 0.82. Figures 6.25 and 6.26 show the regression lines with bounds of one standard deviation.

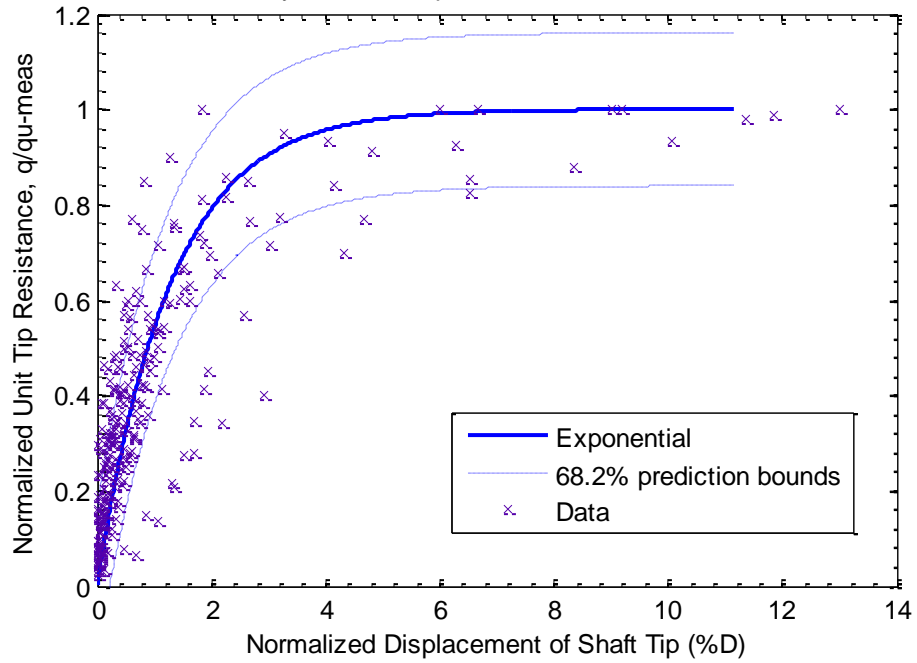


Figure 6.25. Exponential function for tip resistance from ordinary least squares regression.

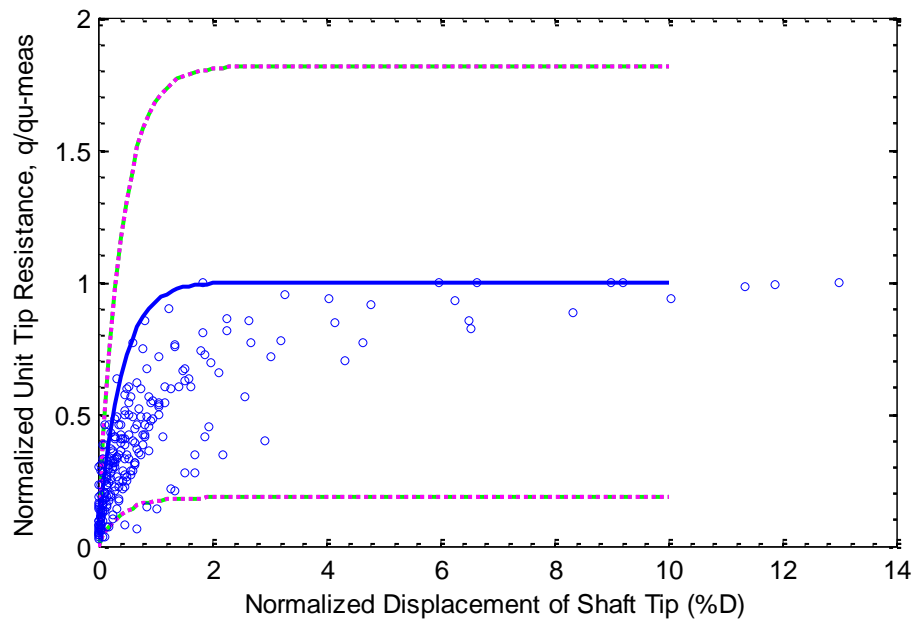


Figure 6.26. Exponential function for tip resistance from weighted least squares regression.

The exponential regression line obtained from ordinary least squares follows the data pattern at the small normalized displacements of less than 4% D; then tracks the upper bound nicely, similar to what was discussed for the unit side resistance. The bounds obtained from the ordinary least squares also predict the variability of future outcomes well.

The model obtained from weighted least squares, as in Figure 6.28, seems to follow the upper bound at very small displacement, which is undesirable. The regression line also over predicts the future data. Moreover, the bounds over predict the variability, manifested in both the large distances from the bounds to the model and the high (0.8) value of *RMSE*. Neither model from the exponential function appear to be a good option for modeling tip resistance data.

The *logarithm function* obtained from ordinary least squares analysis is in the equation:

$$q = d * \ln(x) + e = 0.13 * \ln(w) + 0.52 \quad (6.25)$$

where *d* and *e* are fitting parameters. The regression analyses gave an R^2 of 0.68 and *RMSE* of 0.15. Using weighted least squares regression, the acquired function is:

$$q = d * \ln(x) + e = 0.08 * \ln(w) + 0.44 \quad (6.26)$$

with the *RMSE* of 0.46. The regression lines, the data, and the confidence bounds for new observations at 68.2% are presented in Figure 6.27 (for ordinary least squares regression) and Figure 6.28 (for weighted least squares regression).

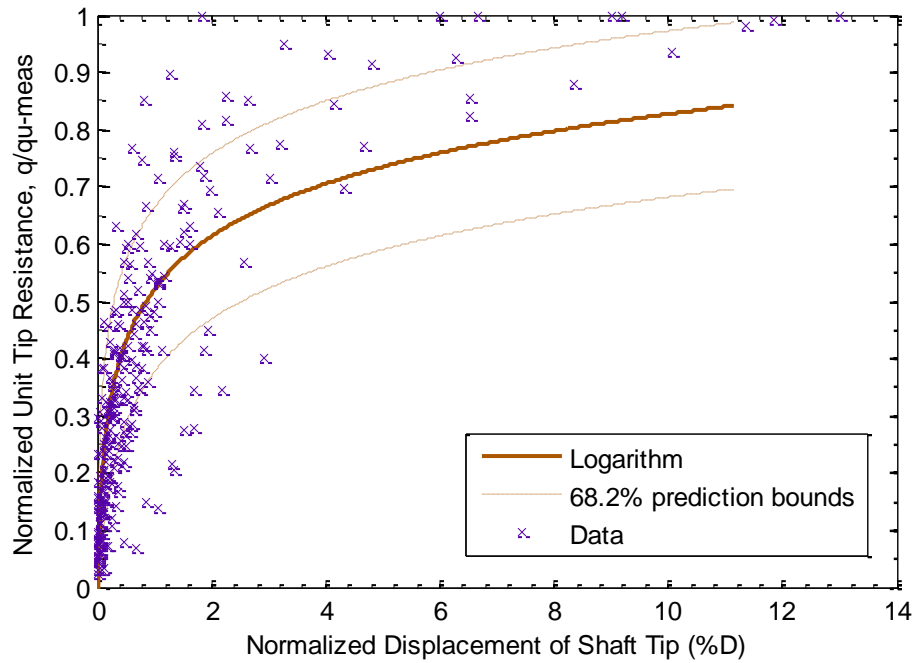


Figure 6.27. Logarithm function for tip resistance from ordinary least squares regression.

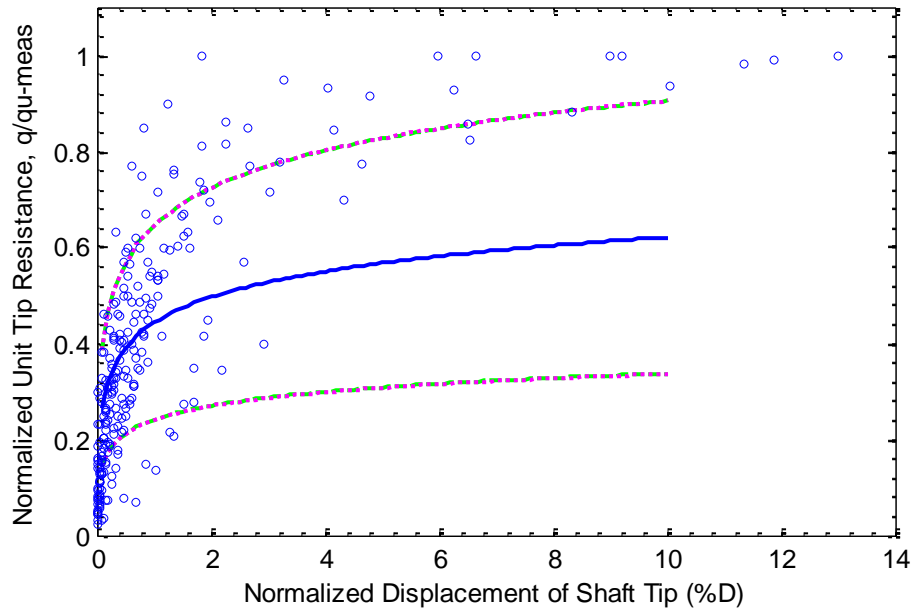


Figure 6.28. Logarithm function for tip resistance from ordinary least squares regression.

The models obtained from both ordinary least squares and weighted least squares regression fit the unit tip resistance data when the displacement is less than about 2% D. Then for larger displacements, the fitting functions underestimate future observations. The logarithm function is the only function of the five analyzed that underestimates the future observations for the unit tip resistance. The standard deviation prediction bounds from ordinary least squares are narrower and more reasonable than those obtained from weighted least squares, the former gave a smaller *RMSE* of 0.15 compared to the latter's 0.46.

The *rational function* obtained from ordinary least square regression is in the form:

$$q = \frac{p_1 x + p_2}{x + q_1} = \frac{1.05 * w + 0.16}{w + 1.36} \quad (6.27)$$

where p_1 , p_2 , and q_1 are fitting parameters. The fit gave an R^2 of 0.74 and an $RMSE$ of 0.13. The rational function obtained from weighted least square regression is:

$$q = \frac{p_1 x + p_2}{x + q_1} = \frac{0.90 * w + 0.07}{w + 0.80} \quad (6.28)$$

Using weighted least squares, the $RMSE$ obtained is 0.41. The regression lines are presented in Figure 6.29 and 6.30 with the plus and minus one standard deviation bounds.

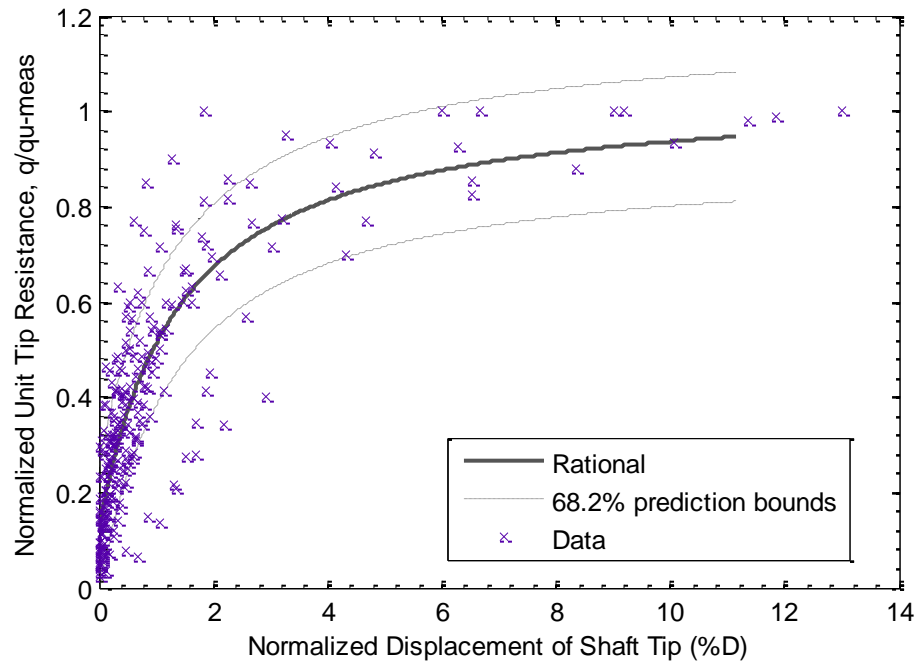


Figure 6.29. Rational function for tip resistance from ordinary least squares regression.

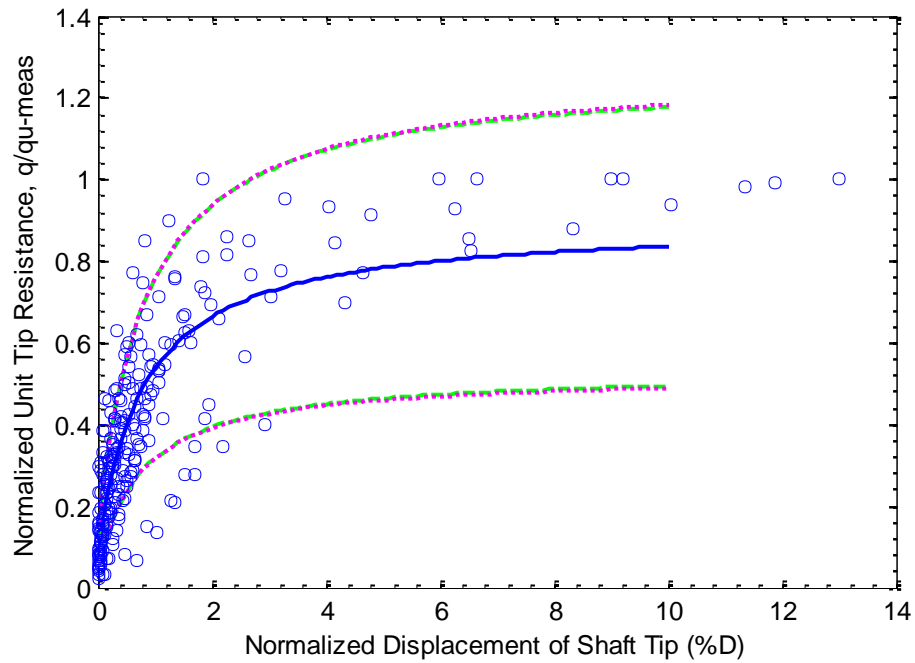


Figure 6.30. Rational function for tip resistance from weighted least squares regression.

The models obtained from the rational function reflect the data well, in terms of both the regression lines and the prediction bounds. The narrowest conditional prediction bounds (manifested by smallest $RMSE = 0.13$) when the five models were applied to unit tip resistance data were from the rational model using ordinary least squares analysis.

However, when evaluating Equations 6.27 and 6.28, the fitting parameter p_2 is not close to zero. This means that when the shaft tip displacement is zero, the unit tip resistance is not equal to zero, but has positive values of 0.16 and 0.07, respectively. The rational regression lines do not pass through the origin, as in Figures 6.29 and 6.30, and this is not favorable. This is a practical consideration that should be considered when

considering the rational fit, similar to the fact that an initial infinite slope is a practical consideration that needs to be considered for the power function.

The *hyperbolic function* of fit obtained from ordinary least square regression on the unit tip resistance data is:

$$q = \frac{x}{ax+b} = \frac{w}{1.1*w+0.72} \quad (6.30)$$

where a and b , are fitting parameters. The analysis gave an R^2 of 0.70 and an $RMSE$ of 0.14. Using weighted least squares regression, the following function is acquired:

$$q = \frac{x}{ax+b} = \frac{w}{1.12 *w+0.69} \quad (6.31)$$

with the $RMSE$ of 0.76. Figures 6.31 and 6.32 present the data, and show the regression lines with the plus and minus one standard deviation bounds.

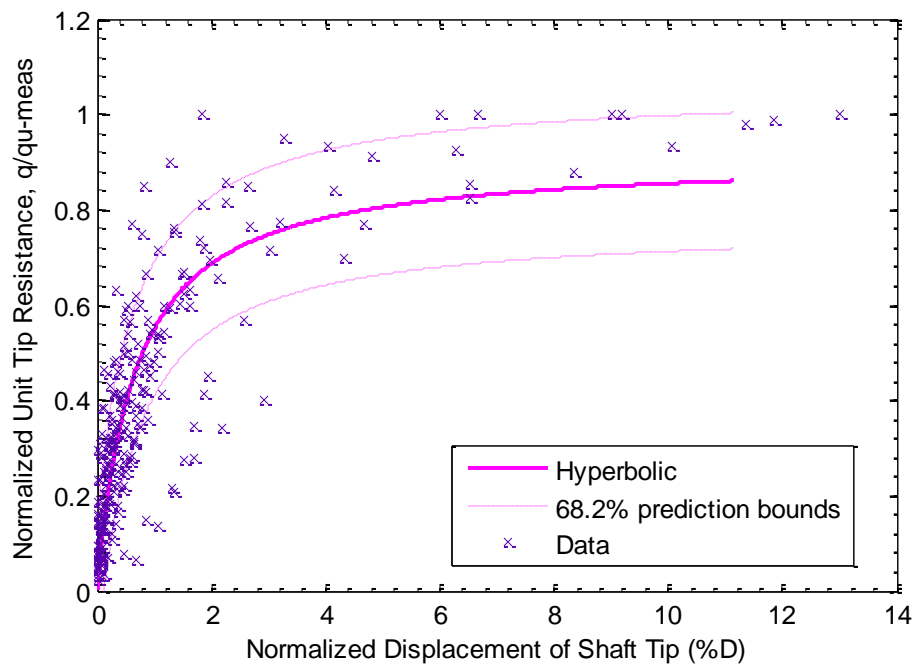


Figure 6.31. Hyperbolic function for tip resistance from ordinary least squares regression.

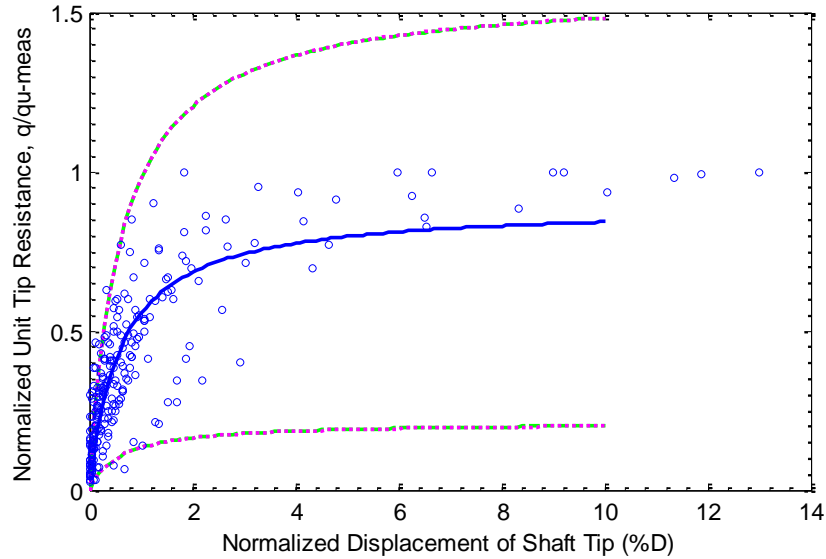


Figure 6.32 Hyperbolic function for tip resistance from weighted least squares egression.

The hyperbolic functions from ordinary and weighted least squares analyses are good fits and the regression lines track the data well. The prediction bounds obtained from ordinary least squares analysis is one of the narrowest of the five functions with a low *RMSE* of 0.14. The bounds obtained from weighted least squares analysis are large, indicating the high uncertainty in the prediction of future outcomes.

For all five functions, when considering small displacements of less than 0.2% shaft diameter, the prediction bounds obtained from the ordinary least squares seem to over predict the variability/uncertainty of the normalized unit resistance. However, at larger displacements, the prediction bounds obtained from ordinary least squares analysis reflect the data variability/uncertainty better than the weighted least squares analysis. Because 0.2% D is especially small when considering tip resistance, the ordinary least squares regression is considered to be the better fit to the data and is recommended for modeling load transfer for unit tip resistance. This conclusion is similar to that reached for the unit side resistance analyses.

The five regression lines from five functions using ordinary least squares regression are graphed together in Figure 6.33. The summary of the function equations, R^2 and $RMSE$ obtained from the regression analyses are in Table 6.6. The hyperbolic model obtained from ordinary least squares analyses is the best model to predict the unit tip resistance data. The criteria for choosing the hyperbolic model was that the model fits the data well and follows the data pattern, while producing low variability prediction bounds. The model does not contain any practical issues such as: infinite slope at origin (the power function) or not passing through origin (the rational function). The fitting parameters of the hyperbolic model have physical meanings as discussed in the previous sections. The variability of the hyperbolic load transfer model is quantified and has the standard deviation of 0.14.

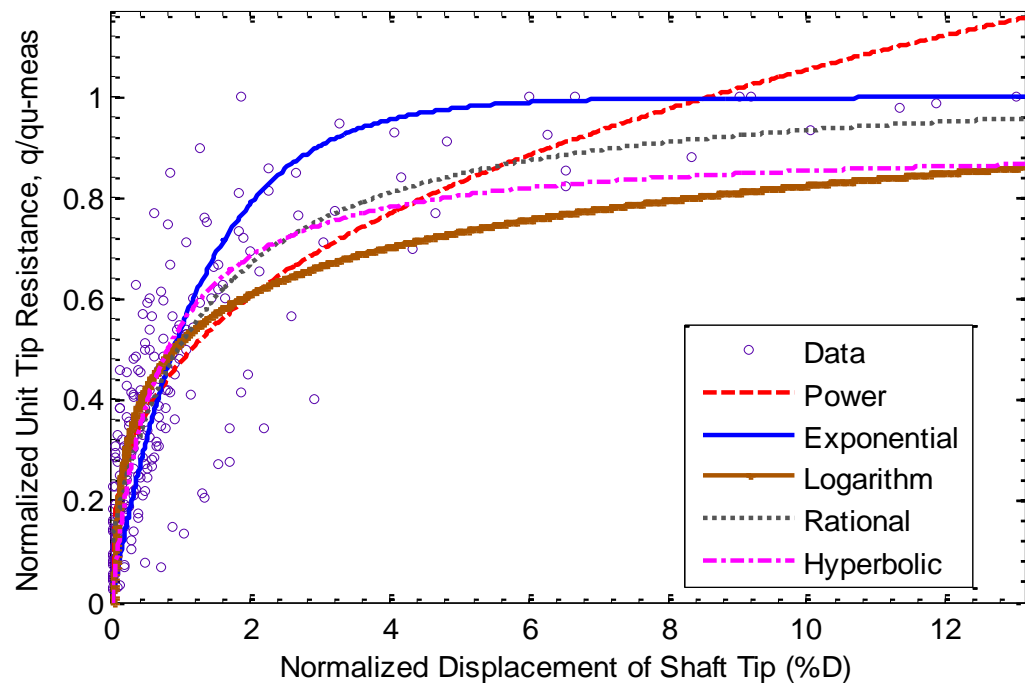


Figure 6.33. Five functions for tip resistance from ordinary least squares regression.

Table 6.8. Summary of fitting models for tip resistance normalized to maximum measured values using collective approach.

Type of Function	Regression Type	Equation	R^2	$RMSE$	Comments
Power	Ordinary least squares	$q = 0.48 * w^{0.34}$	0.73	0.13	+ Fit data relatively well; high R^2 and low $RMSE$. – Infinity slope at origin;
	Weighted least squares	$q = 0.48 * w^{0.39}$	-	0.40	
Exponential	Ordinary least squares	$q = 1 - exp(-0.78 * w)$	0.60	0.16	– Does not fit well when displacement is large; low R^2 , and high $RMSE$.
	Weighted least squares	$q = 1 - exp(-2.55 * w)$	-	0.82	
Logarithm	Ordinary least squares	$q = 0.13 * ln(w) + 0.52$	0.68	0.15	– Under predict data; lower R^2 , and relatively high $RMSE$.
	Weighted least squares	$q = 0.08 * ln(w) + 0.44$	-	0.46	
Rational	Ordinary least squares	$q = \frac{1.05 * w + 0.16}{w + 1.36}$	0.74	0.13	– Does not pass through origin.
	Weighted least squares	$q = \frac{0.90 * w + 0.07}{w + 0.80}$	-	0.41	
Hyperbolic	Ordinary least squares	$q = \frac{w}{1.1 * w + 0.72}$	0.70	0.14	+ Best reflects data, high R^2 and low $RMSE$.
	Weighted least squares	$q = \frac{w}{1.12 * w + 0.69}$	-	0.76	

It was observed that tip resistance data are less scattered, and correspondingly, the $RMSE$ of unit tip resistance for the recommended model is lower than that of the unit side resistance. The best functional form that reflects data of both unit side and tip resistance is hyperbolic. The models and their quantified variability were used for subsequent analyses presented later in this chapter and in succeeding chapters.

6.6.2. Regression Analyses for Tip Resistance – Individual Measurements

Regression analyses were performed individually on each and every shaft segment data. The hyperbolic model was used for ordinary least square regressions analyses. The fitting parameters were determined and are presented in Tables 6.7 (Frankford site) and 6.8 (Warrensburg site).

Table 6.9. Fitting parameters for tip resistance data from Frankford site.

Shaft Segment	Hyperbolic Parameter a	Hyperbolic Parameter b
<i>F1</i>	2.77	0.51
<i>F2</i>	1.84	0.08
<i>F3</i>	Unreasonable	
<i>F4</i>	0.99	0.76
<i>F5</i>	0.96	0.47
<i>F6</i>	1.03	0.82
<i>F7</i>	0.69	1.25
<i>F8</i>	1.51	0.37
<i>F9</i>	1.83	0.33
<i>F10</i>	1.15	0.57

Table 6. 10. Fitting parameters for tip resistance data

from Warrensburg site.

Shaft Segment	Hyperbolic Parameter a	Hyperbolic Parameter b
W1	2.35	0.19
W2	1.09	0.84
W3	Unreasonable	
W4	0.46	1.93
W5	Unreasonable	
W6	1.29	0.77
W7	0.85	3.48
W8	1.04	0.71
W9	Unreasonable	
W10	1.01	0.53
W11	0.74	4.99
W12	0.85	0.54
W13	1.14	0.13
W14	1.01	0.57
W15	0.68	0.20

During load testing, there were some tests that finished when side resistance reached ultimate resistance while the tip resistance was well below its ultimate value. In these cases, the tip resistance versus shaft tip displacement curves were still at the beginning, “linear part” of the curve (Figure 6.34). The regression analyses performed for tip resistance data for those tests using the hyperbolic model produced “unreasonable” hyperbolic fitting parameters (Tables 6.7 and 6.8). For example, for the normalized unit tip resistance of shaft W3 in Figure 6.34 (compare to the reasonable one in Figure 6.35), the asymptote value reached 186 instead of the expected value of around 1.0. This is an unacceptable result. Note that this phenomenon does not depend

on normalization (maximum measured or maximum predicted), but depends on how far a load test went on the load transfer curve for tip resistance at the end of the test.

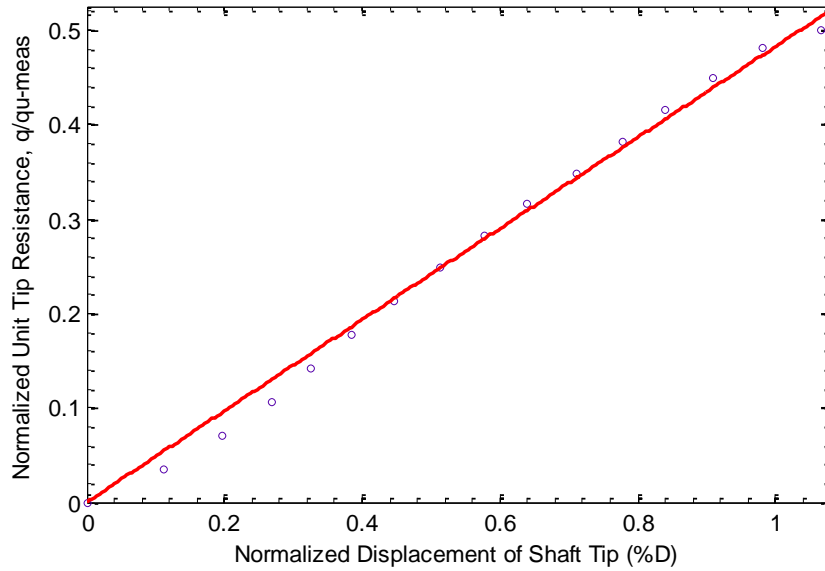


Figure 6.34. Unreasonable tip resistance fit (Shaft W3) with a parameter of 186 instead of approximately 1.0.

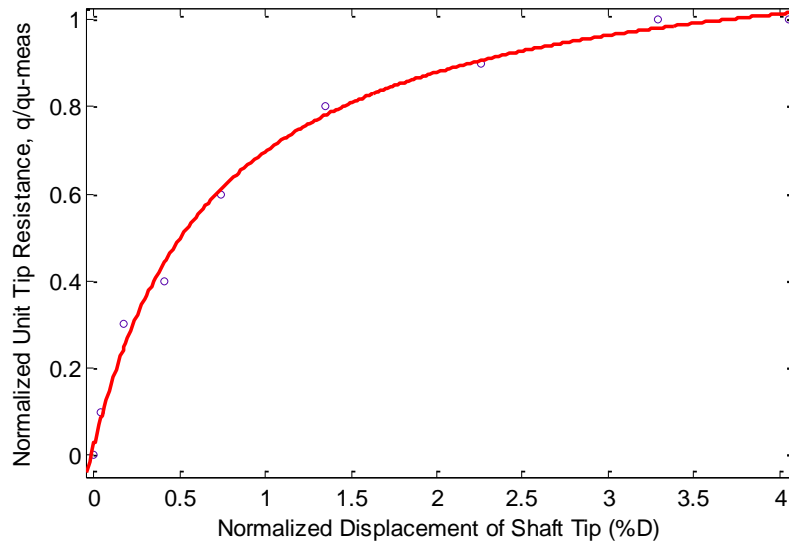


Figure 6.35. Reasonable tip resistance fit (Shaft W12) Parameters a of 0.84 and b of 0.62.

Four shafts (F3, W3, W5 and W9) of the 25 tested shafts showed unreasonable parameters, as indicated in Tables 6.7 and 6.8. All four of these “extreme” tests were eliminated from the analysis of the individual approach. Some other shafts might have ended when the tip resistance had just passed the “linear part” of the curve and would not have given such extreme values to fitting parameter a . The unit tip resistance data from these shafts produced higher values of fitting parameter a than necessary, but are difficult to identify and quantify . This makes the parameter a more variable and scattered, and may be one of the reasons that the average COV of a parameter for tip resistance is 2.7 times larger than that of side resistance (Table 6.9).

Table 6.9 shows the mean values, the standard deviation, the COV and the correlation coefficient of fitting parameters for tip resistance data from the Frankford and the Warrensburg. As for side resistance, the variability of the hyperbolic fitting parameter b are very high; for the Warrensburg site, the COV of b parameter was as high as 121.8 %, indicating the high variability of the initial slope of the tip load transfer curve. The table also shows that the horizontal asymptote ($1/a$) and the initial slope ($1/b$) of the $q-w$ curves were negatively correlated.

Table 6.11. Fitting parameters and their statistics from individual approach for tip resistance.

Site	Frankford		Warrensburg	
Fitting Parameters	Hyperbolic Parameter a	Hyperbolic Parameter b	Hyperbolic Parameter a	Hyperbolic Parameter b
Mean	1.42	0.57	1.04	1.24
Standard Deviation	0.65	0.34	0.47	1.51
COV (%)	45.8	59.6	45.2	121.8
Correlation Coefficient	-0.59		-0.39	

For both side and tip resistance, the variability of b parameter is larger than the variability of a parameter. However, the variability a (horizontal asymptote) for tip resistance is significantly higher than that of side resistance, which is reflected in the COVs, which are 47.5 % (Table 6.10) and 17.6% (Table 6.11) respectively.

The summary of fitting parameters and the quantified variability of the models from the individual and collective regression are shown in Table 6.11. The average fitting parameters for unit tip resistance from all shaft segments are $a_{avg} = 1.20$ and $b_{avg} = 0.95$. The recommended q - w model based on individual analysis of the tip load transfer measurements has the hyperbolic form:

$$q = \frac{w}{a_{avg} * w + b_{avg}} = \frac{w}{1.2 * w + 0.95} \quad (6.32)$$

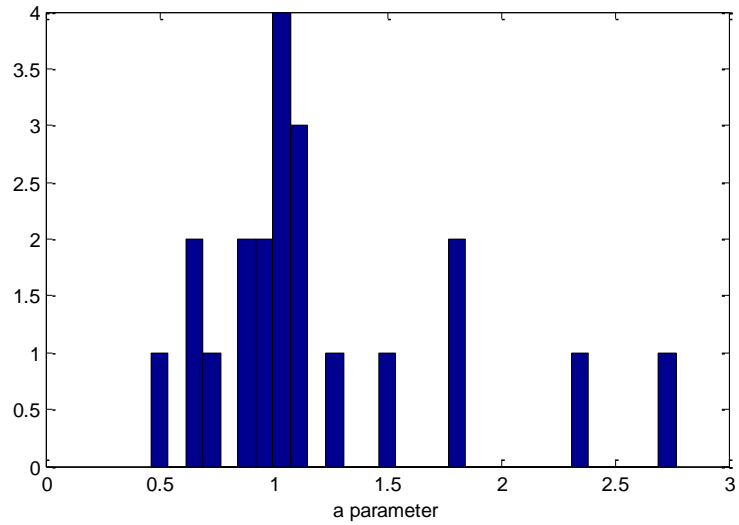
Table 6.12. Fitting parameters and their statistics for tip resistance for collective and individual approaches.

Parameters	Individual Approach		Collective Approach	
	Hyperbolic parameter a	Hyperbolic parameter b	Hyperbolic parameter a	Hyperbolic parameter b
Mean	1.20	0.95	1.098	0.72
Conditional Standard Deviation	0.57	1.19	0.14	
COV (%)	47.5	123.5		
Correlation Coefficient	-0.40			

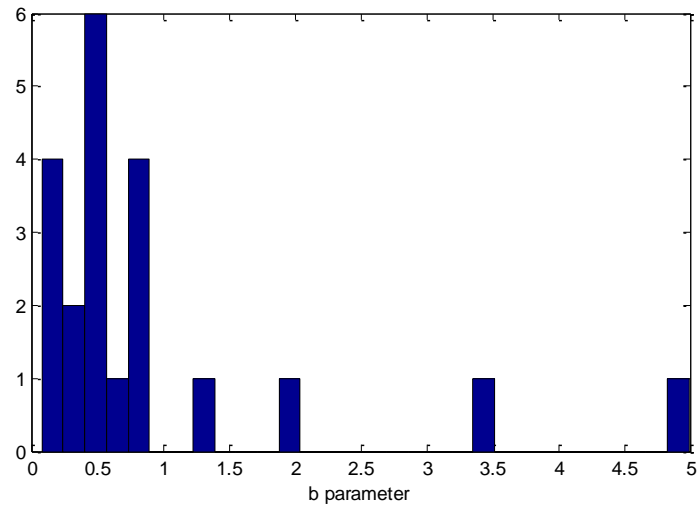
Note that the data from four shafts (F3, W3, W5 and W9) could not be used in the individual approach; however, these data are used in the collective approach. In other words, the individual approach cannot use all the tip resistance data, and the decision of which data should be excluded becomes subjective. This is one of the disadvantages of the individual approach compared to the collective approach in quantifying the tip load transfer model.

The histograms of the fitting parameters a and b are in Figure 6.36. Parameter a does not clearly show a bell-shaped distribution as is the case for side resistance; however, it is assumed that parameter a also has a normal distribution for tip resistance. As in the case of side resistance, parameter b follows a lognormal distribution. The correlation coefficient of the hyperbolic fitting is negative, of -0.40 , showing that the initial slope and the horizontal asymptote of the hyperbolic load

transfer model is inversely proportional. All of this information was used later for the simulation of load transfer data.



a) Histogram of hyperbolic parameter a .



b) Histogram of hyperbolic parameter b .

Figure 6.36. Histograms of hyperbolic fitting parameters for tip resistance.

6.7. Regression Analyses for Tip Resistance - Normalized to Predicted Ultimate Resistance

Analyses utilizing both ordinary and weighted least squares regression were performed on the tip resistance normalized to predicted ultimate values data. The hyperbolic function obtained from ordinary least squares analyses has the form:

$$q = \frac{x}{ax+b} = \frac{w}{0.72*w+0.68} \quad (6.32)$$

The fitting model for tip resistance has a low R^2 of 0.46, and an $RMSE$ of 0.34. Under the weighted least squares analyses, the function obtained for q - w curve is:

$$q = \frac{x}{ax+b} = \frac{w}{0.76*w+0.61} \quad (6.33)$$

The regression analysis gave a high $RMSE$ of 1.1. The hyperbolic fits are presented in Figures 3.37 and 3.38 with the plus and minus one standard deviation bounds.

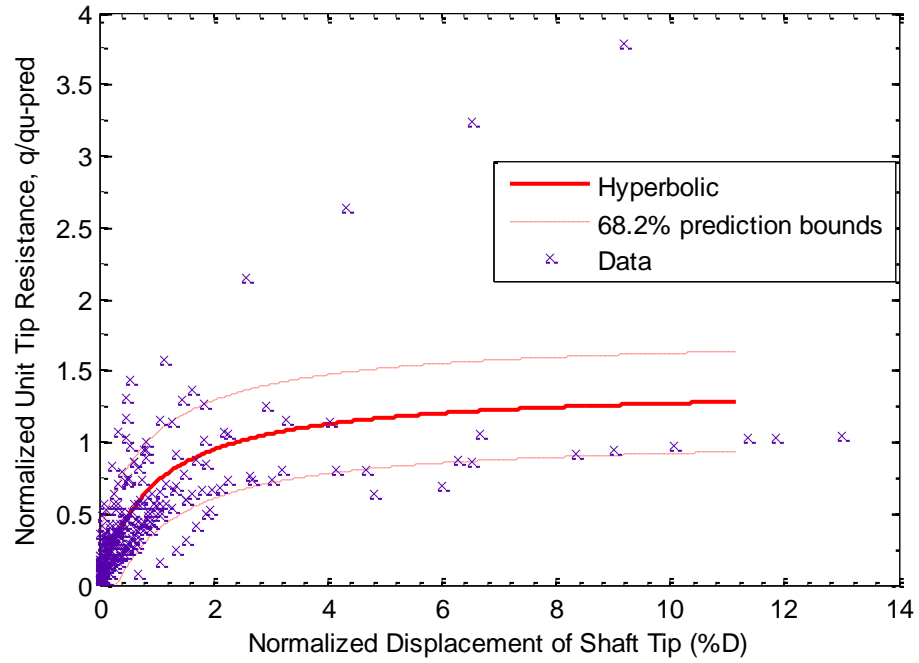


Figure 6.37. Hyperbolic function for tip resistance from ordinary least squares regression.

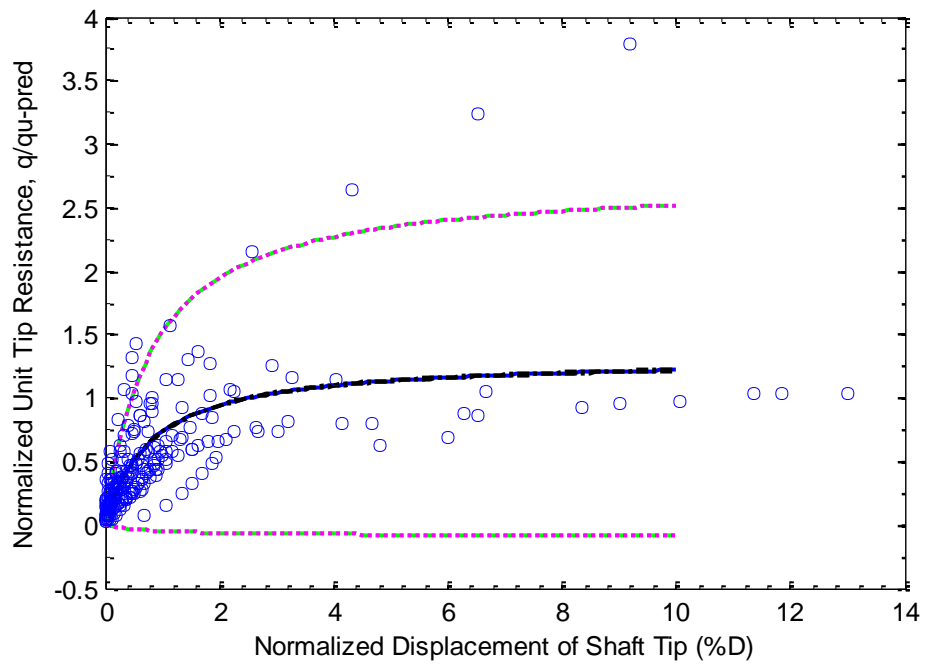


Figure 6.38. Hyperbolic function for tip resistance from weighted least squares regression.

The regression lines from both the ordinary and the weighted least square regression are similar in shape and magnitude. The prediction bounds from weighted least squares regression over estimates the future outcome of the tip resistance data starting at the origin. The bounds widen with increasing shaft tip displacement. Ordinary least squares regression gave better prediction bounds with a lower *RMSE* of 0.34 than the weighted least squares regression *RMSE* 0.75. Therefore, the *q-w* fitting model using ordinary least squares regression (Equation 6.32) was chosen for further analyses in Chapter 8.

6.8. Probabilistic Simulation of Load Transfer Curves

The simulation of load transfer curve depends on how the variability and uncertainty of the load transfer model is represented. The variability of the model obtained from the collective approach of regression analysis is represented by its conditional standard deviation; and that of the individual approach is represented by the standard deviation/and or the COV of its fitting parameters.

The simulated load transfer data are generated using Monte Carlo simulation, which generates random numbers based on the mean value, standard deviation or COV, and the distribution type of the variable. The process of using Monte Carlo simulation to simulate normalized unit resistance for collective and individual regression approaches of regression follows the steps below:

The *collective approach*: Using function $t = \frac{z}{a*z+b} + C$, with two fitting model parameters *a* and *b*; *C* is an added parameter to account for the uncertainty of the

model. Parameter C is normally distributed with a mean of zero and a standard deviation equal to the conditional standard deviation of the data. The reason for adding the parameter C is because the model was obtained from ordinary least squares analysis with constant standard deviation, as discussed in previous sections. (If data followed constant COV, C would be a multiplier with mean C of 1.0). The ordinary least squares regression also assumes the data are normally distributed about the trend line, so parameter C is considered normally distributed. The Monte Carlo technique is used to generate a large set of random C . The fitting parameters a and b are deterministic, and the randomly created parameter C added to the equation makes t the random response variable.

The *individual approach*: Because hyperbolic parameters a and b are correlated, the process of generating a and b involves Monte Carlo simulation utilizing a *random correlated multi variable generation* technique. From Section 6.4.2 and 6.5.2, a is normally distributed and b is lognormally distributed. Because of the difference in the distribution types, the correlation coefficients of parameters a and b cannot be used directly. The simulation process begins with taking the logarithm of b . The logarithm of b , b_L , is now normally distributed.

Covariance correlation coefficients of random variables a and b_L are needed to simulate the correlated random variables a and b_L , and are determined by:

$$C_V(a, b_L) = \sum_{i=1}^N (a_i - a_{avg}) * (b_{L_i} - b_{L_{avg}}) \quad (6.34)$$

$$\rho_{ab_L} = \frac{C_V(a, b_L)}{\sigma_a \sigma_{b_L}} \quad (6.35)$$

where

$C_V(a, b_L)$ = covariance of fitting parameter a and variable b_L ,

a_{avg} , $b_{L_{avg}}$ = average values of fitting parameter a and variable b_L , and

σ_a , σ_{b_L} = standard deviation of fitting parameter a and variable b_L .

Covariance $C_V(a, b_L)$ and correlation coefficient ρ_{ab_L} were then used with function *mvnrnd* in MATLAB® to simulate two large sets of correlated random variables, a and b_L . The random values of fitting parameter b were obtained by taking the exponent of b_L . The final step was to substitute randomly generated a and b back into the function $t = z/(a * z + b)$ to obtain the simulated load transfer data or curves.

A MATLAB® code was developed and used to generate and plot simulated load transfer data (Appendix G). The two approaches of probabilistic simulation of load transfer data were used to create data and plots presented in the next section.

6.9. Comparison of Simulated Data for Collective and Individual Measurements

Two hyperbolic models (for side and tip resistance) obtained from the collective approach and two from the individual approach were used to simulate the resistance data. The process utilized the Monte-Carlo simulation. The simulated data were compared in order to identify the “final model” (Figure 6.2) for the resistance normalized to maximum measured values to be used in subsequent probabilistic analyses.

6.9.1. Generation of Load Transfer Data - Side Resistance

A total of 60,000 normalized displacements and the corresponding 60,000 randomly simulated normalized unit side resistances were generated using the hyperbolic fitting models obtained from the collective approach. In particular, fitting parameters $a = 1.07$, $b = 0.13$ (Equation 6.17) and the added parameter C with a mean value of 0.0 and a standard deviation of 0.17 (Section 6.8) were used to simulate the data. The same number of 60,000 simulated data points was created from the model obtained from the individual approach: $a = 0.91$ with a standard deviation of 0.16; $b = 0.25$ with a standard deviation of 0.38; and a correlation coefficient equal to -0.15 (Table 6.5). The simulations followed the procedures presented in Section 6.8.

Figure 6.39 presents a sample of 270 random side resistance data points created from the collective model. Figure 6.40 presents samples from the individual approach. The field test data were imposed in the figures for comparison. Figures 6.41 and 6.42 are in the expanded scale for displacements less than 2% D.

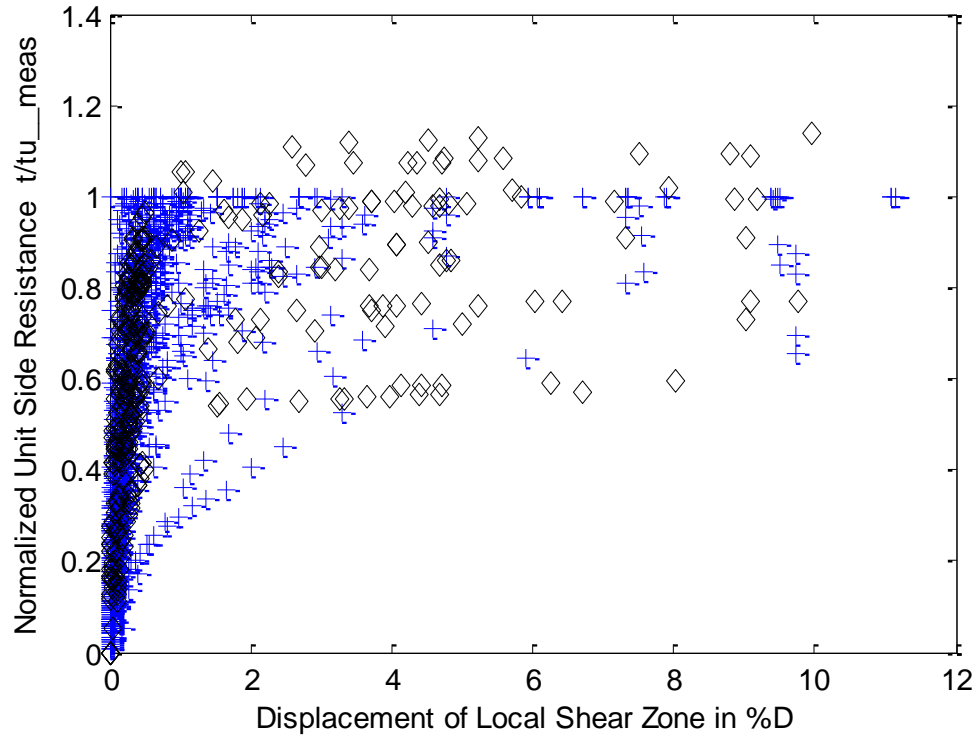


Figure 6.39 Comparison of simulated (\diamond) and measured (+) side resistances for the collective approach.

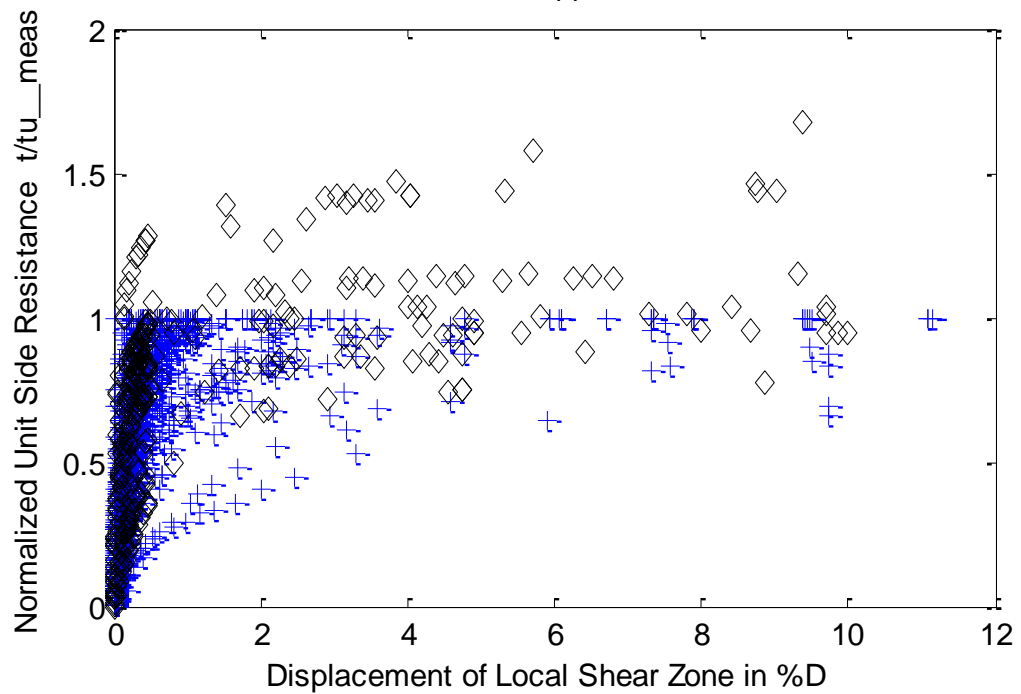


Figure 6.40. Comparison of simulated (\diamond) and measured (+) side resistances for the individual approach.

When displacement was less than 0.4 % D, the collective approach produced simulated resistance that was lower than the field test data. However, when the displacement was larger than 0.4% D, the simulated data compared favorably with the field test data.

On the other hand, the individual approach produced simulated data with values significantly higher than the field test data, especially when the displacement exceeded 0.2% D. The simulated data also seemed to be more scattered than data from field tests.

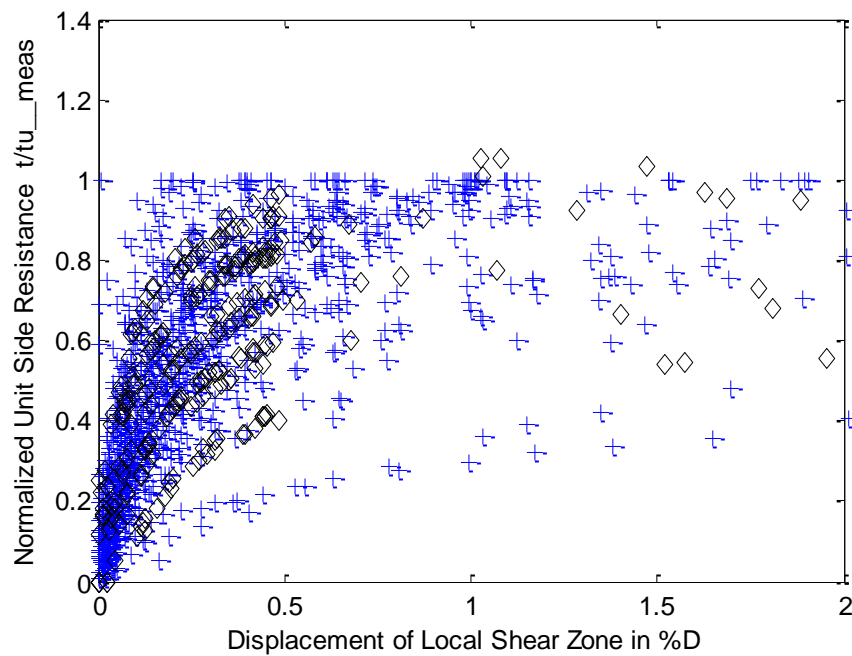


Figure 6.41. Comparison of simulated (\diamond) and measured (+) side resistances for the collective approach—expanded scale.

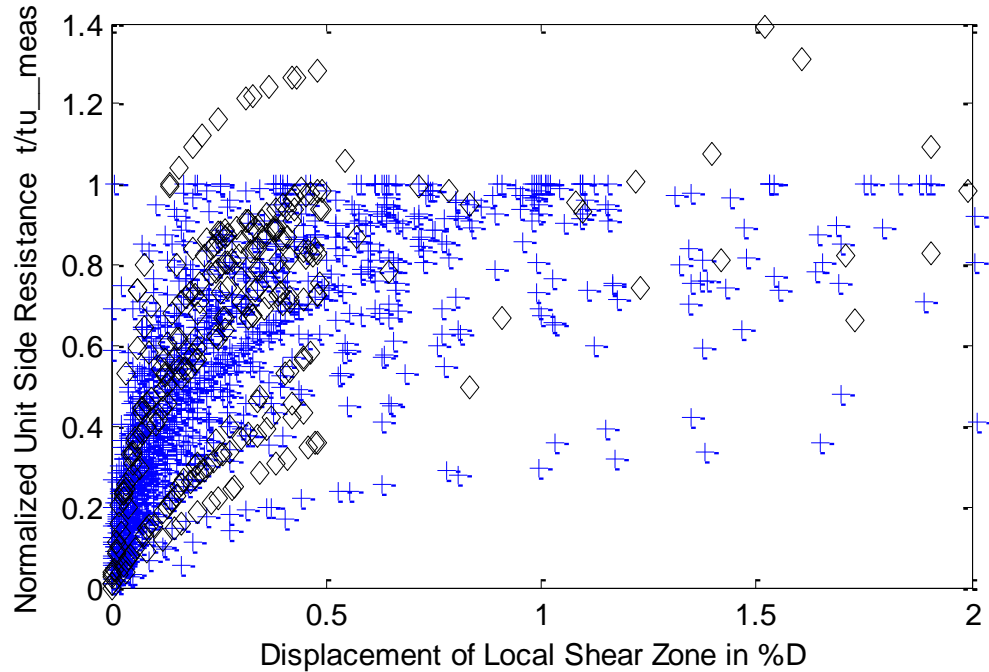


Figure 6.42. Comparison of simulated (\diamond) and measured (+) side resistances for the individual approach - expanded scale.

Regression analyses were performed on the 60,000 simulated data points generated from the model obtained from the collective approach, and on another 60,000 simulated data points from the individual approach. The regression analyses used a hyperbolic function and ordinary least squares analyses. The purpose was to find two “simulated” models and their variability from each approach. Then these models and their variability were compared with those from the field test data. The results are in Table 6.11.

Table 6. 13. Fitting parameters and the variability of simulated data and field test data for side resistance.

	Field Test Data	Collective Approach	Individual Approach
Parameter a	1.07	1.08	0.93
Parameter b	0.13	0.13	0.16
Conditional Standard Deviation	0.17	0.17	0.19

The regression analyses on the simulated data of collective approach produced fitting parameters and an *RMSE* or conditional standard deviation that was almost exactly the same as the field data. On the other hand, the individual approach provided a and b parameters that were not so similar to the field data. Furthermore, the *RMSE* of the simulated data was 0.19, which was higher than the 0.17 of the field test data. The collective approach of regression provided simulated data more similar to field data than did the individual approach.

The normalized unit side resistance versus normalized displacement curves, or t - z curves, were created based on the simulated data points. Figure 6.43 presents 150 random t - z curves created using the collective approach. The simulated t - z curves using the collective approach are “parallel” to each other. Some curves do not start from the origin, with some positive and negative t values at small values of z . The parallel characteristic is attributed to using two deterministic values of parameters, $a = 1.071$ and $b = 0.13$, with all the variability that results from adding the randomly simulated parameter, C . The curves are parallel to each other and are similar to the plus minus one standard deviation bounds which are parallel to the trend line.

On the other hand, Figure 6.44 presents 150 random t - z curves created from the individual approach. These simulated curves intersected one another and have varying shapes because a and b (or the slope and the horizontal asymptote) are randomly created differently for each curve. Furthermore, all the curves were generated using the individual approach fitting parameters pass through the origin.

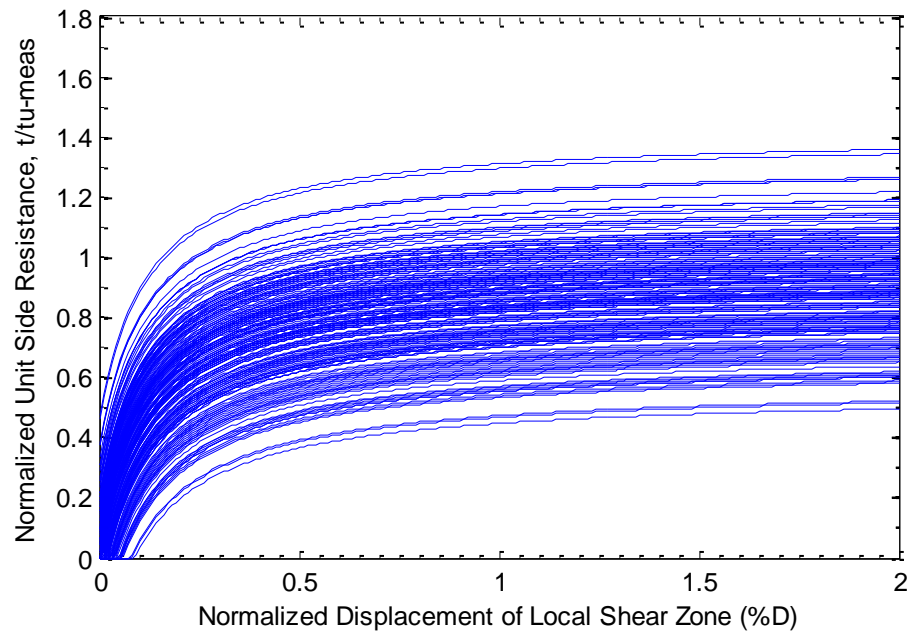


Figure 6.43. Simulated normalized unit side resistance curves from the collective approach.

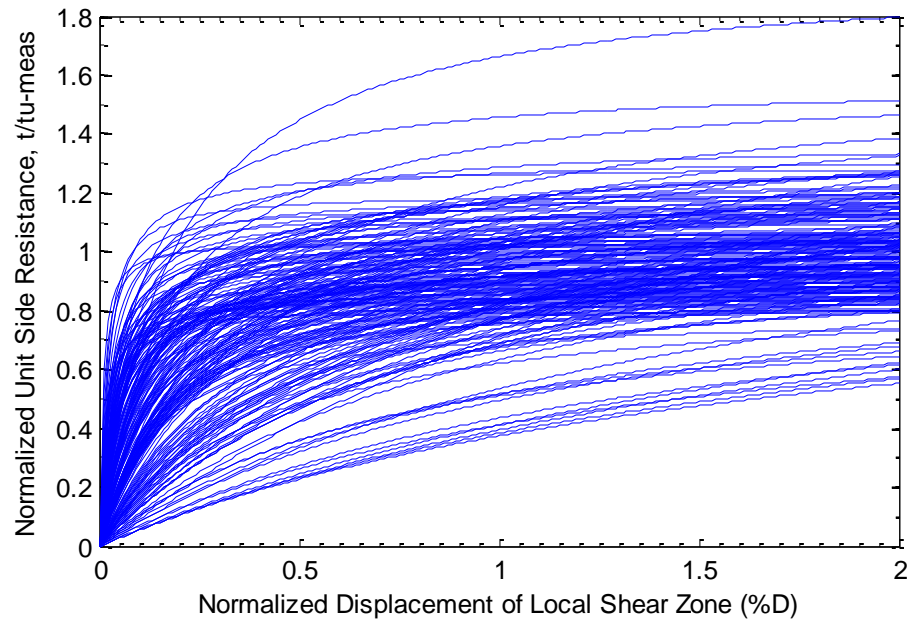


Figure 6.44. Simulated normalized unit side resistance curves
From the individual approach.

The collective approach produced simulated curves that were less scattered compared with the individual approach. One limitation of the collective approach was that some negative values existed for the normalized unit side resistance, t , which appeared at the very beginning of the curves when the normalized displacement z was less than about 0.08% of the shaft diameter. This value is usually small for the range of displacement for the service limit state analysis, which usually considers displacements more than 10 to 20 times greater than 0.08, or about 1 to 2% of shaft diameter.

6.9.2. Generation of Load Transfer Data - Tip Resistance

A total of 60,000 normalized displacements, and the corresponding 60,000 randomly simulated normalized unit tip resistance were generated using the hyperbolic fitting models obtained from the collective approach. The data were simulated using the

fitting parameters $a = 1.10$ and $b = 0.72$ (Equation 6.29), and the parameter C with mean value of 0.0 and standard deviation of 0.14 (Section 6.8).

An equal number of 60,000 simulated data points was created from the model obtained from the individual approach, $a = 0.12$ with a standard deviation of 0.57, $b = 0.95$ with a standard deviation of 1.19, and a correlation coefficient equal to -0.40 (Table 6.5). Because variable b is lognormally distributed, and parameters a and b are correlated, a transformation must be made. Using mean value $\ln(b)$ of -0.54 , and the standard deviation for $\ln(b)$ of 0.99, the new correlation coefficient of a and $\ln(b)$ is founded to be -0.49 . The simulations follow the procedures presented in Section 6.8.

Figure 6.45 presents a sample of 270 random tip resistance data points created from the collective model. Figure 6.46 presents random tips resistances from the individual approach. The field test data were imposed on the figures for comparison. Figure 6.47 and 6.48 are in the expanded scale for displacements less than 2% D.

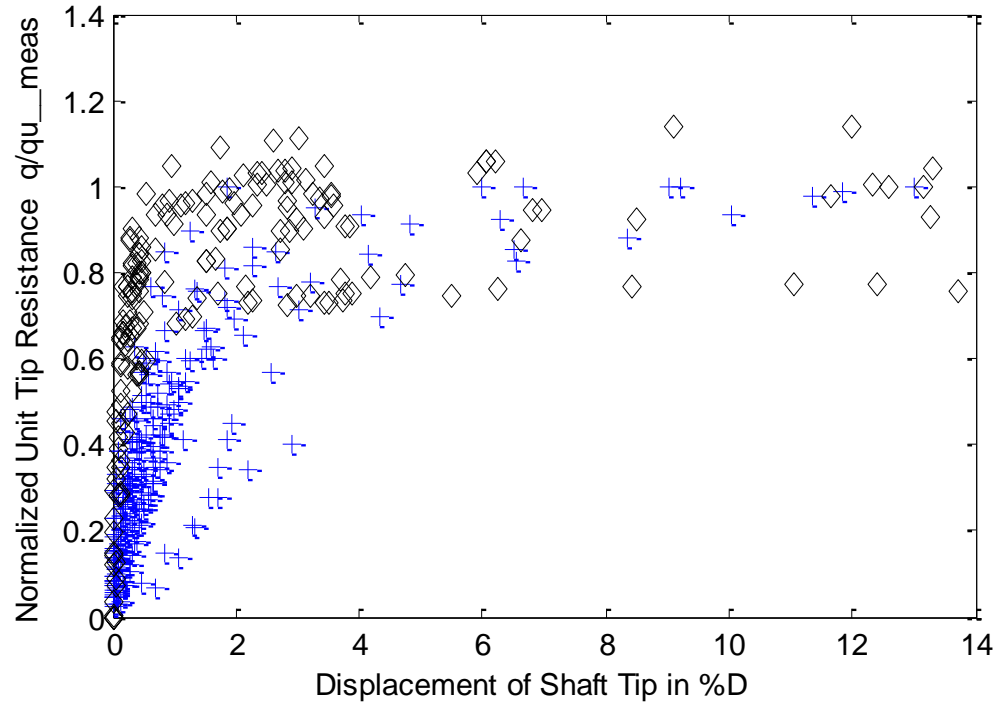


Figure 6.45. Comparison of simulated (\diamond) and measured (+) tip resistances for the collective approach.

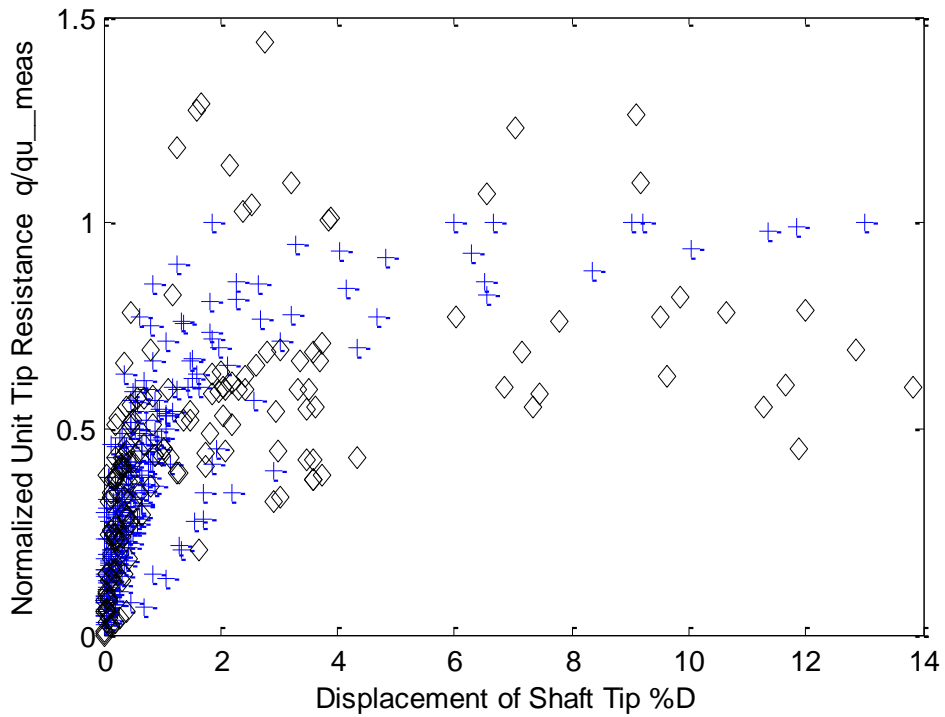


Figure 6.46. Comparison of simulated (\diamond) and measured (+) tip resistances for the individual approach.

When the displacement is less than 1 % D, the simulated data from the collective approach have larger values than the measured data, while those from the individual approach match the measured data more accurately. However, when the whole range of shaft tip displacement is considered, the simulated data from the individual approach are significantly more scattered than the simulated data from the collective approach.

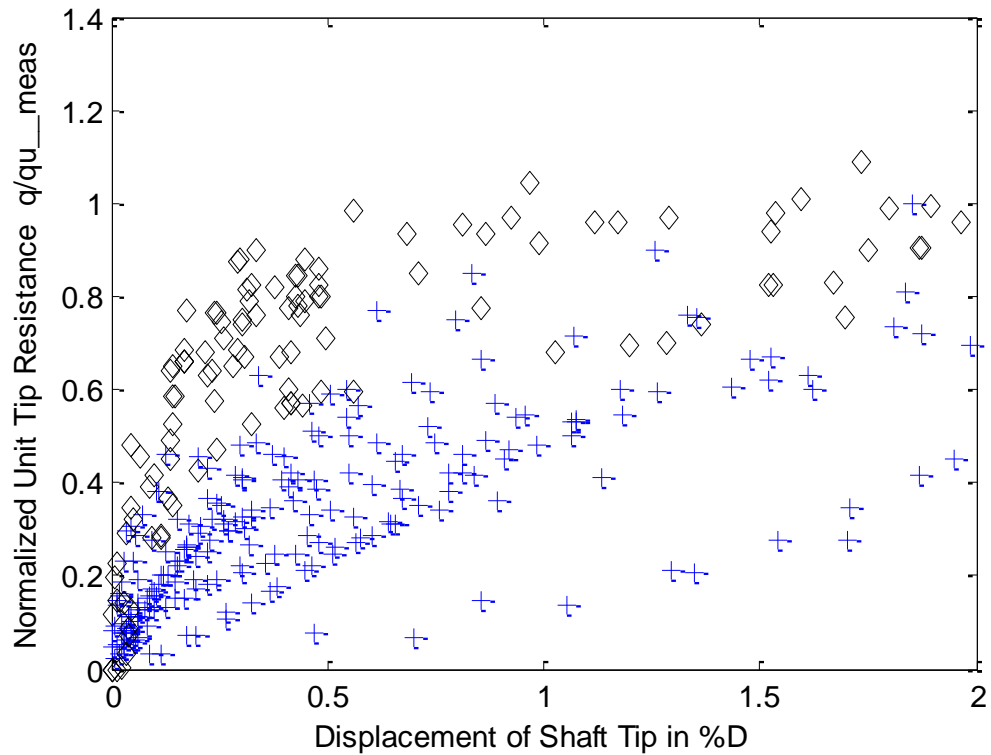


Figure 6.47. Comparison of simulated (\diamond) and measured (+) tip resistances for the collective approach—expanded scale.

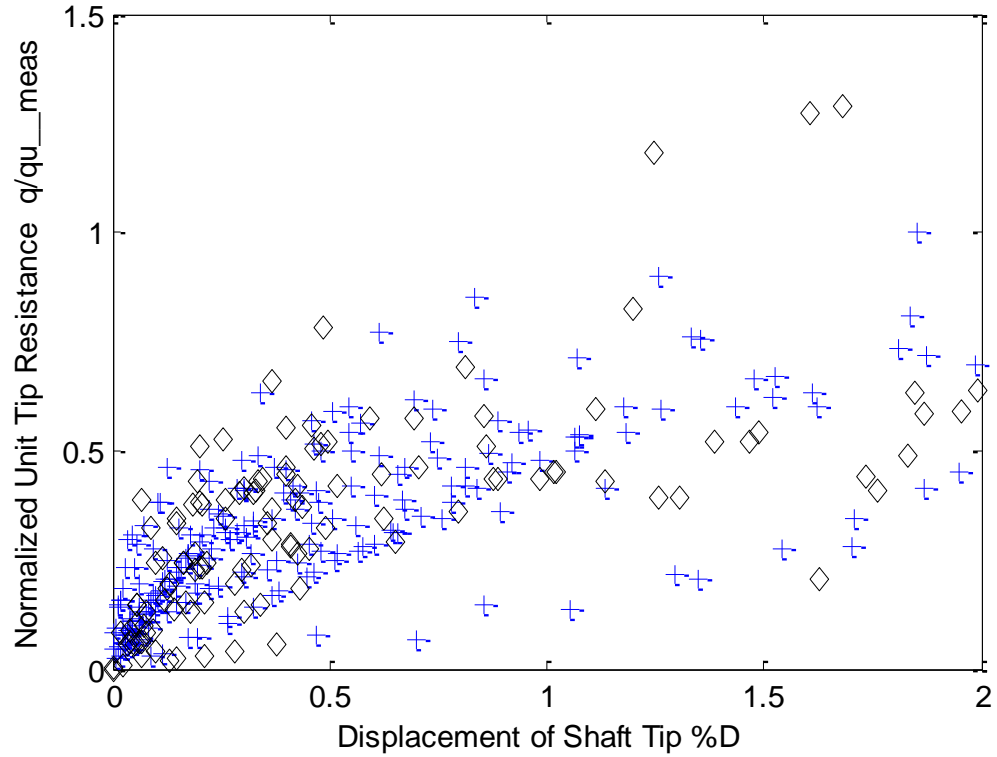


Figure 6.48. Comparison of simulated (\diamond) and measured (+) tip resistances for the individual approach—expanded scale.

Regression analyses were performed on the 60,000 simulated tip resistance data points generated from the model obtained from the collective approach, and another 60,000 data points from the individual approach. The regression used hyperbolic function and ordinary least squares analyses. The purpose was to find two “simulated” models as well as their variability from each approach. Then these models and their variability were compared with the models and variability from the field test data. The results are in Table 6.12.

Table 6.14. Fitting parameters and the variability of simulated data and field test data for tip resistance.

	Field Test Data	Collective Approach	Individual Approach
Parameter a	1.10	1.10	1.05
Parameter b	0.72	0.72	0.79
Conditional standard deviation	0.14	0.14	0.39

The observation is that the fitting parameters and the standard deviation obtained for the collective approach replicated those of the field test data. On the contrary, the individual approach gave $a = 1.054$, and $b = 0.7874$, which were not very close to those of field test data, and the standard deviation of 0.39 greatly exceed the standard deviation (0.138) of the field test data.

The normalized unit tip resistance versus normalized tip displacement $q-w$ curves were created based on the simulated data points. For visual purposes $q-w$ curves from a random subset of 150 data points were plotted in Figures 6.49 and 6.50.

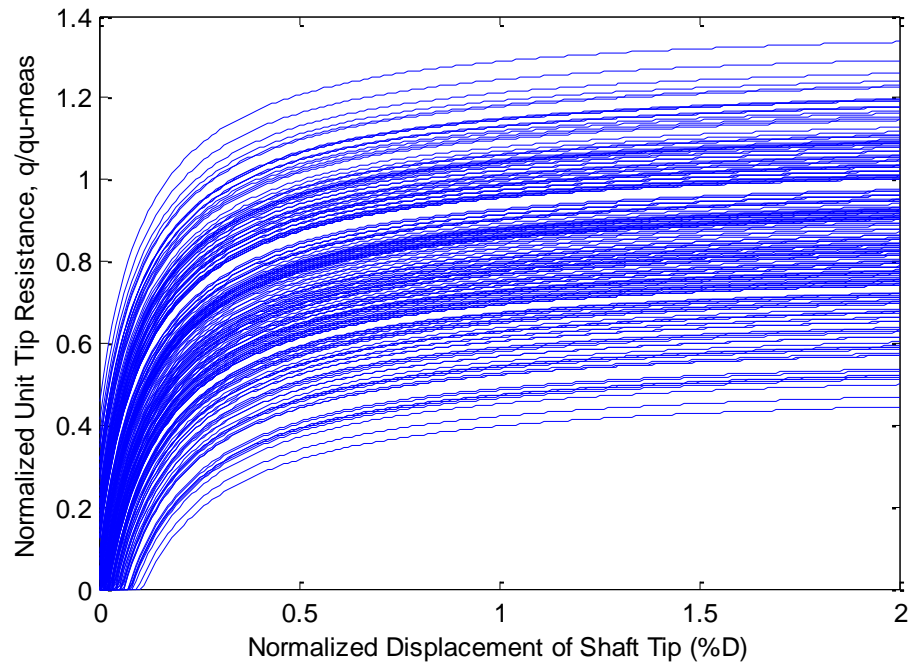


Figure 6.49. Simulated normalized unit tip resistance curves from the collective approach.

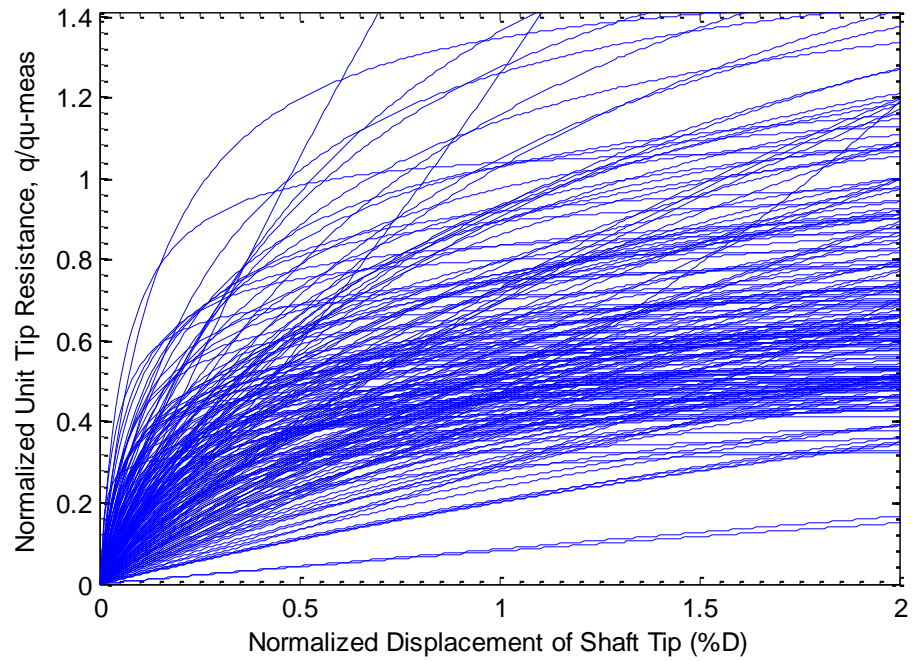


Figure 6.50. Simulated normalized unit tip resistance curves from the individual approach.

The curves generated from the collective approach have the same shape and do not pass through the origin. There are negative values of normalized unit tip resistance q appeared close to the origin, where w is less than about 0.08% of the shaft diameter. However, this value is usually relatively small within service limit state consideration, especially when considering mobilization of tip resistance where the displacement is 5 to 10% D .

The individual approach produces curves that pass through the origin. The curves generated from the individual approach have different slopes and asymptotes, which are similar to curves obtained from the field test. The simulated q - w curves from the individual approach are more scattered compared those from the collective approach.

Some tip resistance data points were not close to fully mobilized, which made the hyperbolic fitting parameters a have higher uncertainty/variability (Section 6.5.2). This is one of the reasons that simulated data from the individual approach are scattered. Another possible reason is the procedure for simulating data from the model obtained from the individual approach seemed to be more “processed”. In particular, these extra process steps included averaging values of a and b for all shaft segments and the transformations required for data simulation. Those steps may have distorted the simulated data from the observed data.

The simulated data points from the collective approach matched well with the field test data points. Therefore, even though the simulated load transfer curves did not pass through the origin at very small displacements, simulated data using the collective approach model gave results with fitting parameters and a standard deviation that

compared favorably with the field test data. Models based on the individual approach were not used for additional analyses.

6.10. Important Findings of this Chapter

- Five functional models were used for regression analyses, and the best model for side and tip load transfer data was found to be hyperbolic which predicts future data and their variability well. Hyperbolic model contains two fitting parameters that have physical meaning: a is the reciprocal of the curve's initial slope and b is the reciprocal of the curve's horizontal asymptote.
- Most models obtained from ordinary least square regression give prediction bounds that overpredict future observations when displacement is less than 0.05% of shaft diameter, but then the bounds predict the future outcome favorably when the displacement is higher than about 0.05% D. Models from weighted least squares regression with the defined weight predict future outcomes well only when the displacement is less than about 0.05%D. For larger displacement, these models overestimate the variability of future observations. Because 0.05%D is a relatively small displacement for SLS design, ordinary least squares regression is recommended for developing load transfer data.
- Uncertainty in load transfer t - z and q - w curves were quantified. The variation/uncertainty of the load transfer for side resistance, which has

constant standard deviation of 0.17 is larger than that for tip resistance, which has constant standard deviation of 0.14.

- Two approaches were presented for regression analysis to obtain functions for load transfer curves:

1) The collective approach, which does regression analysis for a whole set of data at once to obtain two hyperbolic fitting parameters for each side and tip load transfer model; and

2) the individual approach, which analyzes each load transfer curve from each shaft segment to obtain two sets of hyperbolic parameters. The model function was developed based on the parameters that are the average of all fitting parameters. The conclusions and findings about the approaches of regression are as follows:

- The variability and uncertainty of the load transfer models are represented differently for collective and individual approaches, and so is the method for simulating the load transfer curves. Corresponding methods for simulating data from the models of the two approaches were proposed.

- Simulated data points using the collective approach gives fitting parameters a and b that are almost exact matches to those from the field test data base. The standard deviation of the simulated data point from the collective approach is also the same as that of field test data. On the other hand, the individual approach gives different values of the

parameters compared with those from the field tests, especially for the b parameter. The load transfer models from the individual approach overpredict the variability of the future outcome. The collective approach is recommended for performing regression analysis for load transfer data. This is another significant practical implication of the research.

- Some of the simulated load transfer curves from the collective approach do not pass through zero at small displacement, and these curves have the same shape. On the other hand, the curves simulated using the models from the individual approach always pass through origin, and have varying shapes.

- One disadvantage of the individual approach is that the approach cannot utilize all the tip resistances from field test data points available when there are shafts which failed in shear, while the tip resistance was barely mobilized. The fitting parameters for those shafts sometimes are unreasonable and cannot be used to find the average fitting parameters for developing the tip resistance model.

- The two approaches give different load transfer models with different fitting parameters. A slight difference in the hyperbolic a parameters exists. However, the b parameter magnitudes are almost two times different for the two approaches. Parameter b , which represents the initial slope of the curve, is 0.13 for the collective approach, while for the individual approach, it is 0.25.

- The individual approach gives the coefficient of correlation between the two hyperbolic parameters, but the collective approach cannot do that. The coefficients of correlation for both fitting parameters of side and tip resistance curves are negative, meaning that the slope and the asymptote of the load transfer curve are inversely proportional. The individual approach also is able to give the distribution type of the fitting parameters. The distribution type of a parameter is normal, but for the b parameter, it is lognormal.

6.11. Selection of Load Transfer Models

Subsequent probabilistic analyses need load transfer models that are capable of producing probabilistically simulated data that simulate field test load transfer data. Analyses presented in previous sections demonstrate that the hyperbolic model is the best of the five models representing the load transfer measured data. The ordinary least squares regression had advantages over weighted squares regression to model the variability and uncertainty of the measured data. The collective approach created load transfer data that produced hyperbolic fitting parameters and conditional standard deviation which replicated the field test data. Thus, the hyperbolic models from ordinary least square analyses obtained from the collective approach were chosen as the best models for further SLS probabilistic analyses.

Table 6.13 presents the final load transfer models for side and tip unit resistances normalized to the maximum measured values and normalized to the

predicted ultimate values. These models were used in subsequent work for SLS probabilistic analyses presented in Chapter 8.

Table 6.15. Summary of load transfer models and their quantified variability.

	Normalized to Maximum Measured Values		Normalization by Maximum Predicted Values	
	Hyperbolic Function	Conditional Std. Deviation	Hyperbolic Function	Conditional Std. Deviation
Side Resistance	$t = \frac{z}{1.071 * z + 0.13}$	0.17	$t = \frac{z}{1.104 * z + 0.1174}$	0.35
Tip Resistance	$q = \frac{w}{1.098 * w + 0.721}$	0.14	$q = \frac{w}{0.72 * w + 0.68}$	0.34

6.12. Summary

The objective of the analyses presented in this chapter was to identify models for load transfer data and to quantify the variabilities and uncertainties of the models. The hyperbolic function was found to be the best model presenting load transfer data for both unit side and tip resistances. The ordinary least squares regression and the collective approach of regression were recommended for load transfer data analyses. New relationships were proposed for drilled shafts normalized unit side and tip resistance versus normalized displacement in shales, using approaches of normalizing to maximum measured values and predicted ultimate resistance. The load transfer models subsequently were used to predict load-displacement responses in deterministic and

probabilistic analyses in the resistance factor calibrating process, which is presented in Chapter 8.

Chapter 7. Evaluation of Probabilistic and Deterministic Variables

7.1. Introduction

This chapter presents a new framework for service limit states (SLS) design with the utilization of SLS resistance factor, which is used to account for different sources of variability/uncertainty in design. The SLS probabilistic analyses and resistance factor calibration process, which involve a number of deterministic and probabilistic parameters, are presented. This chapter is also about the evaluation of probabilistic and deterministic variables. A sensitivity study was conducted to evaluate the dependency of the resistance factor on each probabilistic variable and on each source of uncertainty, as well as on the deterministic variables. The primary objective of this sensitivity study is to inform implementation of the load and resistance factor design for the SLS design.

7.2. Framework for Load and Resistance Factor Design at Service Limit State

The SLS resistance factor in this research applies to the strength parameter of geomaterials to account for possible sources of uncertainty so that the design can achieve a level of reliability or a target probability of failure. The SLS performance function is:

$$y_a - y^*_{(UCS^*)} \geq 0 \quad (7.1)$$

with

$$UCS^* = \varphi * UCS \quad (7.2)$$

where

$y^*_{(UCS^*)}$ = factored predicted settlement,

y_a = allowable or limiting settlement,

UCS = uniaxial compressive strength,

UCS^* = factored uniaxial compressive strength, and

φ = resistance factor.

The resistance factor is to be used in a newly proposed framework of the SLS design for drilled shafts. The steps for the proposed framework are:

1. Find shaft length and shaft diameter following the ultimate limit state procedure.
2. Use given parameters to obtain an SLS resistance factor. The resistance factor is to account for different sources of variability/uncertainty and is dependent on parameters such as the coefficient of variation (COV) of the UCS , the target probability of failure. How to obtain the resistance factor is discussed in detail in Chapter 8.
3. Calculate a factored UCS^* (Equation 7.2). Use factored UCS^* and shaft dimensions, given loads, and t - z models to calculate the shaft's factored settlement. This value of settlement is associated with the given target probability of failure.
4. Compare the factored settlement with the allowable settlement (Equation 7.1).
If the factored settlement is less than or equal to the allowable settlement, the

SLS check is finished. If not, the shaft dimension is increased and steps 2 to 4 are repeated until Equation 7.1 is satisfied and the SLS design procedure is complete.

An SLS design following this framework is based on direct comparison of the factored predicted settlement with the allowable settlement and does not require probabilistic analyses. A final framework with more details on Steps 2 and 3 is presented in Chapter 9.

7.3. Calibration of Resistance Factors for Service Limit State

This section is divided into two subsections. The first presents the probabilistic analysis of how to obtain a shaft head displacement histogram. The second presents a step-by-step procedure for SLS resistance factor calibration.

7.3.1. Probabilistic Analysis

Deterministic and probabilistic variables for the SLS analysis are in Table 7.1. The t - z and q - w models and the ultimate unit side and tip resistance predictive models are considered to be probabilistic variables with their uncertainties represented by their conditional standard of deviations or COVs.

Table 7.1. Inputs for SLS probability analyses and resistance factor calibration.

#	Variables	Type	
1	Dead load	Probabilistic	
2	Live load	Probabilistic	
3	Uniaxial compressive strength	Probabilistic	
4	Shaft length		Deterministic
5	Shaft diameter	Probabilistic	
6	Concrete Young's modulus	Probabilistic	
7	Target Probability of failure		Deterministic
8	t - z model	Probabilistic	
9	q - w model	Probabilistic	
10	Ultimate side resistance predictive model	Probabilistic	
11	Ultimate tip resistance predictive model	Probabilistic	

Probabilistic analyses were performed using the random number simulation technique, i.e., Monte Carlo simulation (Chapter 4), for probabilistic variables. The generated load transfer model followed the procedure described in Chapter 6. The product of the probabilistic analysis is a set of shaft head displacements, which are shown in a histogram (Figure 7.1)

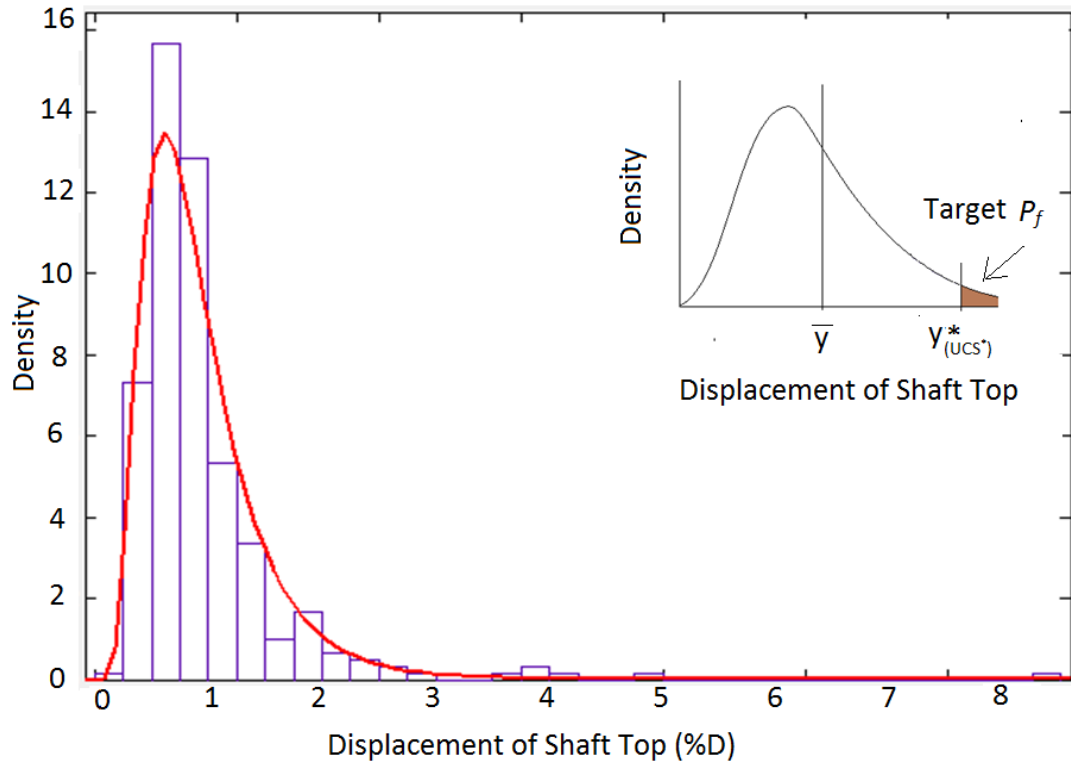


Figure 7.1. Histogram and probability density curve for vertical top shaft displacement.

The probabilistic analysis used the Monte Carlo approach with the number of simulations n equal to 30,000. The detailed procedure is:

1. Generate a set of $n = 30,000$ values for loads (dead loads and live loads) using the loads' means and COVs. This is a probabilistic calculation with the Monte Carlo simulation technique as discussed in Section 4.1.
2. Generate another set of n values of shaft stiffness, EA , using the mean value of EA and its COV.
3. Generate a set of n values of UCS using its mean value COV.
4. Generate n values of ultimate unit side and tip resistance f_{ult} and q_{ult} . This step incorporates the predictive models' variabilities. The models used

were the unit side and tip resistance (f_{ult} and q_{ult}) versus the *UCS* predictive models (Equations 7.7 and 7.8).

5. Generate a set of n load transfer curves from the t - z and q - w models (Table 6.13) and their standard of deviations. This step follows the procedure described in Chapter 6.
6. For one simulation, based on one value of a randomly generated load, *UCS*, *EA*, f_{ult} and q_{ult} , one t - z model and one q - w model, the t - z method (Chapter 3) was used to determine a value of shaft top displacement. For 30,000 simulations, 30,000 values of shaft head displacements were obtained. These values of shaft head displacements were used to create the shaft head histogram, which is the product of the probabilistic analyses.

7.3.2. Resistance Factor Calibration:

From the displacement histogram obtained from the probabilistic analysis described in the previous section, an SLS resistance factor calibration can be found. In general, from the histogram, a specific value of displacement y^* (Figure 7.1) that associates with the target probability of failure, P_f , was determined. Then a factored UCS^* was found based on the condition that if this UCS^* is used, the shaft head displacement obtained is equal to the factored displacement y^* . Then the resistance factor is the ratio of the factored and unfactored *UCS*. The description of the procedure follows.

1. Determine the number of “SLS failure cases” associated with the target probability of failure P_f . The number of failure cases n_f is equal to the target P_f multiplied by the number of simulation n , which is 30,000.

$$n_f = n * P_f = 30,000 * P_f \quad (7.3)$$

2. Find the factored displacement y^* (Figure 7.1) that associates with the number of failure cases n_f . This can be done by sorting the displacement vector in descending order; then, taking the $(n_f + 1)^{th}$ displacement value as y^* . This y^* associates with the target probability of failure P_f as

$$P_{(y>y^*)} = P_f. \quad (7.4)$$

3. Determine the uniaxial compressive strength UCS^* that produces y^* . This step is done by gradually reducing the value of the given UCS . Use the reduced value of UCS to calculate the new shaft top displacement using the t - z method. The process continues until the displacement is equal to y^* . These calculations are deterministic, using the mean values for all parameters except the UCS .
4. Find the SLS resistance factor ϕ , which is the ratio of UCS^*/UCS (as in Equation 7.2)

The SLS resistance factor is calibrated to apply to the UCS in SLS design. Applying the resistance factor reduces UCS so that a design using the nominal values (or mean values) of all parameters and the factored UCS^* produces a factored shaft top vertical displacement that associates with the target probability of failure. The resistance factor

depends upon the histogram of the shaft head displacement, which, in turn, depends on the nominal values and variability of the input variables.

The MATLAB® was used to write a computer program which employs the finite element method described in Chapter 3, Monte Carlo simulation and the SLS probability analyses described in Chapter 4, t - z and q - w models and their simulation procedure established in Chapter 6, and resistance factor calibration procedures presented in the previous section. The computer program is presented in Appendix E.

The resistance factor in this study is presented versus the coefficient of variation of uniaxial compressive strength (*COV of UCS*). The *COV of UCS* is a parameter that has a wide range and often is obtained during site investigations, or if not, can be assumed using “engineering judgment”. Other researchers have also chosen the *COV* of soil or soil/structure property as the independent variable when presenting the resistance factor (Phoon, 1995; Misra and Roberts, 2009). In the computer code, the resistance factor is specified to be rounded to the nearest 0.005. This is two times smaller than the value of 0.01 usually used in the literature.

7.4. Parameter Normalization

During the resistance calibration process, it was noticed that the SLS resistance factor is dependent on nominal values of load, *UCS* and shaft dimensions. This section is about normalization of variables; the presentation on how the resistance factor depends on these normalized variables is in subsequence sections.

One of the examples which shows how the SLS resistance factor depends on nominal values of input parameters (in this case the parameter is load) follows. In a case with inputs as in Table 7.2 where the *COV of UCS* is zero, the resistance factor required to obtain a probability of failure of 1/25 for load (dead load plus live load) of 2000 kips is 0.58. However, when the load is reduced to 1000 kips, the resistance factor drops to 0.46. The load, *UCS* and shaft dimensions are related in the displacement histogram from which the resistance factor is determined, and in similar fashion, the resistance factor depends on the inputs.

In this research, a new parameter named *normalized load*, with the notation of θ , is introduced. The normalized load is the ratio of load over shaft capacity Q_{ult} . Load applied on a shaft is the sum of dead load, *DL*, and live load, *LL*. The normalized load is:

$$\theta = \frac{DL+LL}{Q_{ult}} \quad (7.5)$$

The ultimate shaft capacity is:

$$Q_{ult} = A_s * t_{ult} + A_p * q_{ult} \quad (7.6)$$

where

A_s = the side area of the shaft which is equal to circumference of the shaft times shaft length,

A_p = shaft cross sectional area,

t_{ult} and q_{ult} = ultimate unit side resistance and tip resistance, as a function of UCS , Equations 7.7 and 7.8.

Using the normalized load allows the effects of mean value of load and uniaxial compressive strength (UCS) on the SLS resistance factor to be replaced by the effect of one parameter, the normalized load. Other normalized parameters that are introduced are normalized shaft dimension, which is shaft length over shaft diameter ratio, L/D , and dead load over live load ratio, DL/LL . The effects of the normalized load, normalized shaft dimension, and dead load over live load ratio on the SLS resistance factor are presented in subsequent sections.

It was confirmed in this research that as long as the normalized load and normalized shaft dimension are constant, the resistance factor is a constant regardless of how load, UCS , shaft length or shaft diameter are changed. Figure 7.2 shows calibrated resistance factors for a normalized load θ of 0.3 and a normalized shaft dimension L/D of 10. Different values of UCS from 8 ksf to 50 ksf, shaft length L of 30, 50 and 80 ft., shaft diameter D of 3, 5 and 8 ft., and different corresponding loads to make the normalized load of 0.3, were used in the example. Practically no differences were measured for the obtained resistance factors, indicating that the approach of combining input parameters is effective, and the effect of the change of load, UCS , shaft length or shaft diameter on the resistance factor can be represented by the effect of the change of the normalized load and the normalized shaft dimension.

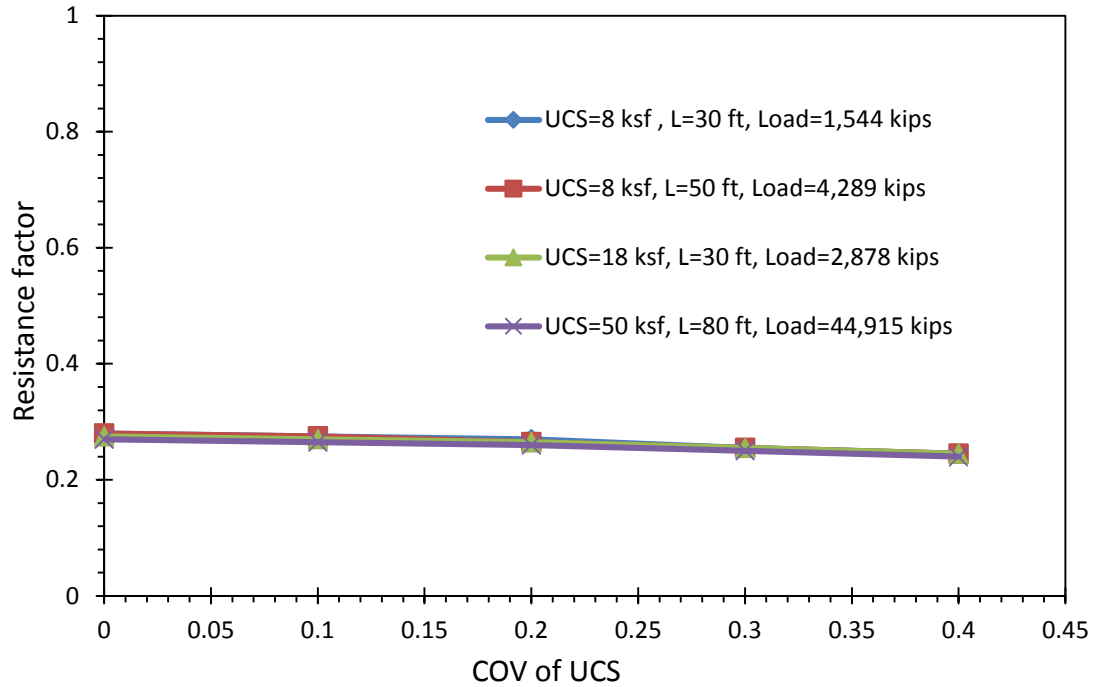


Figure 7.2. Resistance factors for different loads, shaft lengths, shaft diameters and UCSs.

7.5. Impossible Cases

In the process of resistance factor calibration, sometimes there are cases where the randomly simulated loads are high while the randomly simulated shaft resistances (or shaft capacities), are low. When the simulated load is larger than the simulated resistance, the shaft head displacement cannot be calculated. If the number of these cases is larger than the target probability of failure, as illustrated in Figure 7.3, no resistance factor can be obtained to achieve the SLS target probability of failure. This situation is called the “impossible” case. The low shaft resistance comes from a combination of resistance components, such as small t value (from t - z model) or small UCS .

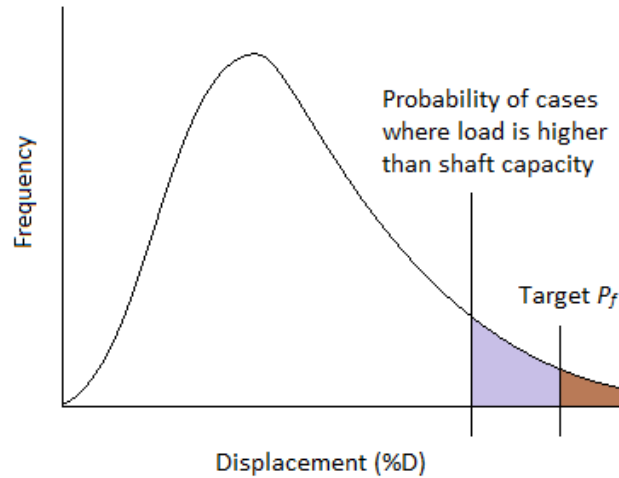


Figure 7.3. Impossible case: the probability of failure cases is larger than the target probability of failure.

To illustrate this concept, an example of 300 Monte Carlo simulations was run using inputs presented in Table 7.2 to obtain a histogram of resulting shaft displacements shown in Figure 7.4. During the calculation, when there was a simulation where the randomly generated load was higher than the randomly generated capacity, the solution for that simulation did not converge. The shaft head displacement could not be determined, and the displacement for this simulation was assigned an arbitrary large displacement, i.e., 14% of the diameter. In Figure 7.4, in one set of 300 simulations, there are 16 simulations where loads were higher than shaft capacity, represented by 16 cases with a very large displacement of 14% shaft diameter.

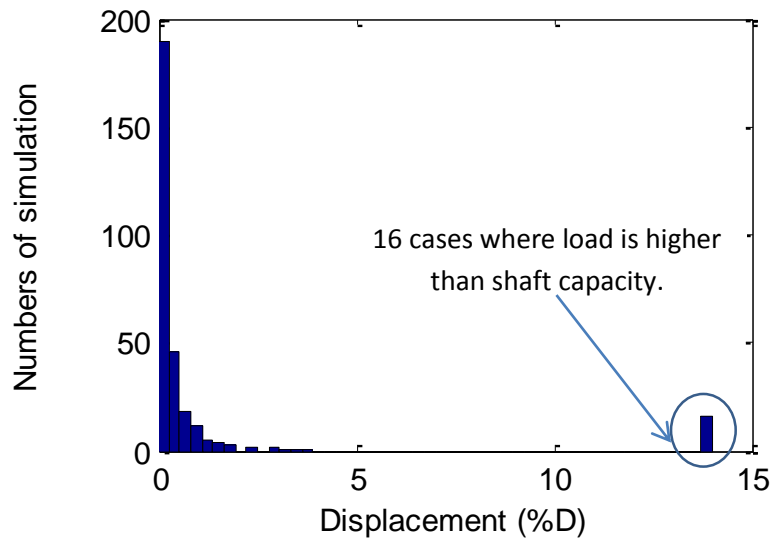


Figure 7.4. Displacement histogram from 300 simulations.

In the example above, with a probability of failure, P_f , of 1/100, which is smaller than 16/300, the resistance factor cannot be determined, and it is the impossible case as illustrated in Figure 7.3. However, if the P_f is 1/15, which is larger than 16/300; then, the resistance factor can be obtained. For circumstances when the normalized load is high, and uncertainty and variability of the resistance of soil/shale properties also are high, the load distribution and the resistance distribution “move” close together (Figure 7.5), the resistance distribution becomes wider, and the overlap area becomes larger. This means that the failure cases have more chances to occur. The number of impossible cases depends on the target probability of failure, on the combination of uncertainty/variability of all parameters, as well as on the magnitude of the applied load. Because of the impossible case concept, the SLS resistance factor can be achieved only in some

given conditions. The appearance and discussion of the impossible case is also found later in this and the next chapter.

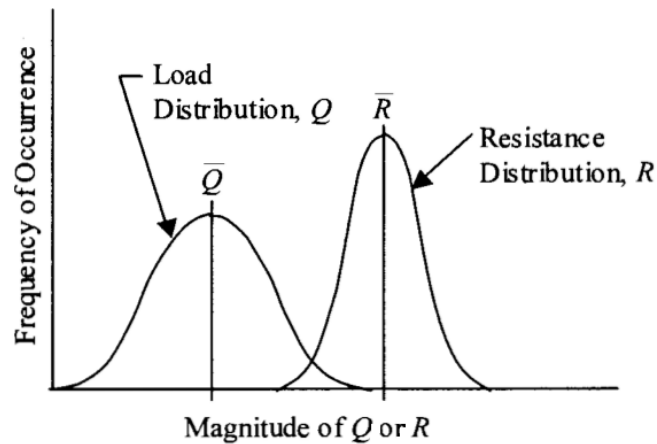


Figure 7.5. Frequency distribution of random values load and resistance (From Allen, 2005).

7.6. Sensitivity Analyses

This section presents the analyses that are the primary objective of this chapter: evaluation of the influence of input variables on the SLS resistance factor.

7.6.1. Inputs for Sensitivity Analyses

An SLS design or a SLS calibration process based on the t - z method, requires a total of 24 inputs, not including types of variables distributions. The 24 inputs have different effects on the resulting shaft displacement, the reliability of the prediction, and eventually on the SLS resistance factors. This section presents the inputs for the analyses of evaluating the sensitivity of the variables. The inputs are listed in Table 7.2. There are sections that use some inputs which were assigned different values; these are specified clearly in those sections.

Table 7.2. Input for SLS probabilistic analyses.

#	Inputs	Values
1	Dead load (kips)	858
2	COV of dead load	0.1
3	Live load (kips)	429
4	COV of live load	0.12
5	UCS (ksf)	8
6	COV of UCS	Independent variable
7	Shaft length (ft.)	50
8	Shaft diameter (ft.)	5
9	Concrete Young's modulus (ksi)	4090
10 & 11	COV of concrete modulus & shaft cross section area	0.15
12	Target Probability of failure	1/25
13	Standard deviation of load transfer - side resistance	0.12
14	Standard deviation of load transfer - tip resistance	0.1
15	COV of unit side resistance prediction model	0.2
16	COV of unit tip resistance prediction model	0.15
17 & 18	Hyperbolic parameters a and b - side resistance	1.07 and 0.13
19 & 20	Hyperbolic parameters a and b - side resistance	1.01 and 0.72
21 & 22	Ultimate predictive model -side resistance (x2)	0.76 and 0.79
23 & 24	Ultimate predictive model -tip resistance (x2)	14.0 and 0.71

In these inputs, the concrete Young's modulus is determined from the concrete strength tests (Chapter 5). The statistics of dead load and live load are values recommended by Kulicki et al. (2007). For the t - z and q - w models, the hyperbolic fitting parameters are obtained from regression analysis as in Chapter 6, i.e., for the t - z , parameters a is 1.07 and b is 0.13, and for q - w model parameters, a is 1.01 and b is 0.72. Inputs for ultimate unit side and tip predictive models (inputs #21 to 24) are obtained from the following models (Loehr et al., 2011):

$$q_s = 0.76 \times UCS^{0.79} \leq 30 \text{ ksf} \quad (7.7)$$

$$q_p = 14 \times UCS^{0.71} \leq 400 \text{ ksf} \quad (7.8)$$

where q_s and q_p are the ultimate unit side and tip resistance. The normalized parameters in Table 7.2 are in a relatively typical range for drilled shafts, with a normalized load of 0.3, a dead load/live load ratio of 2.0, and shaft length over shaft diameter ratio of 10. Other input values were chosen arbitrarily within a practical range.

7.6.2. Effect of Variability of Probabilistic Variables

The influence of variability/uncertainty of each variable on the SLS resistance factor is different depending on the variable. Two variables with the same COV may have different effects on the reliability of the SLS design, and, therefore, on the calibrated resistance factor. This section is to provide an understanding of how the variability probabilistic parameters affect the SLS resistance factor.

Possible sources of uncertainty for service limit state analysis using the t - z method come from the probabilistic variables (Table 7.1). They are dead load, live load, uniaxial compressive strength (UCS) of the geomaterial, shaft stiffness (combined as a product of concrete Young's modulus and cross sectional area), ultimate unit side and tip resistance predictions models, and load transfer models (t - z and q - w curves). In this section (7.6.2), dead load and live load are combined as *load* with one value of COV, so there is a total of seven sources of uncertainty. A sensitivity analysis was conducted by changing the COV of *each* listed probabilistic variable from 0.0 to 0.7 while keeping all other variables deterministic. This allowed investigation of the change in resistance factor caused by the change in the variability of one probabilistic parameter at a time.

All inputs are given in Table 7.2, except that the COV and/or standard deviations of the probabilistic variables were changed as described in this section in order to investigate the sensitivity, and that the normalized load θ here is ≤ 0.5 . The resulting resistance factors are presented in Figure 7.6.

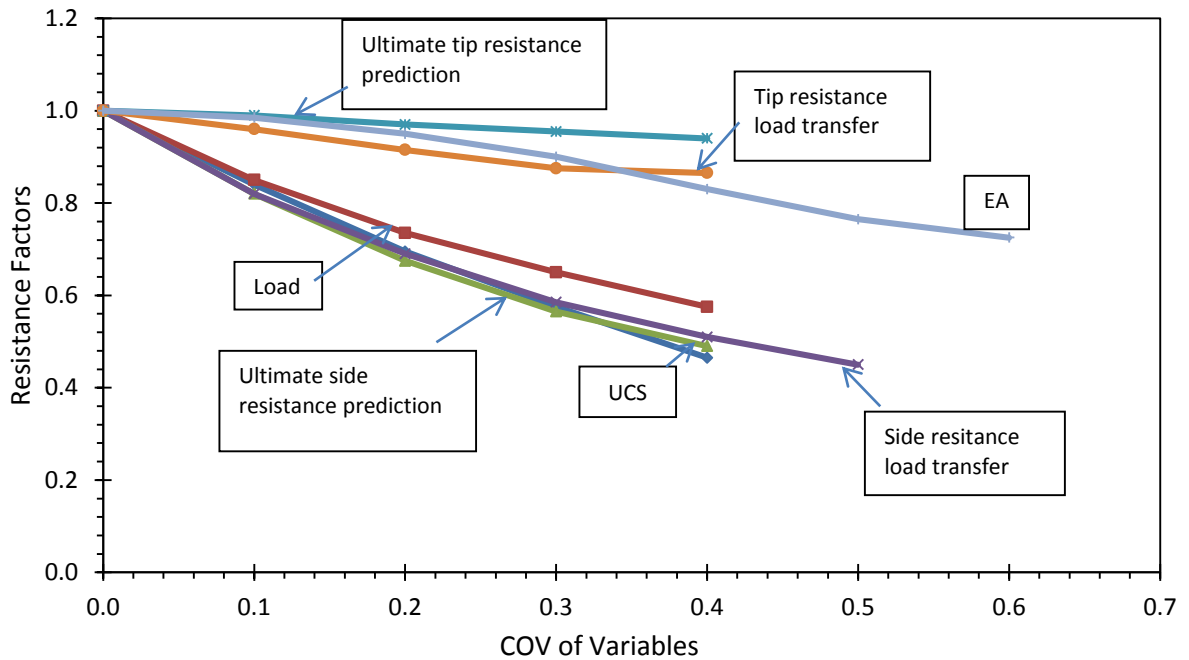


Figure 7.6. Resistance factors versus COV of each probabilistic variable.

The resistance factor is plotted on one line named after each probabilistic variable considered. There are seven probabilistic variables; therefore, there are seven lines presenting the change of the resistance factor on the seven variables (Figure 7.6). When the COV of the investigating variable is zero, the resistance factor is unity. When the COV of the investigating variable *increases*, the resistance factor *decreases*.

The curves separated into two groups, a lower and an upper group. The lower group with a pronounced drop of resistance factor curves shows UCS, ultimate unit side

resistance prediction, side load transfer (t - z) model and load. The upper group with a slower drop of resistance factor curves shows shaft stiffness (EA), tip resistance load transfer and ultimate unit tip resistance prediction. A faster drop in resistance factor line indicates that resistance factor is more sensitive to variability (the COV) of that probabilistic parameter. Therefore, the most influential probabilistic variables on the resistance factor are UCS, side resistance load transfer (t - z) model, the ultimate unit side prediction, and load.

This section presented the effect of the *variability* of probabilistic variables on the SLS resistance factor. The effects of *nominal* value of variables on SLS the resistance factor are presented in the following sections.

7.6.3. Effect of Normalized Load on SLS Resistance Factor

A study was carried out to evaluate the effect of nominal values of normalized load θ on the SLS resistance factor. The resistance factors were calculated for different normalized loads θ , changing from 0.2 to 0.6, which is a typical range of normalized applied load based on ULS considerations. All other deterministic and probabilistic inputs were kept constant as in Table 7.2. The results are presented in Figure 7.7.

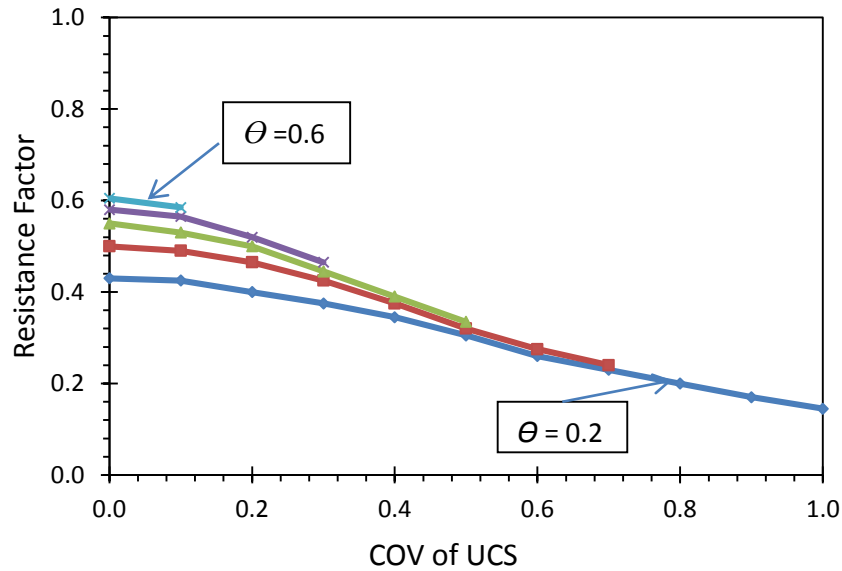


Figure 7.7. Resistance factors for different normalized loads θ from 0.2 to 0.6.

The resistance factor is noticeably dependent on normalized load. As shown in Figure 7.7, at *COV of UCS* equal to zero, the resistance factor significantly decreases from 0.605 to 0.430 when the normalized load θ varies from 0.6 to 0.2.

The curve for higher normalized load of 0.6 truncates when *COV of UCS* is 0.1, meaning that the target probability of failure, which is 1/25 (Table 7.2), cannot be achieved when *COV of UCS* is higher than 0.1. This is attributed to the “impossible case” (Section 7.5) where the load distribution moves close to the resistance distribution, and/or resistance distribution becomes wider. In this situation, the number of cases where the randomly simulated load is higher than the randomly simulated shaft capacity is more than the target probability. For a lower load of 0.2, P_f can be reached even when the *COV of UCS* is as high as 1.0. With the lower normalized load, a design is more likely to achieve the target probability of failure with the higher *COV of UCS*,

and the impossible case has less chance to occur. The curves all appear to converge to an upper bound curve, where all the curves truncate. This could have also resulted from the impossible cases.

As in Figure 7.7, the higher the normalized load is, the lower the resistance factor is. This could be caused by the high non-linearity feature of load transfer curve and can be explained qualitatively using Figure 7.8.

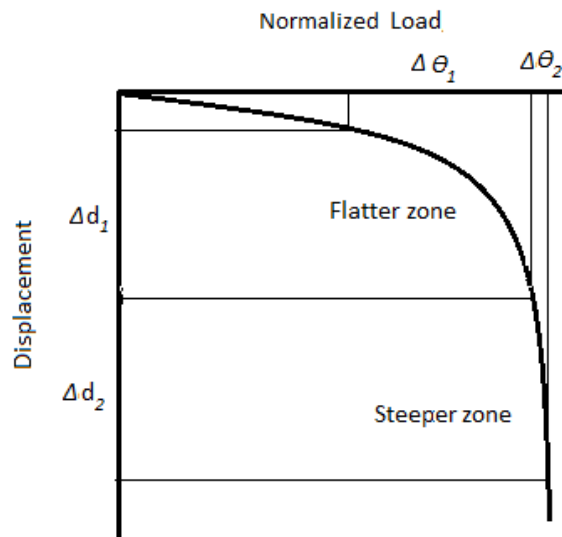


Figure 7.8. Non-linearity of load transfer curve.

The effect of changing the load is *inversely* proportional to the effect of changing the UCS. In the calibration process, the resistance factor is to be used to factor UCS, or to reduce UCS to increase the nominal value of the settlement to the settlement y^* that is associated with the target probability of failure (Figure 7.1). The effect of reducing the UCS is similar to the effect of increasing the load. In Figure 7.8, to obtain the same increasing amount of displacement $\Delta d = \Delta d_1 = \Delta d_2$, the required change in the

normalized load $\Delta\theta_1$ in the flatter zone is much larger than the $\Delta\theta_2$ in the steeper zone. This means that less change in normalized load is required in the flatter zone. The reduced change in load is analogous to less change in UCS (recall they are inversely proportional), and the less change in UCS means a higher resistance factor is needed to obtain the factored displacement y^* . Therefore, the resistance factor is higher for the higher normalized load.

7.6.4. Effect of Dead Load over Live Load Ratio

Applied load consists of dead load and live load, and because they have different COVs, they may have different effects on the resistance factor. In this section, the effect of the dead load over live load ratio on the resistance factor is presented. The resistance factor was calibrated using two values: the dead load/live load ratio of 2 and ½. Other inputs are shown in Table 7.2. The results are presented in Figure 7.9.

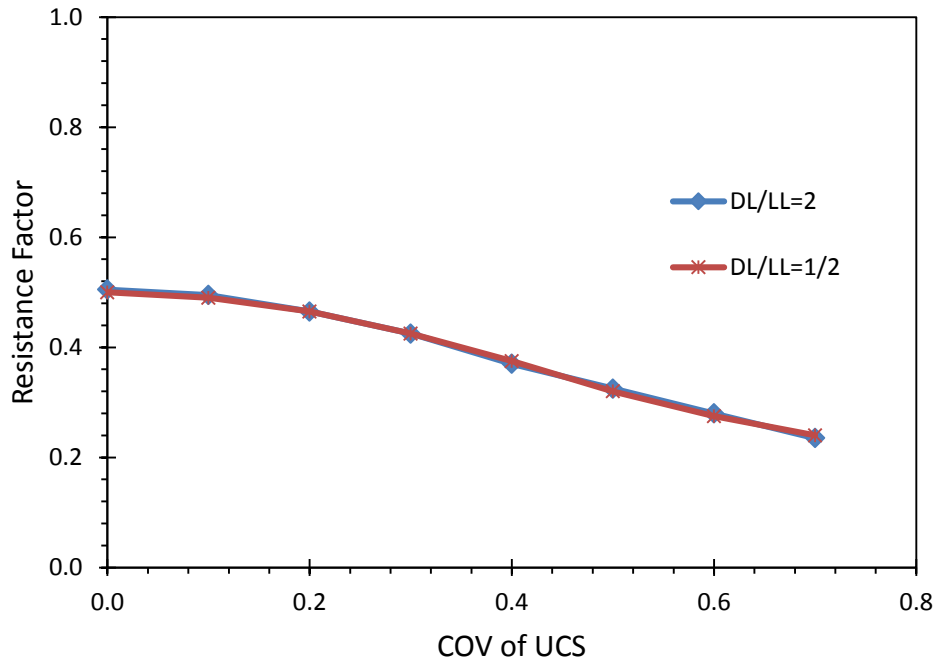


Figure 7.9. Resistance factor for different dead load/live load ratios.

The two resistance factor lines for the dead load/live load ratio coincide, indicating that the resistance factor is not affected by the DD/LL ratio. The values for the two curves have a maximum difference of 0.005 which is effectively “no difference,” because the resistance factor was rounded to the nearest 0.005. This finding is explainable, given that the only difference between the dead load and live load is that the COV of dead load is 0.10 and the COV of live load is 0.12. The difference between COVs of dead load and live load is too small compared with the variability of combinations of all other variables. From the analysis presented above, when using the COV of dead load and live load as recommended by Kulicki (2007), the dead load/live load ratio actually has no effect on the resistance factor for SLS design.

7.6.5. Effect of Target Probability of Failure

The resistance factor is calibrated to achieve a target probability of failure; thus, the resistance factor must be a function of probability of failure P_f . To investigate the changes of resistance factor with different target probabilities of failure, the resistance factor was calibrated for four different levels of probability of failure P_f , which are: 1/25, 1/50, 1/75 and 1/100. These values are recommended by Huaco et al. (2012). The results are shown in Figure 7.10.

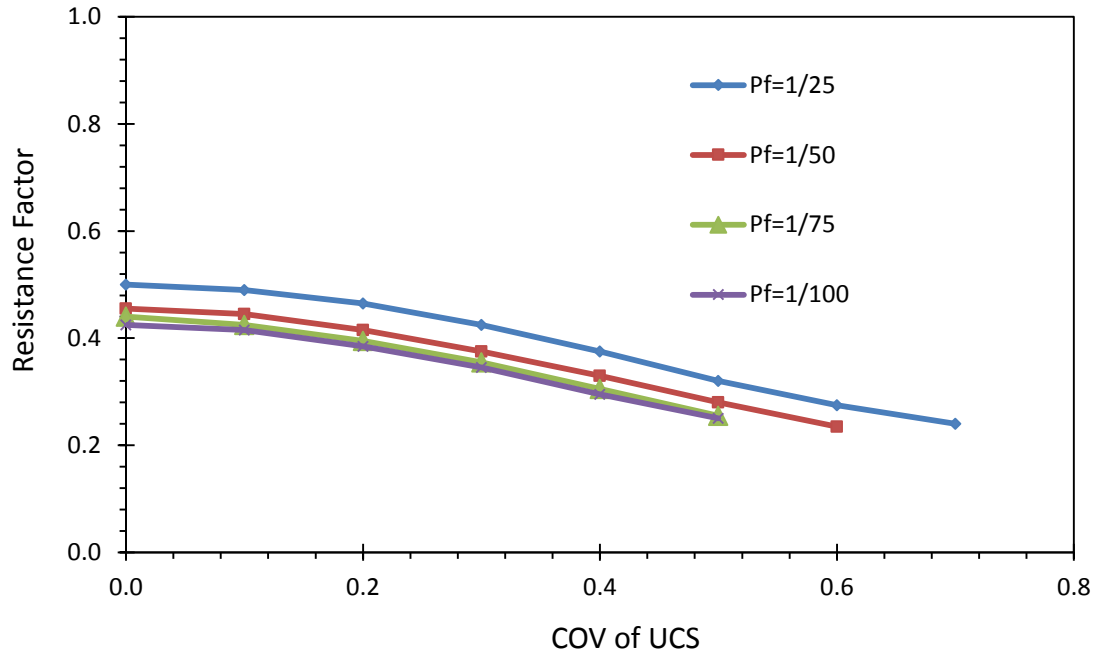


Figure 7.10. Resistance factor for P_f of 1/25-1/100.

The resistance factor decreases with decreasing probability of failure. This is to be expected because using a lower resistance factor means that a lower UCS was used, which produces a design with a higher level of reliability or lower probability of failure.

All the resistance factor curves seem to be parallel to one another. At the COV of UCS of zero, when the probability of failure decreases from 1/25 to 1/100, the resistance factor decreases from about 0.5 to 0.4. This difference in resistance factor for different probabilities of failure does not change with increasing COV of UCS.

7.6.6. Effect of Normalized Shaft Dimension

It was confirmed that the resistance factor stays unchanged for shafts with different nominal values of shaft lengths and shaft diameters as long as the normalized shaft dimension, L/D ratio, is constant (Section 7.4). For a drilled shaft, the shaft length

over shaft diameter ratio is usually within the range of 3 to 30. The effect of shaft length over shaft diameter ratio on the resistance factor was evaluated by changing the ratio within the range. Other inputs are in Table 7.2.

The resulting resistance factors are presented in Figure 7.11. The resistance factor *decreases* with the increase of shaft length over shaft diameter ratio. This can be explained by noting that when the shaft is long, the side resistance contributes more to the overall capacity, which in turn consists of side and tip resistances. The side resistance itself has more uncertainty with the standard deviation of the t - z model which is higher than that of the q - w model (Chapter 6), and the COV of the ultimate predictive model for side resistance of 0.659 is higher than that of the tip resistance of 0.254 (Loehr et al. 2013). Discussion in section 7.6.1 shows that the resistance factor is very sensitive to variability of side resistance models. For longer shafts, the variability of parameters related to side resistance contributes more to the overall variability of the design that causes the resistance factor to decrease. That explains why the resistance factor decreases when the shaft is long or when the L/D ratio increases. Note that the averaging of side resistance is not considered in this research, so the change of the resistance factor is not from side resistance averaging.

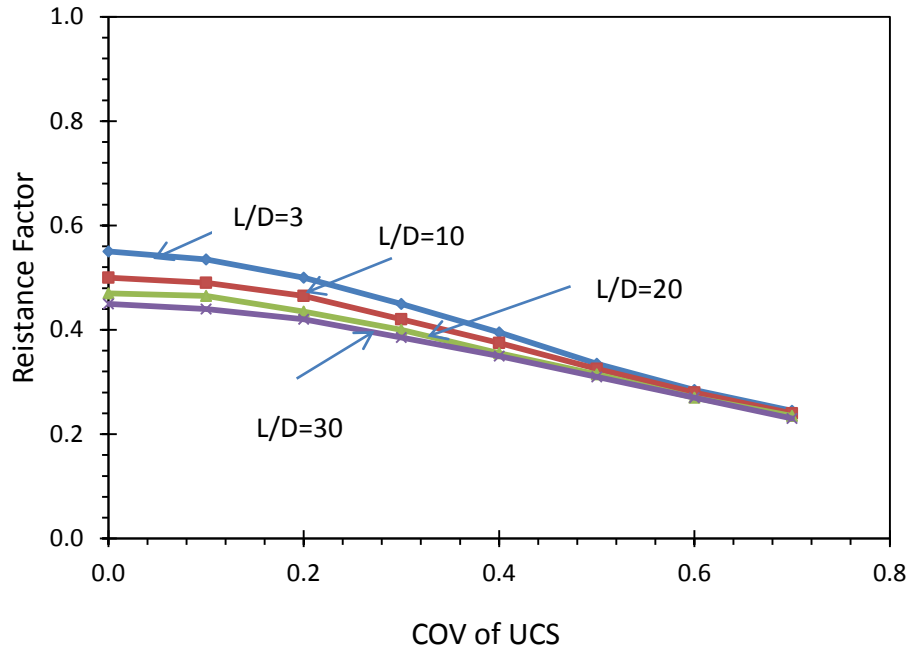


Figure 7.11. Resistance factors for different L/D.

It is also noticeable that the differences among the curves become *smaller* when the *COV of UCS* increases. At *COV of UCS* of zero, the difference between resistance factors for L/D of 3 and 30 is 0.12, while for *COV of UCS* of 0.7, the difference drops to 0.015. In other words, the curves tend to converge to one smaller value.

Comparing the relative magnitude of the change in the resistance factor when *COV of UCS* is zero, the change is higher for the normalized load (θ varies from 0.2 to 0.6), which is 0.17, than for normalized shaft dimension (L/D varies from 3 to 30), which is 0.12. The change in the resistance factor is smaller for target probability failure (P_f from 1/25 to 1/100), which is 0.07.

7.6.7. Effect Reinforced Concrete Young's Modulus

The effect of mean value of concrete Young's modulus was evaluated by using the same input parameters as in Table 7.2 except that the moduli took two values of 4090 ksi (as found in the concrete strength tests, Chapter 5), and an arbitrary high value of 10,000 ksi. The resistance factor is plotted in Figure 7.12.

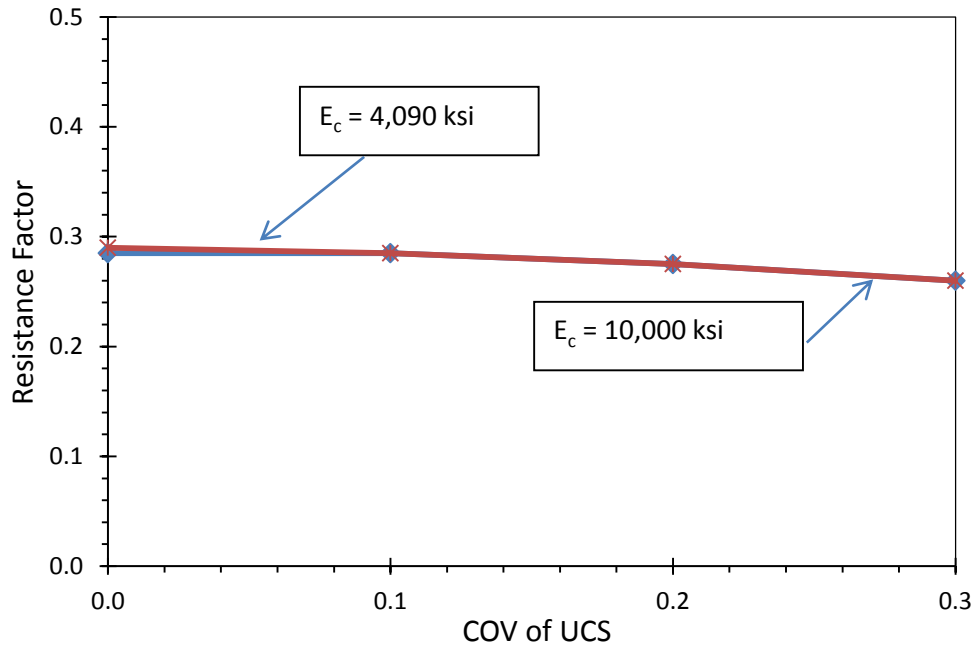


Figure 7.12. Resistance factors for concrete Young's moduli of 4090 ksi and 10,000 ksi.

The resistance factor curves for the two values of concrete Young's moduli almost coincide. This indicates that the resistance factor is not affected by the mean of concrete's Young's modulus. This result is used for the analyses presented later in Chapter 8.

7.6.8. Effect of Adding Probabilistic Variables

This section presents how the number of probabilistic variables considered in the calibration process affects the resistance factor. The analysis was performed using input as in Table 7.2 except that the COVs and standard deviations of parameters were changed for investigation as specified below.

When all variables are set as deterministic (imposing zero COV or standard deviation) the resistance factor is unity. The probabilistic variables were added one-by-one to investigate the change of the resistance factor curve. First, every variable was kept deterministic, except *only* uniaxial compressive strength was considered as a probabilistic variable. The resistance factor was calibrated when the *COV of UCS* changed from 0.0 (deterministic) to 0.7. The resistance factor was plotted as Line 1 in Figure 7.14. There are six more lines in the figure, so for the sake of convenience when discussing the results later, the notation for the resistance factor lines is in Table 7.3.

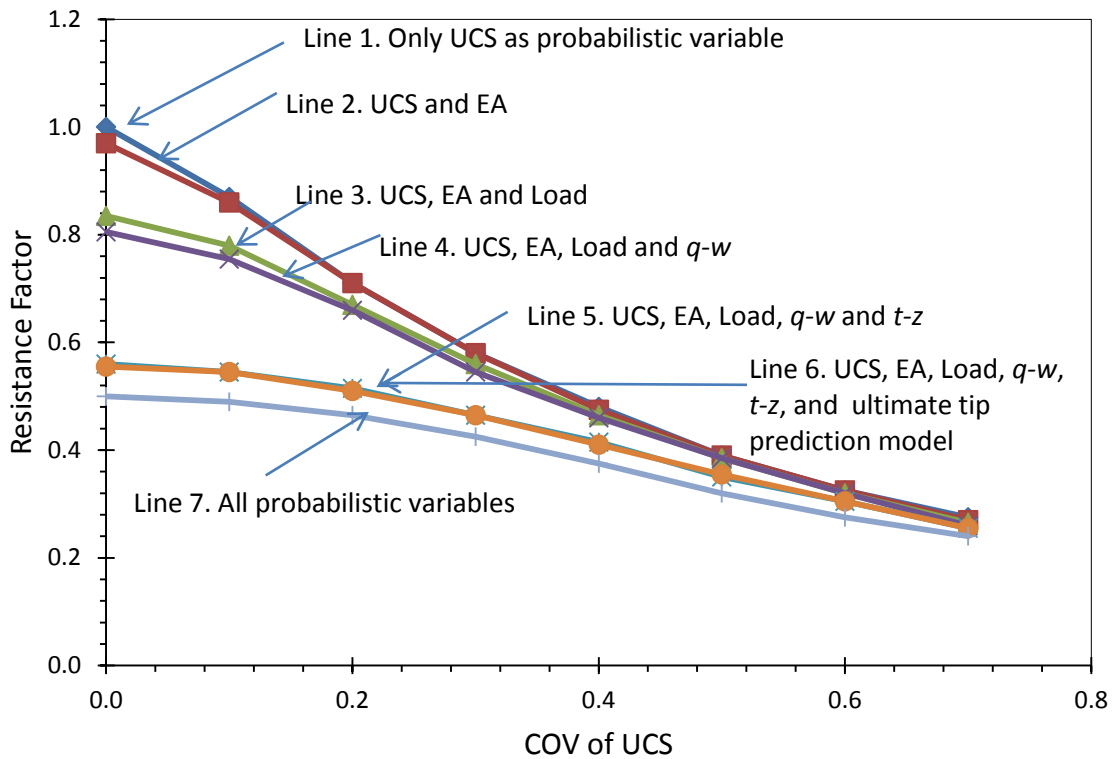


Figure 7.13. Comparing effects of adding probabilistic variables.

Table 7.3. Notation for resistance factor lines.

Symbol	Probabilistic variables
Line 1	UCS
Line 2	UCS and EA
Line 3	UCS, EA and Load
Line 4	UCS, EA, Load and $q-w$
Line 5	UCS, EA, Load, $q-w$ and $t-z$
Line 6	UCS, EA, Load, $q-w$, $t-z$, and ultimate tip prediction model
Line 7	UCS, EA, Load, $q-w$, $t-z$, and ultimate tip and side prediction models

The next step is to consider one more parameter as probabilistic, which is shaft stiffness EA , with COV of EA at 0.15. At this point, the calibration process is considering two variables as probabilistic variables: UCS and EA . The resistance factor was obtained

by keeping the COV of EA unchanged at 0.15 and changing COV of UCS from 0.0 to 0.7. The resistance factor is plotted as Line 2 in Figure 7.14.

Consider one more parameter as a probabilistic variable: this time it is load. For convenience, in this section, dead load and live load are combined as load that has COV of 0.15 (recall that the dead load and live load ratio does not affect the resistance factor). By keeping COV of EA at 0.15, and COV of load at 0.15 (they are equal by coincidence), and by changing the COV of UCS from 0.0 to 0.7, the resistance factor is obtained as in Line 3. The gap between Line 3 and Line 2 is significantly larger than the gap between Line 2 and Line 1. This indicates qualitatively that the variability of load has more influence than the variability EA on the resistance factor.

Load transfer in the tip resistance $q-w$ model was added as the fourth probabilistic variable in the calibration process to make Line 4. This line does not clearly separate from Line 3, showing that adding the $q-w$ model insignificantly affects the resistance factor (when the standard deviation of the model is 0.1 as in Table 7.2).

Load transfer in side resistance of the $t-z$ model was added as the fifth probabilistic variable in the calibration process to make Line 5. The resistance factor is presented by Line 5, which created the greatest plunge from the previous line, Line 4, showing that adding the $t-z$ model greatly affects the resistance factor. Note that for this sensitivity study, the standard deviation of the $t-z$ model took the value of 0.12 (Table 7.2). If the value of the standard of deviation was taken as the field-test-derived of 0.17 (Chapter 6) the gap between Line 4 and Line 5 would be even wider.

The ultimate tip prediction model was considered as a probabilistic variable to create the sixth resistance factor line. Line 6 almost coincides with Line 5. The final variable was the ultimate side prediction model that created Line 7. The gap between Line 7 and Line 6 is considerably noticeable.

As an observation, considering more probabilistic variables in the calibration process decreases the resistance factor. This can be explained by the accumulated effect of variability and the uncertainty of the probabilistic variables. The more variability/uncertainty there is in a problem, the lower the resistance factor required to achieve the target probability of failure.

The more probabilistic variables that are considered, the flatter the resistance factor curve is; or in other words, the less sensitive the resistant factor is to the *COV of UCS*. Line 1 is the steepest curve, which is obtained when UCS is the only probabilistic variable considered. When the *COV of UCS* changes from 0 to 0.7, the resistance factor drops significantly from 1 to 0.275. The flattest is Line 7, when all the variables are considered probabilistic with the resistance factor dropping from 0.5 to 0.24.

It should be noted that all the resistance factor lines tend to converge to one low value. The effect of increasing the number of probabilistic variables is qualitatively similar to the effect of increasing the *COV of UCS* alone.

The biggest gaps between the lines are the gaps between: Line 2 and Line 3, when the load probabilistic variable is added; Line 4 and Line 5, when the side resistance

load transfer variable is added; and Line 6 and Line 7, when ultimate unit side prediction variable is added. Also recall how steep Line 1 is. The resistance factor dropped significantly from 1.0 to 0.86 when the UCS was added as a probabilistic variable with a COV of UCS of 0.1 and further dropped to 0.71 when the COV of UCS was 0.2, which is a significant gap. Qualitatively, these four variables had the biggest impact on the overall resistance factors. This is consistent with results in Section 7.6.1 which showed that the most influential parameters are: UCS, unit side resistance prediction, side load transfer ($t-z$) model and load.

The other three pairs (Lines 1 and 2, Lines 3 and 4, and Lines 5 and 6) almost coincide, showing the effect of variability of EA , tip load transfer model and ultimate tip prediction model - all having little effect on the resistance factor. These observations are used in subsequent analyses presented in Chapter 8.

In the literature, there are several studies on the SLS resistance factor for drilled shafts as mentioned in Chapter 2, but the studies accounted for fewer sources of uncertainty (Misra and Robert, 2006, 2009; Phoon and Kulhawy, 2008). It was shown that considering more probabilistic variables in the SLS analyses makes the resistance factor decrease. This indicates that the SLS resistance factors obtained from the SLS probabilistic analyses that considered fewer variables as probabilistic may be unconservative.

7.7. Important Findings of this Chapter

The evaluation of the dependency of the SLS resistance factor on the input parameters produces the following conclusions and findings:

- The SLS resistance factor is more sensitive to variability/uncertainty of some probabilistic parameters than that of others. The parameters in a descending order of sensitivity are: 1) Uniaxial compressive strength UCS, 2) unit side resistance prediction, 3) side load transfer, 4) load, 5) shaft stiffness EA, 6) tip load transfer and 7) unit tip resistance prediction. The more sensitive group contains the first four parameters, and the less sensitive group contains the last three parameters.
- Mean values of load and of shale uniaxial compressive strength has important effects on the resulting SLS resistance factors. The normalized load was introduced for use so that the effects of the mean values of load and uniaxial compressive strength can be represented by the effect of the normalized load. The SLS resistance factor increases with increasing normalized load.
- Another normalized parameter was introduced which is shaft length over shaft diameter ratio L/D . Resistance factor increases with decreasing L/D . This is explained by noticing that when the shafts are longer, side resistance contributes more to the overall resistance. Note that the resistance factor is strongly sensitive to both unit side resistance prediction and side load transfer's variability/uncertainty, which in turn, is significantly higher than that of tip resistance.
- Dead load over live load ratio does not affect the drilled shaft SLS resistance factors. This is because the only difference between dead load and live load is 2% difference

in their coefficient of variation, which is very small compared to the combined effects of other probabilistic variables.

- There exist impossible cases where probability of failure P_f for a design cannot be achieved because the number of cases, where simulated load that is higher than simulated resistance, is larger than the target probability of failure. If a design is an impossible case, the best way a designer should do is to increase shaft dimensions to reduce normalized load so that the case is possible.
- The number of sources of uncertainties incorporated in the resistance factor calibration process is important. The more variables which are treated as probabilistic in the calibration process, the lower the resistance factor. This indicates that the resistance factors that have been proposed in the literature, which were calibrated considering fewer variables as probabilistic, are unconservative. The resistance factors calibration in this research considered as many sources of variables as possible by using eight probabilistic variables.

7.8. Summary

This chapter covers the framework for SLS design, the probabilistic analyses and the resistance factor calibration. It introduces some concepts that are used in subsequent analyses such as normalized parameters and impossible case. This chapter also presents a study on the effects of probabilistic variables on resistance factors of drilled shafts at service limit state. The most influential probabilistic parameters on the resistance factor are COV of UCS, load, unit side resistance prediction and side load transfer. Effects of other nominal values of parameters are also addressed. The

application of knowledge gained from this study helped establish an equation to calculate resistance factor in the next chapter.

Chapter 8. Procedure for Evaluation of Service Limit State for Drilled Shafts Using LRFD

8.1. Introduction

This chapter presents the procedure for evaluation of the service limit states for drilled shafts based on research results. Objectives of this chapter are to show how to represent the different parameters that influence variability and uncertainty in the predicted settlements or on the SLS resistance factor, combining variables where appropriate and developing relations that make the method practical and accurate and do not require case-by-case probabilistic analyses.

One of the results of the process is that the service limit states (SLS) resistance factors could be calibrated as dependent on only four variables. The resistance factors for SLS drilled shafts are presented as charts. The new equation was developed to calculate the resistance factors for the sake of design convenience. The SLS resistance factors for side and tip resistance are also introduced. The results of this chapter set up the most important step toward establishing the final design procedure of drilled shaft SLS design.

8.2. Input Parameters

8.2.1. Inputs for SLS probabilistic Analyses

A total of 24 inputs was used to probabilistically predict shaft head settlement and for the SLS resistance factor calibration (Chapter 7). The parameters, the values

used in the analyses presented in this chapter, and the sources of the values are presented in Table 8.1.

Table 8.1. Input parameters for the calibration of SLS probabilistic analyses.

#	Input Parameter	Values	Source
1	Dead load (kips)	Varies to make desired L/D	-
2	COV of dead load	0.1	Kulicki et al. (2007)
3	Live load (kips)	1/2 of Dead load	-
4	COV of live load	0.12	Kulicki et al. (2007)
5	UCS (ksf)	8	-
6	COV of UCS	Independent variable	-
7	Shaft diameter (ft.)	3	-
8	Shaft length (ft.)	Varies to make desired L/D ratio	-
9	Concrete Young's modulus (ksi)	4090	Chapter 5
10 & 11	COV of concrete modulus & shaft cross section area	0.15	Tyler (2010) and Chapter 5
12	Target Probability of failure	1/25; 1/50; 1/75 and 1/100	Huaco et. al (2012)
13	Standard deviation of load transfer side resistance	0.17	Chapter 6
14	Standard deviation of load transfer tip resistance	0.14	Chapter 6
15	COV of unit side resistance prediction model	0.659	Loehr et al., (2013)
16	COV of unit tip resistance prediction model	0.254	Loehr et al., (2013)
17 & 18	Hyperbolic parameters <i>a</i> and <i>b</i> side resistance	1.07 and 0.13	Chapter 6
19 & 20	Hyperbolic parameters <i>a</i> and <i>b</i> tip resistance	1.01 and 0.72	Chapter 6
21 & 22	Ultimate prediction model side resistance (x2)	0.76 and 0.79	Loehr et al., (2011)
23 & 24	Ultimate prediction model tip resistance (x2)	14.0 and 0.71	Loehr et al., (2011)

In Table 8.1, the four different target probabilities of failure P_f cover four different categories of bridges at SLS. These values were recommended by Huaco et al., (2012) and are presented in Table 8.2.

Table 8.2. Probability of failure for different bridge categories (Huaco et al. 2012)

Category	Target Probability of Failure P_f
Bridges on Minor Roads	1/25
Bridges on Major Roads	1/50
Major Bridges (< \$100 million)	1/75
Major Bridges (> \$100 million)	1/100

Ultimate unit side prediction and ultimate unit tip prediction both are log-normally distributed (Loehr et al., 2013). As shown in the Engineering Policy Guidelines for Design of Drilled Shafts (Loehr et al., 2011), the ultimate unit side resistance q_s is:

$$q_s = 0.76 \times UCS^{0.79} \quad (8.1)$$

where UCS is mean uniaxial compressive strength of rock core along the shaft segment (ksf), and the ultimate unit tip resistance for a shaft is shown by the equation:

$$q_p = 14 \times UCS^{0.71} \quad (8.2)$$

The predictions show a constant COV of 0.659 for side resistance, and 0.254 for tip resistance, Loehr et al. (2013).

Load transfer relationships are represented by t - z and q - w curves. As presented in Chapter 6, the t - z and q - w models are:

$$t = \frac{z}{1.07 * z + 0.13} \quad (8.3)$$

and

$$q = \frac{w}{1.10*w+0.72} \quad (8.4)$$

where t and q respectively, are unit side and tip resistance normalized by maximum measured unit resistance, and z and w are normalized displacements of the local shear zone and shaft tip. These models were obtained using ordinary least square regression with an assumption that standard deviation was constant. The model for side resistance has a constant standard deviation of 0.17. The model for tip resistance also has a constant standard deviation, which is 0.14.

8.2.2. Variable Combination and Reduction

Each of the 24 input parameters presented above has a different effect on the predicted settlement and on the resistance factor. This section presents the process of combining and reducing the number of input variables in the resistance factor calibration process.

In the analysis presented in Section 7.6.4, dead load over live load ratio does not affect the SLS resistance factor, so they can be combined as “load.” Furthermore, the effects of load and UCS on the resistance factor can be combined as normalized load θ . Therefore three variables, which are dead load, live load and UCS, can be combined into one variable, which is “normalized load” in SLS probabilistic analysis. Shaft length and shaft diameter inputs are combined into one variable which is “normalized shaft dimension” or shaft length over shaft diameter ratio (Section 7.6.6). The resistance factors were calculated for different cases by changing nominal values of five inputs: dead load, live load, UCS, shaft length and shaft diameter, while maintaining specific

values of normalized load θ and L/D ratio (Section 7.4). There were no differences in the SLS resistance factors, indicating the five inputs can be combined and reduced into two variables, i.e., θ and L/D ratio. The resistance factors must be a function of those two variables.

A product of reinforced concrete Young's modulus, E , and shaft area (that solely depends on shaft diameter) is shaft stiffness. The variability of concrete Young's modulus and shaft diameter is the variability of shaft stiffness, so COV of the modulus and the shaft diameter are combined as one input, which is the variability of shaft stiffness. Shaft stiffness has the COV of 0.15 (Section 7.6), and the resistance factor seems to be constant with the change of variability of shaft stiffness, which varies in the range of 0.1 to 0.2. Thus, the two inputs of the variability of concrete Young's modulus and of shaft diameter can be combined as one input, which is COV of EA . The value for COV of EA was set as a constant of 0.15 in the resistance factor calibration process.

The previous discussions are for combining input variables. Some other inputs in the calibration process are required but can be kept at their typical values or as constants and do not affect the resistance factor. One such constant is the mean value of Young's modulus for reinforced concrete. Practically, the mean value of Young's modulus for reinforced concrete does not affect the resistance factor, as in Section 7.6.7. Thus, the nominal value of the modulus is considered as a constant with the value of 4090 ksi as determined from the concrete strength tests (Chapter 5).

The load transfer models are proposed for the SLS design of drilled shafts, and the inputs for side and tip load transfer models and their standard of deviations (Inputs #13, 14 and 17-20, Table 8.1) are also kept constant in the SLS resistance factor calibration process. Similarly, input for the ultimate unit resistance prediction models and their COVs (Inputs #15, 16 and 21-24, Table 8.1) were also kept as constant in the process.

Even though the effect of the change in the COV of load (dead load and live load) has a significant effect on the SLS resistance factor, the COV of dead load and live load practically are often fixed or given (0.1 for dead load and 0.12 for live load, Kulicki et al., 2007). If not, the COV of load still has a narrow range around those values. Section 7.6.8 showed that uncertainty in load has little effect on the resistance factors when the COV of load is 0.15 or less. The COVs of dead load and live load are kept as constant inputs when conducting SLS probabilistic analyses.

The resistance factor significantly depends on the COV of UCS, which has a wide range in practice, making it an important input variable in the calibration process. The resistance factor is calibrated for use in SLS design so that the design can achieve a target probability of failure, which means that P_f must be an input variable for the calibration. The COV of UCS and P_f are sensitive input variables upon which the resistance factors depend.

In short, there are three groups of input parameters for the SLS calibration process:

- *Parameters that are combined consist of:* UCS, dead load, live load, shaft length and shaft diameter. These five parameters are combined into two variables, normalized load, θ , and shaft length over shaft diameter ratio, L/D.

- *Parameters that are insensitive, or have a small range in change and are often given.* These consist of: COV of dead load, COV of live load, COV of concrete Young's modulus combined with COV of shaft area, and the nominal value of the modulus. Those input parameters were used in the calibration process at their typical values (see above list and Table 8.2). Model parameters of t - z and q - w models and ultimate unit resistance prediction models were set as constant inputs in the calibration process.

- *Parameters that are sensitive consist of:* probability of failure P_f and the COV of UCS.

When variables are combined and reduced by keeping insensitive parameters at their typical values, and setting empirical models parameters as constant inputs, only four variables of the original 24 inputs remain for the probabilistic analyses and for developing the resistance factor: normalized load, L/D ratio, P_f , and COV of UCS. The resistance factors for drilled shafts were calibrated following the procedure presented in Chapter 7 and are presented focusing on these four variables in the next section.

8.3. Resistance Factors for Drilled Shaft at Service Limit State

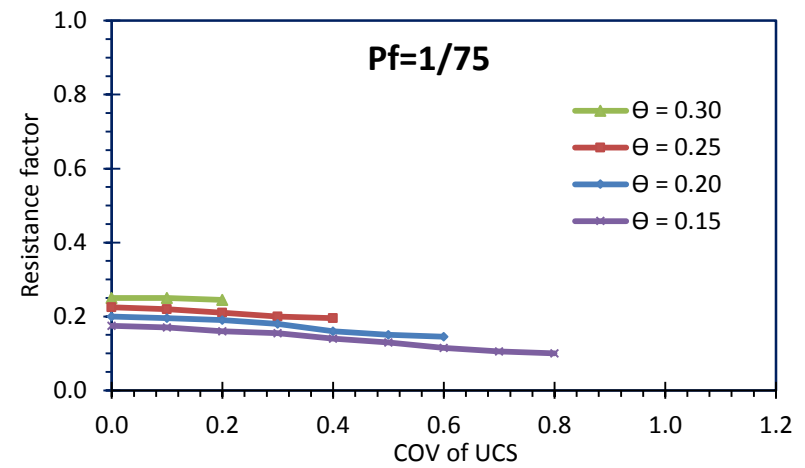
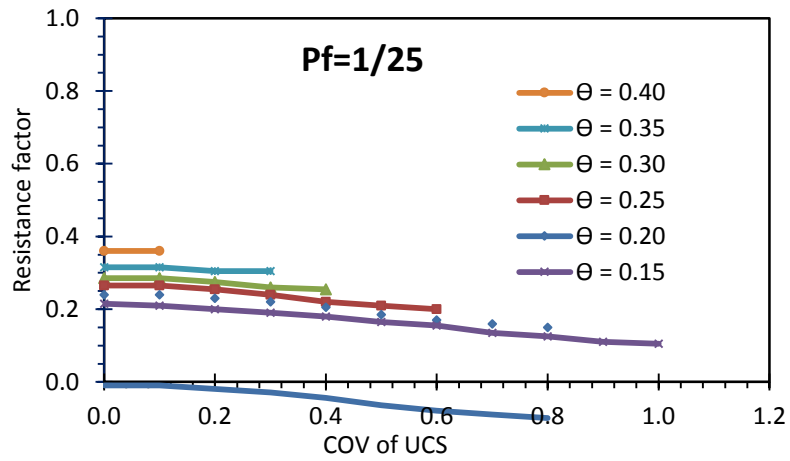
As presented in detail in Section 7.3, the SLS resistance factor φ is applied to uniaxial compressive strength to account for variability and uncertainty in SLS designs. The purpose is to reduce UCS to a factored uniaxial compressive strength so that a design that uses the factored strength will achieve a target reliability level. A designer simply can compare the factored settlement $y^*_{(UCS^*)}$ with the allowable or limiting settlement, y_a directly to check for the SLS condition:

$$y^*_{(UCS^*)} \leq y_a \quad (8.5)$$

$$UCS^* = \varphi * UCS \quad (8.6)$$

where UCS^* and $y^*_{(UCS^*)}$ are the factored strength and factored settlement. If Equation 8.5 satisfies, the SLS design that uses the resistance factor actually reaches the target probability of failure without any probabilistic analyses. By using the computer code (Appendix G), following the procedure presented in Section 7.3 and using inputs as in Table 8.1, the resistance factors were calibrated for different normalized loads θ , P_f and COV of UCS at L/D ratios of 10 and 30. The effects of the L/D ratio on the resistance factors are discussed in Chapter 7 and later in this chapter.

The resistance factors are presented in Figures 8.1 and 8.2 (and in in Appendix H tables). The resistance factors have relatively low values in the range of 0.1 to 0.4. This means that when using the design method with the proposed load transfer models, the



a) Resistance factor for drilled shafts at SLS for $P_f=1/25$.

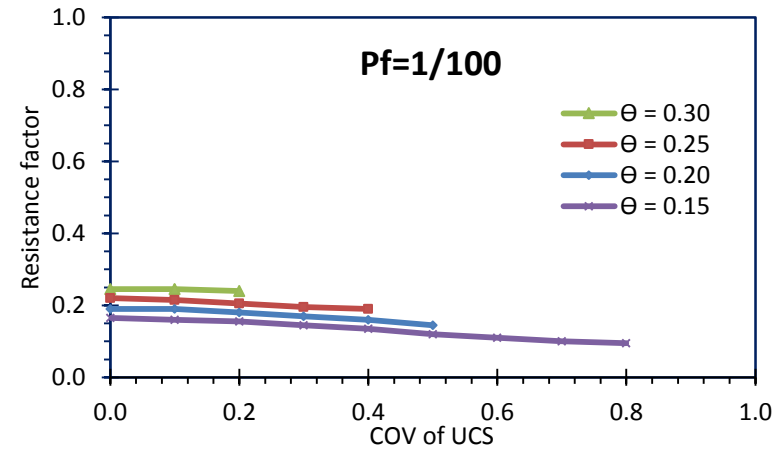
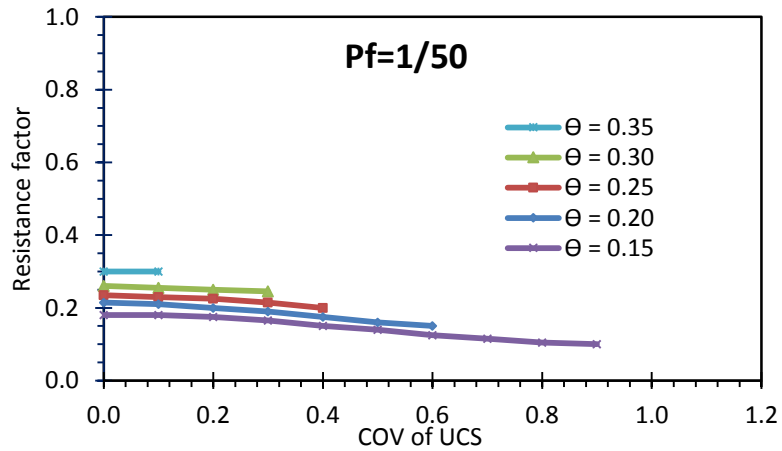
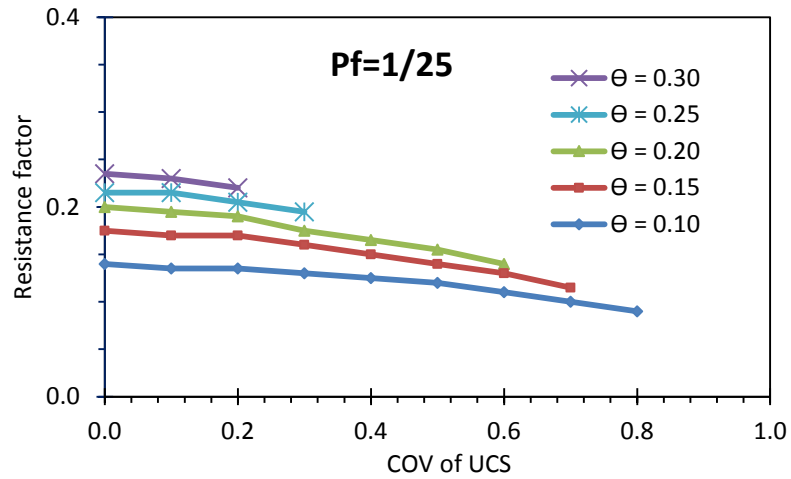
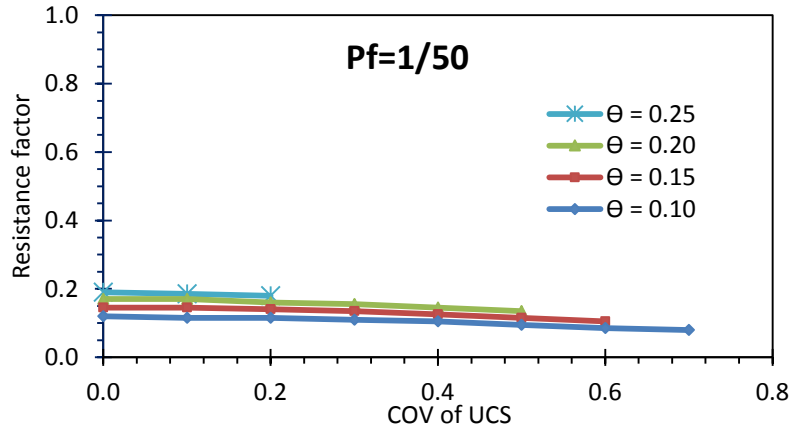
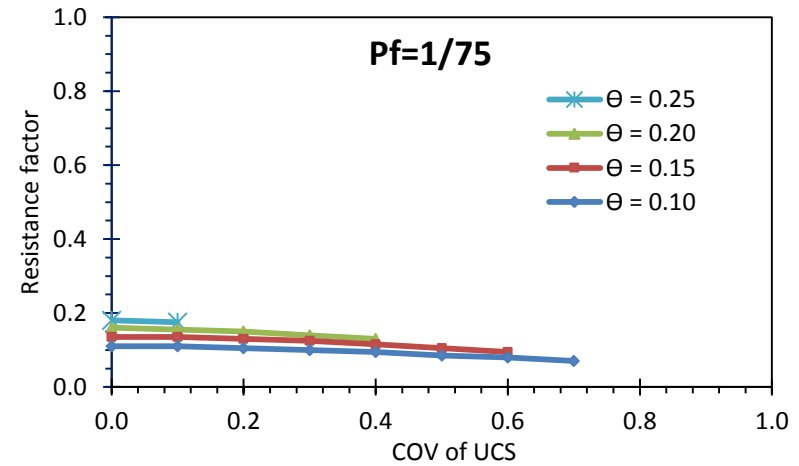
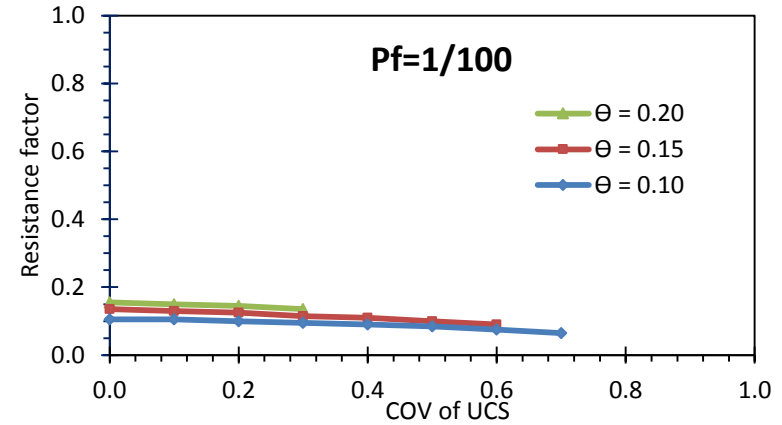


Figure 8.1. Resistance factor for drilled shafts at SLS for $(L/D = 10)$.

a) Resistance factor for drilled shafts at SLS for $P_f=1/25$.b) Resistance factor for drilled shafts at SLS for $P_f=1/50$.c) Resistance factor for drilled shafts at SLS for $P_f=1/75$.d) Resistance factor for drilled shafts at SLS for $P_f=1/100$.Figure 8.2. Resistance factor for drilled shafts at SLS $L/D = 30$.

designer should reduce the mean value of UCS about 60% to 90% in the SLS design to achieve a probability of failure between 1/25 and 1/100. As observed, the resistance factor decreases when the normalized load θ increases and COV of UCS decreases, which is consistent with the results in Chapter 7. The resistance factor also decreases when increasing probability of failure.

As associated with impossible cases discussed in Section 7.5, all the resistance factor curves are truncated at certain values of COV of UCS. The end points on the right hand side of each curve define the boundary between possible and impossible cases (when COV is rounded to 0.1). The impossible/possible boundaries are presented in detail later in Section 8.6.

The maximum normalized load θ that can be obtained for the SLS probability of failure of 1/ is 0.4. Beyond this value of normalized load, it is possible that the design can produce a probability of failure that is substantially higher than 1/25.

The resistance factors presented in this chapter were calibrated using the unit side and tip resistance normalized by maximum measured values by using the load transfer models obtained from the approach, as in Equations 8.1 and 8.2. Then only in Section 8.7, some SLS resistance factors derived from the models of unit side and tip resistances normalized by predicted ultimate resistance are presented solely for comparison purposes.

8.4. Equation to Calculate SLS Resistance Factor

The resistance factors were developed depending on four different variables which are normalized load θ , shaft length/shaft diameter ratio, target P_f , and COV of UCS. The charts above were developed to determine the resistant factor for different probabilities of failure, normalized load θ and COV of UCS, but only one constant value of the fourth variable, which is the ratio of shaft length over shaft diameter at a value 10.0. (The dependence of the resistance on the ratio was presented in detail in Chapter 7). Because the resistance factors should be presented depending on the four variables, it would be cumbersome to present the resistance factors in the form of charts, with the frequent (or common) values of all four parameters. The charts presented in the previous section can be used to evaluate drilled shafts at the service limit state and to achieve settlements that meet the target probability of failure. The use of the charts may often require interpolation within a chart or between charts, which introduces some complexity. It would be advantageous to further simplify the design with an equation, which would provide a better way for design engineers to quickly get the resistance factor to apply to UCS in the SLS design. A mathematical form was chosen, then multiple regression analyses were performed in an effort to find an equation (more details to follow). The following equation was developed and is proposed for calculating the resistance factor:

$$\varphi = \left[\frac{(5-COV)*\theta-COV}{10} + c_{pf} \right] * c_{L/D} \quad (8.7)$$

where:

COV = COV of UCS,

θ = normalized load over capacity,

c_{pf} = coefficient for different probability of failure P_f , and

$c_{L/D}$ = coefficient for different shaft length over shaft diameter L/D .

All of the terms in Equation 8.7 are dimensionless. The coefficients for different probabilities of failure c_{pf} and the coefficients for different shaft length over shaft diameter ratios $c_{L/D}$ are determined from Tables 8.3 and 8.4:

Table 8.3. Coefficient c_{pf}

P_f	Coefficient c_{pf}
1/25	0.145
1/50	0.120
1/75	0.115
1/100	0.105

Table 8.4. Coefficient $c_{L/D}$

L/D	Coefficient $c_{L/D}$
5	1.14
10	1.00
15	0.93
20	0.86
30	0.80

The L/D ratio is usually changed in a design when determining the shaft dimension. For convenience, the coefficient $c_{L/D}$ can be approximately determined from Figure 8.3 or by the following function (for L/D in the range from 5 to 30):

$$c_{L/D} = 1.6 * (L/D)^{-0.2} \quad (8.8)$$

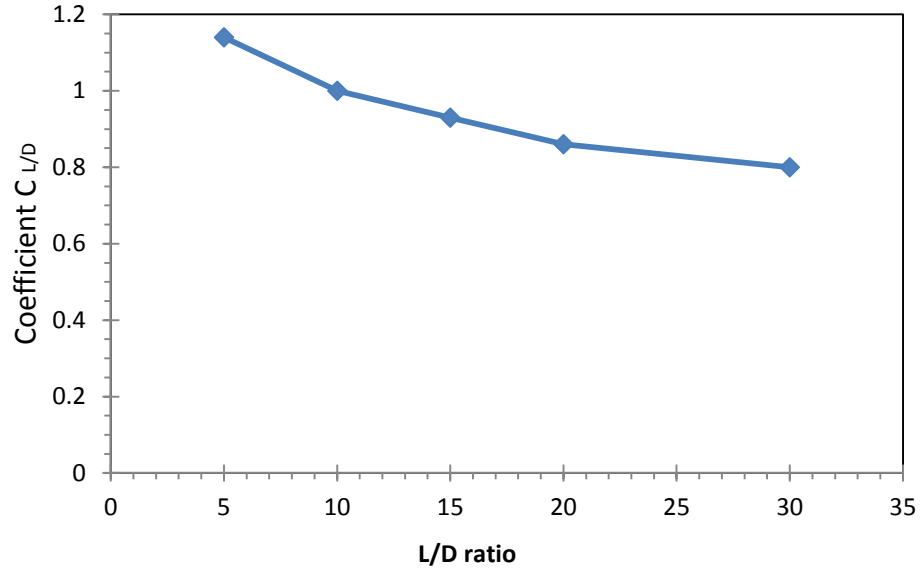


Figure 8.3. Coefficient $C_{L/D}$

The resistance factor in Equation 8.7 and the coefficients were developed based on the following features, which shaped the mathematical form:

- As shown in Figure 7.10, the resistance factor curves for different probabilities of failure are parallel to each other. From that parallel feature, a coefficient presenting P_f should be an *adding* coefficient in the equation.
- The resistance factor curves for different shaft length over diameter (L/D) ratios (as shown in Figure 7.11) are converged. Because of the converged feature, a coefficient presenting L/D is a *multiplying* coefficient in the equation. As shown in the resistance charts above (Figures 8.1), the resistance factor decreases when COV of UCS increases; therefore, COV of UCS should be in the subtracted form (or may be in the denominator) of the equation.

- Also as shown in the resistance charts above, the resistance factor increases when normalized load θ increases (also as in Section 7.6.3), so θ should be in the adding or numerator part of the equation.

Calibration was carried out for cases with different L/D , P_f , COV of UCS and normalized load θ . A large number of curves was constructed to find the pattern for a coefficient representing L/D , and resistance factor curves were also created for different probabilities of failure, P_f , to find a coefficient representing P_f . Regression analyses were performed to find the two coefficients.

Equation 8.7 gives the resistance factors with the precision of ± 0.01 (± 0.015 if COV of UCS < 0.1) compared with the values obtained from rigorous calibration as shown in the following section. The equation is easier to use without interpolating between or within the charts and tables. The proposed equation can be used in an SLS design of drilled shafts for different dead load, live load, uniaxial compressive strength, UCS's variability/uncertainty, shaft length, shaft diameter, and target probability of failure without performing probabilistic analysis on a case-by-case basis.

8.5. Resistance Factor Equation Verification

In this section, examples and comparison graphs for equation verification are presented. In these, "rigorous" resistance factors were calibrated on a case-by-case basis using the computer code and were compared with the resistance factors obtained from Equation 8.7 with the two coefficients. The resistance factors were computed and calibrated for different ranges of the four variables.

8.5.1. Example 1

A case was given where target probability of failure $P_f = 1/100$; $DL = 860$ kips, $LL = 430$ kips, $UCS = 8$ ksf and value of COV of UCS is 0.1. Shaft length was chosen to be 50 ft., with a shaft diameter of 5 ft., so $L/D=10$.

The shaft ultimate capacity was calculated similarly to the calculations from this chapter's previous examples, where the unfactored ultimate capacity is 4290 kips. The normalized load θ is 0.3. The case was run by the computer code and gave a "rigorous" resistance factor of 0.245 (also as in Figure 8.1). With $L/D=10$, Table 8.4 was used to obtain $c_{L/D}$ of 1.0; and with P_f at $1/100$, Table 8.3 was used to obtain coefficient c_{Pf} of 0.105. When the two coefficients are inserted into Equation 8.7, the resistance factor for this case is:

$$\phi = \left[\frac{(5 - 0.1) * 0.3 - 0.1}{10} + 0.105 \right] * 1 = 0.242$$

The results of 0.245 and 0.242 match.

8.5.2. Example 2

For this case, the target probability of failure, COV of UCS, and normalized load are a different range from case 1 as follows: $P_f = 1/25$, $COV=0.6$, $UCS= 30$, $DL=568$ kips, and $LL=284$ kips. Shaft resistance is 4263 kips, and normalized load θ is 0.2

When selecting a design where $L/D=10$ the "rigorous" calibration gave a rigorous resistance factor ϕ of 0.170 (also in Figure 8.1). Now using Equation 8.7 to calculate the

resistance factor, from Table 8.4, $c_{L/D}$ 1.0 was obtained, and from Table 8.3 with P_f at 1/25, coefficient c_{Pf} is 0.105. After substituting the coefficients into Equation 8.7, the resistance factor was:

$$\phi = \left[\frac{(5 - 0.6) * 0.2 - 0.6}{10} + 0.145 \right] * 1 = 0.173$$

The results match.

For this example, but with a different load of 930 kips (DL = 627 kips, LL = 313 kips), and a different L/D of 30, with a shaft diameter of 2 ft. and shaft length of 60 ft., ultimate shaft capacity is 4700 kips and the normalized load θ is 0.2. The computer code was run and gave the rigorous resistance factor of 0.140. The result was compared with the resistance factor that was calculated using the equation. From Table 8.4, constant L/D = 30 gives $c_{L/D} = 0.80$; and the resistance factor is:

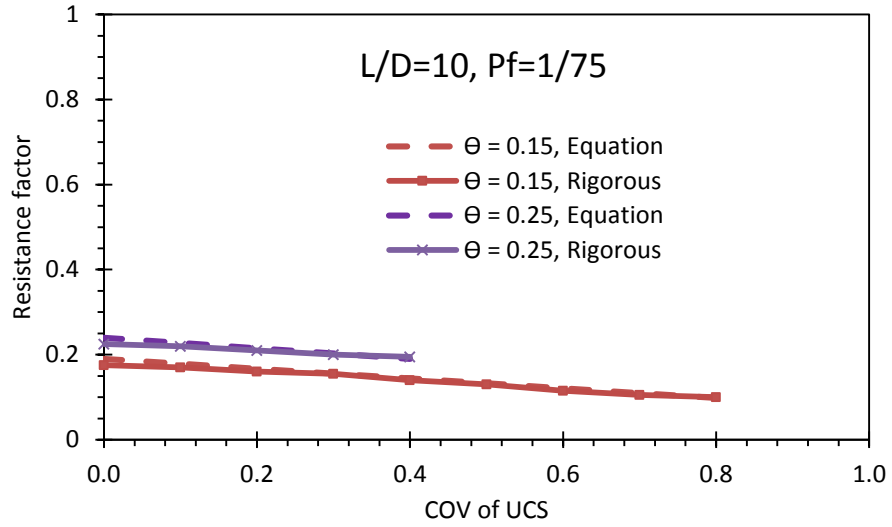
$$\phi = \left[\frac{(5 - 0.6) * 0.2 - 0.6}{10} + 0.145 \right] * 0.80 = 0.138$$

The results match.

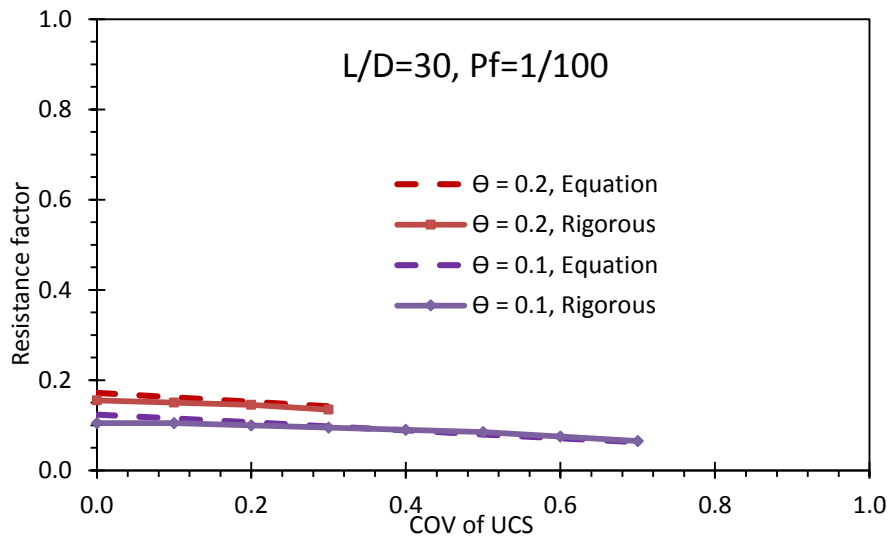
8.5.3. Comparisons with Resistance Factor Curves

Together with the above examples, other examples were made with ranges of the four variables. The resulting resistance factors are presented in Figure 8.4. The results match well with the precision of ± 0.01 (± 0.015 if COV of UCS < 0.1), as in the figure. This indicates that by using Equation 8.7, the resistance factors can be obtained without using a computer program or using any chart and are sufficiently accurate for

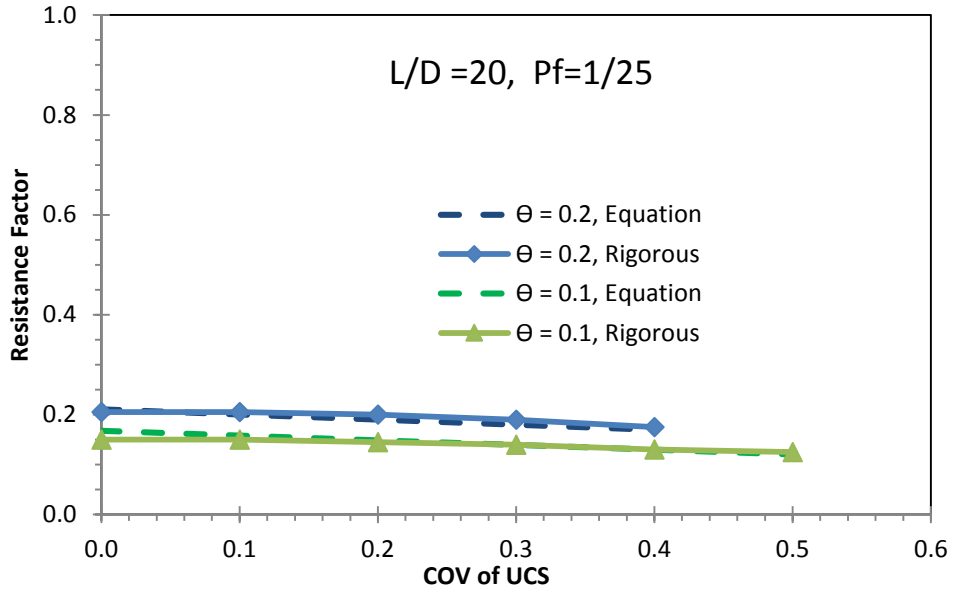
practical use. The use and the application of the equation to calculate resistance in an SLS design procedure design factor are discussed in Chapter 9.



a) L/D=10, Pf=1/75



b) L/D=30, Pf=1/100



c) L/D = 20, Pf = 1/25

Figure 8.4. Comparisons of resistance factors obtained from Equation 8.7 and from rigorous calculations.

8.6. Possible and Impossible Case

As discussed in section 7.5, there exist some combinations of parameters where the target probability of failure could never be obtained, i.e., an “impossible case”. The impossible case exists when the number of cases, in which randomly generated loads are higher than randomly generated shaft capacities, is larger than the target probability of failure. The impossible case for a certain shaft length over diameter ratio is formed by a combination of normalized load θ , COV of UCS and probability of failure P_f . The boundary of the case was found by making the number of the impossible cases equal to the SLS probability of failure. Note that for these cases, in which generated load was equal to or larger than generated capacity, using simulated t - z and q - w models, the

results were different from an ultimate limit state failure because different models and procedures were used (see Section 7.5).

The case boundaries representing a combination of COV of UCS, P_f and θ for the specific shaft length over shaft diameter ratio L/D of 10.0 are presented in Figure 8.5 and Table 8.9. Four curves, as shown in Figure 8.5, are associated with four target probabilities of failure. The *left-and-under* area of each curve can be named the “possible case” for the corresponding P_f , where the resistance factor could be found to achieve the target probability of failure. The *right-and-above* area of each curve, however, is the “impossible case”, where the target probability of failure cannot be achieved no matter how small the resistance factor is. This is unfavorable for a design.

Table 8.5. Combinations for impossible case with L/D of 10.

Normalized Load	COV of UCS			
	Pf=1/25	Pf=1/50	Pf=1/75	Pf=1/100
0.15	1.09	0.9	0.83	0.8
0.2	0.84	0.67	0.61	0.56
0.25	0.63	0.5	0.44	0.4
0.3	0.47	0.33	0.28	0.21
0.35	0.31	0.15		
0.4	0.15			

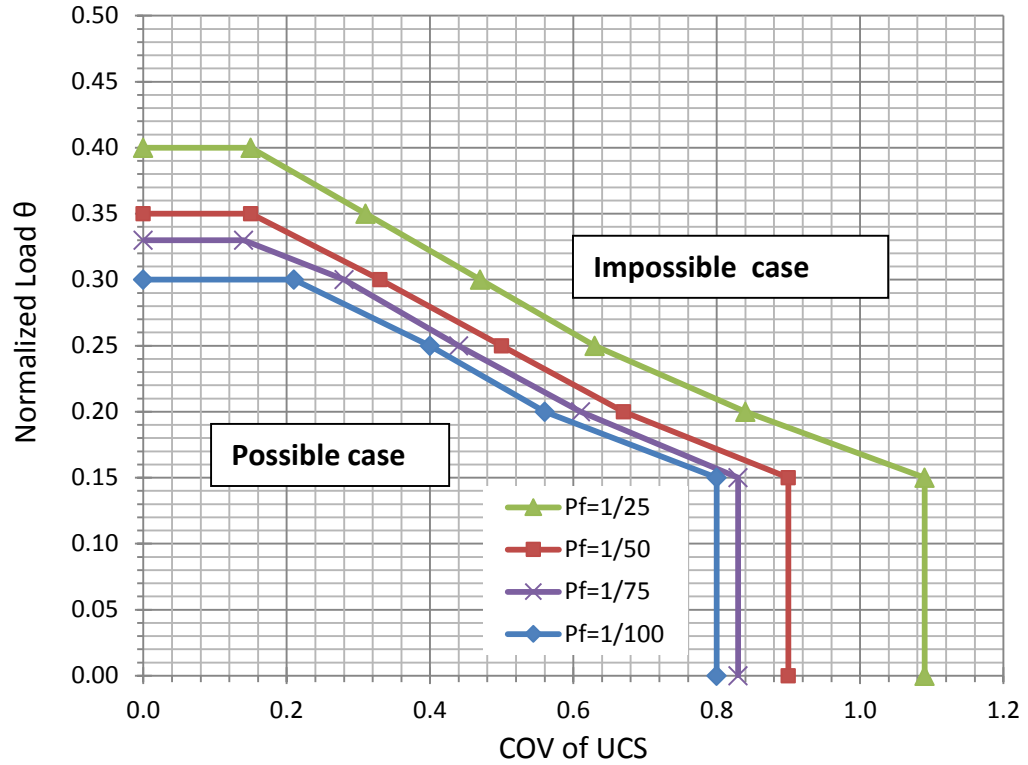


Figure 8.5. Boundaries of possible and impossible cases with L/D of 10.

In an SLS design, if the designed shaft has conditions which fall outside the possible case, three different ways exist whereby conditions can be moved into the impossible case. The designer could increase the shaft length or diameter, so the normalized load θ is reduced where technically the resistance distribution is shifted farther from load distribution. Also, the designer can change *COV of UCS* by conducting more site exploration tests. The last resort is to increase the target probability of failure P_f so the number of cases where load is larger than the displacement is less than the target P_f .

Practically, changing the conditions for COV of UCS or the probability of failure would make a design more costly, or sometimes it is not possible. Hence, increasing the shaft dimension may be the only practical way that a design can achieve target P_f .

It should be of interest to know the relationship of the impossible case with the ultimate limit state (ULS) design criteria. This leads to the question: If a design satisfies the ULS condition, will it fall into a possible case? The following examples show the use of the impossible case concept and the relationship between ULS and impossible case conditions.

8.6.1. Example 1

This example is a design of a shaft under a load of 600 kips with dead load (weight of shaft is included), DL, at 400 kips, and live load, LL, at 200 kips. The factored load is $(1.75 * LL + 1.25 * DL) = (1.75 * 200 + 1.25 * 400) = 870$ kips. The design is for a minor road bridge with a target P_f of 1/25, with a mean UCS of 20 ksf, and a COV of UCS of 0.4.

The chosen shaft length L was 30 ft. and shaft diameter D is 3 ft. Using the Engineering Policy Guidelines for Design of Drilled Shafts (Loehr et al., 2011) with P_f of 1/25 and COV of UCS of 0.4 from Figure 751.37.3.3 of the guidelines (also cited in Figure 9.2), the ULS resistance factor for unit side resistance is 0.22, and from Figure 751.37.3.4 (cited in Figure 9.3), the resistance factor for unit tip resistance is 0.46.

Using Equations 8.1 and 8.2 for ultimate unit resistance prediction:

Ultimate unit side resistance is:

$$q_s = 0.76 * (UCS^{0.79}) = 0.76 * 20^{0.79} = 8.1 \text{ (ksf)} .$$

Ultimate unit tip resistance is:

$$q_t = 14 * (UCS^{0.71}) = 14 * (20^{0.71}) = 117.4 \text{ (ksf)} .$$

$$\begin{aligned} \text{Unfactored shaft resistance} &= (q_s * \pi * D * L) + (q_t * \pi * D^2/4) \\ &= (8.1 * 3.14 * 30 * 3) + (117.4 * 3.14 * 3^2/4) = \\ &3121.2 \text{ (kips)} . \end{aligned}$$

Factored total resistance

$$\begin{aligned} &= (q_s * \pi * D * L) * 0.22 + \left(q_t * \pi * \frac{D^2}{4} \right) * 0.46 = \\ &885.3 \text{ (kips)} . \end{aligned}$$

Factored load = 870 kips < factored resistance = 885.3 kips, and the design satisfies the ULS conditions. Normalized load θ is the ratio of the unfactored load to the unfactored shaft resistance (capacity) = $600/3,121 = 0.19$.

Now consider the impossible case for the combination of $L/D=10$, and COV of UCS of 0.4, minor bridge $P_f=1/25$ and $\theta=0.19$. With these parameters, from Figure 8.5, the maximum possible normalized load for the case to be the possible case is 0.32, which is larger than the value of 0.19 from the ULS design. In this case, the design satisfies the ULS condition and falls well into the possible case, and Equation 8.7 can be applied for the SLS design.

8.6.2. Example 2

This example is a design of a shaft under loading of 1200 kips, with LL = 400 kips, DL = 800 kips, in shale with a higher UCS of 80 ksf. The design is for major bridges costing more than \$100 million, and has a target $P_f=1/100$, and a lower end COV of UCS of 0.2.

The factored load is $(1.75 * LL + 1.25 * DL) = 1.75 * 400 + 1.25 * 800 = 1700$ kips. For this example, the higher end of L/D ratio of 30 was chosen, with a shaft length L of 60 ft., and shaft diameter D of 2 ft. Using Engineering Policy Guidelines for Design of Drilled Shafts (Loehr et al., 2011), the ULS resistance factor for unit side resistance is 0.142 (Figure 9.2); resistance factor for unit tip resistance is 0.44 (Figure 9.3). This example needs boundaries for the case of L/D of 30 and $P_f=1/100$, thus the boundary was established as shown in Figure 8.5.

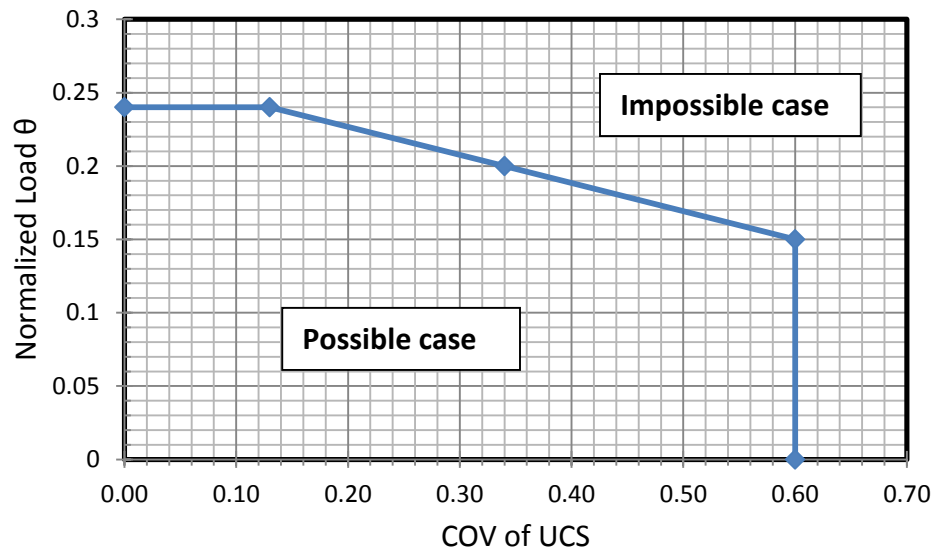


Figure 8.6. Possible/impossible case boundary for Equation 8.7 with L/D of 30 and $P_f=1/100$.

Once more, using Equations 8.1 and 8.2 for ultimate unit resistance prediction, the shaft resistance can be determined as follows:

$$\text{Ultimate unit side resistance } q_s = 0.76 * (80^{0.79}) = 24.22 \text{ (ksf)}$$

$$\text{Ultimate unit tip resistance } q_t = 14 * (80^{0.71}) = 314.3 \text{ (ksf)}$$

$$\text{Unfactored shaft resistance} = q_s * \pi * D * L + q_t * \pi * D^2/4$$

$$24.22 * 3.14 * 2 * 60 + 314.3 * 3.14 * \frac{2^2}{4} = 10,120 \text{ kips}$$

Factored total resistance

$$= (q_s * \pi * D * L * 0.142 + q_t * \pi * D^2/4 * 0.44)$$

$$= (24.22 * 3.14 * 2 * 60) * 0.142 + \left(314.3 * 3.14 * \frac{2^2}{4} \right) * 0.44$$

$$= 1,730 \text{ kips.}$$

Factored load = 1700 kips < factored resistance = 1730 kips, and design satisfies ULS conditions. The normalized load $\theta = 1,200/10,120 = 0.12$.

Now consider the impossible case where L/D=30 with COV of UCS of 0.2, for a minor bridge with target P_f of 1/100, and θ of 0.12; with these, from Figure 8.5, the possible maximum normalized load is 0.23, which is almost two times larger than 0.12 as per ULS criteria, and hence, the case falls into the possible case classification.

Other examples with a wide variety of variable changes were also conducted to find the relationship between the ULS normalized load and the maximum normalized

load to satisfy the SLS possible case. All examples showed that if a design satisfies current ULS design, it lies well within the possible case. This becomes very convenient for shaft designers, because once ULS conditions are met, Equation 8.7 can be applied directly to find the resistance factor for the SLS design without any possible case checking.

8.7. Resistance Factor Calibrated Using Load Transfer Normalized to Predicted Ultimate Values

As discussed in Chapter 6, there are two approaches to obtain load transfer relationships: 1) normalizing the unit side and tip resistance to maximum measured resistance, and 2) normalizing the unit side and tip resistance to the predicted ultimate resistance. The resistance factors outside of this section were calibrated using the former approach. This section provides comparisons between resistance factors obtained from the two approaches.

In the SLS probabilistic analyses, mobilized unit resistance corresponding with a particular normalized displacement can be obtained with some uncertainty by using load transfer models (t - z curves and q - w curves) and prediction models (Equations 8.1 and 8.2). For both approaches of normalization, there are two steps for determining mobilized unit resistance:

- Step 1: Obtain the mobilized normalized unit resistance from the particular normalized displacement using a load transfer relationship.

- Step 2: Multiply the mobilized normalized unit resistance with a predicted ultimate unit resistance (obtained from Equations 8.1 and 8.2) to get the desired mobilized unit resistance.

For the approach of normalizing to maximum measured resistance, the $t-z$ models obtained from the approach have maximum y axis value of unity as in Figure 8.7.a, and the curve carries the load transfer variability/uncertainty only. Thus, the variability of the results in Step 1 comes only from the variability of load transfer (or mobilization). That of Step 2 comes from the variability of the prediction model (Equation 8.1 and 8.2) (or prediction).

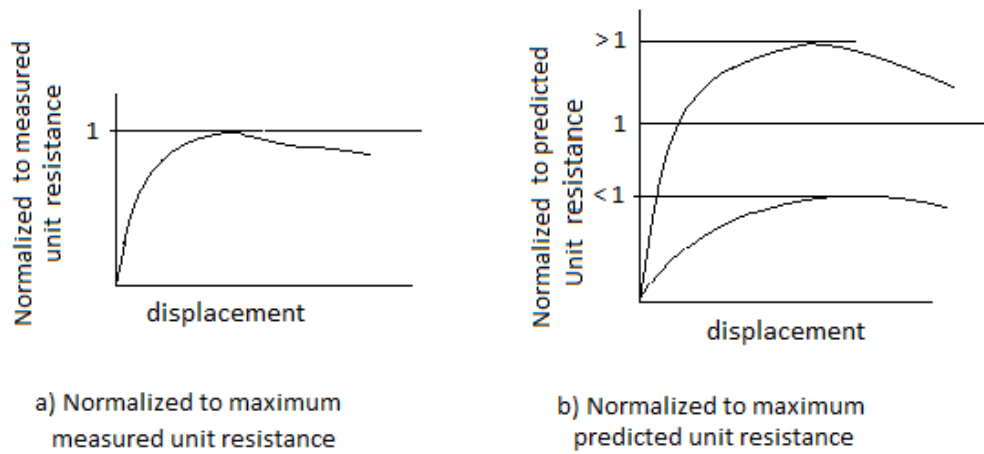


Figure 8.7. The $t-z$ curves for a) normalized to maximum measured unit resistance and b) normalized to maximum predicted unit resistance.

For the approach of normalizing to predicted ultimate resistance, the load transfer curve may have any y axis value (not of unity, as when the load transfer is

normalized to the maximum measured resistance) as shown in Figure 8.7.b. For this approach, a load transfer model carries both the load transfer model's uncertainty (mobilization) and the prediction model's uncertainty (prediction). The reason is that the t - z models used here were obtained by normalizing unit resistance with the predicted ultimate unit resistance, so the uncertainty of the ultimate unit resistance prediction is inherently within the models. Therefore, the variability of the result in Step 1 comes both from the variability of load transfer (or mobilization) and the prediction model's uncertainty (prediction). The variability of the result in Step 2 was set to zero to avoid redundancy.

In the calibration process, the variability/uncertainty of both mobilization and prediction from Steps 1 and 2 must be incorporated. When normalizing to maximum measured unit resistance in the process of generating the t - z curves, the variability of mobilization comes from the variability/uncertainty of load transfer models, which has the variability represented by the standard of deviation of the t - z curve of 0.17, and the q - w of 0.14 (Table 8.1, input #13 and 14). The variability of the prediction comes from the variability/uncertainty of the ultimate unit resistance prediction models represented by COVs of ultimate unit side and tip prediction of 0.659 and 0.254 (Table 8.1, input #15 and 16).

On the other hand, for the approach of normalizing to predicted ultimate unit resistance, the variability/uncertainty of the prediction models was inherently included in the uncertainty of the load transfer models. Therefore, in the process of generating

the t - z curves, when using the standard deviation for t - z and q - w models, the variabilities of both Step 1 (mobilization) and Step 2 (prediction) were already included. The COVs of ultimate unit side and tip prediction models were then set to zero. The variation of the t - z model is represented by its standard deviation of 0.35, and of 0.34 for the q - w model (Table 6.13). Those two values are larger than the values of 0.17 and 0.14 for the approach of normalizing to maximum measured unit resistance.

To compare the resistance factors obtained from the two approaches of normalizing, the resistance factors were calibrated for three sample cases A, B and C. The input parameters in Table 8.1 were used, except that for the approach of normalizing to predicted ultimate unit resistance, the standard deviation and the COV of the load transfer models and prediction models were as specified in the previous paragraph. The cases were for different given probabilities of failure and normalized loads as:

$$\text{Case A: } P_f = 1/25, \theta = 0.3$$

$$\text{Case B: } P_f = 1/50, \theta = 0.25$$

$$\text{Case C: } P_f = 1/100, \theta = 0.2.$$

The obtained resistance factors are presented in Figure 8.8. It is observed that the resistance factors obtained from the approach of normalizing to predicted ultimate values (solid lines) are consistently lower than resistance factors obtained from the approach of normalizing to maximum measured values (dashed lines).

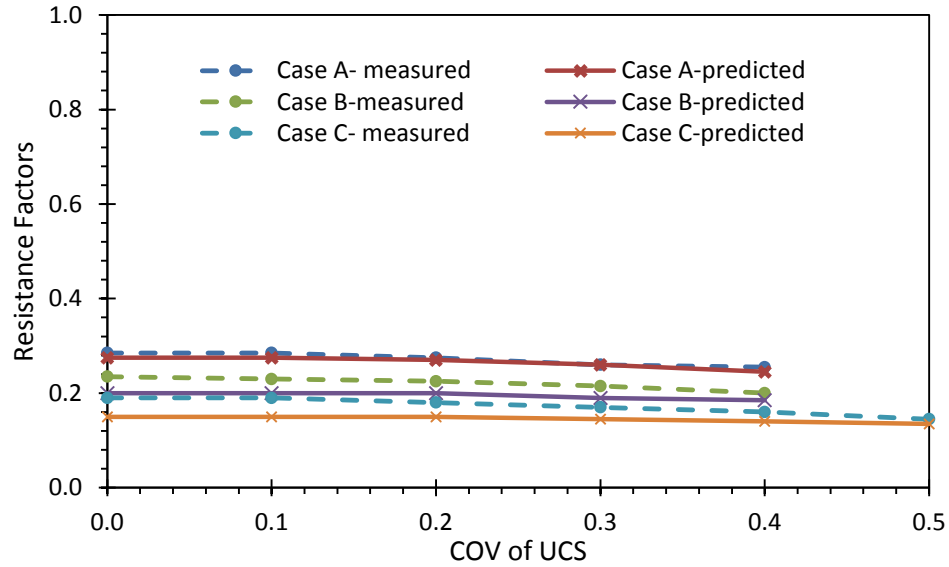


Figure 8. 8. Resistance factors for two approach of normalization.

The two approaches of normalizing to maximum measured values and to predicted ultimate values are inherently different. The t-z models of the former approach carry only the variability of the mobilization of load transfer, while the t-z models of the latter inherently contain the variability of both mobilization and the prediction. This leads to the differences in modeling and simulating the shaft head settlement and the resistance factors. The approach of normalizing to maximum measured resistance produces higher resistance factors, thus the design would be more cost-effective to achieve the same target probability of failure and is recommended for use. The resistance factors recommended in this dissertation (except for this Section 8.7) were calibrated solely by using the approach of normalizing to maximum measured resistance.

8.8. Side Resistance Factor and Tip Resistance Factor

In practice, a design engineer sometimes ignores the shaft tip's resistance, and the shaft resistance is derived from side resistance only. This intentional omission may happen because the design engineer does not want to account for tip resistance, which requires a large displacement, from 5% to 10% of shaft diameter, to fully mobilize; or s/he just does not want to depend on the quality of concrete at the tip of the shaft. In some other special cases, an engineer will rely on tip resistance only. This happens, for example, when the drilled shaft is placed with most of the shaft side in soft soil layers while the shaft tip rests on hard rock. This section presents the resistance factors which were calibrated for side resistance and tip resistance for use in these special cases only. Note that for the case where the overall shaft resistance comes from both side and tip resistance, the side and tip resistance factors presented in this section cannot be used separately instead of using the resistance factors obtained from the charts or the equation proposed in Section 8.4, because the design would then have a different target probability of failure.

As previously discussed, the resistance factors in Section 8.4 depend on four variables: *COV of UCS*, normalized load θ , probability of failure and shaft length over shaft diameter (L/D) ratio. When calibrating for the side and tip resistance factor, the resistance factor must be a function of these first three variables: *COV of UCS*, θ and probability of failure. Also note that the normalized load is now the applied load normalized by the ultimate side resistance when calibrating the side resistance factor,

and by ultimate tip resistance when calibrating the tip resistance factor. Also, the side and tip resistance factors must be independent of length and diameter (or the ratio of L/D). A calculation was carried out to prove this.

Side and tip resistance factors were calibrated for cases with shaft lengths and shaft diameters as indicated in Table 8.6 with $\theta = 0.2$, $P_f = 1/25$, COV of $UCS = 0.2$, and all other inputs are as in Table 8.1. The results are shown in Table 8.6. With the varying shaft lengths and shaft diameters, the side and tip resistance factors are constants.

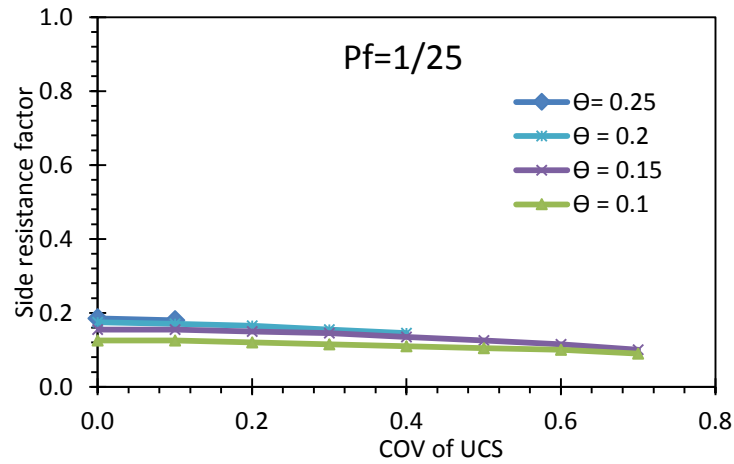
Table 8.6. Side and tip resistance factors.

	Shaft Diameter (Shaft length = 30ft.)			Shaft Length (Shaft diameter = 3 ft.)		
	2 ft.	4 ft.	6 ft.	10 ft.	20 ft.	30 ft.
Side Resistance Factor	0.165	0.165	0.165	0.165	0.165	0.165
Tip Resistance Factors	0.275	0.280	0.280	0.280	0.280	0.280

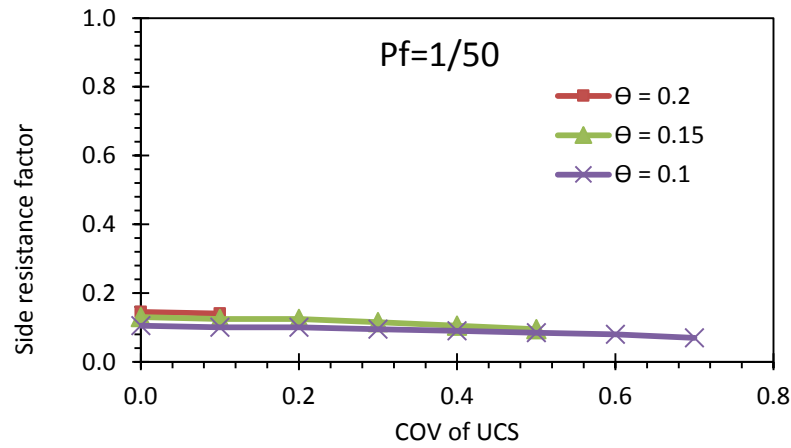
Side resistance factors were calibrated for shafts that gain their resistance from side resistance only; therefore, tip resistance was considered to be zero in the calibration process, and vice versa. Side resistance factors were calibrated depending on the COV of UCS, normalized load and probability of failure and are introduced in Figure 8.9 and in tables in Appendix H. The resistance factors seem small, with values ranging from 0.05 to 0.2. This means that in the design of a shaft that gains its resistance from side resistance solely, the UCS is reduced about 80 to 95% of its value, which is a significant reduction, to achieve a target probability of 1/25 to 1/100.

Tip resistance factors were also calibrated and are presented in Figure 8.10. The tip resistant factors are significantly higher than the side resistance factors in the same conditions. For example, with COV of UCS of 0.2, P_f of 1/25 and normalized load of 0.2, the side resistance factor is 0.165, while the tip resistance factor is 0.280. The difference, again, comes from the fact that the variability and uncertainty of parameters related to the fact that tip resistance is smaller than that from side resistance.

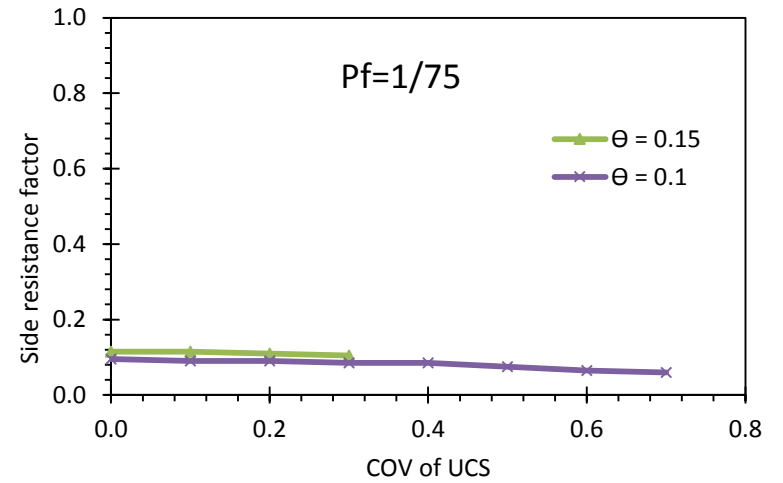
The side and tip resistance factors presented in this section are for the shafts which gain the overall shaft resistance from either side resistance or tip resistance. The resistance factors here cannot be used as separate resistance factors to design regular shafts where the shafts gain resistance from both side and tip, otherwise the design would have an actual probability of failure significantly lower than the target probability of failure, which leads to a costly design. The difference between the actual and the target probability of failure is as much as one order of magnitude.



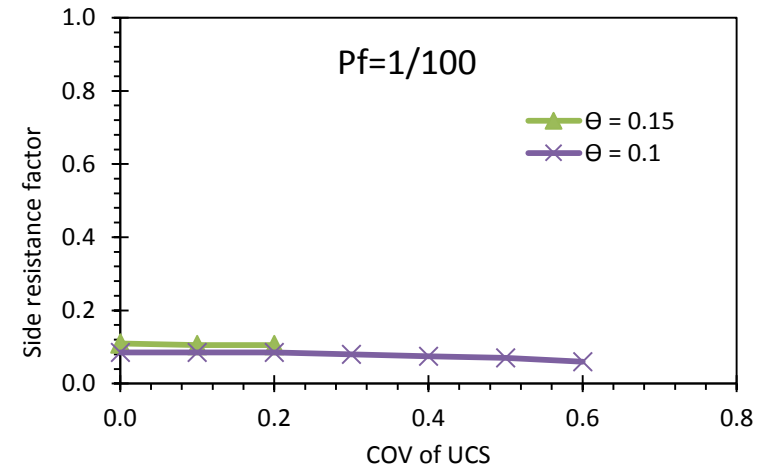
a) Side resistance factor for probability of failure of 1/25.



b) Side resistance factor for probability of failure of 1/50.

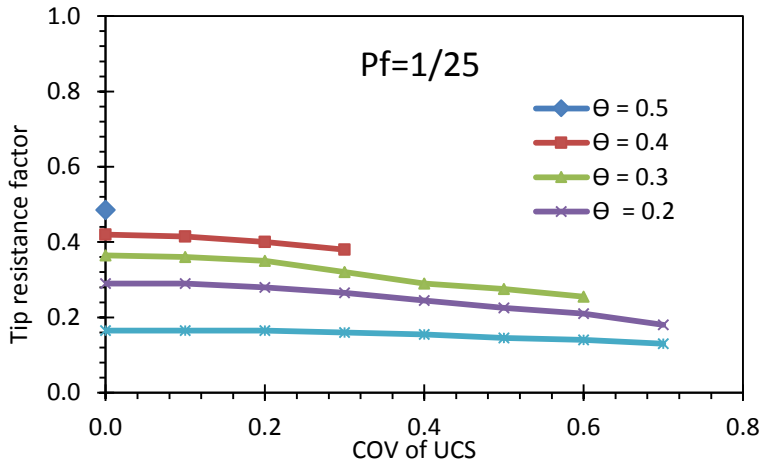


c) Side resistance factor for probability of failure of 1/75.

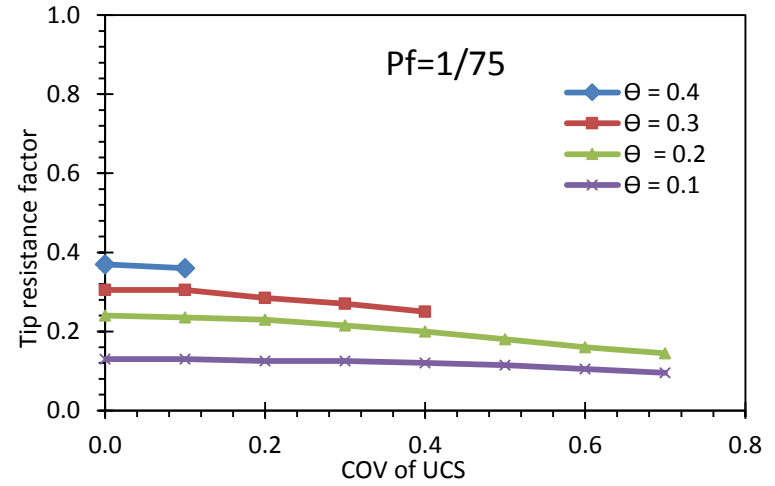


d) Side resistance factor for probability of failure of 1/100.

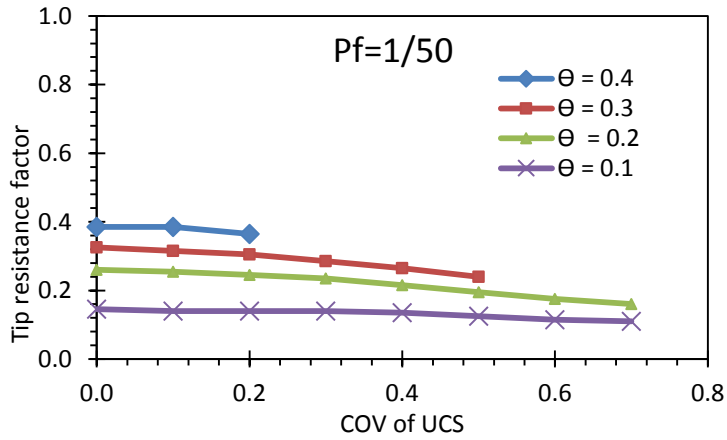
Figure 8.9. Side resistance factors.



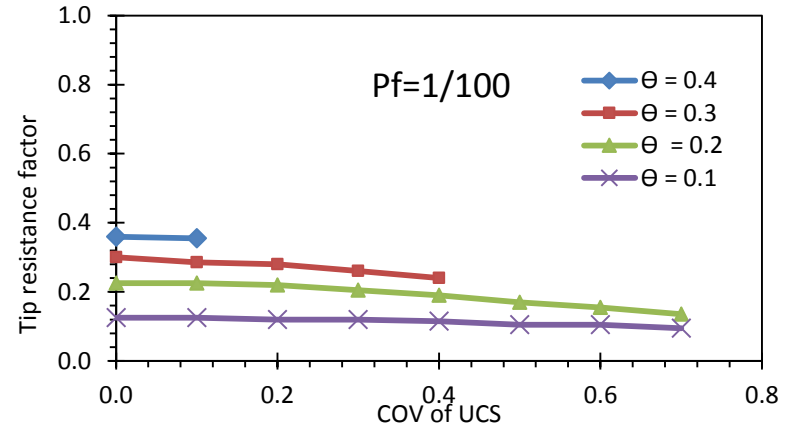
a) Tip resistance factor for probability of failure of 1/25.



c) Tip resistance factor for probability of failure of 1/75.



b) Tip resistance factor for probability of failure of 1/50.



d) Tip resistance factor for Probability of failure of 1/100.

Figure 8.10. Tip resistance factors.

8.9. Summary

This chapter presented the procedure for evaluation of SLS for drilled shafts. The input parameters used in the procedure were evaluated, combined and reduced so that from the original 24 input parameters, the resistance factors were then calibrated depending on only four variables while maintaining accuracy. The resistance factors were calibrated and presented in the form of charts, and an equation to calculate the SLS resistance factor was proposed. The use of the proposed SLS resistance factors makes SLS drilled shaft designs practical, simple and still achieves accurate target probability of failure, while not requiring “case-by-case” probabilistic analyses.

The comparisons in the resistance factors calibrated using load transfer models obtained from two approaches of normalizing - normalizing to maximum measured values and normalizing to predicted ultimate values - are presented. The recommendation was made to calculate resistance factors by using the approach of normalizing to maximum measured values. The side and tip resistance factors for shafts which have overall resistance coming from either side or tip resistance were also presented. This chapter established an important step toward finalizing the SLS design procedure using the proposed resistance factors, which will be discussed further in Chapter 9.

Chapter 9. Application Procedure for Service Limit State Design Using LRFD

9.1. Introduction

In Chapter 2, the literature review describes how the design for drilled shafts at SLS still uses the resistance factor of unity (note that the load factor in SLS design is also assigned a value of unity) or some resistance factors calibrated for specific conditions. Using a resistance factor of unity means that the SLS design procedure is treated as deterministic. Using specifically calibrated resistance factors for some specific values of shaft length, load, allowable settlement or probability of failure means that for other cases, there are no precalibrated resistance factors, and the design must be performed on a case-by-case basis. The fact of the matter is that if a design is done on a case-by-case basis, then the design is not a load and resistance factor design (LRFD) but is really reliability-based design. LRFD is intended to be a practical and straightforward way to account for reliability without having to do reliability-based design, which requires statistical and probabilistic calculations as well as computer programming skills that are not familiar to many geotechnical engineers.

To address this problem, an LRFD design procedure for drilled shafts at the service limit state is proposed. The new procedure addresses existing limitations by using the proposed resistance factors that depend on four variables while still

accounting for different conditions of dead load, live load, geomaterial strength and its variability, shaft length, shaft diameter, allowable settlement, and the target probability of failure. The resistance factor equation was established from models developed from field load tests, from variable sensitivity studies and intensive probability analyses. The use of a new resistance factor equation is the unique feature of the proposed design procedure.

This chapter first presents a step-by-step procedure for application of the proposed methods for service limit state (SLS) design of drilled shafts using LRFD. An example is also provided to illustrate application of the proposed procedure.

9.2. Procedure for Drilled Shaft Design at the Service Limit State

The key steps of the design procedure are presented in Chapter 7. In this chapter, a more detailed design procedure utilizing the resistance factor equation is presented. The proposed design procedure relies on direct comparisons between shaft head displacement and allowable displacement, which makes the design possible without any case-by-case probabilistic analyses. The steps for the proposed design procedure are:

Step 1. Determine initial shaft dimensions using strength limit state criteria. This step requires using the Missouri Department of Transportation's *Engineering Policy Guidelines for Design of Drilled Shafts* (Loehr et al., 2011). In these guidelines, shaft dimensions are established from the ultimate unit side resistance

$$q_s = 0.76 \times UCS^{0.79} \quad (9.1)$$

where UCS is mean uniaxial compressive strength (ksf), and the ultimate unit tip resistance

$$q_p = 14 \times UCS^{0.71} \quad (9.2)$$

After choosing an initial shaft diameter and shaft length, shaft capacity Q_{ult} can be determined from the unit side and tip resistance. Side resistance is equal to the ultimate unit side resistance q_s multiplied by the shaft side area. Tip resistance is equal to the ultimate unit tip resistance q_p multiplied by the shaft tip area. The condition that factored load is equal to or less than shaft resistance Q_{ult} is used to iteratively solve for shaft dimensions that satisfy the strength limit state condition.

Step 2. Determine shaft length over shaft diameter ratio L/D and normalized load θ :

$$\theta = \frac{DL+LL}{Q_{ult}} \quad (9.3)$$

Step 3. Calculate resistance factor ϕ . The resistance factor is a function of the normalized load, θ , the shaft length over shaft diameter ratio, L/D , the coefficient of variation of the uniaxial compressive strength (COV of UCS), and the target probability of failure, P_f :

$$\phi = \left[\frac{(5-COV)*\theta-COV}{10} + c_{pf} \right] * c_{L/D} \quad (9.4)$$

where:

COV = COV of UCS,

θ = normalized load over capacity,

c_{pf} = coefficient for different probability of failure P_f , from Table 8.7,

and

$c_{L/D}$ = coefficient for different shaft length over shaft diameter ratios (L/D) from Table 8.8.

Step 4. Calculate the *factored shaft head vertical displacement* $y^*_{(UCS^*)}$. This is done by first determining the factored uniaxial compressive strength UCS^* :

$$UCS^* = \varphi * UCS \quad (9.5)$$

Then the factored UCS^* , shaft dimensions and given loads are used in the proposed load transfer models to calculate the *factored shaft head displacement* $y^*_{(UCS^*)}$:

$$t = \frac{z}{1.07*z+0.13} \quad (9.6)$$

$$q = \frac{w}{1.10*w+0.72} \quad (9.7)$$

where

t and q = normalized unit side and tip resistance, and

z and w = normalized displacement in % of shaft diameter.

This step of calculating the factored shaft head settlement requires iteration. Designers can use software such as TZPile or SHAFT available from Ensoft, Inc., or some

in-house computer code. The obtained value of factored settlement, $y^*_{(UCS^*)}$, is associated with the given target probability of failure P_f used to determine the resistance factor in Step 3.

Step 5. Compare the factored settlement $y^*_{(UCS^*)}$ with the allowable settlement y_a . The allowable settlement y_a is usually assigned by structural engineers depending on the serviceability and structure type. The equation used for this step is:

$$y^*_{(UCS^*)} \leq y_a \quad (9.8)$$

If the factored settlement is less than the allowable settlement, the SLS check is satisfied and the design is controlled by the strength limit state. The probability of having settlements that exceed the allowable settlement is less than the target value of the probability of failure. In contrast, if the factored settlement is greater than the allowable settlement, the design is controlled by serviceability and the shaft dimensions must be increased and Steps 2 through 5 are repeated to satisfy Eq. 9.8.

The above proposed procedure allows SLS design for drilled shaft to be conducted without any probabilistic analysis. The design procedure uses the resistance factors established from load transfer models and the ultimate resistance prediction models derived empirically from the field load test data. However, both the design procedure and the equation can be used for any soil/shale that shows similar load transfer characteristics. The analysis principles can be further applied for any type of

soil or shale as long as its load transfer curves and ultimate resistance prediction models are given.

9.3. Illustrative Example

An example is presented to illustrate the design procedure. The problem is to design a single drilled shaft to carry a dead load, DL , of 850 kips and live load, LL , of 400 kips; the shaft is in shale that has mean UCS of 10 kips with a COV of 0.1. The sketch for the problem is shown in Figure 9.1.

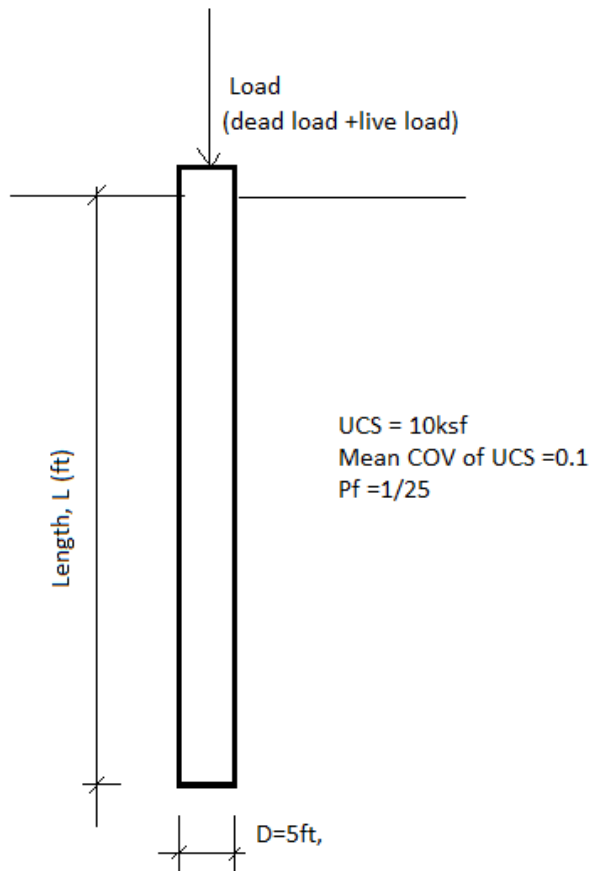


Figure 9.1. Sketch of design problem for a single drilled shaft.

The assigned allowable displacement is taken to be 0.6 inches. The SLS design is for a bridge on a minor road that has a SLS target probability of failure of 1/25. The design follows the five step procedure as follows:

Step 1. Determine shaft dimensions using strength limit state criteria. Choose shaft diameter of D=5 ft. Use the Engineering Policy Guidelines for Design of Drilled Shafts (Loehr et al., 2011) to solve shaft length by the following inequality:

$$(DL + W) * \gamma_{DL} + LL * \gamma_{LL} \leq \phi_s * q_s * + \phi_p * q_p$$

or

$$(DL + W) * \gamma_{DL} + LL * \gamma_{LL} \leq \phi_s * (\pi DL * 0.76 * UCS^{0.79}) + \phi_p * \left(\frac{\pi}{4} D^2 * 14 * UCS^{0.71}\right)$$

where:

γ_{DL} = dead load factor,

γ_{LL} = live load factor,

ϕ_s = resistance factor for unit side resistance for drilled shaft

ϕ_p = resistance factor for unit tip resistance for drilled shaft,

W = weight of the shaft:

$$W = \frac{\pi}{4} D^2 * L * \gamma_c$$

γ_c = unit weight of concrete, which is 150 pcf.

Dead load factor γ_{DL} is 1.75, live load factor γ_{DL} is 1.2. Figures 9.2 and 9.3 (which are Figures 751.37.3.3 and 751.37.3.4 in the Engineering Policy Guidelines for Design of Drilled Shafts, Loehr et al., 2011), P_f of 1/25 for bridges on minor roads,

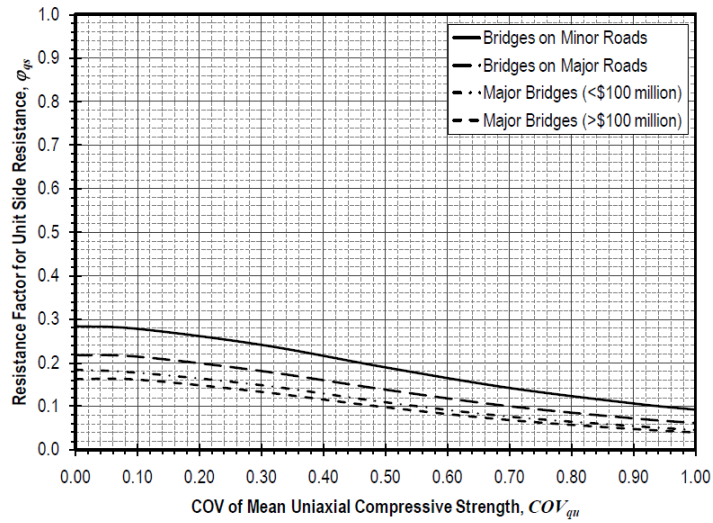


Figure 9.2. Resistance factors for unit side resistance for strength limit states.

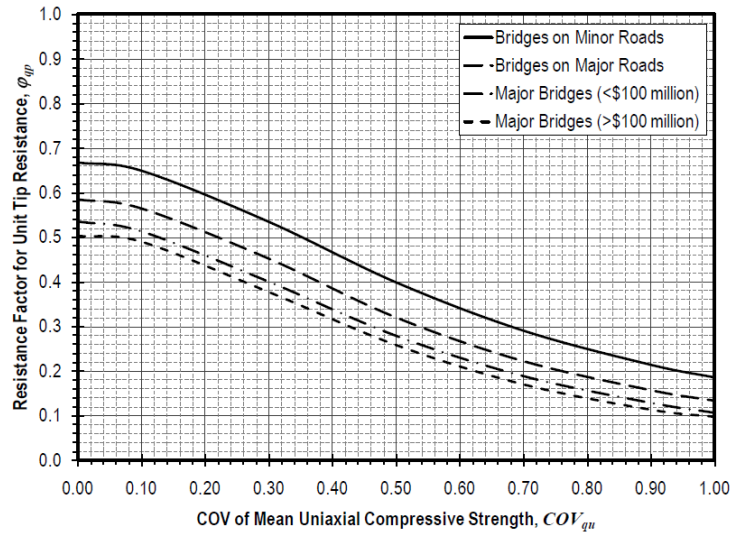


Figure 9.3 Resistance factors for unit tip resistance for strength limit states.

and COV of UCS of 0.1, gives the strength limit state resistance factor for unit side resistance ϕ_s of 0.28. From Figure 9.3, the strength limit state for resistance factor for unit tip resistance ϕ_p is 0.65. Several trials for the shaft length were carried out, and the final trial was L=50 ft.; the weight for the 50-foot-long shaft was 147.26 kips. They are inserted into the above inequality:

$$(850 + 147.26) * 1.25 + 400 * 1.75$$

$$\leq 0.28 * (50 * \pi * 5 * 0.76 * 10^{0.79}) + 0.65 * \left(\frac{\pi}{4} 5^2 * 14 * 10^{0.71}\right)$$

$$1946.5 \text{ kips} \leq 1946.9 \text{ kips} .$$

Shaft dimensions of D=5 ft. and L=50 ft. satisfy strength limit state condition.

Step 2. Determine the shaft length over shaft diameter ratio L/D and normalized load θ which is the ratio of given loads over Q_{ult} . For D=5 feet and L=50 feet, the shaft length over shaft diameter ratio is 10. The nominal shaft capacity Q_{ult} is

$$Q_{ult} = (50 * \pi * 5 * 0.76 * 10^{0.79}) + \left(\frac{\pi}{4} 5^2 * 14 * 10^{0.71}\right)$$

$$Q_{ult} = 5090 \text{ Kips}$$

The normalized load θ is

$$\theta = \frac{(\text{DL} + \text{shaft weight} + \text{LL})}{5090} = \frac{(850 + 147.2 + 400)}{5090} = 0.275.$$

Step 3. Calculate the resistance factor. With given $P_f=1/25$, from Table 8.7, c_{pf} is 0.145. Use Table 8.8 where $L/D=10$ to obtain $c_{L/D}=1.0$. Substitute θ , c_{pf} , $c_{L/D}$ and COV of UCS into the resistance factor equation:

$$\varphi = \left[\frac{(5 - COV) * \theta - COV}{10} + c_{pf} \right] * c_{L/D}$$

$$\varphi = \left[\frac{(5 - 0.1) * 0.275 - 0.1}{10} + 0.145 \right] * 1.0$$

$$\varphi = 0.267$$

Step 4. Calculate the *factored shaft head displacement* $y^*_{(UCS^*)}$. First calculate the factored uniaxial compressive strength UCS^* , which is UCS multiplied by the resistance factor

$$UCS^* = \varphi * UCS$$

$$UCS^* = 0.267 * 10 = 2.67 \text{ ksf}$$

Use factored UCS of 2.67 ksf in calculation and the t - z models as in Equations 9.5 and 9.6 to find factored settlement $y^*_{(UCS^*)}$. For this example, the finite element computer code is used to obtain the factored displacement of **0.66** inches.

Step 5. Compare the factored settlement $y^*_{(UCS^*)}$ with allowable settlement y_a . The shaft displacement of 0.66 inches is larger than allowable displacement of 0.6 inches; hence, the shaft needs to be longer or larger diameter. The shaft length is increased to 52 ft., then 53 ft. For each shaft length, a new Q_{ult} for a new shaft weight and new normalized load were calculated and used to calculate new resistance factors as shown in Table 9.1. The shaft length of 53 ft. gives a shaft head displacement of 0.59

inches, which is smaller than the allowable settlement of 0.6 in. A final $D=5$ ft. and $L =53$ ft. were chosen for the design.

In this illustrative example, strength limit state design requires a shaft length of 50 feet; however, SLS design for this case requires a shaft length of 53 feet which is *longer* than 50 feet, from strength limit state criteria in order to obtain the probability of 1/25.

Table 9.1. Calculation of factored settlements

Shaft Length	50 (ft.)	52(ft.)	53(ft.)
L/D	10	10.4	10.6
$C_{L/D}$	1	0.984	0.9807
Shaft Weight (kips)	147	153	156
Load (kips)	1397	1403	1406
Q_{ult} (kips)	5090	5238	5311
Normalized Load	0.274	0.268	0.265
Resistance Factor	0.267	0.262	0.260
Factored Settlement	0.660	0.614	0.587

If this case was designed using Allowable Stress Design or was designed following current ASSHTO (2007) specifications using an SLS resistance factor of 1.0, the nominal displacement calculated by using t-z method is 0.054 inches, which is significantly less than the allowable displacement of 0.6 inches. A shaft length of 50 feet then satisfies the SLS check, but the probability of failure is apparently much higher than 1/25.

For this example, a rigorous resistance factor was calculated for the case of $L = 53$ ft. obtaining a resistance factor of 0.255. The result matches the resistance factor in Table 9.1, which is 0.26 (note that the precision of the number is to 0.005). Another rigorous calculation was conducted to see if using the calculated resistance factor of 0.26, provides the “calculated” probability of failure P_f that is equal to the target P_f of $1/25$. The procedure is similar to the procedure presented in Sections 4.4 in Chapter 4. A simulation of 100,000 shaft head displacements using a resistance factor of 0.26, resulted in 4032 failure cases where shaft head displacements were larger than the factored shaft displacement $y^*_{(UCS^*)}$ of 0.59, making a “calculated” P_f of 0.04, which is the same as the target P_f of $1/25$. When the resistance factor equation was used the probability of failure condition was met without conducting any rigorous probabilistic calculation.

9.4. Summary

In this chapter, a design procedure for drilled shaft SLS design is proposed. A new step-by-step procedure for the SLS drilled shaft design is introduced. Using the design procedure makes the SLS drilled shaft design possible without probabilistic calculation on a case-by-case basis; this saves time and money. An illustrative example, which follows the new design calculation, was presented to demonstrate the use of the new design procedure.

Chapter 10. Summary, Findings, Practical Implications and Conclusions

10.1. Summary of the Study

For current AASHTO load and resistance factor design, the resistance factor for drilled shafts at the service limit states (SLS) is recommended to have a value of 1.0 (AASHTO, 2007). This implies that the design for the SLS is treated as deterministic, while the design for the strength limit states is probabilistic. Even though some SLS resistance factors have been introduced in the literature, these factors were calibrated for some specific conditions of load, shaft length or allowable settlement. In other cases, under different conditions, the designs are recommended to be analyzed on a case-by-case basis.

This study focuses on probabilistic analyses, establishing an SLS design procedure, and developing resistance factors for design of drilled shafts in shale at the service limit state. Load transfer models for drilled shafts were developed from field load test measurements. The dependency of SLS resistance factors on different parameters was studied. Then, an approach of combining variables and eliminating variables was used to develop a method for design of drilled shafts at the SLS, based on resistance factors that are taken to be a function of four variables. A new equation to calculate the resistance factors was also established as a function of the four variables.

The proposed design procedure allows for design of drilled shafts at the service limit state without requiring case-by-case probabilistic analyses for the specific conditions encountered, as has been recommended for SLS design problems in the literature. The proposed method allows for account of different dead loads, live loads, geomaterial strengths, geomaterial strength variability, shaft lengths, shaft diameters, allowable settlements, and the target probability of failure.

Chapter 2 summarizes recent studies on development of resistance factors for drilled shafts and other deep foundations at the service limit state. The current issue is that the recommended resistance factors for drilled shafts at the SLS were calibrated for specific shaft lengths, applied loads, allowable displacements, etc. Therefore, for other cases with different conditions, it has been recommended that the probabilistic design should be carried out using specific case inputs.

Chapter 3 describes the method for deterministic prediction of settlement using the load-transfer method, or t - z method. This method is based on non-linear load transfer curves. A numerical approach using the finite element method applied to the t - z method was presented in detail.

Chapter 4 describes methods used for probabilistic prediction of shaft settlement using the Monte Carlo simulation method. Discussions about the process of generating simulated random data, the number of simulations required, and the inputs for the calibration process were presented.

The Missouri Department of Transportation (the sponsor of this study) authorized load tests on 25 drilled shafts for research purposes. Details of the two test sites, shaft designations, load testing procedure, data reduction and data analyses are provided in Chapter 5. Empirical load transfer curves were developed from results of this testing program and compared with the well-known O'Neil and Reese (1999) load transfer curves.

Chapter 6 describes regression analyses performed on the measured load transfer data to establish load transfer models that represent the data. Models for the load transfer curves were found, and the variability/uncertainty in the load transfer models was characterized and quantified using several different approaches of normalization and regression. Two different approaches of generating load transfer data were proposed and the simulated load transfer data were compared with the field test data to find the best approach.

Chapter 7 describes the procedure used for calibration of resistance factors and the step-by-step use of the resistance factors for SLS design of drilled shafts. A sensitivity study to investigate the dependence of SLS resistance factors for drilled shafts on deterministic and probabilistic variables was also described.

Based on the results of the sensitivity study, the input variables were combined and reduced so that resistance factors could be calibrated based on four variables. The variables are: 1) probability of failure, 2) normalized load, 3) shaft length over shaft diameter ratio and 4) the uniaxial compressive strength's coefficient of variation. The

SLS resistance factors for drilled shaft in shale are found and presented in Chapter 8 and equations are proposed to calculate the SLS resistance factors. The approach of using resistance factors as presented in Chapter 8 frees SLS design for drilled shafts from depending on case-by-case analyses.

Chapter 9 presents a procedure developed for evaluating drilled shafts at the SLS to achieve a target probability of failure. A step-by-step procedure for design is introduced and an accompanying example was presented to illustrate application of the proposed procedure for design.

10.2. Findings and Practical Implications

The findings, conclusion and practical implications of this study are grouped in four different categories.

10.2.1. Load Transfer Characteristics

The following findings and conclusions on the load transfer characteristics were based on analysis of the load test data:

- Field test data show that side resistance requires displacement of up to 10% shaft diameter to fully mobilize. This number is significantly larger than that of O'Neil and Reese (1999) load transfer curves which showed that side resistance is fully mobilized when settlement reaches 0.8% of shaft diameter. The displacement of 10% of shaft diameter is also higher than the displacement of 5% shaft diameter required for shaft resistance

to be fully mobilized as assigned in ASSHTO (2007). Similarly for tip resistance, the displacement required for full mobilization of tip resistance is higher than that established by O'Neil and Reese (1999), and greater than the 5%D provided in ASSHTO (2007). This is an important practical implication for SLS design.

- Load transfer models were developed for side and tip resistance for drilled shafts in shale. Five functional models were used for regression analyses and the best model for side and tip load transfer data was found to be a hyperbolic function. The hyperbolic model predicts future data and their variability of well. This model contains two fitting parameters that have physical meaning: a is the reciprocal of the curve's initial slope and b is the reciprocal of the curve horizontal asymptote.
- Most of the models obtained from ordinary least square regression give prediction bounds that overpredict future observations when displacement is less than 0.05% of shaft diameter, but then the bounds predict the future outcome favorably when the displacement is higher than about 0.05% D. The models from weighted least squares regression with the defined weight, on the other hand, predict future outcomes well only when the displacement is less than about 0.05%D. For larger displacement, the models overestimate the variability of future observations. Because 0.05%D is a relatively small displacement for SLS

design, the ordinary least squares regression is recommended for developing models of load transfer data.

- Uncertainty in t - z and q - w curves were quantified. The variation/uncertainty of the load transfer for side resistance is greater than that of load transfer for tip resistance. The variation of both t - z and q - w curves for field test data are significantly larger than the range suggested by Reese and O'Neil (1999).

10.2.2. Regression Approaches

Two approaches were presented for regression analysis to obtain functions for load transfer curves: a collective approach in which regression analyses were performed for the collective set of data at once to obtain two hyperbolic fitting parameters for side and tip load transfer, respectively, and an individual approach in which regression analyses were performed for individual load transfer curves from each shaft segment to obtain two sets of hyperbolic parameters. The model function was developed based on the parameters that are the average of all fitting parameters. The conclusions and findings about the approaches to regression are as follows:

- The variability and uncertainty of the load transfer models are represented differently for the collective and individual approaches, and so is the method for simulating the load transfer curves. Corresponding methods for simulating data from the models for the two approaches were proposed.

- Simulated data points using the collective approach produces fitting parameters a and b that are almost exact matches to those from the field test data. The standard deviation of the simulated data points from the collective approach is also similar to that of the field test data. On the other hand, the individual approach gives different values of the parameters compared with those from the field tests, especially for the b parameter, which represents the inverse of the initial slope of the load transfer curves. The load transfer models from the individual approach tend to over-predict the variability of future outcomes. The collective approach is recommended for performing regression analysis for load transfer data. This is another significant practical implication of the research.
- Some of the simulated load transfer curves from the collective approach do not pass through zero at zero displacement, and the curves have the same shape. On the other hand, the curves simulated using the models from the individual approach always pass through origin, and have varying shapes.
- One disadvantage of the individual approach is that the approach cannot utilize all the tip resistances from field test data points available when there are shafts that failed in shear, while the tip resistance was barely mobilized. The fitting parameters for those shafts sometimes are

unreasonable and cannot be used to find the average fitting parameters for developing the tip resistance model.

- The two approaches give different load transfer models with different fitting parameters. A slight difference for the hyperbolic a parameter exists, but the b parameter magnitudes are almost two times different for the two approaches. Parameter b , which represents the initial slope of the curve, is 0.13 for the collective approach, while for the individual approach, it is 0.25.
- The individual approach gives the coefficient of correlation between the two hyperbolic parameters, but the collective approach does not. The coefficients of correlation for both fitting parameters for side and tip resistance curves are negative, meaning that the slope and the asymptote of the load transfer curve are inversely proportional. The individual approach also is able to give the distribution type of the fitting parameters; the distribution type for the a parameter is normal, and for the b parameter, it is lognormal.

10.2.3. Sensitivity of SLS Resistance Factors on Variables

One of the important contributions of this research is the evaluation of the dependency of SLS resistance factors on different input parameters for probabilistic prediction of settlement. The conclusions and findings from these evaluations are as follows:

- SLS resistance factors are more sensitive to the variability/uncertainty of some probabilistic variables than of others. In a descending order of sensitivity, these variables are: 1) Uniaxial compressive strength UCS, 2) ultimate unit side resistance prediction, 3) side resistance load transfer, 4) applied load, 5) shaft stiffness EA, 6) tip resistance load transfer and 7) ultimate unit tip resistance prediction. They are clearly separated into two groups. The more sensitive group consists of the first four variables, and the less sensitive group consists of the last three as summarized in Table 10.1.

Table 10.1. Probabilistic Variables Listed According to Sensitivity.

Most Sensitive Variables	Least Sensitive Variables
Uniaxial compressive strength	Shaft Stiffness
Unit Side Resistance Prediction	Tip Load Transfer
Side Load Transfer	Unit Tip Resistance Prediction
Load	

- SLS resistance factors depend on mean values of load and on shale uniaxial compressive strength. The normalized load, which is the ratio of the sum of dead load and live load divided by the total shaft capacity, is introduced for use so that the effect of the mean values of load and uniaxial compressive strength can be represented by the effect of the normalized load. It was found that the SLS resistance factors increase with increasing normalized load.

- The dead load over live load ratio does not substantially affect the SLS resistance factors. This is because the only difference between dead load and live load is 2% difference in their coefficient of variation, which is small compared to the combined effects of other probabilistic variables.
- Resistance factors increase with decreasing shaft length over shaft diameter ratio L/D . This is explained by noticing that when the shafts are longer, side resistance contributes more to the overall resistance, and the resistance factor is strongly sensitive to both the ultimate unit side resistance prediction and side resistance load transfer's variability/uncertainty, which, in turn, is significantly higher than that of tip resistance. A coefficient to predict the change of the SLS resistance factor on L/D ratio was also proposed.
- There exist impossible cases where the probability of failure P_f for a design cannot be achieved. These cases are formed by a combination of the coefficient of variation of uniaxial compressive strength (COV of UCS), normalized load, L/D ratio and probability of failure P_f . If the design case is an impossible case, the designer should increase shaft dimensions to reduce normalized load or perform more site investigation tests to reduce the COV of UCS, so that the case is possible. It was found that if a case satisfies current Strength Limit States, the case will not be "impossible"
- SLS resistance factors strongly depend on how many input variables are considered probabilistic. The more variables that are treated as probabilistic

in the calibration process, the lower the resistance factor. If fewer variables are treated as probabilistic, the resulting SLS designs will be unconservative. The resistance factors developed in this research considered as many sources of variables as possible by using eight probabilistic variables.

10.2.4. Proposed Procedure and Resistance Factors for SLS Design

This research proposes a new design procedure for SLS design of drilled shafts. The procedure makes use of resistance factors to account for different sources of uncertainty in design. Details follow:

- There are 24 input parameters for probabilistic analysis of drilled shafts for the service limit state. By using the results from sensitivity analyses to identify which parameters are most important, and by combining and reducing the number of variables, the proposed resistance factors were calibrated depending on only four input variables: COV of UCS, normalized load, L/D ratio and probability of failure P_f . This is one of the significant practical implications of this work.
- SLS resistance factors for drilled shafts in shale were calibrated and introduced in the form of charts. An equation was also developed to calculate resistance factors based on four input variables. This is an important contribution of this dissertation.
- Resistance factors were also calibrated for shafts that gain their resistance from side resistance or from tip resistance only. These resistance factors do

not depend on L/D ratio, but only on the COV of UCS, the normalized load and the target probability of failure P_f . The resistance factors for tip resistance are significantly greater than the resistance factors for side resistance, because the variability and uncertainty of tip resistance are less than for side resistance.

- A new procedure for SLS drilled shaft design is proposed. By using the proposed resistance factors or the resistance factor equation, no probabilistic analysis is needed for different cases with different loads, probability of failure or allowable displacement. In other words, the design is not case-by-case based. Design-specific allowable displacement is used in direct comparison during the design process. This is the most important practical implication of this research.
- The resistance factors were calibrated based on t - z and q - z curves, which were obtained from two approaches of normalizing the unit side and tip resistance data: normalized by the maximum measured unit resistance and normalized by the predicted ultimate unit resistance. In the same conditions, the approach of normalizing to the maximum measured unit resistance gives a higher resistance factor to obtain the same target probability of failure. The latter leads to less costly designs and is recommended for developing load transfer curves.

- The SLS equation was developed based on empirical load transfer models. The principles of deriving this equation can be applied for any other type of soil. The only differences in inputs are load transfer curve characteristics and unit side and tip resistance prediction characteristics.

10.3. Conclusions

This dissertation presents new models for load transfer data with the variability/uncertainty quantified. A new equation is proposed to calculate resistance factor for drilled shafts in shale at the SLS that depends on only four variables. A procedure for SLS design of drilled shafts using the equation was established, freeing designers from using SLS resistance factor of 1.0 or performing probabilistic analyses on a case-by-case basis.

10.4. Recommendations for Future Research

Some areas in this study can be extended or improved. Recommendations for future work are as follows:

- Ordinary least squares regression (with constant standard deviation) and the chosen weighted least squares regression (that produces constant coefficient of variation) both have disadvantages in predicting variability of future observations. A better approach of weighting should be found for the weighted least square that produces load transfer models to better reflect the variability of the data.

- The collective and individual approaches of performing regression both have advantages and disadvantages. The collective approach was recommended for the regression analyses. However, the simulated load transfer data using the load transfer models from this approach sometimes produces negative values of unit resistance when the displacement is small. A better approach of doing regression, or a better way of representing the variability of the load transfer model should be found to minimize the disadvantages.
- The resistance factor calibration process considered the geomaterial as one layer with all the variability/uncertainty of the geomaterial strength represented by its coefficient of variation. The calibrated resistance factors should further consider multi-layered geomaterials.
- The SLS resistance factors proposed in this research were based on load transfer data for drilled shafts in shale. The methodology can be extended to other soil materials such as clay and sand, and for other types of foundations.
- Resistance factors for the O'Neil and Reese (1999) method should be calibrated because O'Neil and Reese method of design for deep foundation is widely used (AASHTO; O'Neil & Reese, 1999).
- Effects of variability caused by construction methods on the SLS resistance factors for drilled shafts should also be studied when establishing new design methods.

APPENDIX

Appendix A. MATLAB® Code for Shaft Top Displacement Calculation

A.1. Main Program:

```
function pilesolve(tzcode)
data.P = 1000; % tip load (kips);
data.Nnodes = 20; % number of nodes
data.tzcode = 1;

data.diam = 5.04*12; % diameter (inches)
data.L = 17*12; % total length (inches)

data.Emodulus = [30E3 4.09E3]; % pile moduli [steel concrete] (ksi)
data.Apercent = .9; % percent area that is steel
data.A = [1.1706 1.4215];
data.b = [0.4641 0.6253]; %y = 0x
data.tULT = 3600; % side ultimate shear (pounds/sqft)
data.tULT = (data.tULT/1000)/144; % in kips per square inch
data.qULT = 60000; % 78 000 do lun lon hon side ultimate shear
(pounds/sqft)
data.qULT = (data.qULT/1000)/144; % in kips per square inch
realQult=
(data.tULT*pi*data.diam*data.L/data.A(1)+data.qULT*pi*(data.diam^2)/4/d
ata.A(2))
maxiter = 50;
u0 = zeros(1,data.Nnodes);
disp('NR ITERATION HISTORY [iter residual]')
loai=0;
[u,numiter,loai] = NewtonRaphson (@getNRdata,u0,maxiter,1E-
6,data,loai);
loai

maxminu = [max(u) min(u)];
x = linspace(0,data.L/12,data.Nnodes);
plot(x,u)
xlabel('length along pile (ft)')
ylabel('pile displacement (in)')
end

function [f,df] = getTZ(u,data)
A = data.A; b = data.b;
L = data.L; diam = data.diam;
```

```

N = data.Nnodes;
% calculate areas
h = L/(N-1);
Aside = ones(1,N)*pi*diam*h;
Aside([1 N]) = Aside([1 N])/2;
Abase=zeros(1,N);
Abase(1) = pi*(diam^2)/4;
% zero TZ values
t = zeros(1,N); dt = t;
q = zeros(1,N); dq = q;
z = u; w = u(1);

switch data.tzcode
case 1

% SIDE TZ hyperbolic curve
t = z./(A(1).*z+b(1));

dt = b(1)./(A(1).*(z)+(b(1))).^2;

% BASE QW hyperbolic curve
q(1) = w./(A(2).*w+b(2));

dq(1) = b(2)./(A(2).*w+(b(2))).^2;
case 2
% EXPONENTIAL
% SIDE TZ exponential curve
t = 1-exp(-z);
dt = exp(-z);
% BASE QW exponential curve
% tb(1) = 1-exp(-z(1));
% dtb(1) = exp(-z(1));
end
%
f = Aside.*t*data.tULT+ Abase.*q*data.qULT;
df = Aside.*dt*data.tULT+ Abase.*dq*data.qULT;
end

function [E,F,G,R] = getNRdata(u,data)
diam = data.diam;
L = data.L;
N = data.Nnodes;
P = data.P;
Esteel = data.Emodulus(1);
Econcrete = data.Emodulus(2);
Apercent = data.Apercent;

% calculate spring rate
h = L/(N-1);
Abase = pi*(diam^2)/4;
Emod = (Apercent*Esteel + (100-Apercent)*Econcrete)/100;
Kspring = Abase*Emod/h;

% calculate forces and force derivatives

```

```

[f,df] = getTZ(u,data);

% define force (RHS) vector and Jacobian
E = zeros(1,N); F = df; G = zeros(1,N); R = f;

for i = 1:N-1
    Ke = Kspring*[1 -1;-1 1];
    Fe = Ke*u(i:i+1)';
    E(i+1) = E(i+1) + Ke(2,1);
    F(i:i+1) = F(i:i+1) + diag(Ke)';
    G(i) = G(i) + Ke(1,2);
    R(i:i+1) = R(i:i+1) + Fe';
end
R(N) = R(N) - P;
end

```

A.2. Function NewtonRaphson

```

function [xi,i,loai] = NewtonRaphson (fun,xi,imax,es,data,loai)
% This M-File computes the root of a
% nonlinear equation using the Newton Raphson
% iteration method. Inputs are as follows:
% fun = name of M-File that computes f and df/dx
% xi = initial guess
% imax = max number of iterations allowed
% es = convergence criteria
for i = 1:imax
    loai=loai+1;
    [e,f,g,r] = feval(fun,xi,data);
    % disp('=====') disp([i
sqrt(dot(r,r)])
    if sqrt(dot(r,r)) < es, break, end
    dx = Tridiagonal(e,f,g,r);
    if dx<-2
        dx=.05;
    end
    xi = xi - dx;
end
end

```

A.3. Function Tridiagonal

```

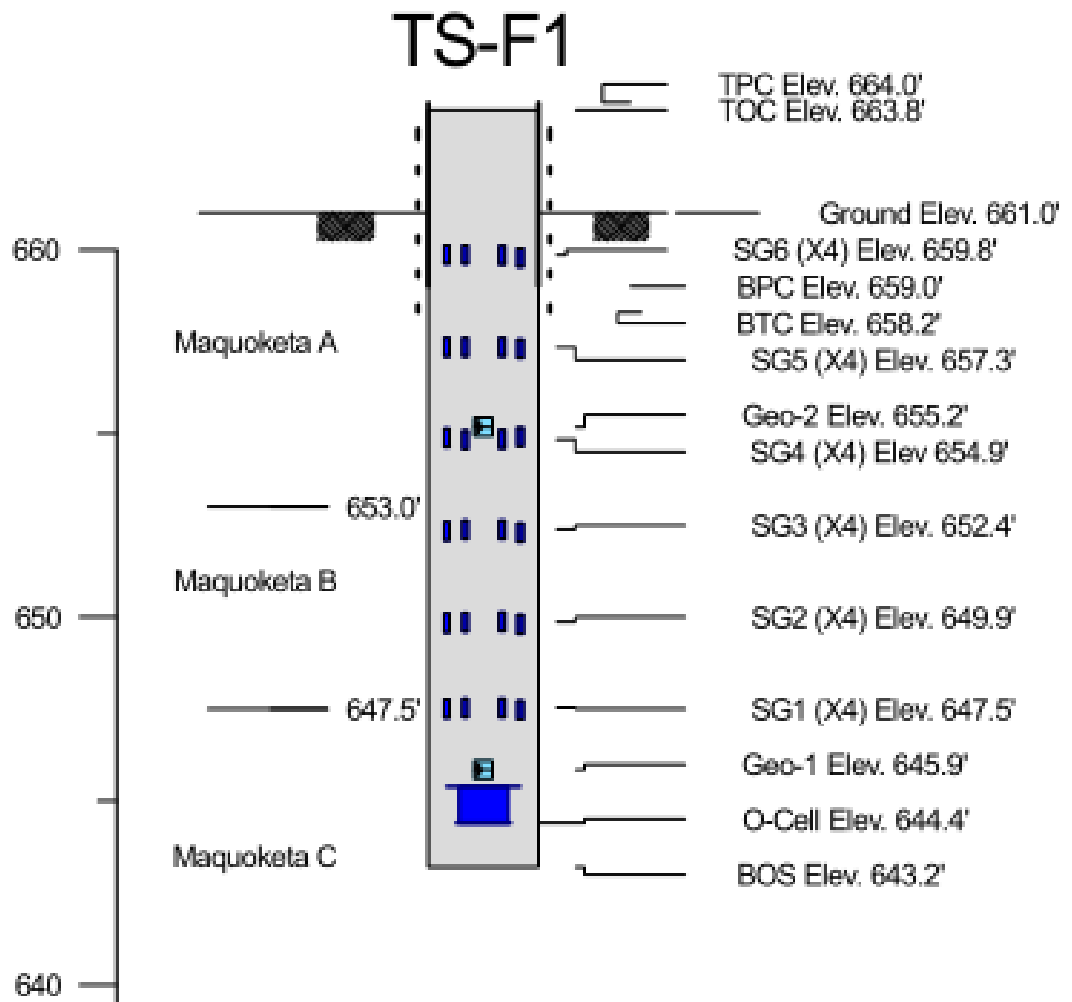
function x = Tridiagonal (e,f,g,r)
% this mfile solves a linear tridiagonal
% system of equations
n=length(f);
% decomposition
for k=2:n
    e(k)=e(k)/f(k-1);
    f(k)=f(k)-e(k)*g(k-1);
end

```

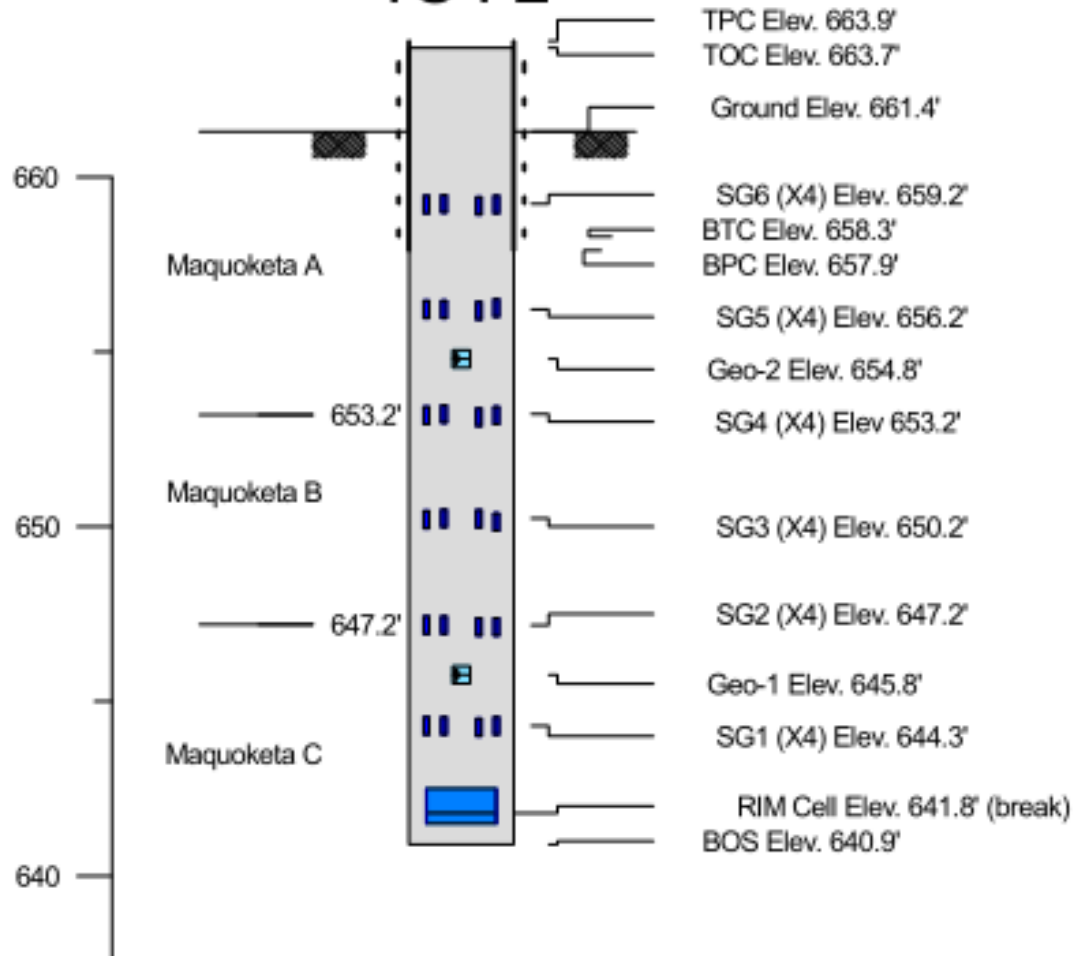
```
% forward substitution
for k=2:n
    r(k)=r(k)-e(k)*r(k-1);
end
% backward substitution
x(n)=r(n)/f(n);
for k=n-1:-1:1
    x(k)=(r(k)-g(k)*x(k+1))/f(k);
end
```

Appendix B. As-built Shaft Information

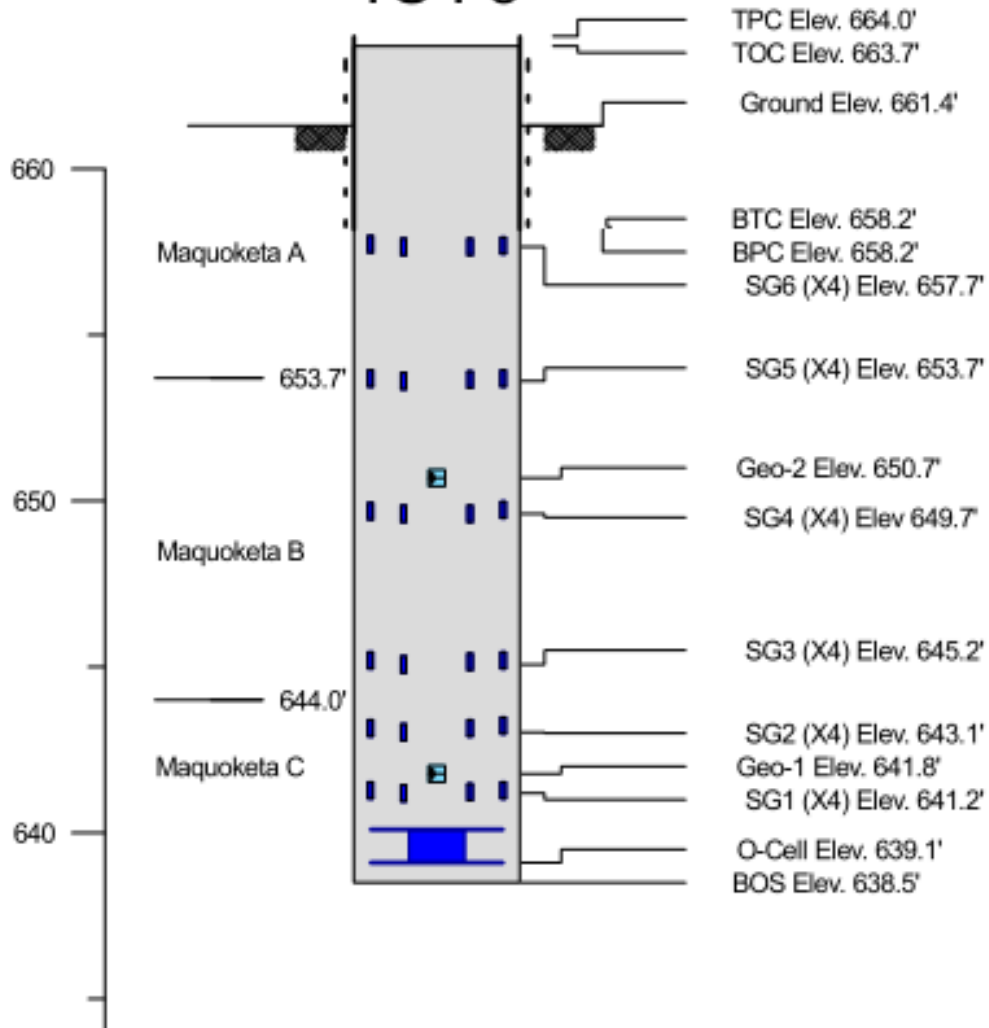
B.1. As-Built Shaft Dimensions:



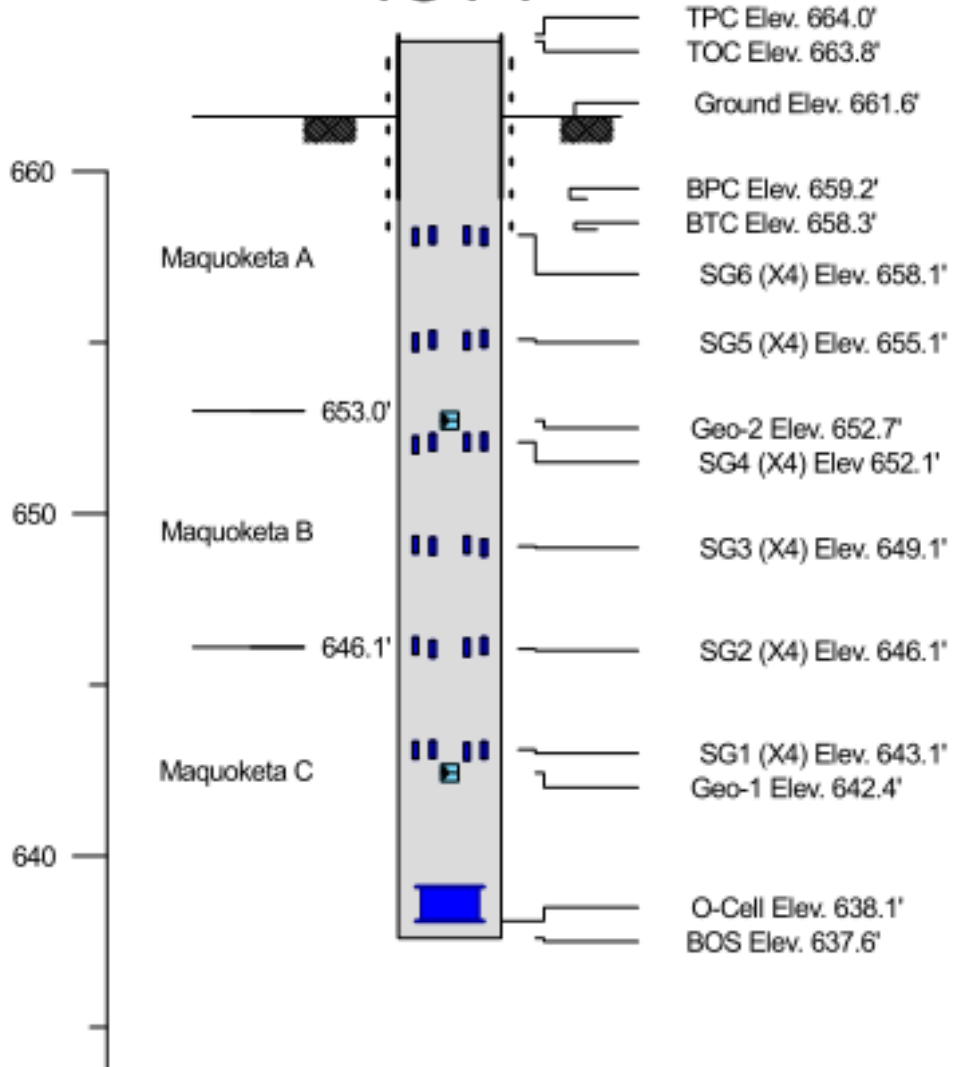
TS-F2



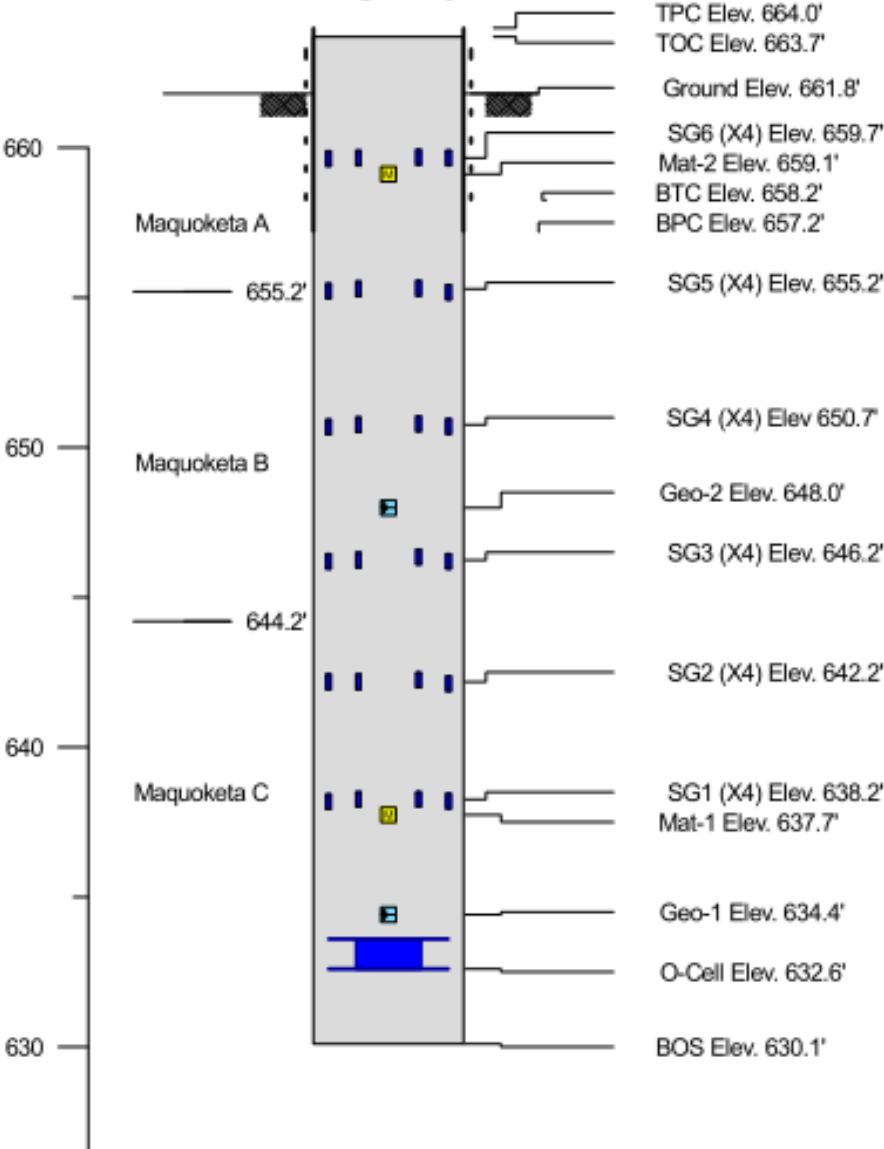
TS-F3

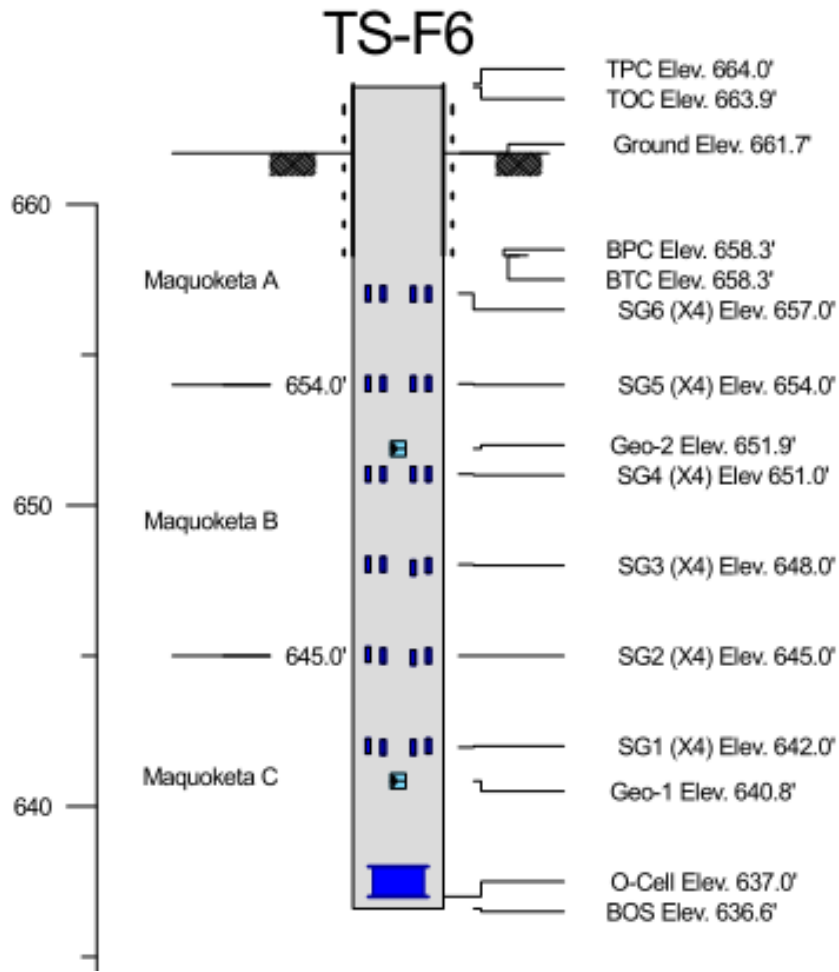


TS-F4

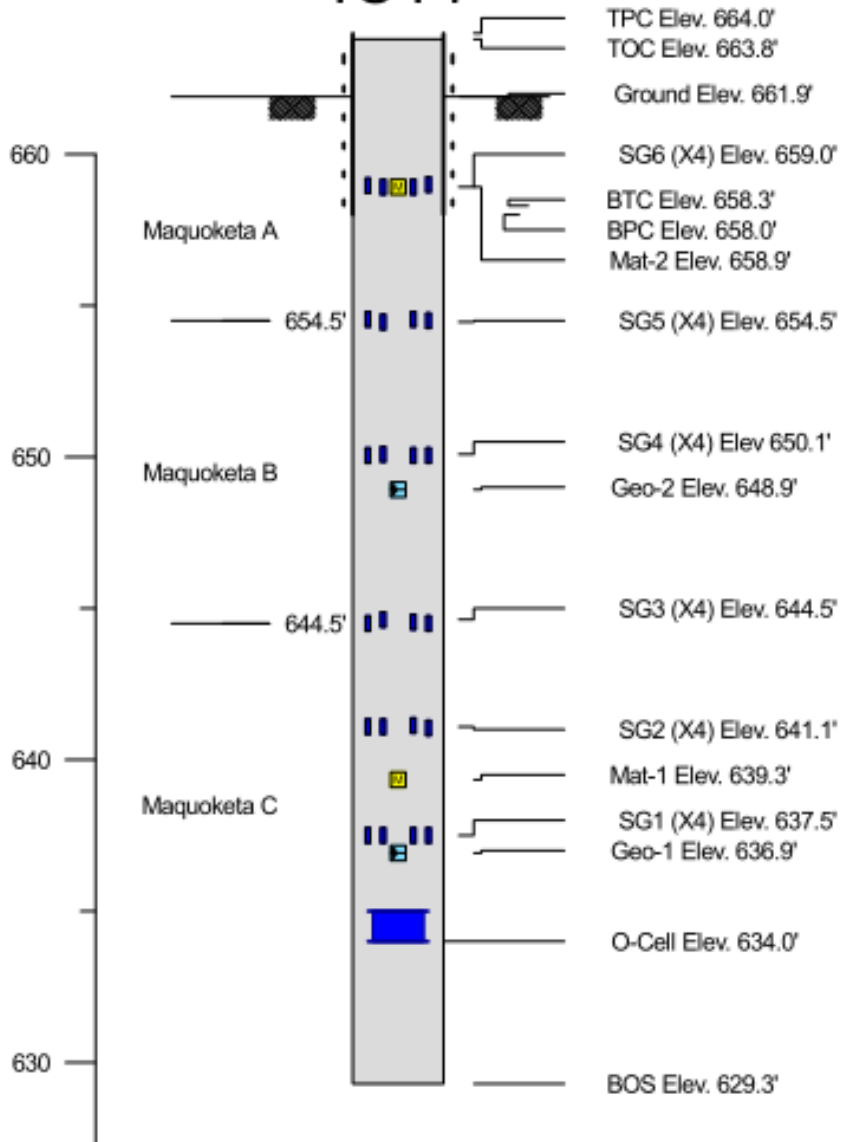


TS-F5

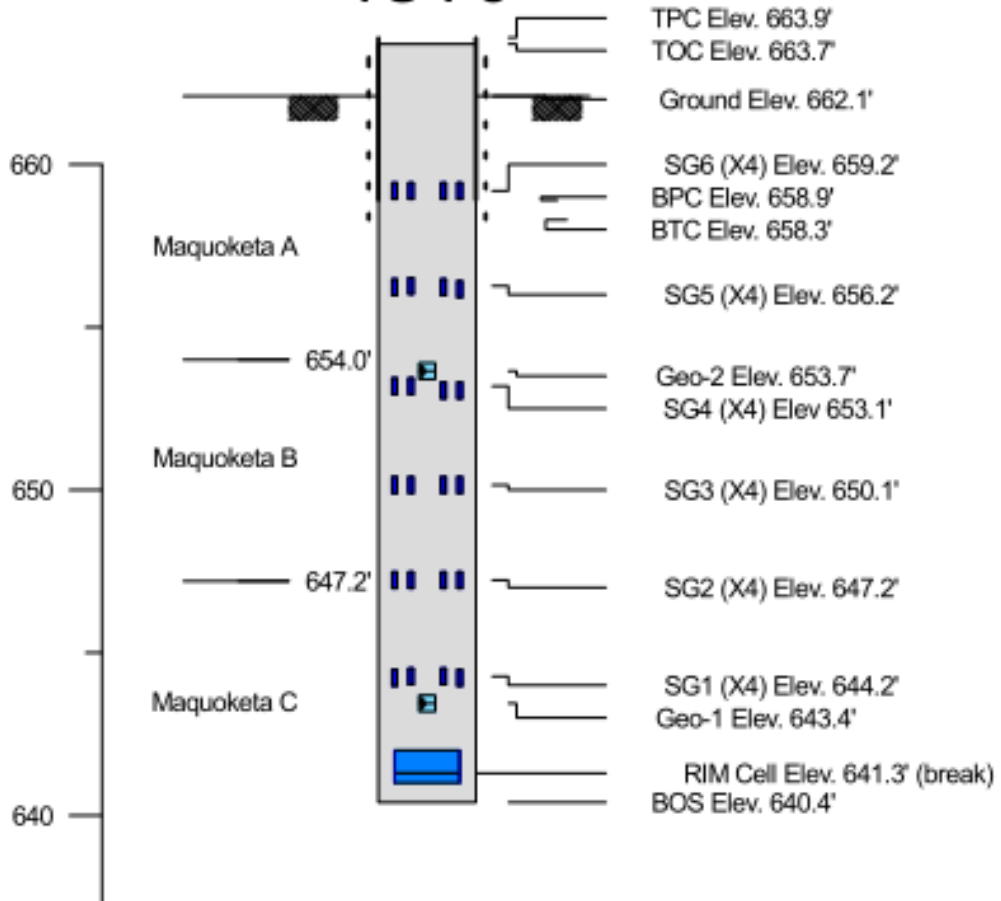




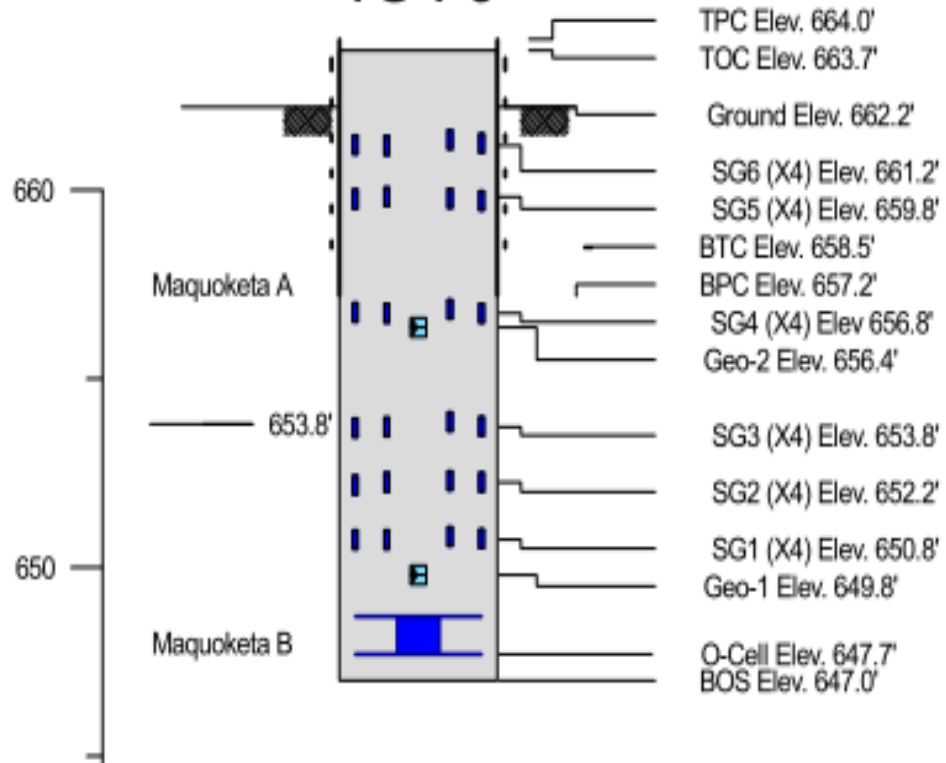
TS-F7



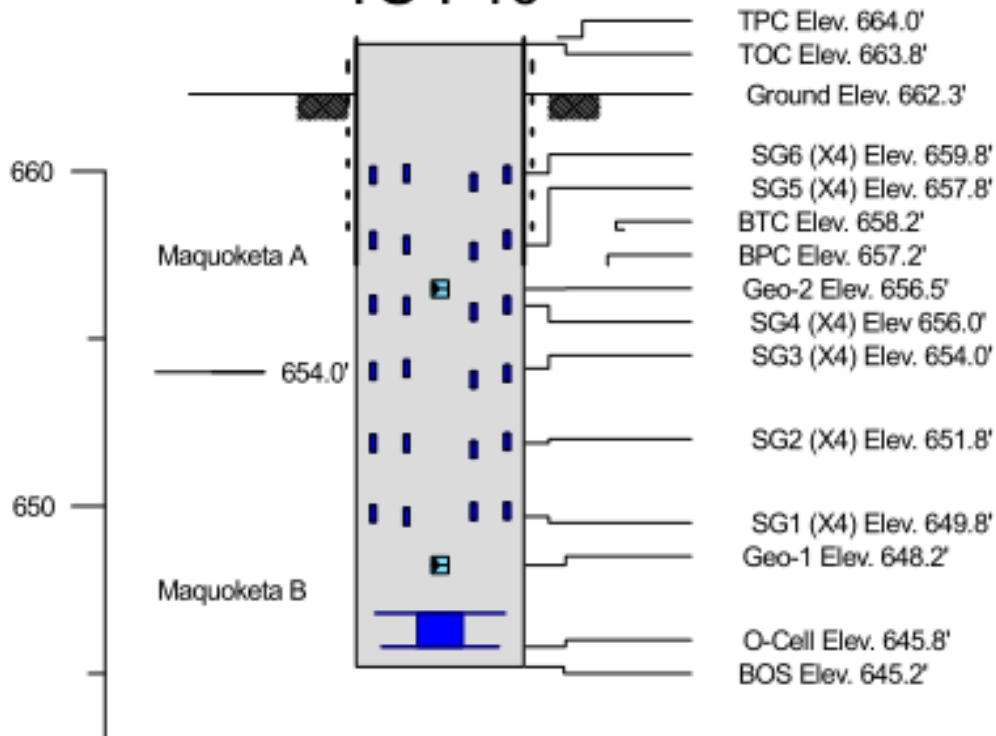
TS-F8

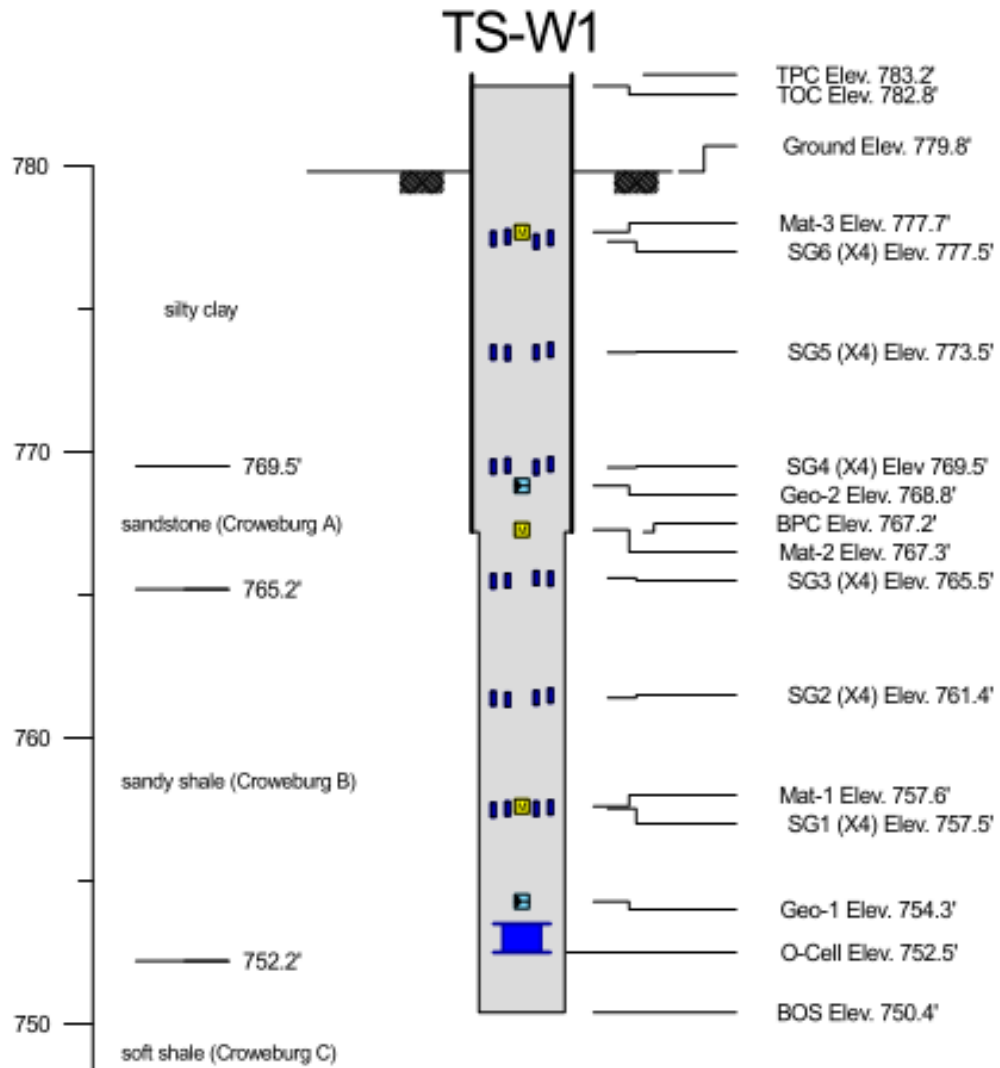


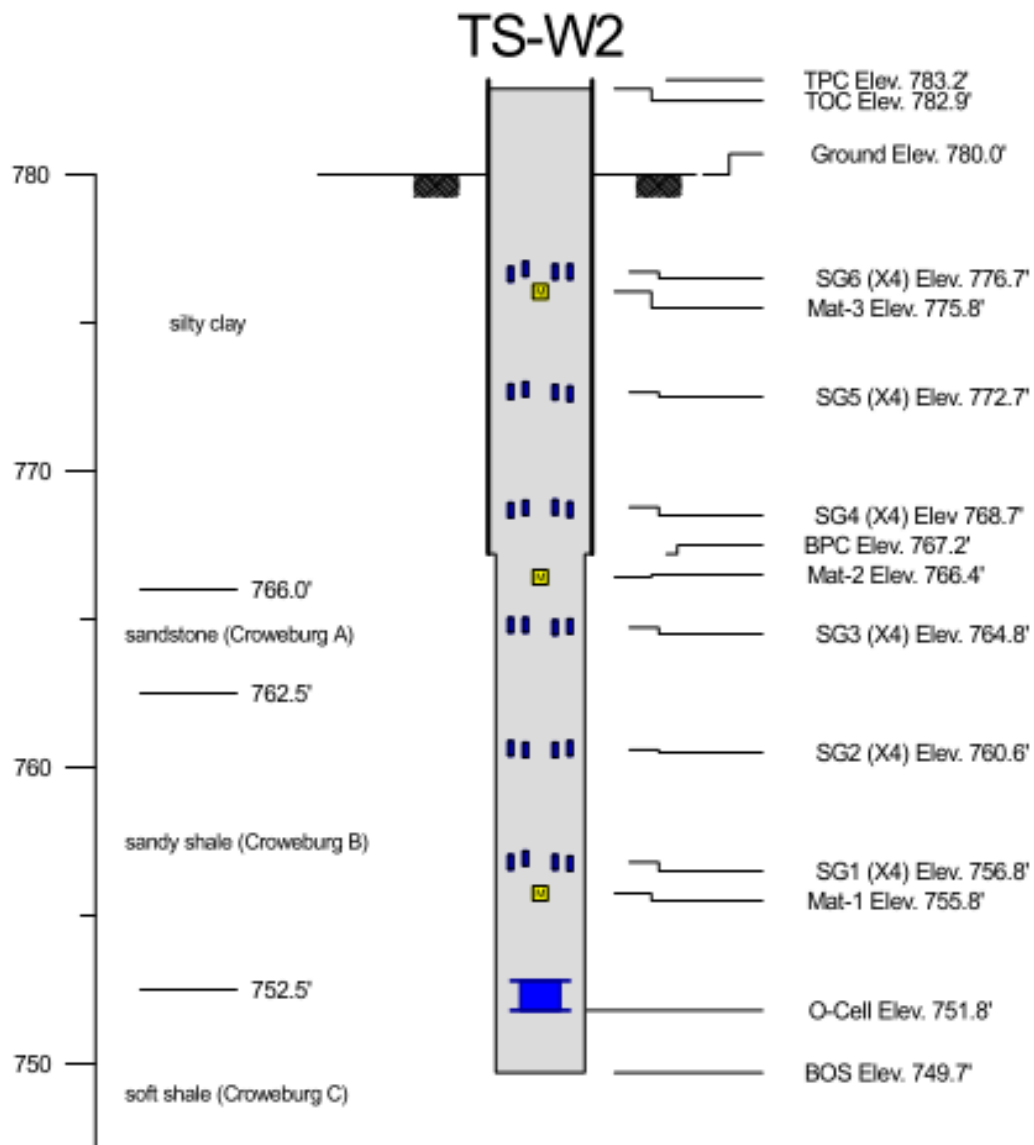
TS-F9

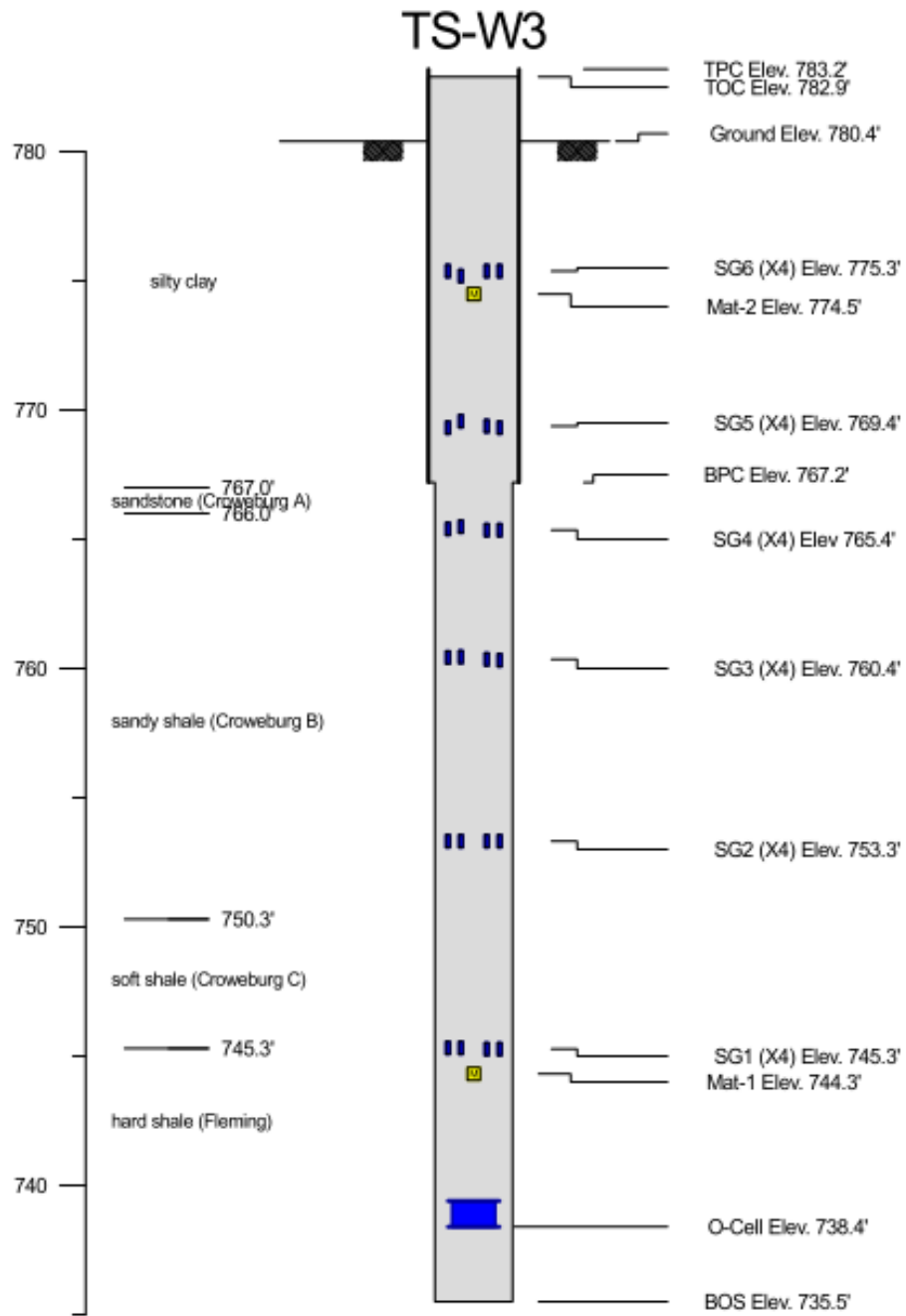


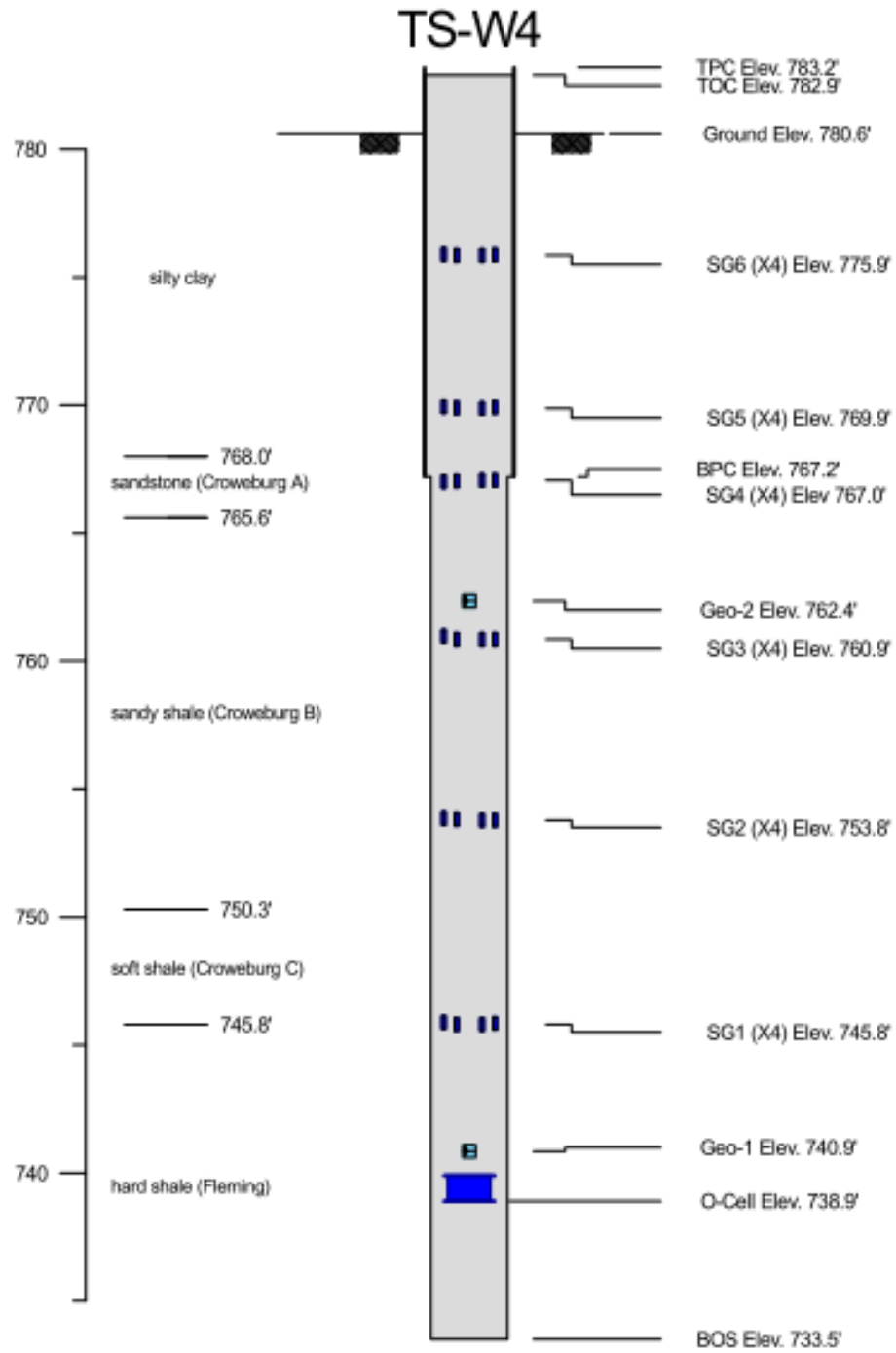
TS-F10



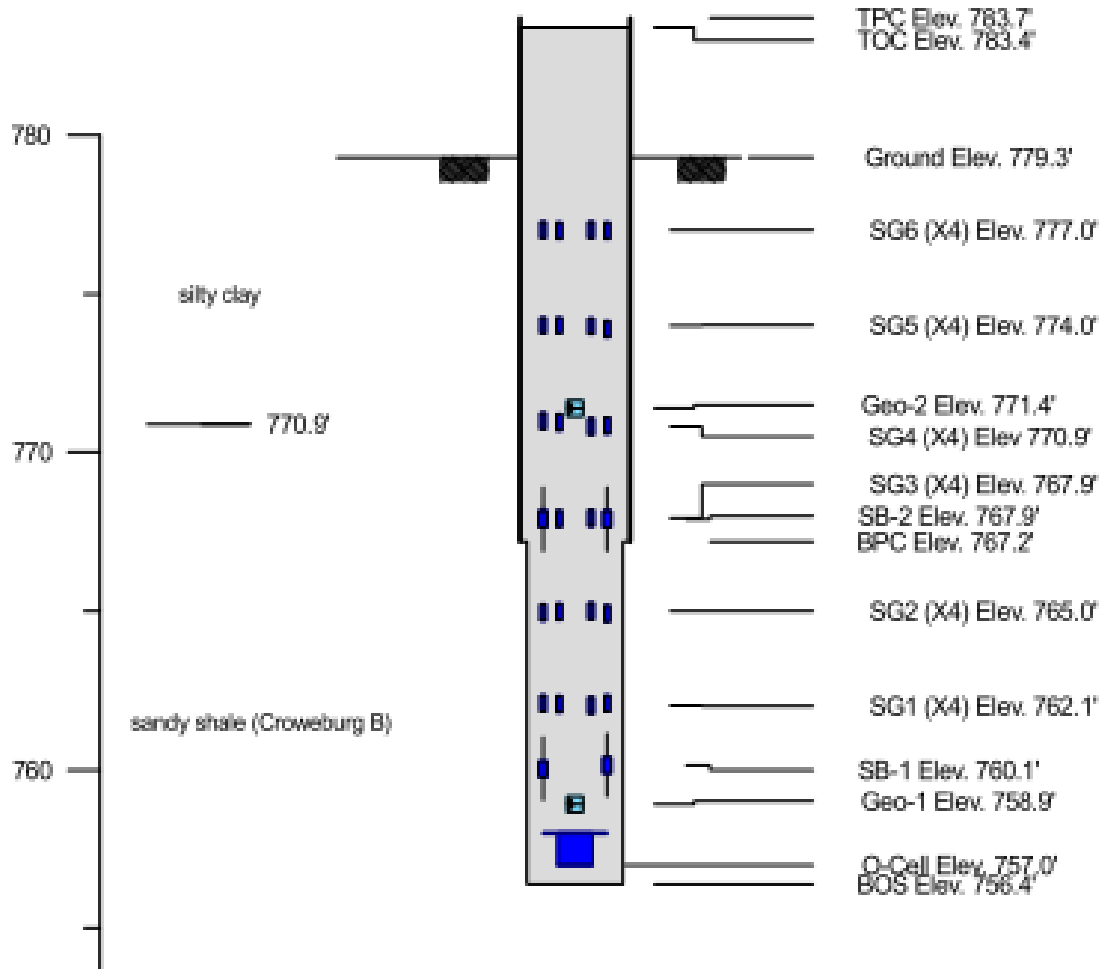


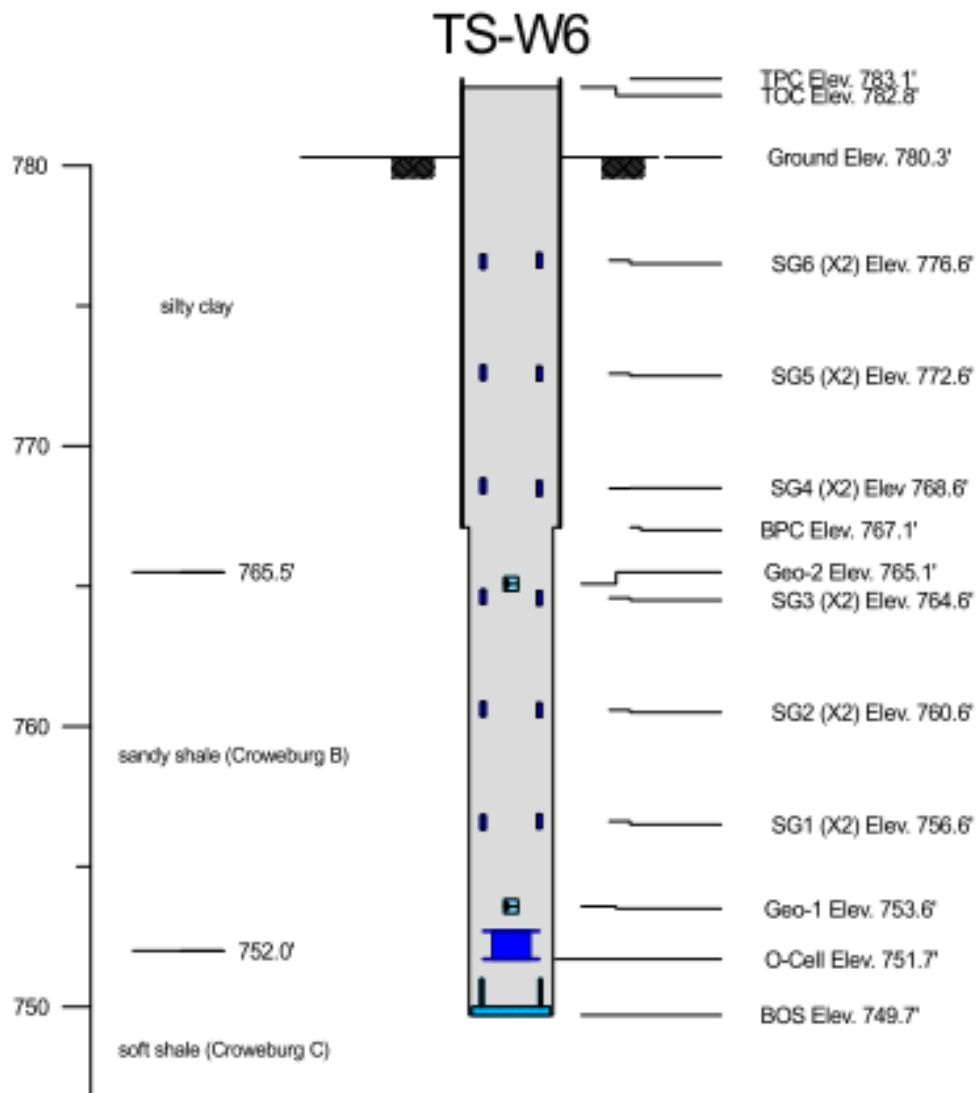


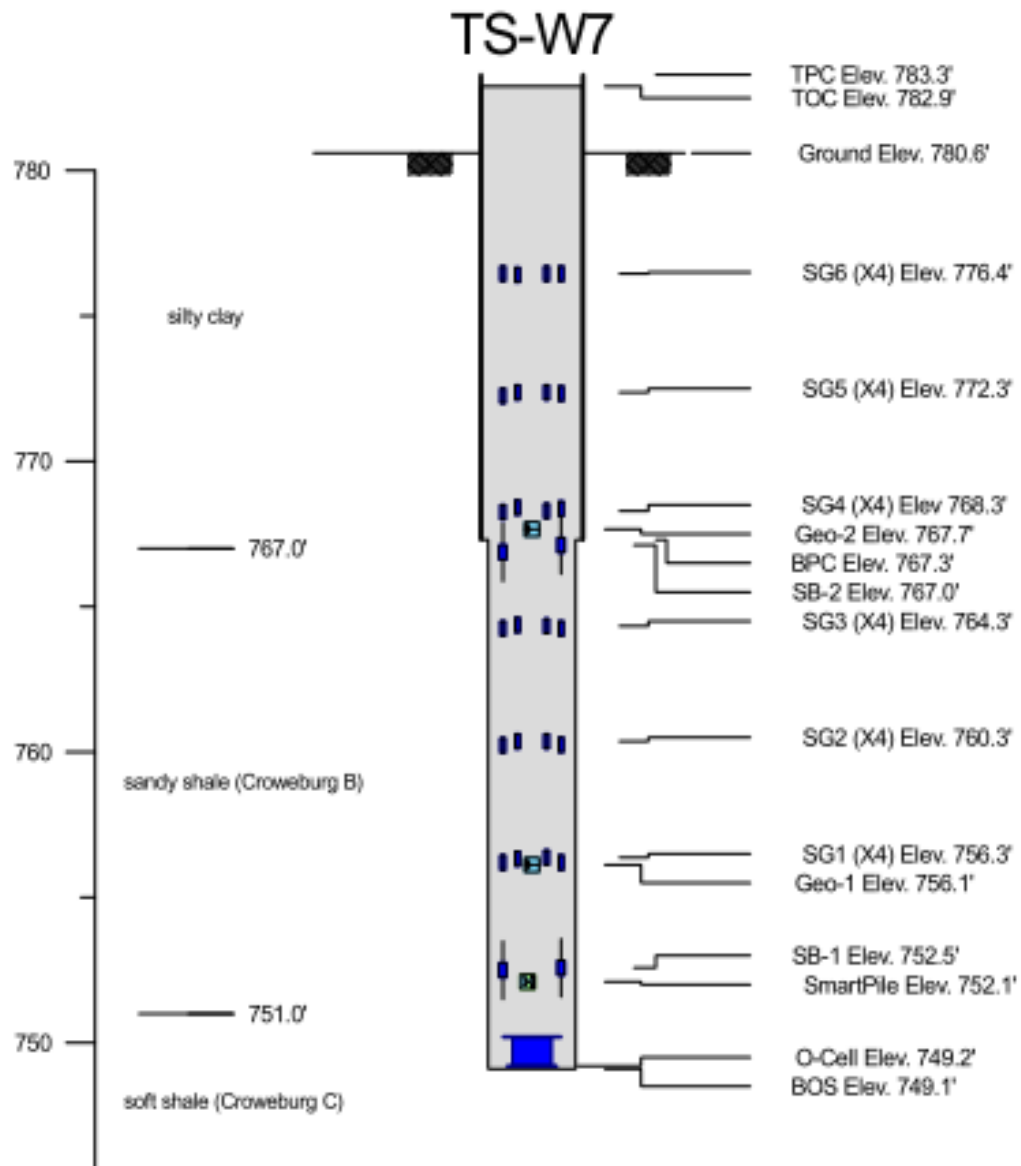


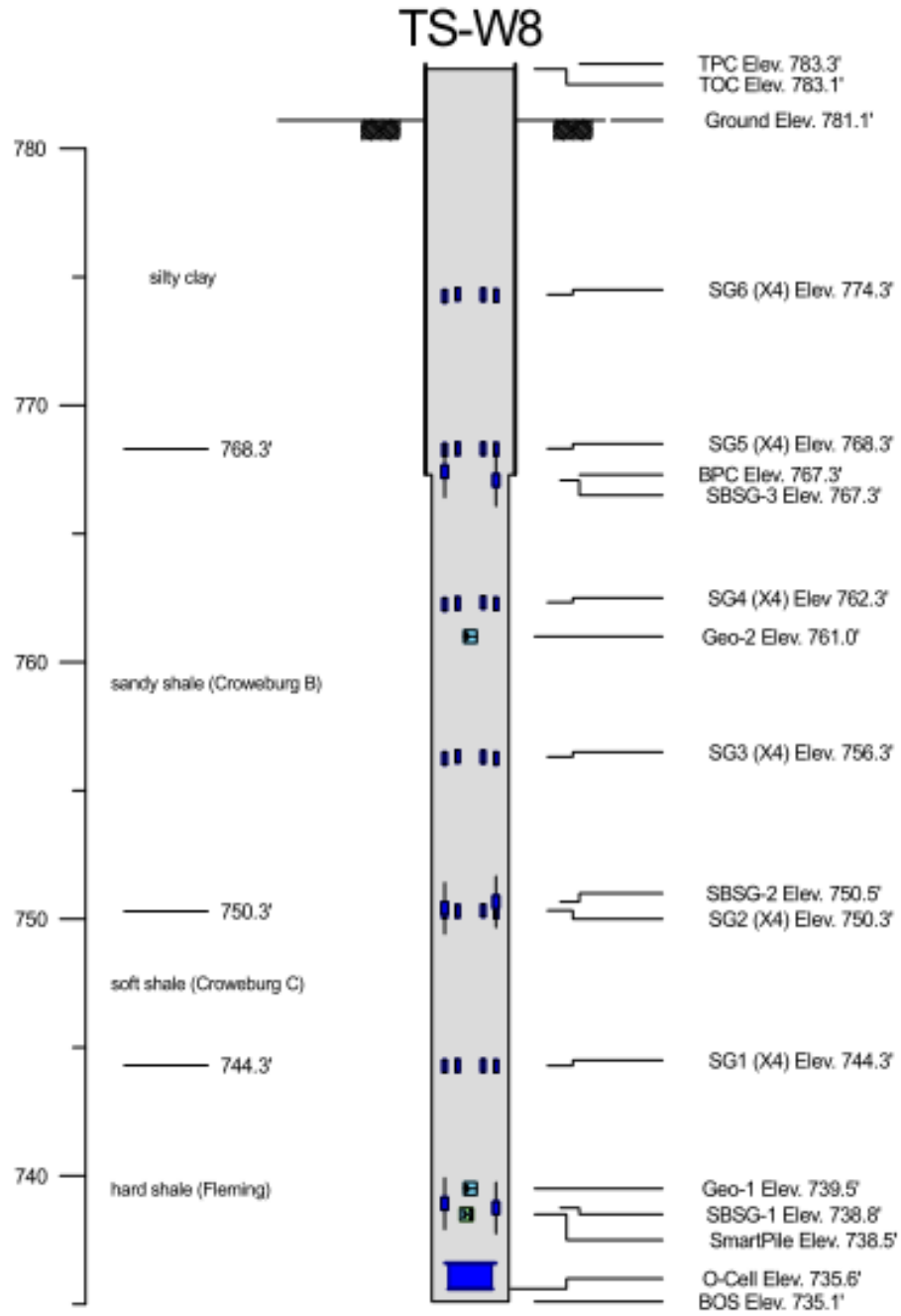


TS-W5

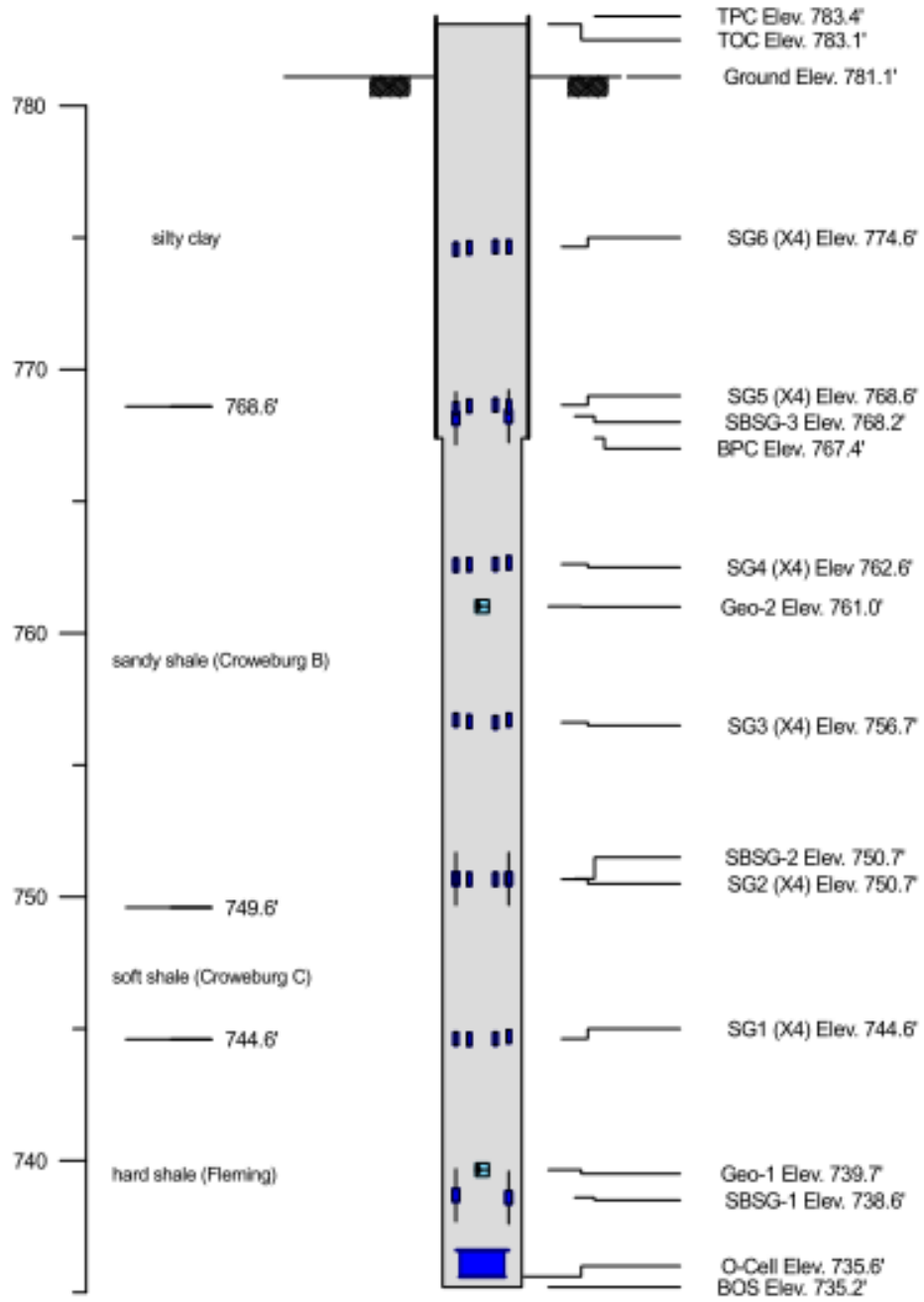


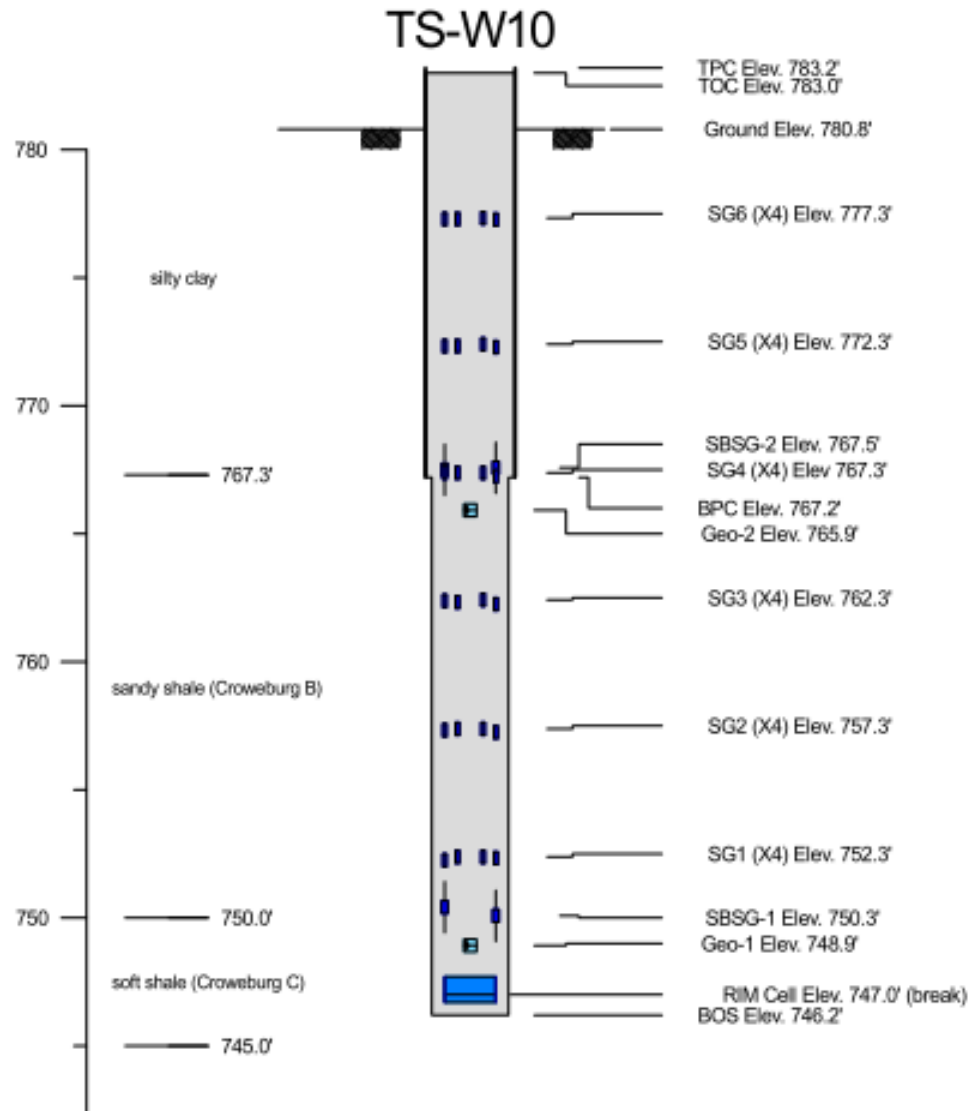


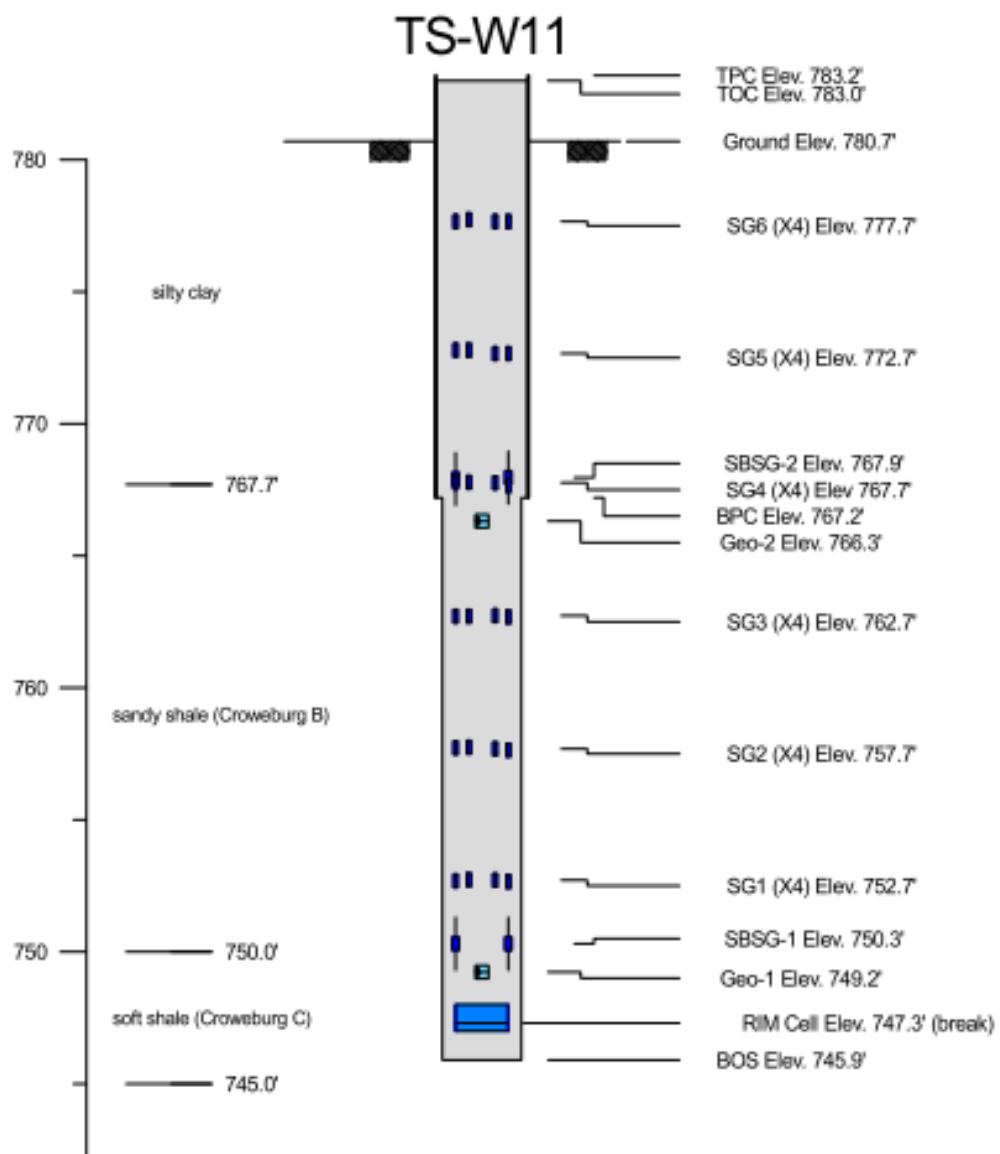




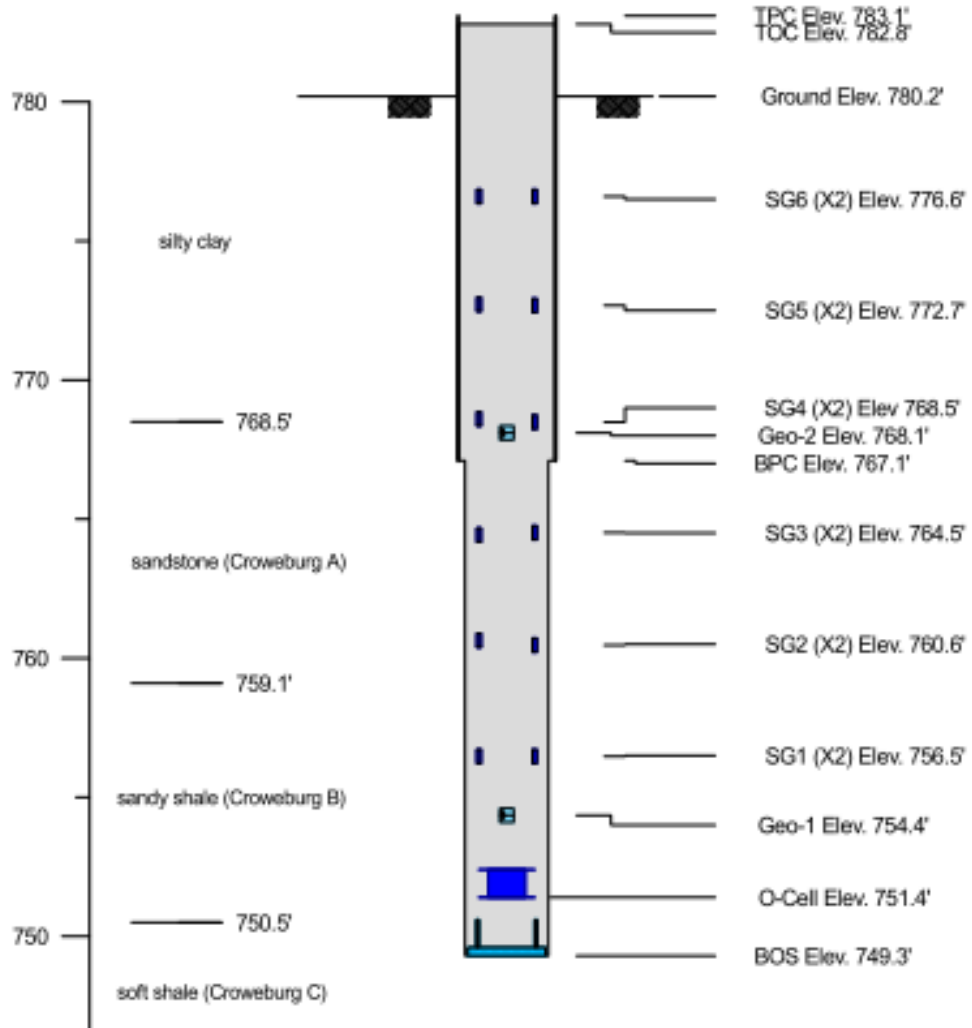
TS-W9



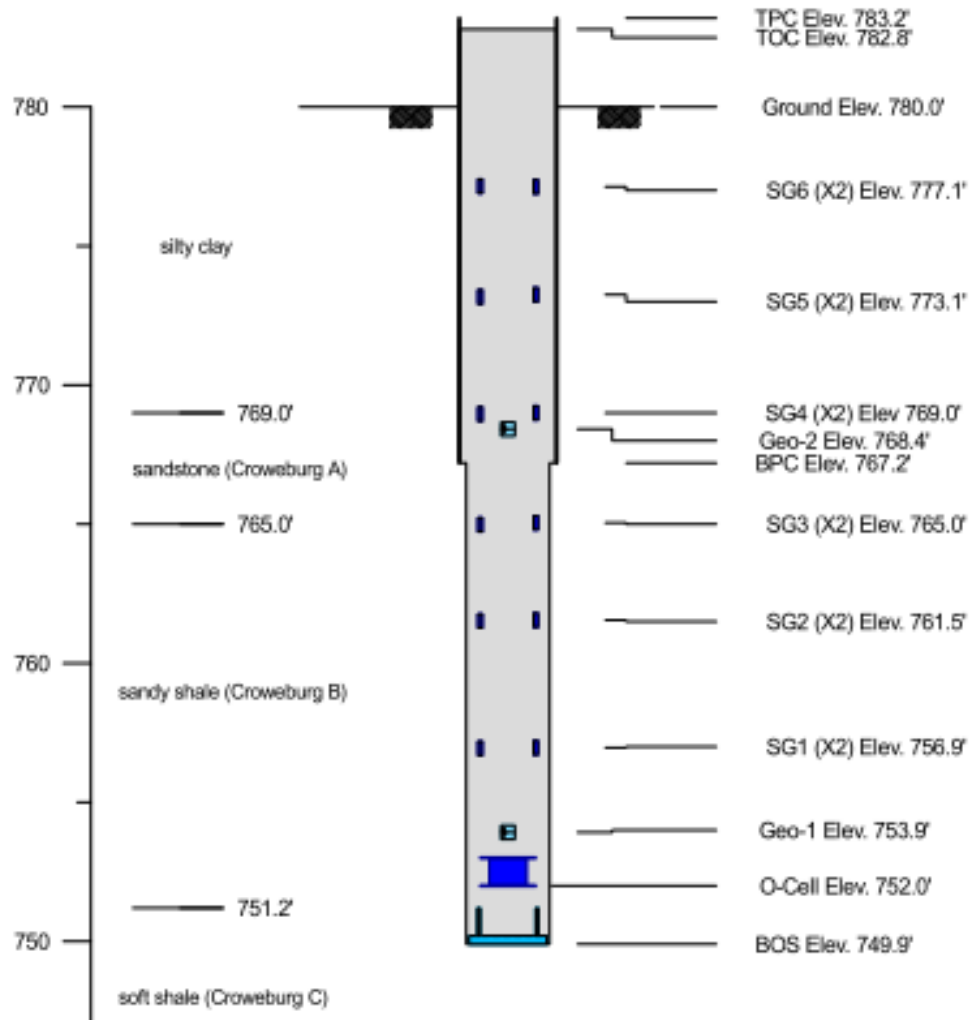


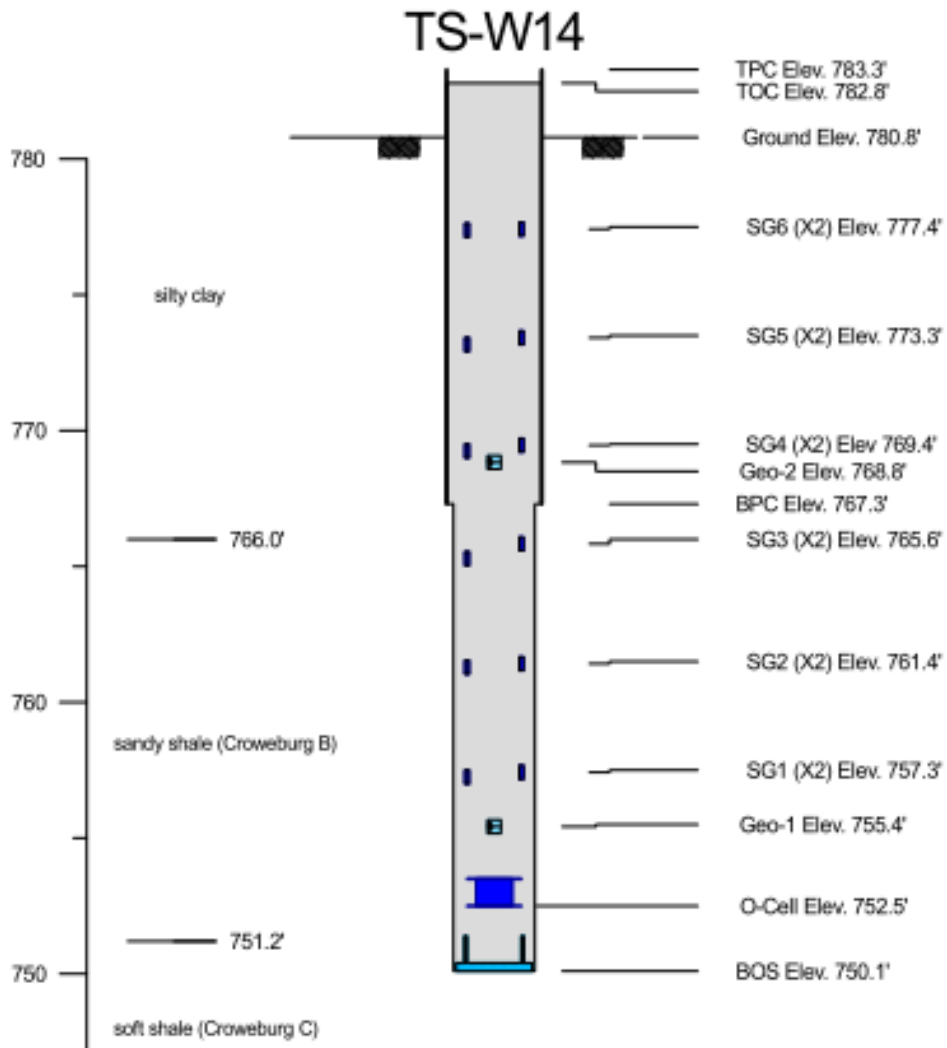


TS-W12

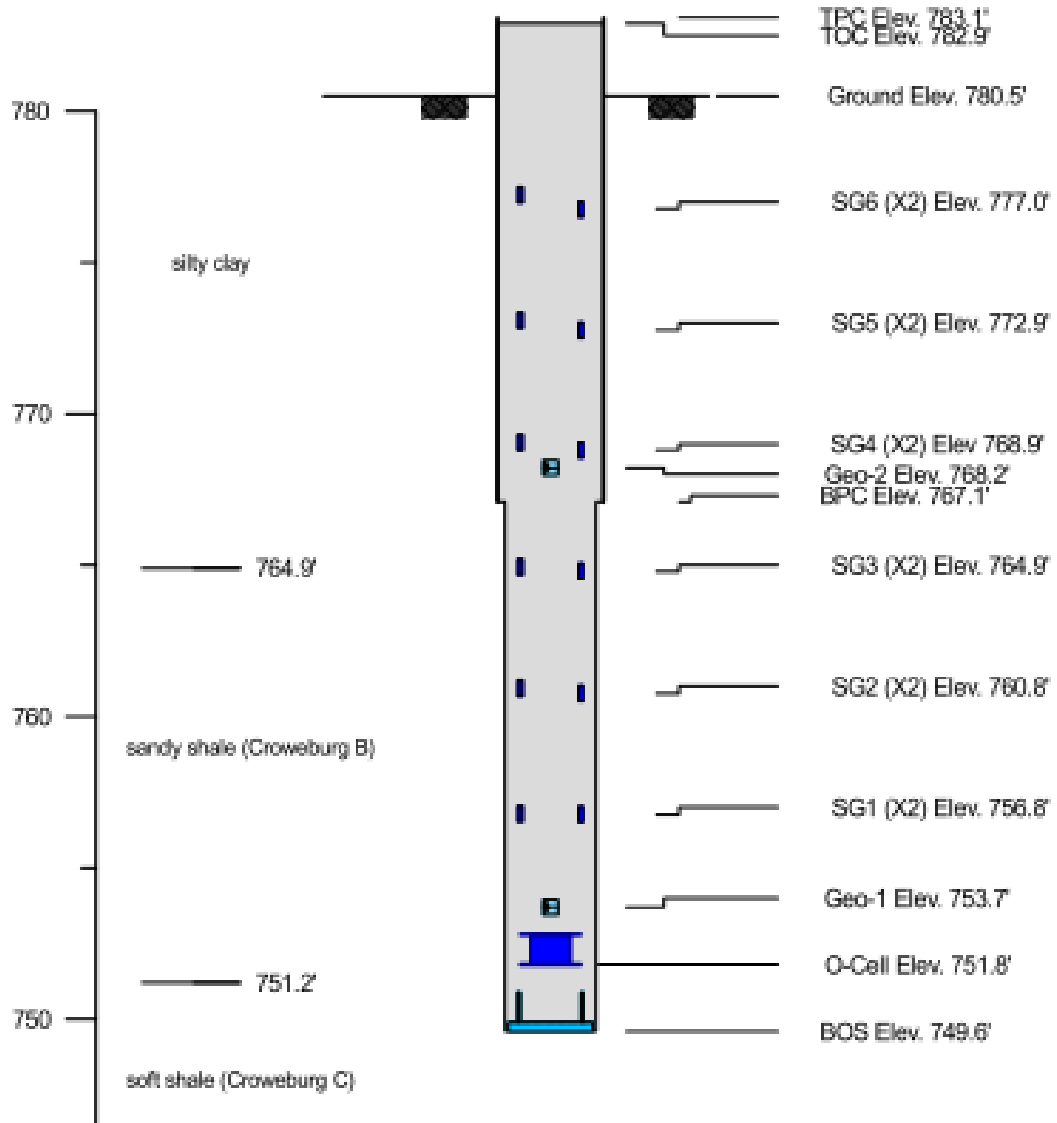


TS-W13





TS-W15



B.2. As-Built Shaft Elevation, Diameter and Area of steel.

Notation F1 is for Test shaft F1 from the Frankford site.

F1			
Parameters	Elevation (ft.)	Shaft Diameter (ft.)	Area of Steel (in ²)
Shaft Tip	643.2	3.2	0.0
O-Cell Bottom plate	644.4	3.2	20.3
O-Cell Top plate	645.5	3.2	20.3
SG1	647.5	3.3	20.3
SG2	649.9	3.3	20.3
SG3	652.4	3.5	20.3
SG4	654.9	3.2	20.3
SG5	657.3	3.3	20.3
SG6	659.8	3.0	62.7
Shaft Top	664	3.0	62.7

F2			
Parameters	Elevation (ft.)	Shaft Diameter (ft.)	Area of Steel (in ²)
Shaft Tip	640.9	3.2	0.0
O-Cell Bottom plate	641.8	3.2	20.3
O-Cell Top plate	641.81	3.2	20.3
SG2	647.2	3.3	20.3
SG3	650.2	3.3	20.3
SG4	653.2	3.4	20.3
SG5	656.2	3.3	20.3
SG6	659.2	3.0	48.5
Shaft Top	663.9	3.0	48.5

F3			
Parameters	Elevation (ft.)	Shaft Diameter (ft.)	Area of Steel (in ²)
Shaft Tip	638.5	5.2	0.0
O-Cell Bottom plate	639.1	5.2	20.3
O-Cell Top plate	640.2	5.2	20.3
SG2	643.1	5.2	20.3
SG3	645.2	5.3	20.3
SG4	649.7	5.4	20.3
SG5	653.7	5.4	20.3
SG6	657.7	5.3	20.3
Shaft Top	664	5.1	116.1

F4			
Parameters	Elevation (ft.)	Shaft Diameter (ft.)	Area of Steel (in ²)
Shaft Tip	637.6	3.3	0.0
O-Cell Bottom plate	638.1	3.3	20.3
O-Cell Top plate	639.2	3.3	20.3
SG1	643.1	3.3	20.3
SG2	646.1	3.3	20.3
SG3	649.1	3.3	20.3
SG4	652.1	3.3	20.3
SG5	655.1	3.3	20.3
SG6	658.1	3.5	20.3
Shaft Top	664	3.0	62.7

F5			
Parameters	Elevation (ft.)	Shaft Diameter (ft.)	Area of Steel (in ²)
Shaft Tip	630.1	5.1	0.0
O-Cell Bottom plate	632.6	5.1	20.3
O-Cell Top plate	633.7	5.1	20.3
SG1	638.2	5.1	20.3
SG2	642.2	5.1	20.3
SG3	646.2	5.1	20.3
SG4	650.7	5.2	20.3
SG5	655.2	5.2	20.3
SG6	659.7	5.1	165.2
Shaft Top	664	5.1	165.2

F6			
Parameters	Elevation (ft.)	Shaft Diameter (ft.)	Area of Steel (in ²)
Shaft Tip	636.6	3.2	0.0
O-Cell Bottom plate	637	3.2	20.3
O-Cell Top plate	638.1	3.2	20.3
SG1	642	3.2	20.3
SG2	645	3.2	20.3
SG3	648	3.2	20.3
SG4	651	3.2	20.3
SG5	654	3.2	20.3
SG6	657	3.2	20.3
Shaft Top	664	3.0	62.7

F7			
Parameters	Elevation (ft.)	Shaft Diameter (ft.)	Area of Steel (in ²)
Shaft Tip	629.3	3.2	0.0
O-Cell Bottom plate	634	3.2	20.3
O-Cell Top plate	635.1	3.2	20.3
SG1	637.5	3.2	20.3
SG2	641.1	3.1	20.3
SG3	644.5	3.2	20.3
SG4	650.1	3.2	20.3
SG5	654.5	3.2	20.3
SG6	659	3.0	76.8
Shaft Top	664	3.0	76.8

F8			
Parameters	Elevation (ft.)	Shaft Diameter (ft.)	Area of Steel (in ²)
Shaft Tip	640.41	3.4	0.0
O-Cell Bottom plate	641.27	3.4	20.3
O-Cell Top plate	641.27	3.4	20.3
SG1	644.2	3.4	20.3
SG2	647.2	3.4	20.3
SG3	650.1	3.4	20.3
SG4	653.1	3.3	20.3
SG5	656.2	3.3	20.3
SG6	659.2	3.0	62.7
Shaft Top	663.91	3.0	62.7

F9			
Parameters	Elevation (ft.)	Shaft Diameter (ft.)	Area of Steel (in ²)
Shaft Tip	647	5.3	0.0
O-Cell Bottom plate	647.7	5.3	20.3
O-Cell Top plate	648.8	5.3	20.3
SG1	650.8	5.3	20.3
SG2	0	0.0	0.0
SG3	653.8	5.3	20.3
SG4	656.8	5.3	20.3
SG5	659.8	5.0	161.7
SG6	661.2	5.0	161.7
Shaft Top	664	5.0	161.7

F10			
Parameters	Elevation (ft.)	Shaft Diameter (ft.)	Area of Steel (in ²)
Shaft Tip	645.2	4.9	0.0
O-Cell Bottom plate	645.8	5.0	20.3
O-Cell Top plate	647	5.1	20.3
SG1	649.8	5.1	20.3
SG2	651.8	5.0	20.3
SG3	654	5.1	20.3
SG4	656	5.0	20.3
SG5	657.8	5.0	161.6
SG6	659.8	5.0	161.6
Shaft Top	664	5.0	161.6

W1			
Parameters	Elevation (ft.)	Shaft Diameter (ft.)	Area of Steel (in ²)
Shaft Tip	750.4	3.1	0.0
O-Cell Bottom plate	752.5	3.0	20.3
O-Cell Top plate	753.6	3.0	20.3
SG1	0	0.0	0.0
SG2	761.4	3.1	20.3
SG3	765.5	3.2	20.3
SG4	769.5	3.5	53.3
SG5	773.5	3.5	53.3
SG6	777.5	3.5	53.3
Shaft Top	783.2	3.5	53.3

W2			
Parameters	Elevation (ft.)	Shaft Diameter (ft.)	Area of Steel (in ²)
Shaft Tip	749.7	3.1	0.0
O-Cell Bottom plate	751.8	3.1	20.3
O-Cell Top plate	752.9	3.1	20.3
SG2	760.6	3.2	20.3
SG3	764.8	3.1	20.3
SG4	768.7	3.5	53.3
SG5	772.7	3.5	53.3
SG6	776.7	3.5	53.3
Shaft Top	783.2	3.5	53.3

W3			
Parameters	Elevation (ft.)	Shaft Diameter (ft.)	Area of Steel (in ²)
Shaft Tip	735.5	3.0	0.0
O-Cell Bottom plate	738.4	3.0	20.3
O-Cell Top plate	739.5	3.1	20.3
SG1	745.3	3.1	20.3
SG2	753.3	3.1	20.3
SG3	760.4	3.2	20.3
SG4	765.4	3.2	20.3
SG5	769.4	3.5	53.3
SG6	775.3	3.5	53.3
Shaft Top	783.2	3.5	53.3

W4			
Parameters	Elevation (ft.)	Shaft Diameter (ft.)	Area of Steel (in ²)
Shaft Tip	733.5	3.1	0.0
O-Cell Bottom plate	738.9	3.1	20.3
O-Cell Top plate	740	3.1	20.3
SG1	745.8	3.1	20.3
SG2	753.8	3.1	20.3
SG3	760.9	3.1	20.3
SG4	767	3.1	20.3
SG5	769.9	3.5	53.3
SG6	775.9	3.5	53.3
Shaft Top	783.2	3.5	53.3

W5			
Parameters	Elevation (ft.)	Shaft Diameter (ft.)	Area of Steel (in ²)
Shaft Tip	756.4	3.0	0.0
O-Cell Bottom plate	757	3.1	20.3
O-Cell Top plate	758.1	3.1	20.3
SG1	762.1	3.2	20.3
SG2	765	3.1	20.3
SG3	767.9	3.5	53.3
SG4	770.9	3.5	53.3
SG5	774	3.5	53.3
SG6	777	3.5	53.3
Shaft Top	783.7	3.5	53.3

W6			
Parameters	Elevation (ft.)	Shaft Diameter (ft.)	Area of Steel (in ²)
Shaft Tip	749.7	3.2	0.0
O-Cell Bottom plate	751.7	3.0	11.4
O-Cell Top plate	752.8	3.0	11.4
SG1	756.6	3.2	11.4
SG2	760.6	3.2	11.4
SG3	764.6	3.2	11.4
SG4	768.6	3.5	44.4
SG5	772.6	3.5	44.4
SG6	776.6	3.5	44.4
Shaft Top	783.1	3.5	44.4

W7			
Parameters	Elevation (ft.)	Shaft Diameter (ft.)	Area of Steel (in ²)
Shaft Tip	749.1	3.0	0.0
O-Cell Bottom plate	749.2	3.0	20.3
O-Cell Top plate	750.3	3.1	20.3
SG1	756.3	3.2	20.3
SG3	764.3	3.1	20.3
SG4	768.3	3.5	53.3
SG5	772.3	3.5	53.3
SG6	776.4	3.5	53.3
Shaft Top	783.3	3.5	53.3

W8			
Parameters	Elevation (ft.)	Shaft Diameter (ft.)	Area of Steel (in ²)
Shaft Tip	735.1	3.3	0.0
O-Cell Bottom plate	735.6	3.3	20.3
O-Cell Top plate	736.7	3.2	20.3
SG1	744.3	3.2	20.3
SG2	750.3	3.2	20.3
SG3	756.3	3.2	20.3
SG4	762.3	3.2	20.3
SG5	768.3	3.5	53.3
SG6	774.3	3.5	53.3
Shaft Top	783.3	3.5	53.3

W9			
Parameters	Elevation (ft.)	Shaft Diameter (ft.)	Area of Steel (in ²)
Shaft Tip	735.2	3.1	0.0
O-Cell Bottom plate	735.6	3.1	20.3
O-Cell Top plate	736.7	3.2	20.3
SG1	744.6	3.2	20.3
SG3	756.7	3.1	20.3
SG4	762.6	3.1	20.3
SG5	768.6	3.5	53.3
SG6	774.6	3.5	53.3
Shaft Top	783.4	3.5	53.3

W10			
Parameters	Elevation (ft.)	Shaft Diameter (ft.)	Area of Steel (in ²)
Shaft Tip	746.2	3.3	0.0
O-Cell Bottom plate	747	3.3	20.3
O-Cell Top plate	747.8	3.3	20.3
SG1	752.3	3.2	20.3
SG3	762.3	3.1	20.3
SG4	767.3	3.5	53.3
SG5	772.3	3.5	53.3
SG6	777.3	3.5	53.3
Shaft Top	783.2	3.5	53.3

W11			
Parameters	Elevation (ft.)	Shaft Diameter (ft.)	Area of Steel (in ²)
Shaft Tip	745.9	3.2	0.0
O-Cell Bottom plate	747.3	3.2	20.3
O-Cell Top plate	748	3.2	20.3
SG1	752.7	3.2	20.3
SG2	757.7	3.3	20.3
SG3	762.7	3.1	20.3
SG4	767.7	3.5	20.3
SG5	772.7	3.5	53.3
SG6	777.7	3.5	53.3
Shaft Top	783.2	3.5	53.3

W12			
Parameters	Elevation (ft.)	Shaft Diameter (ft.)	Area of Steel (in ²)
Shaft Tip	749.3	3.1	0.0
O-Cell Bottom plate	751.4	3.1	11.4
O-Cell Top plate	752.4	3.1	11.4
SG1	756.5	3.2	11.4
SG2	760.6	3.2	11.4
SG3	764.5	3.2	11.4
SG4	768.5	3.5	44.4
SG5	772.7	3.5	44.4
SG6	776.6	3.5	44.4
Shaft Top	783.1	3.5	44.4

W13			
Parameters	Elevation (ft.)	Shaft Diameter (ft.)	Area of Steel (in ²)
Shaft Tip	749.9	3.1	0.0
O-Cell Bottom plate	752	3.0	11.4
O-Cell Top plate	753.1	3.1	11.4
SG1	756.9	3.1	11.4
SG2	761.5	3.2	11.4
SG3	765	3.1	11.4
SG4	769	3.5	44.4
SG5	773.1	3.5	44.4
SG6	777.1	3.5	44.4
Shaft Top	783.2	3.5	44.4

W14			
Parameters	Elevation (ft.)	Shaft Diameter (ft.)	Area of Steel (in ²)
Shaft Tip	750.1	3.0	0.0
O-Cell Bottom plate	752.5	3.1	11.4
O-Cell Top plate	753.5	3.1	11.4
SG1	757.3	3.3	11.4
SG2	761.4	3.1	11.4
SG3	765.6	3.2	11.4
SG4	769.4	3.5	44.4
SG5	773.3	3.5	44.4
SG6	777.4	3.5	44.4
Shaft Top	783.3	3.5	44.4

W15			
Parameters	Elevation (ft.)	Shaft Diameter (ft.)	Area of Steel (in ²)
Shaft Tip	749.6	2.9	0.0
O-Cell Bottom plate	751.8	3.1	11.4
O-Cell Top plate	752.8	3.1	11.4
SG1	756.8	3.2	11.4
SG2	760.8	3.2	11.4
SG3	764.9	3.2	11.4
SG4	768.9	3.5	44.4
SG5	772.9	3.5	44.4
SG6	777	3.5	44.4
Shaft Top	783.1	3.5	44.4

Appendix C. Measured Side and Tip Resistances

C.1. Side Resistance

C.1.1. Frankford Site

Test Shaft	Interval Elevations.		Measured Side resistance		Mean	Standard Deviation of UCS		
	Lower	Upper	(ksf)	% of Ultimate		Model	Data	Total
	(ft)	(ft)			(ksf)	(ksf)	(ksf)	(ksf)
F1	657.3	659.8		100	3.3	0.2	0.6	0.59
	654.9	657.3	0.7	100	3.3	0.2	0.6	0.59
	652.4	654.9	1.9	100	10.4	1.6	7.3	7.42
	649.9	652.4	8.4	100	10.4	1.6	7.3	7.42
	647.5	649.9	6.1	100	10.4	1.6	7.3	7.42
	644.4	647.5	21.4	100	66.2	2.2	14	14.21
F2	656.2	659.2		100	3.3	0.2	0.6	0.59
	653.2	656.2	0.9	100	7.5	1	4.6	4.68
	650.2	653.2	6.1	50	10.4	1.6	7.3	7.42
	647.2	650.2	3.7	70	10.4	1.6	7.3	7.42
	641.8	647.2	12.5	50	66.2	2.2	14	14.21
F3	653.7	657.7	0.6	100	3.3	0.2	0.6	0.59
	649.7	653.7	6.7	100	10.4	1.6	7.3	7.42
	645.2	649.7	6.2	100	10.4	1.6	7.3	7.42
	643.1	645.2	10.6	100	34.3	1.8	10.2	10.32
	639.1	643.1	42.9	100	66.2	2.2	14	14.21
F4	655.1	658.1	0.6	100	3.3	0.2	0.6	0.59
	652.1	655.1	2.4	100	5.4	0.6	2.6	2.63
	649.1	652.1	10.9	100	10.4	1.6	7.3	7.42
	646.1	649.1	8.4	100	10.4	1.6	7.3	7.42
	643.1	646.1	23.9	100	66.2	2.2	14	14.21
	638.1	643.1	27.5	100	66.2	2.2	14	14.21

Test Shaft	Interval Elevations.		Measured Side resistance		Mean (ksf)	Standard Deviation of UCS		
	Lower	Upper	(ksf)	% of Ultimate		Model	Data	Total
	(ft)	(ft)				(ksf)	(ksf)	(ksf)
F5	655.2	659.7		100	3.3	0.2	0.6	0.59
	650.7	655.2	4.2	100	10.4	1.6	7.3	7.42
	646.2	650.7	5.2	100	10.4	1.6	7.3	7.42
	642.2	646.2	12.2	100	38.3	1.9	10.6	10.81
	638.2	642.2	19.2	90	66.2	2.2	14	14.21
	632.6	638.2	37.3	95	66.2	2.2	14	14.21
F6	654	657	1.3	95	5.6	0.7	2.8	2.86
	651	654	9.2	80	10.4	1.6	7.3	7.42
	648	651	5	100	10.4	1.6	7.3	7.42
	645	648	6.7	80	10.4	1.6	7.3	7.42
	642	645	18.6	80	66.2	2.2	14	14.21
	637	642	34.3	80	66.2	2.2	14	14.21
F7	654.5	659		100	3.3	0.2	0.6	0.59
	650.1	654.5	8.9	100	10.4	1.6	7.3	7.42
	644.5	650.1	5.8	100	10.4	1.6	7.3	7.42
	641.1	644.5	20.7	100	66.2	2.2	14	14.21
	637.5	641.1	32.3	100	66.2	2.2	14	14.21
	634	637.5	36.8	100	66.2	2.2	14	14.21
F8	656.2	659.2		90	3.3	0.2	0.6	0.59
	653.1	656.2	1.7	90	5.3	0.6	2.5	2.57
	650.1	653.1	8.4	50	10.4	1.6	7.3	7.42
	647.2	650.1	1.6	90	10.4	1.6	7.3	7.42
	644.2	647.2	5.2	60	66.2	2.2	14	14.21
	641.3	644.2	9.3	60	66.2	2.2	14	14.21
F9	659.8	661.2		100	3.3	0.2	0.6	0.59
	656.8	659.8		100	3.3	0.2	0.6	0.59
	653.8	656.8	1	100	3.3	0.2	0.6	0.59
	650.8	653.8	8.5	100	10.4	1.6	7.3	7.42
	647.7	650.8	9.8	100	10.4	1.6	7.3	7.42
F10	657.8	659.8		100	3.3	0.2	0.6	0.59
	656	657.8	0.9	100	3.3	0.2	0.6	0.59
	654	656	1.1	100	3.3	0.2	0.6	0.59
	651.8	654	6.2	100	10.4	1.6	7.3	7.42
	649.8	651.8	9.1	100	10.4	1.6	7.3	7.42
	645.8	649.8	9	100	10.4	1.6	7.3	7.42

C.1.2. Warrensburg Site

Test Shaft	Interval Elevations.		Measured Side resistance		Mean	Standard Deviation of UCS		
	Lower	Upper				Model	Data	Total
	(ft)	(ft)	(ksf)	% of Ultimate	(ksf)	(ksf)	(ksf)	(ksf)
W1	773.5	777.5		100	4.5	1.2	5.1	5.19
	769.5	773.5		100	4.5	1.2	5.1	5.19
	765.5	769.5		100	15	2	13.2	13.38
	761.4	765.5	2.1	100	15	2	13.2	13.38
	752.5	761.4	3.3	100	15	2	13.2	13.38
W2	772.7	776.7		100	4.5	1.2	5.1	5.19
	768.7	772.7		100	4.5	1.2	5.1	5.19
	764.8	768.7		90	7.7	1.4	7.6	7.7
	760.6	764.8	6.3	100	15	2	13.2	13.38
	751.8	760.6	2.6	100	15	2	13.2	13.38
W3	769.4	775.3		100	4.5	1.2	5.1	5.19
	765.4	769.4		100	8.7	1.5	8.3	8.46
	760.4	765.4	6.5	100	15	2	13.2	13.38
	753.3	760.4	4.6	95	15	2	13.2	13.38
	745.3	753.3	5.8	100	9	1.3	6.4	6.49
W4	738.4	745.3	4.6	95	74.7	9.5	56.2	57.03
	769.9	775.9		100	4.5	1.2	5.1	5.19
	767	769.9		100	8.1	1.5	7.9	8.01
	760.9	767	5.6	95	15	2	13.2	13.38
	753.8	760.9	2.3	95	15	2	13.2	13.38
	745.8	753.8	5.3	95	9	1.3	6.4	6.49
	738.9	745.8	5.3	90	74.7	9.5	56.2	57.03

Test Shaft	Interval Elevations.		Measured Side resistance		Mean	Standard Deviation of UCS		
	Lower	Upper				Model	Data	Total
	(ft)	(ft)	(ksf)	% of Ultimate	(ksf)	(ksf)	(ksf)	(ksf)
W5	774	777		50	4.5	1.2	5.1	5.19
	770.9	774		50	4.5	1.2	5.1	5.19
	767.9	770.9		50	15	2	13.2	13.38
	765	767.9		50	15	2	13.2	13.38
	762.1	765	1.5	50	15	2	13.2	13.38
	757	762.1	1.8	50	15	2	13.2	13.38
W6	772.6	776.6		100	4.5	1.2	5.1	5.19
	768.6	772.6		100	4.5	1.2	5.1	5.19
	764.6	768.6		85	6.8	1.4	6.9	7.03
	760.6	764.6	4.7	80	15	2	13.2	13.38
	756.6	760.6	3.8	100	15	2	13.2	13.38
	751.7	756.6	5.2	100	15	2	13.2	13.38
W7	772.3	776.4		100	4.5	1.2	5.1	5.19
	768.3	772.3		100	4.5	1.2	5.1	5.19
	764.3	768.3		90	11.6	1.7	10.6	10.71
	756.3	764.3	2.4	80	15	2	13.2	13.38
			2.9					
	749.2	756.3	2.9	65	15	2	13.2	13.38
W8	768.3	774.3		100	4.5	1.2	5.1	5.19
	762.3	768.3		100	15	2	13.2	13.38
	756.3	762.3	3.2	95	15	2	13.2	13.38
	750.3	756.3	5.9	100	15	2	13.2	13.38
	744.3	750.3	5.3	90	5.4	0.8	2.3	2.39
	735.6	744.3	16.1	100	74.7	9.5	56.2	57.03
W9	768.6	774.6		90	4.5	1.2	5.1	5.19
	762.6	768.6		100	15	2	13.2	13.38
	756.7	762.6	3.7	100	15	2	13.2	13.38
	744.6	756.7	3.7	85	11.1	1.5	8.7	8.82
	735.6	744.6	4	60	74.7	9.5	56.2	57.03
W10	772.3	777.3		10	4.5	1.2	5.1	5.19
	767.3	772.3		10	15	2	13.2	13.38
	762.3	767.3	1.2	10	15	2	13.2	13.38
	752.3	762.3	2.1	10	15	2	13.2	13.38
	747	752.3	3.3	100	15	2	13.2	13.38

Test Shaft	Interval Elevations.		Measured Side resistance		Mean	Standard Deviation of UCS		
	Lower	Upper				Model	Data	Total
	(ft)	(ft)	(ksf)	% of Ultimate	(ksf)	(ksf)	(ksf)	(ksf)
W11	772.7	777.7		100	4.5	1.2	5.1	5.19
	767.7	772.7		100	4.5	1.2	5.1	5.19
	762.7	767.7	1.8	85	15	2	13.2	13.38
	757.7	762.7	2.8	75	15	2	13.2	13.38
	752.7	757.7	1.4	80	15	2	13.2	13.38
	747.3	752.7	3.7	60	15	2	13.2	13.38
W12	772.7	776.6		100	4.5	1.2	5.1	5.19
	768.5	772.7		100	4.5	1.2	5.1	5.19
	764.5	768.5		100	15	2	13.2	13.38
	760.6	764.5	1	100	15	2	13.2	13.38
	756.5	760.6	3.8	95	15	2	13.2	13.38
	751.4	756.5	8.8	95	15	2	13.2	13.38
W13	773.1	777.1		100	4.5	1.2	5.1	5.19
	769	773.1		100	4.5	1.2	5.1	5.19
	765	769		100	15	2	13.2	13.38
	761.5	765	2.3	100	15	2	13.2	13.38
	756.9	761.5	1.9	100	15	2	13.2	13.38
	752	756.9	7.4	100	15	2	13.2	13.38
W14	773.3	777.4		100	4.5	1.2	5.1	5.19
	769.4	773.3		100	4.5	1.2	5.1	5.19
	765.6	769.4		100	4.5	1.2	5.1	5.19
	761.4	765.6	2.5	100	15	2	13.2	13.38
	757.3	761.4	2.4	100	15	2	13.2	13.38
	752.5	757.3	5	100	15	2	13.2	13.38
W15	772.9	777		100	4.5	1.2	5.1	5.19
	768.9	772.9		100	4.5	1.2	5.1	5.19
	764.9	768.9		100	4.5	1.2	5.1	5.19
	760.8	764.9	3	100	15	2	13.2	13.38
	756.8	760.8	4.5	100	15	2	13.2	13.38
	751.8	756.8	6.2	100	15	2	13.2	13.38

C.2. Tip Resistance

C.2.1. Frankford Site

Test Shaft	Tip Elevation	Measured tip resistance		Mean	Std. Dev.		
	(ft)	(ksf)	% of Ultimate		Model	Data	Total
				(ksf)	(ksf)	(ksf)	(ksf)
F1	643.2	78.1	31	66.2	2.2	14	14.2
F2	640.9	121.1	48	66.2	2.2	14	14.2
F3	638.5	134.3	54	66.2	2.2	14	14.2
F4	637.6	271.4	100	66.2	2.2	14	14.2
F5	630.1	190.2	76	66.2	2.2	14	14.2
F6	636.6	297.5	100	66.2	2.2	14	14.2
F7	629.3	211.4	85	66.2	2.2	14	14.2
F8	640.4	84.7	34	66.2	2.2	14	14.2
F9	647	29.4	35	10.4	1.6	7.3	7.4
F10	645.2	44.5	52	10.4	1.6	7.3	7.4

C.2.2. Warrensburg Site.

Test Shaft	Tip Elev.	Q _{u-max}		Mean	Std. Dev.		
	(ft)	(ksf)	% ult		Model	Data	Total
				(ksf)	(ksf)	(ksf)	(ksf)
W1	750.4	41.8	42	5.4	0.8	2.3	2.4
W2	749.7	63.1	63	5.4	0.8	2.3	2.4
W3	735.5	175	50	74.7	9.5	56.2	57
W4	733.5	134	36	74.7	9.5	56.2	57
W5	756.4	100.3	100	15	2	13.2	13.4
W6	749.7	58.7	59	5.4	0.8	2.3	2.4
W7	749.1	188.6	100	5.4	0.8	2.3	2.4
W8	735.1	251.6	72	74.7	9.5	56.2	57
W9	735.2	158.9	45	74.7	9.5	56.2	57
W10	746.2	32.1	100	5.4	0.8	2.3	2.4
W11	745.9	57.9	40	5.4	0.8	2.3	2.4
W12	749.3	53.7	95	5.4	0.8	2.3	2.4
W13	749.9	44.1	85	5.4	0.8	2.3	2.4
W14	750.1	45.1	50	5.4	0.8	2.3	2.4
W15	749.6	66.9	60	5.4	0.8	2.3	2.4

Appendix D. Measured and Predicted Ultimate Resistance

D.1. Side Resistance

D.1.1. Frankford Site

F1	UCS (ksf)	Measured maximum resistance (ksf)	Predicted Ultimate resistance (ksf)	Displacement at maximum resistance (%D)
O-SG1	66.2	20.5	20.86	0.646
SG1-SG2	10.4	5.8	4.83	0.638
SG2-SG3	10.4	8.4	4.83	0.634
SG3-SG4	10.4	1.7	4.83	0.632
SG4-SG5	3.3	0.7	1.95	0.631
SG5-SG6	3.3	0.6	1.95	0.631

F2	UCS (ksf)	Measured maximum resistance(ksf)	Predicted Ultimate resistance (ksf)	Displacement at maximum resistance (%D)
O-SG2	66.2	13.1	20.86	0.394
SG2-SG3	10.4	3.8	4.83	0.383
SG3-SG4	10.4	5.6	4.83	0.379
SG4-SG5	7.5	0.7	3.73	0.377
SG5-SG6	3.3	0.4	1.95	0.377

F3	UCS (ksf)	Measured maximum resistance(ksf)	Predicted Ultimate resistance (ksf)	Displacement at maximum resistance (%D)
SG1-SG2	66.2	42.9	20.86	1.087
SG2-SG3	34.3	9.8	12.41	1.075
SG3-SG4	10.4	5.6	4.83	1.071
SG4-SG5	10.4	6.7	4.83	1.068
SG5-SG6	3.3	0.4	1.95	1.067

F4	UCS (ksf)	Measured maximum resistance(ksf)	Predicted Ultimate resistance (ksf)	Displacement at maximum resistance (%D)
O-SG1	66.2	25.3	20.86	0.942
SG1-SG2	66.2	23.6	20.86	0.911
SG2-SG3	10.4	7.5	4.83	0.898
SG3-SG4	10.4	8.6	4.83	0.891
SG4-SG5	5.4	2.3	2.88	0.888
SG5-SG6	3.3	0.6	1.95	0.888

F5	UCS (ksf)	Measured maximum resistance(ksf)	Predicted Ultimate resistance (ksf)	Displacement at maximum resistance (%D)
O-SG1	66.2	37.3	20.86	1.021
SG1-SG2	66.2	19.2	20.86	0.998
SG2-SG3	38.3	11.8	13.54	0.987
SG3-SG4	10.4	4.9	4.83	0.981
SG4-SG5	10.4	4.2	4.83	0.979
SG5-SG6	3.3	-0.2	1.95	0.978

F6	UCS (ksf)	Measured maximum resistance(ksf)	Predicted Ultimate resistance (ksf)	Displacement at maximum resistance (%D)
O-SG1	66.2	32.6	20.86	1.157
SG1-SG2	66.2	17.8	20.86	1.124
SG2-SG3	66.2	6.2	20.86	1.109
SG3-SG4	10.4	4.8	4.83	1.099
SG4-SG5	10.4	9.2	4.83	1.093
SG5-SG6	5.6	1.3	2.96	1.091

F7	UCS (ksf)	Measured maximum resistance(ksf)	Predicted Ultimate resistance (ksf)	Displacement at maximum resistance (%D)
O-SG1	66.2	36.0	20.86	1.881
SG1-SG2	66.2	32.3	20.86	1.831
SG2-SG3	66.2	18.0	20.86	1.793
SG3-SG4	10.4	5.8	4.83	1.768
SG4-SG5	10.4	8.9	4.83	1.752
SG5-SG6	3.3	1.2	1.95	1.748

F8	UCS (ksf)	Measured maximum resistance(ksf)	Predicted Ultimate resistance (ksf)	Displacement at maximum resistance (%D)
O-SG1	66.2	9.3	20.86	0.410
SG1-SG2	66.2	5.2	20.86	0.400
SG2-SG3	10.4	1.6	4.83	0.392
SG3-SG4	10.4	7.3	4.83	0.387
SG4-SG5	5.3	1.7	2.84	0.385
SG5-SG6	3.3	0.6	1.95	0.384

F9	UCS (ksf)	Measured maximum resistance(ksf)	Predicted Ultimate resistance (ksf)	Displacement at maximum resistance (%D)
O-SG1	10.4	9.8	4.83	2.294
SG1-SG3	10.4	6.9	4.83	2.292
SG3-SG4	3.3	0.8	1.95	2.291
SG4-SG5	3.3	0.0	1.95	2.291
SG5-SG6	3.3	0.3	1.95	2.291

F10	UCS (ksf)	Measured maximum resistance(ksf)	Predicted Ultimate resistance (ksf)	Displacement at maximum resistance (%D)
O-SG1	10.4	9.0	4.83	1.533
SG1-SG2	10.4	9.1	4.83	1.531
SG2-SG3	10.4	6.0	4.83	1.530
SG3-SG4	3.3	0.4	1.95	1.530
SG4-SG5	3.3	0.9	1.95	1.530
SG5-SG6	3.3	2.2	1.95	1.530

D.1.2. Warrensburg Site

W1	UCS (ksf)	Measured maximum resistance(ksf)	Predicted Ultimate resistance (ksf)	Displacement at maximum resistance (%D)
O-SG2	15	3.3	6.46	6.709
SG2-SG3	15	2.0	6.46	6.702
SG3-SG4	15	1.0	6.46	6.701
SG4-SG5	4.5	0.0	2.49	6.701
SG5-SG6	4.5	0.1	2.49	6.701

W2	UCS (ksf)	Measured maximum resistance(ksf)	Predicted Ultimate resistance (ksf)	Displacement at maximum resistance (%D)
O-SG2	15	2.4	6.46	3.147
SG2-SG3	15	5.9	6.46	3.138
SG3-SG4	7.7	1.3	3.81	3.135
SG4-SG5	4.5	0.2	2.49	3.135
SG5-SG6	4.5	0.4	2.49	3.134

W3	UCS (ksf)	Measured maximum resistance(ksf)	Predicted Ultimate resistance (ksf)	Displacement at maximum resistance (%D)
O-SG1	74.7	4.6	22.95	9.496
SG1-SG2	9	4.7	4.31	9.492
SG2-SG3	15	4.6	6.46	9.487
SG3-SG4	15	5.8	6.46	9.483
SG4-SG5	8.7	2.0	4.20	9.482
SG5-SG6	4.5	0.3	2.49	9.481

W4	UCS (ksf)	Measured maximum resistance(ksf)	Predicted Ultimate resistance (ksf)	Displacement at maximum resistance (%D)
O-SG1	74.7	4.0	22.95	9.433
SG1-SG2	9	6.6	4.31	9.400
SG2-SG3	15	1.8	6.46	9.376
SG3-SG4	15	5.2	6.46	9.365
SG4-SG5	8.1	0.7	3.97	9.362
SG5-SG6	4.5	0.2	2.49	9.362

W5	UCS (ksf)	Measured maximum resistance(ksf)	Predicted Ultimate resistance (ksf)	Displacement at maximum resistance (%D)
O-SG1	15	1.7	6.46	0.170
SG1-SG2	15	1.3	6.46	0.168
SG2-SG3	15	0.8	6.46	0.167
SG3-SG4	15	0.4	6.46	0.167
SG4-SG5	4.5	-0.1	2.49	0.167
SG5-SG6	4.5	0.3	2.49	0.167

W6	UCS (ksf)	Measured maximum resistance(ksf)	Predicted Ultimate resistance (ksf)	Displacement at maximum resistance (%D)
O-SG1	15	4.9	6.46	4.783
SG1-SG2	15	3.0	6.46	4.770
SG2-SG3	15	4.7	6.46	4.762
SG3-SG4	6.8	1.0	3.46	4.758
SG4-SG5	4.5	0.3	2.49	4.757
SG5-SG6	4.5	0.2	2.49	4.756

W7	UCS (ksf)	Measured maximum resistance(ksf)	Predicted Ultimate resistance (ksf)	Displacement at maximum resistance (%D)
O-SG1	15	2.2	6.46	0.990
SG1-SG3	15	2.4	6.46	0.982
SG3-SG4	11.6	1.3	5.27	0.978
SG4-SG5	4.5	0.1	2.49	0.977
SG5-SG6	4.5	0.2	2.49	0.977

W8	UCS (ksf)	Measured maximum resistance(ksf)	Predicted Ultimate resistance (ksf)	Displacement at maximum resistance (%D)
O-SG1	74.7	15.8	22.95	7.311
SG1-SG2	5.4	5.2	2.88	7.269
SG2-SG3	15	4.7	6.46	7.250
SG3-SG4	15	3.2	6.46	7.238
SG4-SG5	15	2.2	6.46	7.233
SG5-SG6	4.5	0.2	2.49	7.232

W9	UCS (ksf)	Measured maximum resistance(ksf)	Predicted Ultimate resistance (ksf)	Displacement at maximum resistance (%D)
O-SG1	74.7	3.9	22.95	11.136
SG1-SG3	11.1	3.7	5.09	11.099
SG3-SG4	15	3.6	6.46	11.077
SG4-SG5	15	3.0	6.46	11.071
SG5-SG6	4.5	0.2	2.49	11.069

W10	UCS (ksf)	Measured maximum resistance(ksf)	Predicted Ultimate resistance (ksf)	Displacement at maximum resistance (%D)
O-SG1	9.6	1.2	4.54	0.209
SG1-SG3	15	1.0	6.46	0.201
SG3-SG4	15	1.2	6.46	0.195
SG4-SG5	4.5	0.5	2.49	0.193
SG5-SG6	4.5	0.3	2.49	0.193

W11	UCS (ksf)	Measured maximum resistance(ksf)	Predicted Ultimate resistance (ksf)	Displacement at maximum resistance (%D)
O-SG1	10.2	3.5	4.76	1.011
SG1-SG2	15	1.4	6.46	1.001
SG2-SG3	15	2.8	6.46	0.994
SG3-SG4	15	1.8	6.46	0.991
SG4-SG5	4.5	0.2	2.49	0.989
SG5-SG6	4.5	0.2	2.49	0.989

W12	UCS (ksf)	Measured maximum resistance(ksf)	Predicted Ultimate resistance (ksf)	Displacement at maximum resistance (%D)
O-SG1	15	8.4	6.46	3.603
SG1-SG2	15	3.6	6.46	3.594
SG2-SG3	15	0.7	6.46	3.591
SG3-SG4	15	0.2	6.46	3.589
SG4-SG5	4.5	0.7	2.49	3.587
SG5-SG6	4.5	0.6	2.49	3.586

W13	UCS (ksf)	Measured maximum resistance(ksf)	Predicted Ultimate resistance (ksf)	Displacement at maximum resistance (%D)
O-SG1	15	6.4	6.46	2.116
SG1-SG2	15	1.9	6.46	2.115
SG2-SG3	15	1.2	6.46	2.114
SG3-SG4	15	1.2	6.46	2.114
SG4-SG5	4.5	0.1	2.49	2.114
SG5-SG6	4.5	0.2	2.49	2.114

W14	UCS (ksf)	Measured maximum resistance(ksf)	Predicted Ultimate resistance (ksf)	Displacement at maximum resistance (%D)
O-SG1	15	5.0	6.46	6.091
SG1-SG2	15	2.4	6.46	6.084
SG2-SG3	15	2.5	6.46	6.080
SG3-SG4	4.5	0.3	2.49	6.078
SG4-SG5	4.5	0.1	2.49	6.078
SG5-SG6	4.5	0.1	2.49	6.078

W15	UCS (ksf)	Measured maximum resistance(ksf)	Predicted Ultimate resistance (ksf)	Displacement at maximum resistance (%D)
O-SG1	15	6.2	6.46	7.893
SG1-SG2	15	4.5	6.46	7.882
SG2-SG3	15	2.9	6.46	7.878
SG3-SG4	4.5	-0.1	2.49	7.876
SG4-SG5	4.5	0.0	2.49	7.875
SG5-SG6	4.5	0.3	2.49	7.875

D.2. Tip Resistance

D.2.1. Frankfort Site

Test Shaft	UCS (ksf)	Measured Maximum Resistance (ksf)	Estimated % of Measured Ultimate (ksf)	Estimated Ultimate Measured Resistance (ksf)	Predicted Ultimate Resistance (ksf)	Displacement at Maximum Resistance (%D)
F1	66.2	78.1	31	252	275	0.65
F2	66.2	114.6	48	239	275	0.3
F3	66.2	134.2	54	249	275	0.54
F4	66.2	259.9	100	260	275	9.02
F5	66.2	190	76	250	275	1.34
F6	66.2	286.4	31	924	275	13
F7	66.2	210.1	85	247	275	2.63
F8	66.2	80.4	34	237	275	0.26
F9	10.4	27.2	35	78	74	0.37
F10	10.4	44.5	52	86	74	0.73

D.2.2. Warrensburg Site

Test Shaft	UCS (ksf)	Measured Maximum Resistance (ksf)	Estimated % of Measured Ultimate (ksf)	Estimated Ultimate Measured Resistance (ksf)	Predicted Ultimate Resistance (ksf)	Displacement at Maximum Resistance (%D)
W1	5.4	41.5	42	99	46	0.81
W2	5.4	60.4	63	96	46	1.44
W3	74.7	171.4	50	343	299	1.07
W4	74.7	131.3	36	365	299	0.89
W5	15	100.3	100	100	96	6.65
W6	5.4	58.7	59	99	46	1.85
W7	5.4	175.3	100	175	46	22.98
W8	74.7	251.6	72	349	299	1.88
W9	74.7	158.9	45	353	299	1.95
W10	5.4	32.1	31	103	46	5.99
W11	5.4	57.9	40	145	46	2.92
W12	5.4	53.7	95	57	46	3.29
W13	5.4	39.9	85	47	46	0.61
W14	5.4	45.1	50	90	46	0.55
W15	5.4	66.4	60	111	46	0.54

Appendix E. Weighted Least Square Regression Code

This computer code is for performing data analyses using weighted squares regression. Outputs are fitting parameters and root mean square error RMSE.

E.1. Inputs and Type Function for Modeling

```
load END_Measuredd_PERCENTD

Displace=END_MEASURED(:,1);
NorUnitSide=END_MEASURED(:,2);
x=Displace;
y=NorUnitSide;

f=zeros(1,length(x));

deltaf = y-(0.9341*x) ./ (x + 0.1215)

bin = -.6:0.05:1;
hist(deltaf)
hist(deltaf,bin)

Normalized_Displacement=x;
Normalized_SideShear=y;

start=[1,1,1];
xvalues=[0:0.1:10]';
%func= @(b,x) b(1).*(x.^b(2))
% func= @(b,x) b(1).*log(x)+b(2);

%func= @(b,x) (1-exp(x*b)); % -9.6727

%func= @(b,x) x./((b(1).*x)+b(2));
func= @(b,x) (b(1).*x+b(2))./(x+b(3));

[coeffs,modelvalues,modelstd,randomstd,totalsd,covariance,RMSE] =
nlfit_constcov(x,y,func,start,xvalues)

Normalized_Displacement_Percent_of_D=x;
Normalized_SideShear_to_Max_Measured=y;
% Create xlabel
xlabel('Normalized Displacement of Shaft Tip (%D)');

% Create ylabel
ylabel('Normalized Unit Tip Resistance, q/qu-meas');
```

E.2. Weighted Least Squares Regression

```
function [coeffs,modelvalues,modelstd,randomsd,totalsd,covariance,RMSE]
= nlfitt_constcov(x,y,func,start,xvalues)
% nlfitt_constcov determines the least square best fit coefficients for
func
% under the assumption of a constant coefficient of variation
% INPUT
%   x - array of measured x-values to be fit
%   y - array of measured y-values to be fit
%   func - function handle for functional form of fit
%   start - array of initial estimates for non-linear fit
%   xvalues - values of x to compute model, random, and total stdev

% initialize variables
tolerance=1.e-5;
maxiterations=500;
iteration=0;

% establish initial fit from OLS and initialize loop variables
[coeffs,r,J,covb,mse]=nlinfit(x,y,func,start);
w=1./func(coeffs,x).^2;
delta=w-0;

% repeatedly re-evaluate function and weights until they don't
change
while norm(delta)>tolerance && iteration<maxiterations
    weightedy=sqrt(w).*y;
    weightedfunc=@(b,x) sqrt(w).*func(b,x);
    [coeffs,r,J,covb,mse]=nlinfit(x,weightedy,weightedfunc,start);
    old=w;
    w=1./func(coeffs,x).^2;
    delta=w-old;
    iteration=iteration+1;
end

if iteration>=maxiterations
    display('\rWARNING: fit did not converge!!\r\r');
end

% compute model values and model standard deviations for provided
xvalues
% xvalues=transpose(xvalues);

[modelvalues,modelstd]=nlpredci(func,xvalues,coeffs,r,'covar',covb,'alph
a',0.318,'mse',mse,'predopt','curve');
% compute model values and non-simultaneous prediction standard
deviations for provided xvalues
% NOTE: cannot use nlpredci for this because it will use the
nominal
% mse rather than the mse values associated with each x-value
```

```

%
[modelvalues,totalsd]=nlpredci(func,x,coeffs,r,'covar',covb,'alpha',0.3
18,'mse',mse,'predopt','observation');
w=1./func(coeffs,xvalues).^2;
randomsd=sqrt(mse./w);
totalsd=hypot(modelsd,randomsd);

covariance=covb
RMSE=sqrt(mse);

% create a plot showing data and standard deviation bounds
figure1 = figure;

% Create axes
axes1 = axes('Parent',figure1,'YMinorTick','on','XMinorTick','on');
box(axes1,'on');
hold(axes1,'all');

% Create multiple lines using matrix input to plot
plot1 = plot(xvalues,[modelvalues,...
    modelvalues+modelsd,modelvalues-modelsd,...
    modelvalues+randomsd,modelvalues-randomsd,...
    modelvalues+totalsd,modelvalues-
totalsd],'LineWidth',2,'Parent',axes1);
set(plot1(1),'DisplayName','model');
set(plot1(2),'LineStyle','-.','DisplayName','model std. dev.',...
    'Color',[0 0 0]);
set(plot1(3),'LineStyle','-.','DisplayName','model std. dev.',...
    'Color',[0 0 0]);
set(plot1(4),'LineStyle','--','Color',[0 1 0],...
    'DisplayName','random std. dev. ');
set(plot1(5),'LineStyle','--','Color',[0 1 0],...
    'DisplayName','random std. dev. ');
set(plot1(6),'LineStyle',':','Color',[1 0 1],...
    'DisplayName','total std. dev. ');
set(plot1(7),'LineStyle',':','Color',[1 0 1],...
    'DisplayName','total std. dev. ');

% Create xlabel
xlabel('Normalized displacement of local shear zone (%D)');

% Create ylabel
ylabel('Normalized unit side resistance');

% Create plot
plot(x,y,'Parent',axes1,'MarkerSize',5,'Marker','o',...
    'LineStyle','none','DisplayName','Measured Values');

% Create legend
legend1 = legend(axes1,'show');
set(legend1,'Location','NorthWest');

```

end

Appendix F. Simulation of Load transfer Data/Curves

F.1. Randomly Simulated Load Transfer With Measured Data Imposed.

This computer code is for generation random points from load transfer models and their constant standard of deviation. The measured data then are imposed on top of the simulated data. Outputs are figures with random data and measured data.

```
clc; clear;
load SS_REmoved

DataX=SS_REmoved(:,1);
DataY=SS_REmoved(:,2);

FFa =[0.624609619    0.868809731    0.674763833    0.849617672    0.826446281
0.580383053    0.736377025    0.628535512    0.982318271    0.838222967
0.825082508    0.986193294    0.958772771    1.138822458    0.819672131    0.69637883
0.8    0.945179584    0.918273646    1.081197967    0.847457627    0.745712155
0.812347685    0.982318271    0.917431193    0.807102502    0.687285223    0.840336134
0.696864111    0.741289844    0.982318271    0.811030008    0.693481276    0.744047619
0.945179584    0.870322019    1.00623868    0.526315789    0.690131125    0.81366965
0.509943906    0.963391137    0.948766603    1.090393632    1.043405676
0.617665225    0.935453695    1.20105693];
FFb =[0.184322299    0.069756733    0.21437247    0.051682243    0.143719008
0.142890308    0.099410898    0.116781898    0.020736739    0.235456832
0.167161716    0.08739645    0.077315436    0.016080173    0.191557377    0.236142061
0.17592    0.308601134    0.041726354    0.070472484    0.201101695    0.289410887
0.138261576    0.082701375    0.076082569    0.260129136    0.323298969    0.135042017
0.351149826    0.294514455    0.064636542    0.211435523    0.461997226    0.308333333
0.193005671    0.230896432    0.095431676    0.188789474    0.121256039    0.084133442
0.228964814    0.042379576    0.126850095    0.008153964    0.095722037
0.566707844    0.136108513    0.004252943];;

WARa=[1.197461382    1.007861318    0.969932105    1.00050025
0.793650794    0.938967136    1.128158845    0.946969697    1.185958254
0.994035785    0.88028169    0.968992248    1.118067979    0.869565217
0.57208238    1.025535842    1.002405774    0.942507069    1.094331364
0.814332248    0.943396226    0.901713255    0.922509225    0.88028169
0.980392157    1.101685579    0.934579439    0.868055556    1.113461753
1.02396068    1.013068585    0.954198473    0.863557858
0.881834215    0.989119683    0.893655049    0.837520938    1.191753069
1.13999088    1.065416578    1.203948953    0.962463908    1.18708452
```

```

1.092776746 1.001903617 0.964320154          1.055408971 1.027221366
0.927643785];
WARb=[0.155550234    0.081586374          0.158292919 0.357778889
2.081746032 0.560093897 0.260040614 0.361079545          0.340014231
0.058976143 0.617077465 0.122093023          0.001702818 0.051095652
0.085411899          0.054014973 0.094597033 0.631008483 0.204858831
0.248615635 0.123867925 0.070477908          0.532103321 2.430457746
0.399411765 0.199735595 0.203084112          2.077256944 0.291392941
0.219332378 0.233917536          0.016479008 0.043825561
0.187037037 0.070445104 0.132439678 0.152261307          0.128709331
0.139534884 0.038909013          0.0759451 0.152646776 0.084591643
0.061206426 0.1330528 0.575699132          0.047271768 0.203081664
0.624860853];;

```

```

%log value of b
FFb=log(FFb);
WARb=log(WARb);

```

```

% X is of a and ln(b)
X=[FFa' FFb';WARa' WARb'];
figure(7)
hist(X(:,1),50)
xlabel('a')

```

```

figure(8)
hist(10.^(X(:,2)),50)
xlabel('b')

```

```

meanA=mean(X)
stdA=std(X)

```

```

CC=corrcoef(X)
SIGMA=cov(X)
r = mvnrnd(meanA, SIGMA, 15);

```

```

aa=r(:,1);
% back to regular b, b: log normal, so cant be negative!
bb=exp(r(:,2));
mean(bb)

```

```

t=0;
for i=1:length(aa)
    if bb(i)>0
        t=t+1;
        a(t)=aa(i);
        b(t)=bb(i);
    end
end

```

```

end
a=a';
b=b';
figure(5)
%x=[0:0.1:1 1:0.2:3 3:0.5:11];
x=[1/2*rand(1,15) 5*rand(1,5) 10*rand(1,3)];

Point=[0 0];
countC=0;
for j=1:length(a)
    x=[1/2*rand(1,15) 5*rand(1,5) 10*rand(1,3)];
    for i=1:length(x)
        y(i)=x(i)/(a(j)*x(i)+b(j));;

        if y(i)<0
            y(i)=0
            countC=countC+1;
        end
        if y(i)>2
            y(i)=2
            countC=countC+1;
        end
        Point=[Point(:,1) Point(:,2);x(i) y(i)];
    end

end

PX=Point(:,1);
Py=Point(:,2);
scatter(PX,Py, 'o')
hold on
scatter(DataX,DataY, '*')

xlabel('Displacement of Local Shear Zone in %D Individual')
ylabel('Normalized Unit Side Resistance t/tu__meas')
hold off

std_F=0.1718;
C_MC =std_F*randn(1,15);

        Old_A = 1.071 ;
        Old_B = 0.13 ;
        count=0;
Point=[0 0];
figure(6)
for j=1:length(C_MC)
    x=[1/2*rand(1,15) 5*rand(1,5) 10*rand(1,3)];
    for i=1:length(x)

```

```

y(i)=x(i)/(Old_A*x(i)+Old_B)+ C_MC(j);;

if y(i)<0
    y(i)=0;
    count=count+1;
end

Point=[Point(:,1) Point(:,2);x(i) y(i)];

end

end

PX_SD=Point(:,1);
Py_SD=Point(:,2);

scatter(PX_SD,Py_SD, 'o')
hold on
scatter(DataX,DataY, '*')
xlabel('Displacement of Local Shear Zone in %D ---Collective')
ylabel('Normalized Unit Side Resistance t/tu__meas')

hold off

```

F.2. Randomly Simulated Load Transfer Data For Regression Analyses.

After running this code, call *cftool* for regression analyses on the data set of `PX_A2` and `Py_A2`

```
clc; clear;
```

```

FFa =[0.624609619    0.868809731  0.674763833  0.849617672  0.826446281
0.580383053  0.736377025  0.628535512  0.982318271    0.838222967
0.825082508  0.986193294  0.958772771  1.138822458  0.819672131  0.69637883
0.8  0.945179584  0.918273646  1.081197967  0.847457627  0.745712155
0.812347685  0.982318271  0.917431193  0.807102502  0.687285223  0.840336134
0.696864111  0.741289844  0.982318271  0.811030008  0.693481276  0.744047619
0.945179584  0.870322019  1.00623868  0.526315789  0.690131125  0.81366965
0.509943906  0.963391137    0.948766603  1.090393632    1.043405676
0.617665225  0.935453695  1.20105693];

```

```

FFb =[0.184322299    0.069756733  0.21437247  0.051682243  0.143719008
0.142890308  0.099410898  0.116781898  0.020736739    0.235456832
0.167161716  0.08739645  0.077315436  0.016080173  0.191557377  0.236142061
0.17592  0.308601134  0.041726354  0.070472484  0.201101695  0.289410887
0.138261576  0.082701375  0.076082569  0.260129136  0.323298969  0.135042017
0.351149826  0.294514455  0.064636542  0.211435523  0.461997226  0.308333333
0.193005671  0.230896432  0.095431676  0.188789474  0.121256039  0.084133442
0.228964814  0.042379576    0.126850095  0.008153964    0.095722037
0.566707844  0.136108513  0.004252943];

```

```

WARa=[1.197461382    1.007861318                                0.969932105  1.00050025
0.793650794  0.938967136  1.128158845  0.946969697                1.185958254
0.994035785  0.88028169   0.968992248                1.118067979  0.869565217
0.57208238                1.025535842  1.002405774  0.942507069  1.094331364
0.814332248  0.943396226  0.901713255                0.922509225  0.88028169
0.980392157  1.101685579  0.934579439                0.868055556  1.113461753
1.02396068    1.013068585                                0.954198473  0.863557858
0.881834215  0.989119683  0.893655049  0.837520938                1.191753069
1.13999088    1.065416578                                1.203948953  0.962463908  1.18708452
1.092776746  1.001903617  0.964320154                1.055408971  1.027221366
0.927643785];
WARb=[0.155550234    0.081586374                                0.158292919  0.357778889
2.081746032  0.560093897  0.260040614  0.361079545                0.340014231
0.058976143  0.617077465  0.122093023                0.001702818  0.051095652
0.085411899                0.054014973  0.094597033  0.631008483  0.204858831
0.248615635  0.123867925  0.070477908                0.532103321  2.430457746
0.399411765  0.199735595  0.203084112                2.077256944  0.291392941
0.219332378  0.233917536                                0.016479008  0.043825561
0.187037037  0.070445104  0.132439678  0.152261307                0.128709331
0.139534884  0.038909013                                0.0759451   0.152646776  0.084591643
0.061206426  0.1330528   0.575699132                0.047271768  0.203081664
0.624860853];

FFb=log(FFb)
WARb=log(WARb)

% X is of a and ln(b)
X=[FFa' FFb';WARa' WARb'];

meanA=mean(X);
stdA=std(X);

ttt=60000 % (number of simulation)
CC=corrcoef(X)
SIGMA=cov(X)
r = mvnrnd(meanA, SIGMA, ttt);

a=r(:,1);
b=exp(r(:,2));
mean(b)

x=0:0.1:3;
Point=[0 0]
for j=1:length(a)
for i=1:length(x)
y(i)=x(i)/(a(j)*x(i)+b(j));;
Point=[Point(:,1) Point(:,2);x(i) y(i)];
end

%plot(x,y)
hold on
end

```

```

PX=Point(:,1);
Py=Point(:,2);

std_F=0.1718;
    C_MC =std_F*randn(1,ttt);

        Old_A = 1.071 ;
        Old_B = 0.13 ;
        count=0

% figure(6)
Point_A2=[0 0]
for j=1:length(C_MC)
    for i=1:length(x)

y(i)=x(i)/(Old_A*x(i)+Old_B)+ C_MC(j);

Point_A2=[Point_A2(:,1) Point_A2(:,2);x(i) y(i)];
% if y(i)<0
%     y(i)=0;
%     count=count+1;
end
end

PX_A2=Point_A2(:,1);
Py_A2=Point_A2(:,2);

```

Appendix G. Computer Codes for Resistance Factor Calibration

The codes contains one main program with four scripts, as follow:

G.1. Main Program

```
clc;clear; tic;data.tzcode=1;maxiter = 20;ttt=30000; NOO=1;UCS=20;
%kips
data.Nnodes = 20; % number of nodes
data.diam = 3*12; % diameter (inches)5.04
data.L =30*12; % total length (inches)17

        data.A = [1.071 1.098];
        data.b = [0.13 0.721];

Inverse_Pf=25;

COV_EA=15;

COV_DL=10;
COV_LL=12;
DeadLoad=10460*0.2*(2/3);%4289
LiveLoad=10460*0.2*(1/3);%      *.5*(2/3);10460%

std_F=0.1718; %%0.12;Load transfer variability
        C_MC =std_F*randn(1,ttt);
std_Q= 0.1395 %; 0.1;%
        C_Q_MC =std_Q*randn(1,ttt);

COV_f= 65.9;%20;% % qult and UCS prediction0;%
COV_q= 25.4; % 15;%% UCS prediction

Load=DeadLoad+LiveLoad;
std_DL=1/100*COV_DL*DeadLoad;
std_LL=1/100*COV_LL*LiveLoad;
Qgiven=DeadLoad+ std_DL*randn(1,ttt) +LiveLoad+ std_LL*randn(1,ttt);

        data.Emodulus = [30E3 4090]; % pile moduli [steel concrete]
(ksi)30E3
        data.Apercent = .9; % percent area that is steel
        Esteel = data.Emodulus(1);
        Econcrete = data.Emodulus(2);
        Apercent = data.Apercent;

        % calculate spring rate
        h = data.L/(data.Nnodes-1);
        Emod = (Apercent*Esteel + (100-Apercent)*Econcrete)/100;
```

```

        Abase = pi*(data.diam^2)/4;
                                %Cal. shaft capacity
                                Aside =
pi*data.diam*data.L;

data.tULT=0.76*(UCS.^0.79)/144; %side ultimate shear % in kips per
square inch

data.qULT=14*(UCS.^0.71)/144;

UltLoad=(data.tULT*Aside+data.qULT*Abase);

realQult=          (data.tULT*Aside/data.A(1)+data.qULT*Abase/data.A(2));
sort(Qgiven);

u0 =zeros(1,data.Nnodes);
        Kspring_b4_MC = Abase*Emod/h;

        std_EA=COV_EA/100*Kspring_b4_MC;
        Kspring_MC=Kspring_b4_MC+std_EA*randn(1,ttt);
        Displacement=zeros(1,ttt);

%generate t simulations for uncertainty in t-z and q-w curves
PhiD=zeros(1,NOO);
COV=-10;

for j=1:NOO
    COV=COV+70

sdUCS_Shale=1/100*COV.*UCS;
aaa=UCS;
bbb=sdUCS_Shale;
    eta=(reallog(1+(bbb.^2)/(aaa.^2))).^0.5;
    lamda = log(aaa)-0.5*eta.^2;
UCS_dist_MC_Shale = (lamda+eta.*randn(1,ttt));
UCS_log=exp(UCS_dist_MC_Shale); %in ksf

mean_f =0.76*UCS_log.^0.79/144; %ksf
mean_q=14*(UCS_log.^0.71)/144; %ksf

loaiNumber(j)=0;
out_2(j)=0;
for i=1:ttt

    data.P = Qgiven(i);
    aaa=mean_f(i);
    bbb=COV_f*mean_f(i)/100;
    eta=(log(1+(bbb.^2)/(aaa.^2))).^0.5;
    lamda = log(aaa)-0.5*eta.^2;
    GO = lamda+eta.*randn(1);
    f_ult_MC=exp(GO);

```

```

aaa=mean_q(i);
bbb=COV_q*mean_q(i)/100;
eta=(log(1+(bbb.^2)/(aaa.^2))).^0.5;
lamda = log(aaa)-0.5*eta.^2;
GO = lamda+eta.*randn(1);
q_ult_MC=exp(GO);

data.C = [C_MC(i) C_Q_MC(i)];
data.tULT = f_ult_MC; % side ultimate shear in kips per square inch
data.qULT = q_ult_MC; % side ultimate shear in kips per square inch

realQultMC(i)=
(data.tULT*Aside*(1/data.A(1)+data.C(1))+data.qULT*Abase*(1/data.A(2)+d
ata.C(2)));

data.Kspring=Kspring_MC(i);
loai=0;
[u,loai] = thuynewCOV3(data,u0,maxiter,loai);
Displacement(i)=u(data.Nnodes);
if loai==maxiter
    loaiNumber(j)=loaiNumber(j)+1;
end

if data.P>=realQultMC(i)
    out_2(j)=out_2(j)+1;
    Displacement(i)=10;
end

end
if out_2(j)>1/Inverse_Pf*ttt
Phi=Phiplot'
toc
return

end
%
BB=isnan(Displacement);
Displacement(BB)=[];

Dstd=std(Displacement);
mS=mean(Displacement);
eta=(log(1+Dstd^2/mS^2)).^0.5;
lamda=log(mS)-.5*eta.^2;
Displacement=sort(Displacement);
S_Star=(Displacement(ttt-ttt/Inverse_Pf+1)+Displacement(ttt-
ttt/Inverse_Pf))/2;
PhiD(j)=mS/S_Star;
Phi=1;
loaiNumber2=0;
while S_Star-mS>.005

```

```

    Phi=Phi-.005;
    UCS=UCS*Phi;
    data.P =Load; % tip load (kips)

data.tULT=0.76*(UCS.^0.79)/144; %side ultimate shear % in kips per
square inch
data.qULT=14*(UCS.^0.71)/144; %tip in kips per square inch

    data.Kspring=Kspring_b4_MC;
    data.C = [0 0];
    [u,loai] = thuynewCOV3(data,u0,maxiter,loai);
    if loai==maxiter
        loaiNumber2=loaiNumber2+1;
    end
    mS=u(data.Nnodes);
    if Phi<0
        Phi=Phiplot'

        return
    end
    UCS=UCS/Phi;

end
    Phiplot(j)=Phi
    COVplot(j)=COV;
end
plot(COVplot,Phiplot);

loaiNumber'
loaiNumber2
Phiplot'

hold on
grid on
toc
title(num2str('Probability of failure = 1%'))
xlabel('COV of UCS'); ylabel('Resistant factor for Displacement');

```

G.2. Scripts

This script requires two functions presented in Appendix A.2 and A.2 which are the NewtonRaphson and the Tridiagonal to run.

```

function [u,loai] = thuynewCOV2(data,u0,maxiter,loai)

[u,numiter,loai] = NewtonRaphson(@getNRdata,u0,maxiter,1E-6,data,loai);

end

```

```

function [f,df] = getTZ(u,data)
A = data.A; b = data.b; C=data.C;
L = data.L; diam = data.diam;
N = data.Nnodes;
% calcualte areas
h = L/(N-1);
Aside = ones(1,N)*pi*diam*h;
Aside([1 N]) = Aside([1 N])*3/2;
Abase(1) = pi*(diam^2)/4;
% zero TZ values
t = zeros(1,N); dt = t;
q = zeros(1,N); dq = q;
z = u; w = u(1);
switch data.tzcode
case 1

% SIDE TZ hyperbolic curve
t = z./(A(1).*z+b(1))+C(1);
if t<0 t=0; end
dt = b(1)./(A(1).*(z)+(b(1))).^2;

% BASE QW hyperbolic curve
q(1) = w./(A(2).*w+b(2))+C(2);
if q(1)<0 q(1)=0; end
dq(1) = b(2)./(A(2).*w+(b(2))).^2;

% POWER CURVE
% t = A(1)*sign(z).*(abs(z)).^b(1);
% dt = A(1)*b(1)*(abs(z)).^(b(1)-1);
% % BASE QW power curve
% q(1) = A(2)*sign(w)*(abs(w))^b(2);
% dq(1) = A(2)*b(2)*(abs(w))^(b(2)-1);
%
case 2
% EXPONENTIAL
% SIDE TZ exponential curve
t = 1-exp(-z);
dt = exp(-z);
% BASE QW exponential curve
% tb(1) = 1-exp(-z(1));
% dtb(1) = exp(-z(1));
end
%
f = Aside.*t*data.tULT+ Abase.*q*data.qULT;
df = Aside.*dt*data.tULT+ Abase.*dq*data.qULT;
end

function [E,F,G,R] = getNRdata(u,data)
diam = data.diam;
L = data.L;
N = data.Nnodes;
P = data.P;
Kspring=data.Kspring;

```

```

% calculate forces and force derivatives
[f,df] = getTZ(u,data);

% define force (RHS) vector and Jacobian
E = zeros(1,N); F = df; G = zeros(1,N); R = f;

for i = 1:N-1
    Ke = Kspring*[1 -1;-1 1];
    Fe = Ke*u(i:i+1)';
    E(i+1) = E(i+1) + Ke(2,1);
    F(i:i+1) = F(i:i+1) + diag(Ke)';
    G(i) = G(i) + Ke(1,2);
    R(i:i+1) = R(i:i+1) + Fe';
end
R(N) = R(N) - P;
end

```

Appendix H. Drilled Shaft SLS Resistance Factors

H.1. Resistance factors

Table H.1.1 Resistance factors for drilled shaft at SLS ($L/D = 10$), $P_f=1/25$

COV of UCS	Resistance Factors for $P_f=1/25$					
	$\theta = 0.15$	$\theta = 0.2$	$\theta = 0.25$	$\theta = 0.3$	$\theta = 0.35$	$\theta = 0.4$
0.0	0.215	0.24	0.265	0.285	0.315	0.36
0.1	0.210	0.24	0.265	0.285	0.315	0.36
0.2	0.200	0.23	0.255	0.275	0.305	Impossible Case
0.3	0.190	0.22	0.24	0.26	0.305	
0.4	0.18	0.205	0.22	0.255		
0.5	0.165	0.185	0.21			
0.6	0.155	0.17	0.20			
0.7	0.135	0.16				
0.8	0.125	0.15				
0.9	0.11					
1	0.105					

Table H.1.2 Resistance factors for drilled shaft at SLS ($L/D = 10$), $P_f=1/50$

COV of UCS	Resistance Factors for $P_f=1/50$				
	$\theta = 0.15$	$\theta = 0.2$	$\theta = 0.25$	$\theta = 0.3$	$\theta = 0.35$
0.0	0.18	0.215	0.235	0.26	0.30
0.1	0.18	0.21	0.23	0.255	0.30
0.2	0.175	0.2	0.225	0.25	Impossible Case
0.3	0.165	0.19	0.215	0.245	
0.4	0.15	0.175	0.20		
0.5	0.14	0.16			
0.6	0.125	0.15			
0.7	0.115				
0.8	0.105				
0.9	0.10				

Table H.1.3 Resistance factors for drilled shaft at SLS ($L/D = 10$), $P_f=1/75$

COV of UCS	Resistance Factors for $P_f=1/75$			
	$\theta = 0.15$	$\theta = 0.2$	$\theta = 0.25$	$\theta = 0.3$
0.0	0.17	0.20	0.225	0.25
0.1	0.17	0.195	0.22	0.25
0.2	0.160	0.19	0.21	0.245
0.3	0.155	0.18	0.20	Impossible Case
0.4	0.14	0.16	0.195	
0.5	0.13	0.15		
0.6	0.115	0.145		
0.7	0.105			
0.8	0.10			

Table H.1.4 Resistance factors for drilled shaft at SLS ($L/D = 10$), $P_f=1/100$

COV of UCS	Resistance Factors for $P_f=1/100$			
	$\theta = 0.15$	$\theta = 0.2$	$\theta = 0.25$	$\theta = 0.3$
0.0	0.165	0.19	0.22	0.245
0.1	0.16	0.19	0.215	0.245
0.2	0.155	0.18	0.205	0.24
0.3	0.145	0.17	0.195	Impossible Case
0.4	0.135	0.16	0.19	
0.5	0.12	0.145		
0.6	0.11			
0.7	0.10			
0.8	0.095			

Table H.1.5 Resistance factors for drilled shaft at SLS ($L/D = 30$), $P_f=1/25$

COV of UCS	$\theta = 0.10$	$\theta = 0.15$	$\theta = 0.20$	$\theta = 0.25$	$\theta = 0.30$
0	0.140	0.175	0.200	0.215	0.235
0.1	0.135	0.170	0.195	0.215	0.230
0.2	0.135	0.170	0.190	0.205	0.220
0.3	0.130	0.160	0.175	0.195	
0.4	0.125	0.150	0.165	0.180	
0.5	0.120	0.140	0.155		
0.6	0.110	0.130	0.140		
0.7	0.100	0.115	Impossible	cases	
0.8	0.090				

Table H.1.6 Resistance factors for drilled shaft at SLS ($L/D = 30$), $P_f=1/50$

COV of UCS	$\theta = 0.10$	$\theta = 0.15$	$\theta = 0.20$	$\theta = 0.25$
0	0.120	0.145	0.170	0.190
0.1	0.115	0.145	0.170	0.185
0.2	0.115	0.140	0.160	0.180
0.3	0.110	0.135	0.155	
0.4	0.105	0.125	0.145	
0.5	0.095	0.115	0.135	
0.6	0.085	0.105	Impossible	cases
0.7	0.080	0.095		

Table H.1.7 Resistance factors for drilled shaft at SLS ($L/D = 30$), $P_f=1/75$

COV of UCS	$\theta = 0.10$	$\theta = 0.15$	$\theta = 0.20$	$\theta = 0.25$
0	0.110	0.135	0.160	0.180
0.1	0.110	0.135	0.155	0.175
0.2	0.105	0.130	0.150	Impossible cases
0.3	0.100	0.125	0.140	
0.4	0.095	0.115	0.130	
0.5	0.085	0.105		
0.6	0.080	0.095		
0.7	0.070			
0.8				

Table H.1.8 Resistance factors for drilled shaft at SLS ($L/D = 30$), $P_f=1/100$

COV of UCS	$\theta = 0.10$	$\theta = 0.15$	$\theta = 0.20$
0	0.105	0.135	0.155
0.1	0.105	0.130	0.150
0.2	0.100	0.125	0.145
0.3	0.095	0.115	0.135
0.4	0.090	0.110	Impossible cases
0.5	0.085	0.100	
0.6	0.075	0.090	
0.7	0.065		
0.8			

H.2. Side Resistance Factors

Table H.2.1 Side resistance factor for P_f of 1/25

COV	$\theta = 0.1$	$\theta = 0.15$	$\theta = 0.2$	$\theta = 0.25$
0	0.125	0.155	0.175	0.185
0.1	0.125	0.155	0.17	0.18
0.2	0.12	0.15	0.165	Impossible cases
0.3	0.115	0.145	0.155	
0.4	0.11	0.135	0.145	
0.5	0.105	0.125		
0.6	0.1	0.115		
0.7	0.09	0.1		

Table H.2.2 Side resistance factor for P_f of 1/50.

		$P_f = 1/50$		
COV	$\theta = 0.1$	$\theta = 0.15$	$\theta = 0.2$	
0	0.105	0.13	0.145	
0.1	0.1	0.125	0.14	
0.2	0.1	0.125		Impossible cases
0.3	0.095	0.115		
0.4	0.09	0.105		
0.5	0.085	0.095		
0.6	0.08			
0.7	0.07			

Table H.2.3 Side resistance factor for P_f of 1/75.

$P_f = 1/75$		
COV	$\theta = 0.1$	$\theta = 0.15$
0	0.095	0.115
0.1	0.09	0.115
0.2	0.09	0.11
0.3	0.085	0.105
0.4	0.085	Impossible cases
0.5	0.075	
0.6	0.065	
0.7	0.06	

Table H.2.4 Side resistance factor for P_f of 1/100.

$P_f = 1/100$		
COV	$\theta = 0.1$	$\theta = 0.15$
0	0.085	0.11
0.1	0.085	0.105
0.2	0.085	0.105
0.3	0.08	Impossible cases
0.4	0.075	
0.5	0.07	
0.6	0.06	
0.7		

H.3. Tip resistance factors

Table H.3.1 Tip resistance factor for $P_f = 1/25$

COV	$\theta = 0.1$	$\theta = 0.2$	$\theta = 0.3$	$\theta = 0.4$	$\theta = 0.5$
0	0.165	0.29	0.365	0.42	0.485
0.1	0.165	0.29	0.36	0.415	Impossible cases
0.2	0.165	0.28	0.35	0.4	
0.3	0.16	0.265	0.32	0.38	
0.4	0.155	0.245	0.29		
0.5	0.145	0.225	0.275		
0.6	0.14	0.21	0.255		
0.7	0.13	0.18			

Table H.3.2 Tip resistance factor for $P_f=1/50$

COV	$\theta = 0.1$	$\theta = 0.2$	$\theta = 0.3$	$\theta = 0.4$
0	0.145	0.26	0.325	0.385
0.1	0.14	0.255	0.315	0.385
0.2	0.14	0.245	0.305	0.365
0.3	0.14	0.235	0.285	Impossible cases
0.4	0.135	0.215	0.265	
0.5	0.125	0.195	0.24	
0.6	0.115	0.175	Impossible	
0.7	0.11	0.16		

Table H.3.3. Tip resistance factor for $P_f=1/75$

COV	$\theta = 0.1$	$\theta = 0.2$	$\theta = 0.3$	$\theta = 0.4$
0	0.13	0.24	0.305	0.37
0.1	0.13	0.235	0.305	0.36
0.2	0.125	0.23	0.285	Impossible cases
0.3	0.125	0.215	0.27	
0.4	0.12	0.2	0.25	
0.5	0.115	0.18		
0.6	0.105	0.16	Impossible	
0.7	0.095	0.145		

Table H.3.4 . Tip resistance factor for $P_f=1/100$

COV	$\theta = 0.1$	$\theta = 0.2$	$\theta = 0.3$	$\theta = 0.4$
0	0.125	0.225	0.3	0.36
0.1	0.125	0.225	0.285	0.355
0.2	0.12	0.22	0.28	Impossible cases
0.3	0.12	0.205	0.26	
0.4	0.115	0.19	0.24	
0.5	0.105	0.17		
0.6	0.105	0.155	Impossible	
0.7	0.095	0.135		

References

- AASHTO, LRFD Bridge Design Specifications. 2007. *American of State Highway and Transportation Officials, Washington, DC.*
- Allen, T. M., Nowak, A. S., & Bathurst, R. J. (2005). Calibration to determine load and resistance factors for geotechnical and structural design. *Transportation Research E-Circular(E-C079).*
- Ang, A. H. S., & Tang, W. H. (2004). Probability concepts in engineering. *Planning, 1(4),* 1.3-5.
- ASTM Standard D1143, (2009). Standard Test Methods for Deep Foundations under Static Axial Compressive Load. ASTM International, West Conshohocken, PA, 2003, DOI: 10.1520/C0033-03, www.astm.org.
- Baecher, G., & Christian, J. (2003). *Reliability and statistics in geotechnical engineering:* John Wiley & Sons Inc.
- Becker, D. E. (1996). Eighteenth Canadian Geotechnical Colloquium: Limit states design for foundations. Part I. An overview of the foundation design process. *Canadian Geotechnical Journal, 33(6),* 956-983.
- Brown, D. A., Turner, J. P., & Castelli, R. J. (2010). *Drilled shafts: Construction procedures and LRFD design methods:* US Department of Transportation, Federal Highway Administration.
- Chapra, S. C. (2005). *Applied Numerical Methods: With MATLAB for Engineers and Scientists,* McGraw-Hill Science Engineering.

- Duncan, J. M., & Chang, C.-Y. (1970). Nonlinear analysis of stress and strain in soils. *Journal of the Soil Mechanics and Foundations Division*, 96(5), 1629-1653.
- Duncan, J. M. (2000). "Factors of safety and reliability in geotechnical engineering." *Journal of Geotechnical and Geoenvironmental Engineering* **126**(GEOBASE): 307-316.
- Fenton, G., & Griffiths, D. (2007). Reliability-Based Deep Foundation Design. *Proceedings of GeoDenver2007: new peaks in geotechnics—ASCE, Reston. Paper no. GSP, 170.*
- Griffiths, D. V., & Fenton, G. A. (2007). *Probabilistic methods in geotechnical engineering* (Vol. 491): Springer Wien New York.
- Haldar, S., & Babu, G. (2008). Load Resistance Factor Design of Axially Loaded Pile Based on Load Test Results. *Journal of Geotechnical and Geoenvironmental Engineering*, 134, 1106.
- Harr, M. E. (1987). Reliability based design in civil engineering (reprint 1996 of the original edition 1987) paper. *Recherche*, 67, 02.
- Honjo, Y., Yoshida, I., Hyodo, J., & Paikowski, S. (2005). Reliability Analysis for Serviceability and the Problems of Code Calibration. *ERTC10/GeoTechNet WP2 Workshop, evaluation of Eurocode7, Trinity College, Dublin.*
- Huaco, D. R., Bowders, J. J., & Loehr, J. E. (2012). *Method to Develop Target Levels of Reliability for Design Using LRFD*. Paper presented at the Transportation Research Board 91st Annual Meeting.
- Kulicki, J. M., Prucz, Z., Clancy, C. M., Mertz, D. R., & Nowak, A. S. (2007). "Updating the calibration report for AASHTO LRFD code." Final Rep. for National Cooperative Highway Research Program (NCHRP): 20-27.

- Loehr, J. E., Bowders, J. J., Ge, L., Likos, W.J., Luna, R., Maerz, N., Stephenson, R.W. (2011). Engineering Policy Guidelines For Design Of Drilled Shafts. No. NUTC R243-2/R244-2
- Loehr, J.E., B.L. Rosenblad, T.T. Vu (2013), *MoDot transportation Geotechnics research program: Drilled shaft axial load test program interpretation report*, Missouri Department of Transportation (In preparation)
- Misra, A., & Roberts, L. (2006a). Axial service limit state analysis of drilled shafts using probabilistic approach. *Geotechnical and Geological Engineering*, 24(6), 1561-1580.
- Misra, A., & Roberts, L. (2006b). Probabilistic analysis of drilled shaft service limit state using the "t-z" method. *Canadian Geotechnical Journal*, 43(12), 1324-1332.
- Misra, A., & Roberts, L. A. (2009). Service limit state resistance factors for drilled shafts. *Geotechnique*, 59(Compendex), 53-61.
- O'Neil, M. W., & Reese, L. C. (1999). Drilled shafts: Construction procedures and design methods. TRB Report, 794 p.
- Orr, T. L., & Farrell, E. R. (1999). *Geotechnical design to Eurocode 7*.
- Paikowsky, S. and Lu, Y. (2006) Establishing Serviceability Limit State in the Design of Bridge Foundations. *Foundation Analysis and Design*: pp. 49-58.
- Phoon, K.-K., Kulhawy, F. H., & Grigoriu, M. D. (2003). Development of a reliability-based design framework for transmission line structure foundations. *Journal of Geotechnical and Geoenvironmental Engineering*, 129(9), 798-806.
- Phoon, K. K., Kulhawy, F. H. (2008). Serviceability limit state reliability-based design. *Reliability-based Design in Geotechnical Engineering—Computations and Applications*, 344–384.

- Phoon, KK., Kulhawy, FH, & Grigoriu, MD, (1995) "Reliability-Based Design of Foundations for Transmission Line Structures", Report TR-105000, Electric Power Research Institute, Palo Alto, CA, , 380 p.
- Roberts, L.A., Gardner, B., & Misra, A. (2008). *Multiple Resistance Factor Methodology for Service Limit State Design of Deep Foundations Using a "t z" Model Approach*.
- Roberts, L. A., & Misra, A. (2010). Performance-Based Design of Deep Foundation Systems in Load and Resistance Factor Design Framework. *Transportation Research Record: Journal of the Transportation Research Board*, 2186(-1), 29-37.
- Wang, Y., Au, S. K., & Kulhawy, F. H. (2011). Expanded Reliability-Based Design Approach for Drilled Shafts. *Journal of Geotechnical and Geoenvironmental Engineering*, 137, 140.
- Zhang, L. and L. Chu (2009). "Calibration of methods for designing large-diameter bored piles: Serviceability limit state." *Soils & Foundations* 49(6): 897-908.
- Zhang, L. and Chu, F. (2009) Developing Partial Factors for Serviceability Limit State Design of Large-Diameter Bored Piles. *Contemporary Topics in In Situ Testing, Analysis, and Reliability of Foundations*: pp. 262-269.
- Zhang, L., & Ng, A. (2005). Probabilistic limiting tolerable displacements for serviceability limit state design of foundations. *Geotechnique*, 55(2), 151-162.

VITA

Thuy Vu obtained her bachelor from Hanoi Architecture University and her Master's from National University of Civil Engineering in Vietnam. She began her doctoral study in Geotechnical program at Civil and Environment Department at University of Missouri in August 2009, and is completing the program in July 2013. Upon her graduation, she would like to be a faculty member teaching at a US institution.

Thuy is married to Thang Pham, who also has a degree in geotechnical engineering from University of Colorado. They are parents to three girls: Fonda Pham, Mai Pham and Tracy Pham.